Network pharmacology for mechanistically redefined comorbidities

Network Pharmacology for Mechanistically Redefined Comorbidities

Network pharmacology for mechanistically redefined comorbidities

Doctoral Thesis, Maastricht University, Maastricht, The Netherlands

ISBN: 978-94-6402-326-8

Design and layout: M. H. Elbatrik

Printed by Gildeprint

Network Pharmacology
For Mechanistically Redefined Comorbidities

DISSERTATION

To obtain the degree of Doctor at the Maastricht University,
on the authority of the Rector Magnificus,
Prof. Dr. Rianne M. Letschert
in accordance with the decision of the Board of Deans,
to be defended in public on Wednesday 26th August 2020, at 12:00 hours

by

Mahmoud Hassan Mahmoud Elbatrik

Born on 05 October 1987, Egypt

Supervisor

Prof. Dr. Harald H.H.W. Schmidt

Co-supervisor

Dr. Ana I. Casas Guijarro

Assessment Committee

Prof. Dr. Jos H.H.J. Prickaerts (Chair)

Prof. Dr. Arjan Blokland

Dr. Stine Mencl (Clinic for Neurology, University Hospital Essen, Germany)

Prof. Dr. Dr Casper Schalkwijk

Prof. Dr. Jörg Schulz (University Hospital RWTH Aachen, Germany)

Table of Contents

1

INTRODUCTION TO NETWORK PHARMACOLOGY FOR ROS-cGMP RELATED COMORBIDITIES

The increasing number of individuals with co- and multimorbidities poses an urgent need to improve the management of patients with multiple coexisting diseases [1]. About one in four adults has at least two chronic conditions, and more than half of older adults have three or more chronic conditions [2, 3]. Those "complicated" patients with multimorbidities are usually excluded from clinical research [4]. On top of that, most of the current therapies only reduce symptoms and are often not curative and rather imprecise, as represented by a high number needed to treat (NNT), i.e. the number of patients that need to be treated within a certain time window to achieve a relevant benefit for 1 patient. For example, one of the statins, which are considered the most important advance in stroke prevention [5], pravastatin has a NNT of 642 i.e. 642 individuals would need to be treated for 5 years with pravastatin in order to prevent one stroke [6]. Likewise, for antihypertensive drugs i.e. angiotensin receptor blockers, 409 and 338 patients have to be treated for 4 years to prevent one cardiovascular death or or a myocardial infarct, respectively [7]; with respect to antidiabetic drugs, 63 patients have to be treated with empagliflozin for 3 years in order to prevent one cardiovascular event [8].

A key and conceptual medical knowledge gap contributing to these therapeutic inefficacies and limitations pertains to our current disease definitions. Many common and complex diseases are defined by a symptom in one organ, the phenotype, but not by an underlying causal mechanism, the mechanotype. Common diseases, such as hypertension for example, represent a descriptive umbrella term most likely for different, unknown disease mechanisms that share a common prominent symptom, but may have different comorbidities. The mechanotype of a common disease is not defined through a single target protein, unlike in rare mono-genetic diseases, but by a dysregulated signaling network or module. Therapeutically, such modules are best treated by a combination of drugs, often in lower doses than in monotherapy, targeting different components of the same network in a synergistic manner, an approach that has been termed network pharmacology [9, 10].

A key step in overcoming organ-based disease approaches was the construction of the first human disease network (diseasome) [11] in which diseases are nodes linked common risk genes as edges. Within the diseasome, clusters of diseases form through shared risk genes, collectively representing one or more underlying, hidden common

mechanotypes. Importantly, these common mechanism clusters represent the leads towards molecular re-definitions of these disease phenotypes and allow drug repurposing within the same cluster [12]. One example, a cluster of twelve cardiovascular, neuronal, metabolic and pulmonary disease phenotypes with high unmet medical need was found to be related to a causal signaling network comprised of reactive oxygen species formation (ROS) and dysfunctional cyclic GMP signaling (ROCG) [12] (Fig. 1).

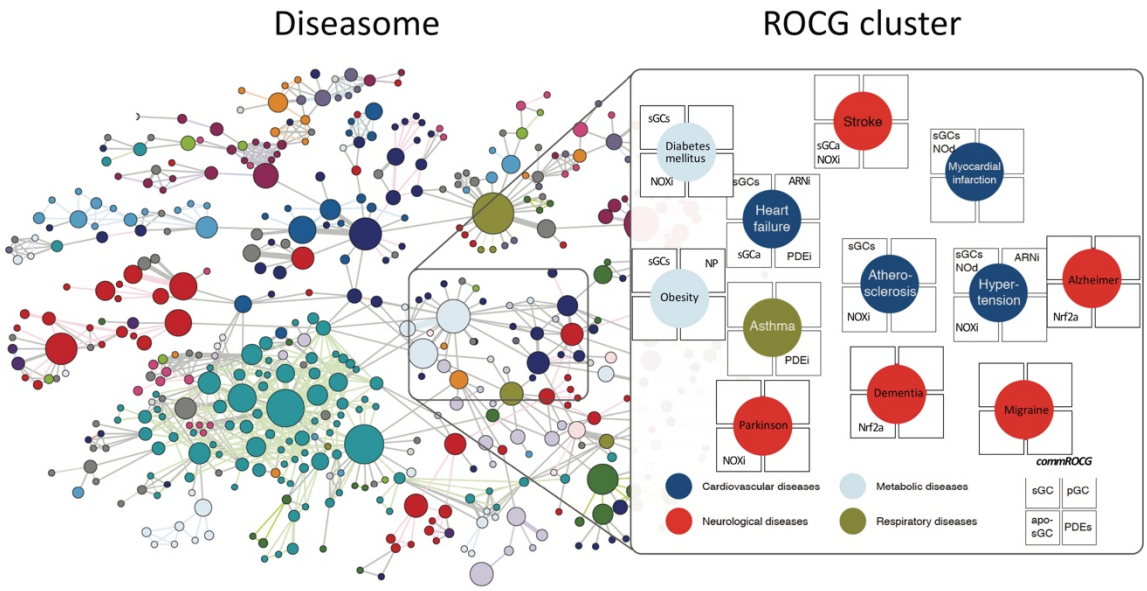

Fig. 1| ROCG cluster (adapted from [12]).

The evidence for these disease-pathway associations stems from genes associated from GWAS studies [13-15], specific genetic risks [16-18] and clinically effective drugs targeting the gene products (Table 1, chapter 2). Moreover, the cluster was revalidated not only based on genes, but also when reconstructed based on protein-protein interactions or comorbidity analysis [12]. Importantly, however, not all of the cluster phenotypes will have a dysregulation of the ROCG pathway as their underlying cause. Instead there will be other mechanisms that can lead to similar phenotypes, each representing an endophenotype, most likely associated with different comorbidities. Moreover, for two acute disease states in the above clusters, stroke or myocardial infarction, at least two types of causal mechanisms are likely to exist, one that increases the risk of a stroke and myocardial infarction, and another

that causes the tissue damage during a stroke and myocardial infarction. The latter are expected to be more uniform than the former as there are many different pathologies that can have a stroke or myocardial infarction as an outcome, whilst the acute scenario during such an event is likely to be very similar.

With this in mind, the present thesis focusses on the dysregulation of the ROCG network as an alternative, mechanistic disease definition for some of the patients with the above cluster phenotypes. To be of clinical relevance, a mechanistically defined disease should be able to be precisely diagnosed and subsequently not only treated but cured. Thus, a detailed understanding and validation of the ROCG network is essential as are rigid and transparent criteria which proteins/drug targets belong to it and which not. The ROCG network can be divided into two interfering pathways, NADPH oxidase (NOX)-induced ROS formation and nitric oxide (NO)-cGMP signaling. Both on their own are *per se* physiological signaling pathways.

ROS include species such as superoxide and hydrogen peroxide (H_2O_2). These are generated by the partial, 1- or 2-electron, reductions of oxygen and play several important roles in many biological processes, regulating cellular physiology and function [19]. Dysfunction of ROS signaling is associated with several disease conditions such as diabetes, atherosclerosis, hypertension, asthma and stroke [10, 20-23]. ROS are produced by several sources including mitochondria, xanthine oxidase, uncoupled nitric oxide (NO) synthase (uc-NOS) and NADPH oxidase (NOX) family [24, 25]. The latter has no other known function than to produce ROS, while other sources only produce ROS as a byproduct or upon protein damage, e.g. by pre-existing ROS [24, 26, 27]. NOX are therefore key therapeutic targets for being the primary sources of ROS in different disease conditions. Seven NOX isoforms exist, NOX1-5 and the dual oxidases, DUOX1-2. Each isoform has a particular pattern of activity regulation, tissue expression, type of ROS produced, and function [25].

The other pathway component, NO-cGMP signaling, is ubiquitously expressed and performs a plethora of physiological functions such as relaxation of vascular smooth muscle cells (blood pressure regulation), inhibiting leukocyte adhesion in endothelial cells (atheroprotective effect) and inhibiting platelet adhesion and aggregation (protective against blood clotting in stroke and myocardial infarction) [28, 29]. NO is produced from three NO synthase (NOS1-3) isoforms and most of its

functions are exerted via activation of the cGMP forming enzyme, soluble guanylate cyclase (sGC). cGMP works as a second messenger that activates cGMP-dependent protein kinase (PKG) to phosphorylate a number of biologically important targets and this is regulated via phosphodiesterases (PDEs) which metabolize cGMP [30, 31].

Within the ROCG disease module, ROS interfere with NO/cGMP at different points (Fig. 2). First, ROS can oxidize the NOS cofactor, tetrahydrobiopterin (H_4Bip), thus converting NOS to uc-NOS which produces superoxide instead of NO [32]. Second, superoxide can interact directly with NO leading to the formation of the potent oxidant, peroxynitrite, which induces cytotoxicity [31]. Third, ROS can oxidize sGC resulting in the formation of oxidized sGC or heme-free sGC (apo-sGC) which is NO-insensitive [33-35].

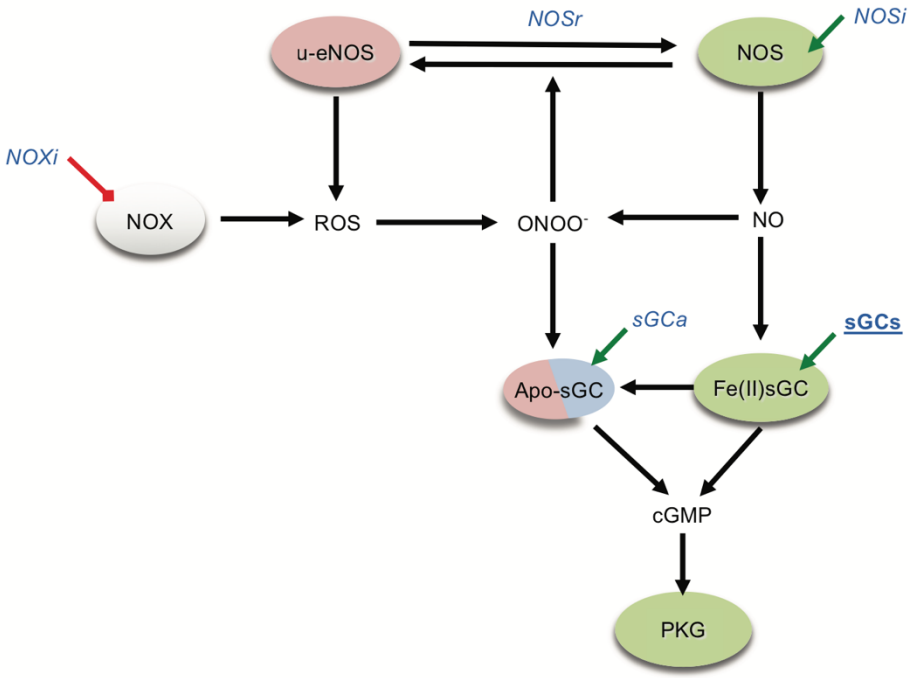

Fig. 2| ROCG network. Reactive oxygen species (ROS) from NADPH oxidase (NOX) interfere with nitric oxide (NO)/ cGMP pathway via interaction of NO to form peroxynitrite ($ONOO^-$), uncoupling of NO synthase (NOS) and oxidation of soluble guanylate cyclase (sGC) to form NO-unresponsive apo-sGC. Several activators and inhibitors, which are shown in blue and indicated by green arrows and red blocks respectively, can activate physiological and inhibit pathophysiological signaling. Drugs written in bold are already in the market while those written in italic are still in clinical trials. NOSi, NOS inhibitors; NOSr, NOS recoupling agents; NOXi, NOX inhibitors; sGCa, sGC activators; sGCs, sGC stimulators. Adapted from [33].

The ROCG network can be targeted by different drug classes in order to maintain normal and functional signaling (Fig 2). NOX inhibitors show promising results in preclinical trials and are now in clinical trials stage focusing on diabetic, neurovascular and fibrotic diseases [36, 37]. However, development of specific and isoform-selective NOX inhibitors is still lagging behind [24, 38]. NOS inhibitors display neuroprotective effects in stroke and are now tested clinically [39]. NOS recoupling agents are used to revert uc-NOS to NOS, and this could be useful in chronic conditions exhibiting low NO bioavailability such as diabetes, atherosclerosis and hypertension [21, 32]. sGC stimulators, recently approved for pulmonary hypertension, activate sGC and synergize with low NO levels [40]. Finally, sGC activators, in phase III clinical trials, can activate apo-sGC [41]. Based on disease mechanism, these drug classes can be used in different low-dose combinations.

Taken together, the following research questions will be addressed subsequently in this thesis through reviews and original work:

1. What are the roles of ROCG in different stages of diabetes and diabetic-end organ damage? (review)
2. Are there isoform-selective NOX inhibitors? How to validate them?
3. Why are sGC activators/stimulators superior to NO donors in chronic conditions?
4. Is network pharmacology (by targeting ROCG) useful in stroke with/without diabetes?
5. Does NOX5, absent in rodents, play a role in diabetic stroke and diabetes-accelerated atherosclerosis?
6. Can network pharmacology predict a ROCG target in hypertension? How to validate this target?

References

1. A. G. Ording, H. T. Sorensen, Concepts of comorbidities, multiple morbidities, complications, and their clinical epidemiologic analogs. Clin Epidemiol 5, 199-203 (2013).
2. c. Guiding principles for the care of older adults with multimorbidity: an approach for, Guiding principles for the care of older adults with multimorbidity: an approach for clinicians: American Geriatrics Society Expert Panel on the Care of Older Adults with Multimorbidity. J Am Geriatr Soc 60, E1-E25 (2012).
3. K. Barnett et al., Epidemiology of multimorbidity and implications for health care, research, and medical education: a cross-sectional study. Lancet 380, 37-43 (2012).
4. S. W. Mercer, S. M. Smith, S. Wyke, T. O'Dowd, G. C. Watt, Multimorbidity in primary care: developing the research agenda. Fam Pract 26, 79-80 (2009).
5. L. Castilla-Guerra, M. Del Carmen Fernandez-Moreno, M. A. Colmenero-Camacho, Statins in Stroke Prevention: Present and Future. Curr Pharm Des 22, 4638-4644 (2016).
6. C. R. Kumana, B. M. Cheung, I. J. Lauder, Gauging the impact of statins using number needed to treat. JAMA 282, 1899-1901 (1999).
7. J. J. Brugts et al., Impact of renin-angiotensin system inhibitors on mortality and major cardiovascular endpoints in hypertension: A number-needed-to-treat analysis. Int J Cardiol 181, 425-429 (2015).
8. Should All Patients with Type 2 Diabetes Mellitus and Cardiovascular Disease Receive an SGLT2 Inhibitor? Can J Hosp Pharm 71, 282-285 (2018).
9. A. L. Hopkins, Network pharmacology: the next paradigm in drug discovery. Nat Chem Biol 4, 682-690 (2008).
10. A. I. Casas et al., From single drug targets to synergistic network pharmacology in ischemic stroke. Proc Natl Acad Sci U S A 116, 7129-7136 (2019).
11. K. I. Goh et al., The human disease network. Proc Natl Acad Sci U S A 104, 8685-8690 (2007).

12. F. Langhauser et al., A diseasome cluster-based drug repurposing of soluble guanylate cyclase activators from smooth muscle relaxation to direct neuroprotection. NPJ Syst Biol Appl 4, 8 (2018).
13. C. A. D. Consortium et al., Large-scale association analysis identifies new risk loci for coronary artery disease. Nat Genet 45, 25-33 (2013).
14. J. Zheng, D. C. Rao, G. Shi, An update on genome-wide association studies of hypertension. Applied Informatics 2, 10 (2015).
15. A. T. Kraja et al., New Blood Pressure-Associated Loci Identified in Meta-Analyses of 475 000 Individuals. Circ Cardiovasc Genet 10, (2017).
16. J. Erdmann et al., Dysfunctional nitric oxide signalling increases risk of myocardial infarction. Nature 504, 432-436 (2013).
17. A. Akomolafe et al., Genetic association between endothelial nitric oxide synthase and Alzheimer disease. Clin Genet 70, 49-56 (2006).
18. M. Jachymova et al., Association of the Glu298Asp polymorphism in the endothelial nitric oxide synthase gene with essential hypertension resistant to conventional therapy. Biochem Biophys Res Commun 284, 426-430 (2001).
19. D. Vara, G. Pula, Reactive oxygen species: physiological roles in the regulation of vascular cells. Curr Mol Med 14, 1103-1125 (2014).
20. S. P. Gray et al., NADPH oxidase 1 plays a key role in diabetes mellitus-accelerated atherosclerosis. Circulation 127, 1888-1902 (2013).
21. M. H. Elbatreek, M. P. Pachado, A. Cuadrado, K. Jandeleit-Dahm, H. Schmidt, Reactive Oxygen Comes of Age: Mechanism-Based Therapy of Diabetic End-Organ Damage. Trends Endocrinol Metab, (2019).
22. P. A. Henricks, F. P. Nijkamp, Reactive oxygen species as mediators in asthma. Pulm Pharmacol Ther 14, 409-420 (2001).
23. B. Lassegue, K. K. Griendling, Reactive oxygen species in hypertension; An update. Am J Hypertens 17, 852-860 (2004).
24. V. T. Dao et al., Isoform-selective NADPH oxidase inhibitor panel for pharmacological target validation. Free Radic Biol Med, (2019).
25. A. I. Casas et al., Reactive Oxygen-Related Diseases: Therapeutic Targets and Emerging Clinical Indications. Antioxid Redox Signal 23, 1171-1185 (2015).

26. A. I. Casas et al., Reactive Oxygen-Related Diseases: Therapeutic Targets and Emerging Clinical Indications. Antioxidants & redox signaling 23, 1171-1185 (2015).
27. V. T. Dao et al., Pharmacology and Clinical Drug Candidates in Redox Medicine. Antioxid Redox Signal 23, 1113-1129 (2015).
28. J. Davignon, P. Ganz, Role of endothelial dysfunction in atherosclerosis. Circulation 109, III27-32 (2004).
29. A. Puzserova, I. Bernatova, Blood pressure regulation in stress: focus on nitric oxide-dependent mechanisms. Physiol Res 65, S309-S342 (2016).
30. F. Z. Monica, K. Bian, F. Murad, The Endothelium-Dependent Nitric Oxide-cGMP Pathway. Adv Pharmacol 77, 1-27 (2016).
31. P. Pacher, J. S. Beckman, L. Liaudet, Nitric oxide and peroxynitrite in health and disease. Physiol Rev 87, 315-424 (2007).
32. J. F. Gielis et al., Pathogenetic role of eNOS uncoupling in cardiopulmonary disorders. Free Radic Biol Med 50, 765-776 (2011).
33. J. M. Oettrich et al., Clinical relevance of cyclic GMP modulators: A translational success story of network pharmacology. Clin Pharmacol Ther 99, 360-362 (2016).
34. J. P. Stasch et al., Targeting the heme-oxidized nitric oxide receptor for selective vasodilatation of diseased blood vessels. J Clin Invest 116, 2552-2561 (2006).
35. O. V. Evgenov et al., NO-independent stimulators and activators of soluble guanylate cyclase: discovery and therapeutic potential. Nat Rev Drug Discov 5, 755-768 (2006).
36. G. Teixeira et al., Therapeutic potential of NADPH oxidase 1/4 inhibitors. Br J Pharmacol 174, 1647-1669 (2017).
37. S. R. Lee, E. J. An, J. Kim, Y. S. Bae, Function of NADPH Oxidases in Diabetic Nephropathy and Development of Nox Inhibitors. Biomol Ther (Seoul) 28, 25-33 (2020).
38. F. Augsburger et al., Pharmacological characterization of the seven human NOX isoforms and their inhibitors. Redox Biol 26, 101272 (2019).
39. L. M. A. Favie et al., Nitric Oxide Synthase Inhibition as a Neuroprotective Strategy Following Hypoxic-Ischemic Encephalopathy: Evidence From Animal Studies. Front Neurol 9, 258 (2018).

40. H. A. Ghofrani et al., Riociguat for the treatment of chronic thromboembolic pulmonary hypertension. N Engl J Med 369, 319-329 (2013).
41. P. Sandner et al., Soluble Guanylate Cyclase Stimulators and Activators. Handb Exp Pharmacol, (2019).

2

REACTIVE OXYGEN COMES OF AGE: MECHANISM-BASED THERAPY OF DIABETIC END-ORGAN DAMAGE

Elbatreek MH, Pachado MP, Cuadrado A, Jandeleit-Dahm K, Schmidt H. Reactive Oxygen Comes of Age: Mechanism-Based Therapy of Diabetic End-Organ Damage. Trends Endocrinol Metab. 2019.

Highlights

- Lack of comprehensive understanding of DM and its complications, together with its increasing prevalence, represent a major unmet medical need. There is quite a lot known about its mechanisms, but more is needed.
- Reactive oxygen species (ROS) may hold the answer to this need, but long-standing misconceptions about oxidative stress and the inefficacy of antioxidants have prevented clinical breakthroughs.
- A new understanding of ROS as both essential signaling molecules and pathomechanism have led to the identification, at different stages of diabetes, of different therapeutically relevant sources and targets of ROS.
- Network pharmacology and precision diagnostics, currently in advanced stages of clinical development, in conjunction with essential lifestyle changes, will revolutionize the therapy and prevention of diabetes and its end-organ damage.

Abstract

Reactive oxygen species (ROS) have been mainly viewed as unwanted by-products of cellular metabolism, oxidative stress, a sign of a cellular redox imbalance, and potential disease mechanisms, such as in diabetes mellitus (DM). Antioxidant therapies, however, have failed to provide clinical benefit. This paradox can be explained by recent discoveries that ROS have mainly essential signaling and metabolic functions and evolutionally conserved physiological enzymatic sources. Disease can occur when ROS accumulate in nonphysiological concentrations, locations, or forms. By focusing on disease-relevant sources and targets of ROS, and leaving ROS physiology intact, precise therapeutic interventions are now possible and are entering clinical trials. Their outcomes are likely to profoundly change our concepts of ROS in DM and in medicine in general.

A New Approach to Diabetes Mellitus and Reactive Oxygen Species

Diabetes mellitus (DM) and its related end-organ damage, such as diabetic nephropathy, neuropathy, retinopathy, and cardiomyopathy, are major causes of death and long-term disability. Their underlying mechanisms are incompletely understood, which is why none of the current antidiabetic therapies target the underlying causes or are curative, but focus instead on normalizing surrogate parameters or risk factors such as blood glucose or hypertension [1]. Hence, our lack of mechanistic understanding of lifestyle change-resistant diabetic end-organ damage, together with the increasing prevalence of DM, represent a significant major unmet medical need.

One mechanism that has been suggested for decades to cause pancreatic β cell dysfunction and diabetic end-organ damage is '**oxidative stress**' (see Glossary), originally defined as an overproduction of **reactive oxygen species (ROS)**. Antioxidants were considered the obvious therapeutic countermeasure but, clinically, have consistently disappointed [2]. Even worse, meta-analyses of clinical trials show that antioxidants may not only be ineffective, but harmful, and even increase mortality [2].

Recently, however, important conceptual breakthroughs in our understanding of ROS in general and DM in particular explain the failure of antioxidants and point towards entirely different mechanism-based and possibly curative therapeutic approaches. Our new understanding of ROS requires that many long-held misconceptions, such as the '**redox balance hypothesis**' and the view that ROS are primarily stressors, disease triggers, and metabolic waste products, must be overcome. Instead, the many physiological roles of ROS and the existence of at least seven evolutionarily conserved ROS-producing enzymes (NOX1–5, DUOX1–2), in addition to their alternatively spliced variants, should be recognized. In particular, the discovery of **NADPH oxidase** isoforms, whose only known function is to produce ROS [i.e., NOX1, NOX2 (aka gp91phox) NOX3, NOX4, and NOX5], made it clear that ROS are not merely waste or toxic by-products that need to be removed in order to prevent cellular damage (Box 1).

Box 1

NADPH Oxidase Family

Unlike several ROS sources (e.g., mitochondria, xanthine oxidase, cytochrome P450 enzymes, and uncoupled NOS), NADPH oxidases are the only enzyme family known to produce ROS as their primary and sole function [5]. NADPH oxidases are enzyme complexes with a membrane spanning catalytic NOX subunit in addition to other membrane and cytosolic proteins. There are seven identified members of the NADPH oxidase family, NOX1–5, and two dual oxidases (DUOX), DUOX1 and DUOX2. In humans, all seven enzymes are expressed and each NOX isoform has specific tissue expression, regulation, and type of ROS produced 3, 5.

The main NOX isoforms to be considered in pathophysiology of DM are NOX1 and NOX5, which produce superoxide, and NOX4, which produces H_2O_2. NOX3 and the DUOXs have very limited roles in the inner ear and in the synthesis of thyroid hormone, respectively [87]. NOX2 is a key enzyme of the innate and inflammatory response and its inhibition or genetic defects are associated with immune deficiency and increased risk of infection, in particular in DM [13]. In addition, NOX2 has been suggested to be involved in an excessive and unlikely number of disease models [5], which indicates a possible positive publication bias, as shown by a meta-analysis of NOX2 studies in stroke [88], or an epiphenomena without therapeutic relevance.

In contrast, ROS are part of signaling networks that include ROS targets, such as **nitric oxide synthase (NOS)** and **soluble guanylate cyclase (sGC)**, and ROS-metabolizing enzymes, in particular those genetically regulated by **nuclear factor (erythroid-derived 2)-like 2 (NRF2)** [3, 4]. The differential expression of these players in different subcellular compartments [5] suggests that a homogenous cell-wide redox level or balance does not exist, but in fact points to there being differential asynchronous hot spots of ROS signaling within the cell. This then makes ROS quite similar to other classical signaling mechanisms [6], including those inducing post-translational protein modifications such as phosphorylation.

ROS signaling contributes to physiological functions and processes such as the oxidative burst of the innate immune response, cell proliferation and angiogenesis,

vasodilation, hearing, hormone synthesis, insulin secretion, and insulin sensitivity [3, 7, 8]. Dysfunction in ROS signaling includes formation of excessive amounts of ROS, appearance of ROS at nonphysiological subcellular sites or in cell types that normally do not form relevant amounts of ROS, or shifting from a physiological to a nonphysiological type of ROS [e.g., from hydrogen peroxide (H_2O_2) to superoxide].

These mechanistic insights are now leading to new therapeutic concepts for which DM is one of best understood and most suitable pathologies. Moving forward, ROS-related drug development will have to focus on the delicate task of identifying the main disease-relevant sources of deleterious ROS while at the same time leaving essential physiological sources of ROS and their signaling pathways intact. One example is the selective inhibition of specific NOX isoforms or the use of NRF2 agonists that enhance the expression of endogenous antioxidant enzymes at their physiological sites, which is qualitatively different to exogenous scavenging antioxidants acting broadly, in all cells and all cellular compartments, and thus in a nonphysiological manner. As a complicating factor, during the course of disease, the enzymatic sources of ROS may change. One example of this is the triggering of vascular dysfunction by NOX1, leading to uncoupling of NOS3, which may become a secondary, yet quantitatively more relevant source of ROS [9]; another example is ROS-induced ROS release in mitochondria [10].

In addition to preventing ROS synthesis and metabolism, ROS-induced damage can also be repaired at both the molecular and functional level. This is exemplified by recoupling of **uncoupled NOS**, allosteric sensitization of the nitric oxide (NO) receptor, sGC, for lowered NO levels, and the activation of oxidatively damaged, heme-free apo-sGC by heme-mimetics, respectively [3, 5]. Collectively, these discoveries have revolutionized the field of ROS in general and, as indicated by one of first clinical applications, DM.

We here review, first, the physiological roles of ROS (e.g., NO, H_2O_2, superoxide, and peroxynitrite) in insulin secretion and signaling (Box 2), as well as in physiology and pathophysiology of organs affected by functional and structural damage due to type 2 DM (T2DM). Importantly, the sources and mechanisms of ROS differ in health, early and late stages of disease, and with respect to different cells and organs (Figure 1, Key Figure), sometimes even qualitatively. These differences need to be carefully dissected

and defined for T2DM and its characteristic complications as well as other conditions in order to allow future precision antidiabetic interventions. With respect to ROS, the relevant therapeutic targets (see above) form a causal signaling network and in T2DM will be best targeted by mechanism-based network pharmacology, where multiple drugs are combined to synergistically correct a pathological into a near-physiological state [11]. These drugs include some new compound classes that act directly on ROS sources and targets but also some registered drugs, which act, at least in part, through indirectly modulating the ROS network. Finally, mechanism-based diagnostics may enrich these new therapeutic approaches with respect to ROS and DM in order to stratify patients for personalized and precision therapy.

Box 2

Insulin and ROS

Pancreatic β Cells

The secretion of insulin from pancreatic β cells is mainly regulated by plasma glucose levels. Glucose is taken up via the glucose transporter 2 (GLUT2) and thereafter oxidized to produce ATP. This leads to the closure of KATP channels, depolarization of the plasma membrane, opening of voltage-dependent Ca^{2+} channels, and a subsequent increase in intracellular Ca^{2+}, which enables exocytotic insulin release [89]. Two ROS species, NO and H2O2, increase intracellular Ca^{2+} and thereby facilitate insulin release. Low levels of NO from NOS1 do so by stimulating cGMP formation through sGC, and cGMP in turn activates cGMP-dependent protein kinase (PKG), which inhibits KATP channels [90]; mitochondrial glucose metabolism leaks small amounts of superoxide, which, upon dismutation to H2O2, stimulates ryanodine receptors to also increase intracellular Ca^{2+} [7, 89]. Importantly, the use of ROS by pancreatic β cells comes at a risk. Compared with most other cells, pancreatic β cells have some of the lowest expression and activity levels of ROS-metabolizing (antioxidant) enzymes [7], making them more vulnerable than other cells to the potential cytotoxic effects of ROS, such as DNA and protein damage.

In early stages of T2DM, production of NO and ROS begins to exceed the antioxidant resistance of pancreatic β cells. Peripheral **insulin resistance** (see below) and high

glucose and fatty acid levels trigger pancreatic β cells to compensate by releasing more and more insulin in a mitochondrial ROS-dependent manner [91]. In later stages, this mechanism is exhausted as superoxide anion induces a leak of protons across the mitochondrial inner membrane, decreases the mitochondrial membrane potential and ATP production, and eventually leads to a lower insulin secretion [92]. Moreover, upregulation of the renin-angiotensin system (RAS) and inflammatory cytokines further increase superoxide overproduction from additional sources (Figure 1) (i.e., NOX1 and NOX2) [87]. The additional induction of NOS2, which produces NO, toxifies superoxide to yield peroxynitrite which not only further reduces insulin secretion but also induces pancreatic β cell death [93].

Insulin-Sensitive Tissues

In peripheral insulin-sensitive tissues such as skeletal muscle, fat cells, and liver, insulin controls the switch from lipolysis/fatty oxidation during fasting to lipid storage/glucose oxidation following feeding [94]. Binding of insulin to the insulin receptor (IR) phosphorylates substrate proteins, IRS1 and IRS2, activating phosphatidylinositol 3-kinase (PI3K)-Akt (protein kinase B) signaling, which leads to the translocation and activation of glucose transporters (mainly GLUT4 in muscles and fat cells) and subsequent glucose uptake [94, 95].

ROS come into play in insulin signaling through activation of PI3K and alternative protein kinase C (PKC) activation to increase NOX4 activity, forming H_2O_2 [95]. H_2O_2 augments insulin-IR-PI3K signaling twofold, by inhibiting protein tyrosine phosphatase 1B (PTP1B) and the phosphatase and tensin homologue, PTEN, which dephosphorylates IR and downregulates PI3K signaling [94, 95], and by activating MAP kinase phosphatase-1, which dephosphorylates IRS1 [96].

Further increased ROS production is associated with peripheral insulin resistance, a main feature of T2DM [97]. In early stages of T2DM, NOX4 causes fat and liver cell apoptosis, fibrosis, and inflammation [97, 98]; NOX2 decreases skeletal muscle insulin-induced Akt phosphorylation, GLUT4 expression and translocation, and thereby glucose uptake [99]. In later stages, mitochondrial ROS formation is induced in skeletal muscles, fat cells, and liver, activating serine kinases and further impeding

insulin signaling [97, 98]. In skeletal muscles, upregulation of the RAS system further activates NOX2 to aggravate insulin resistance [99].

ROS in Diabetic End-Organ Damage/Injury

The most patient-relevant end-organ complications in DM include chronic kidney disease (CKD) (27.8% of patients with DM), retinopathies (18.9%), heart attack (9.8%), and stroke (6.6%) [12]. In all of these, ROS have been suggested to play a causal role 13, 14, 15. Collectively, these represent major causes of disability and death in diabetics and are only moderately prevented by most glucose-lowering antidiabetic drugs, in particular diabetic kidney disease [16]. Although ROS play detrimental roles in these complications, certain ROS forms fulfil important physiological functions in several organs, for example, NO, which is produced by constitutive NOS enzymes (i.e., NOS1 and NOS3) and H_2O_2, which is produced by NOX4. Some examples of these are discussed in the following sections.

Indeed, in T2DM, several events such as hyperglycemia, dyslipidemia, advanced glycation end-products (AGEs), and upregulation of the **renin-angiotensin system (RAS)** contribute to detrimental ROS production. Despite the fact that many enzymes are, in principle, capable of forming ROS, NOXs appear to often be the primary source and disease trigger [14]. Importantly, they represent the only enzyme family with no other known function than to produce ROS [5]. All other ROS sources have other primary functions and ROS production is a biochemical 'accident' often requiring a prior (often ROS-induced) damage or uncoupling before ROS formation is initiated. Therefore, we will focus here on the role of main NOX isoforms (Box 1) in diabetic end-organ damage. The roles played by other ROS sources, such as mitochondria and xanthine oxidase (XO), and the ROS-toxifying enzyme, myeloperoxidase (MPO) as well as NRF2 are briefly discussed in Box 3.

ROS in Blood Vessels

In a normal blood vessel wall, NO produced by NOS3 activates sGC, resulting in cGMP-dependent inhibition of smooth muscle contraction. In human vascular cells, NO shows atheroprotection by inhibiting leukocyte adhesion in endothelial cells and proliferation of smooth muscle cells [17, 18]. NO also displays antithrombotic properties in human

endothelial cells by inhibiting platelet adhesion and aggregation [18]. H_2O_2 produced by endothelial NOX4 enhances vasodilation in mice [8], both in a cGMP-dependent manner, by increasing the expression and activity of NOS3 [19, 20], and in a cGMP-independent manner, by oxidative activation of protein kinase G I (PKGIα) [21]. Moreover, H_2O_2 is a key signal in angiogenesis in both human and animal vascular cells [22, 23].

Vascular Disease/Atherosclerosis

In blood vessels, ROS have been suggested to cause hypertension, atherosclerosis, and a prothrombotic stage, either directly or by interfering with protective NO [13, 24]. In large- and medium-sized arteries, ROS-induced atherosclerosis is thought to be further accelerated by DM [13]. Surprisingly, however, this does not account for all ROS; NOX4-derived H_2O_2 is antiatherosclerotic by reducing fibrosis and proliferation of smooth muscle cells [25]. Conversely, a different type and source of ROS (i.e., NOX1- [13] and possibly NOX5-derived [26] superoxide), may be proatherosclerotic in DM. These examples show the complexity of ROS pathobiology with different sources/types of ROS having qualitatively opposing effects, making precise targeting of the most disease-relevant isoform pertinent for any chronic therapy in T2DM. Nonspecific, chronic NOX inhibition may interfere with angiogenesis, collateral formation, capillarization, and may also be proatherosclerotic and immunocompromising.

Superoxide appears to be the most disease-relevant type of ROS. It can decrease NO biophase levels by direct chemical scavenging, leading to intermediate peroxynitrite, protein tyrosine nitration, reducing endothelial insulin receptor expression, and inhibiting phosphatidylinositol 3-kinase (PI3K)-Akt-NOS3 signaling in the endothelium [24, 27] (Figure 1). In addition, superoxide uncouples NOS3, which decreases NO production and simultaneously increases superoxide production from uncoupled NOS3 [9] (i.e., an example of ROS-induced ROS). This has also been coined as the 'kindling-bonfire-radical' hypothesis [28] (Figure 1), because the total amounts of ROS formed from uncoupled NOS can eventually exceed those of the initial trigger enzyme, NOX. Finally, superoxide and/or peroxynitrite can damage the NO receptor, sGC [29, 30], leading to a collectively threefold interruption of NO-cGMP signaling by: (i) scavenging of NO, (ii) uncoupling NOS3, and (iii) damaging the NO receptor sGC.

ROS in the Kidney

In normal kidney, ROS regulate urine excretion and blood pressure, and H_2O_2 stimulates prorenin-induced sodium reabsorption in mouse kidney [31] and vasodilates intrarenal arteries from human and rat through indirect NO-dependent mechanisms [19, 32]. NO promotes natriuresis in animals by inhibiting tubular sodium reabsorption [33], promotes diuresis by increasing both total and regional renal blood flow through functional antagonism of the vasoconstrictor tone induced by renal sympathetic neurons [33, 34], and blunts the **tubuloglomerular feedback** response by afferent arteriolar dilatation [35].

Diabetic Kidney Disease

Besides ROS, multiple inflammatory, fibrotic, and apoptotic signaling pathways are also implicated in the different stages of diabetic kidney disease. ROS, however, appear to integrate these and thereby play a crucial role in the initiation and progression of diabetic end-organ damage and thus represent an ideal target [14]. For this, diabetic nephropathy represents the clinically most advanced therapeutic approach (Table 1), where disease-relevant (not protective!) H_2O_2 is produced from NOX4, and superoxide, from NOX5. Despite being chemically distinct, both ROS seem to trigger kidney fibrosis, renal hypertrophy, and albuminuria [36, 37]. H_2O_2 also increases the expression of vascular endothelial growth factor (VEGF) and profibrotic markers [36] and induces **glomerular hyperfiltration**, possibly by increasing intrarenal NOS expression [38]. While the disease progresses, several other renal mediators, such as angiotensin II, AGEs, transforming growth factor (TGF)-β, and protein kinase C (PKC), further increase the activity of NOX enzymes, resulting in a further aggravated renal damage [14]. Impaired cGMP signaling by ROS uncoupling of NOS3 and oxidizing sGC (Figure 1) may further aggravate tubulointerstitial damage and fibrosis [39].

ROS in Other Organs

In the retina, NO is necessary for visual function by increasing retinal blood flow, to maintain adequate nourishment and meet the high metabolic demand of the retina. In animal retina, NO modulates synaptic transmission from photoreceptors and activates sGC to produce cGMP, which is a key intermediate in the visual transduction cascade (reviewed in [40]). H_2O_2 may also act as an intracellular messenger in the human retina. Its physiological roles, however, are unclear [41].

In the brain of animals, NO functions as a neurotransmitter and neuromodulator, regulating synaptic plasticity, which is involved in cognitive functions such as memory formation and mediates neurovascular coupling [42]. H_2O_2 contributes to neurogenesis and differentiation, and neuronal plasticity [43]. In the peripheral nervous system of animals, NO also serves as a neurotransmitter of so-called nonadrenergic-noncholinergic nerves, which induce smooth muscle relaxation [42]. H_2O_2 stimulates axon growth and nerve regeneration [43, 44]. The human cell culture data [17, 18, 23, 32, 41] as well as the results in animals described above, if translatable to humans, would suggest that ROS contribute significantly and in multiple manners to human physiology.

Box 3

ROS Sources and Metabolism

Mitochondria, XO, and MPO

In addition to NOXs and uncoupled NOS, mitochondria and XO as alternative ROS sources, and MPO as an important ROS-toxifying enzyme may also contribute to the pathogenesis of diabetic end-organ damage. XO produces ROS such as superoxide and H_2O_2 during oxidative conversion of xanthine to uric acid [5]. Mitochondria produce superoxide, by one electron reduction of O_2, which is then dismutated to H_2O_2 by SOD [100]. MPO is a heme peroxidase expressed in neutrophils and monocytes and is important for innate immune system. MPO converts NOX- or XO-derived H_2O_2 in conjunction with halides and nitrite to more reactive species such as hypochlorous acid [5] and, in conjunction with nitrite, represents an alternative source for peroxynitrite, besides the canonical NO and superoxide interaction [101]. Importantly, elevated XO activity and MPO levels correlate with the development of T2DM and diabetic end-organ damage 102, 103 (e.g., in kidney fibrosis and proteinuria [104], neuropathy [105], and atherosclerosis [103]). Mitochondrial ROS also have been suggested as causative factors of insulin resistance and implicated in initiation and progression of diabetic complications [14]. Therefore, targeting mitochondria, XO, and MPO may be of additional benefit in DM and, indeed, mitochondrial-targeted

antioxidants, XO, and MPO inhibitors are in clinical development (see below) (Table 1).

NRF2

Besides ROS-forming and -metabolizing enzymes, there appears to also be a therapeutic option via endogenous ROS-eliminating (antioxidant) enzymes, in particular those genetically regulated by the transcription factor NRF2. In vasculature, NRF2 is stimulated in response to steady laminar shear stress and ROS to promote atheroprotection. Conversely, oscillatory shear stress and endothelial dysfunction are associated with decreased NRF2 activity and atherogenesis [106]. In the diabetic milieu, NRF2 and its target genes increase in response to hyperglycemia and high fat, suggesting adaptive activation against increased ROS [107]. However, chronic hyperglycemia and prolonged ROS production inhibit NRF2 activation, which is associated with endothelial cell death and foam cell formation [108]. In the diabetic kidney, high glucose and increased ROS production are accompanied by NRF2 upregulation, which initially protects against injury via inhibition of TGF-β and accumulation of extracellular matrix [109]. Sustained hyperglycemia and formation of AGEs, however, downregulate NRF2 and decrease its activity in the kidney, which is associated with increased fibrosis and renal dysfunction [110]. Moreover, in CKD patients, a decrease in the NRF2 signature of peripheral blood mononuclear cells correlates with increased NF-κB related proinflammatory responses [111]. Retinal NRF2 activation is increased in DM, which is thought to protect against ROS overproduction and inflammatory cytokines as well as blood–retina barrier dysfunction, however, the DNA binding activity of NRF2 is decreased [112]. Similarly, in diabetic nerves, acute and chronic hyperglycemia are associated with increased and decreased levels of NRF2, respectively [113]. Thus, in addition to NOX, XO, MPO, NOS, and sGC, NRF2 also has to be considered for the treatment or prevention of diabetic end-organ damage and all of these targets may form a causal inter-related signaling network for mechanism-based network pharmacology (Figure 2).

Key Figure

Differential Roles of ROS in Physiology and DM

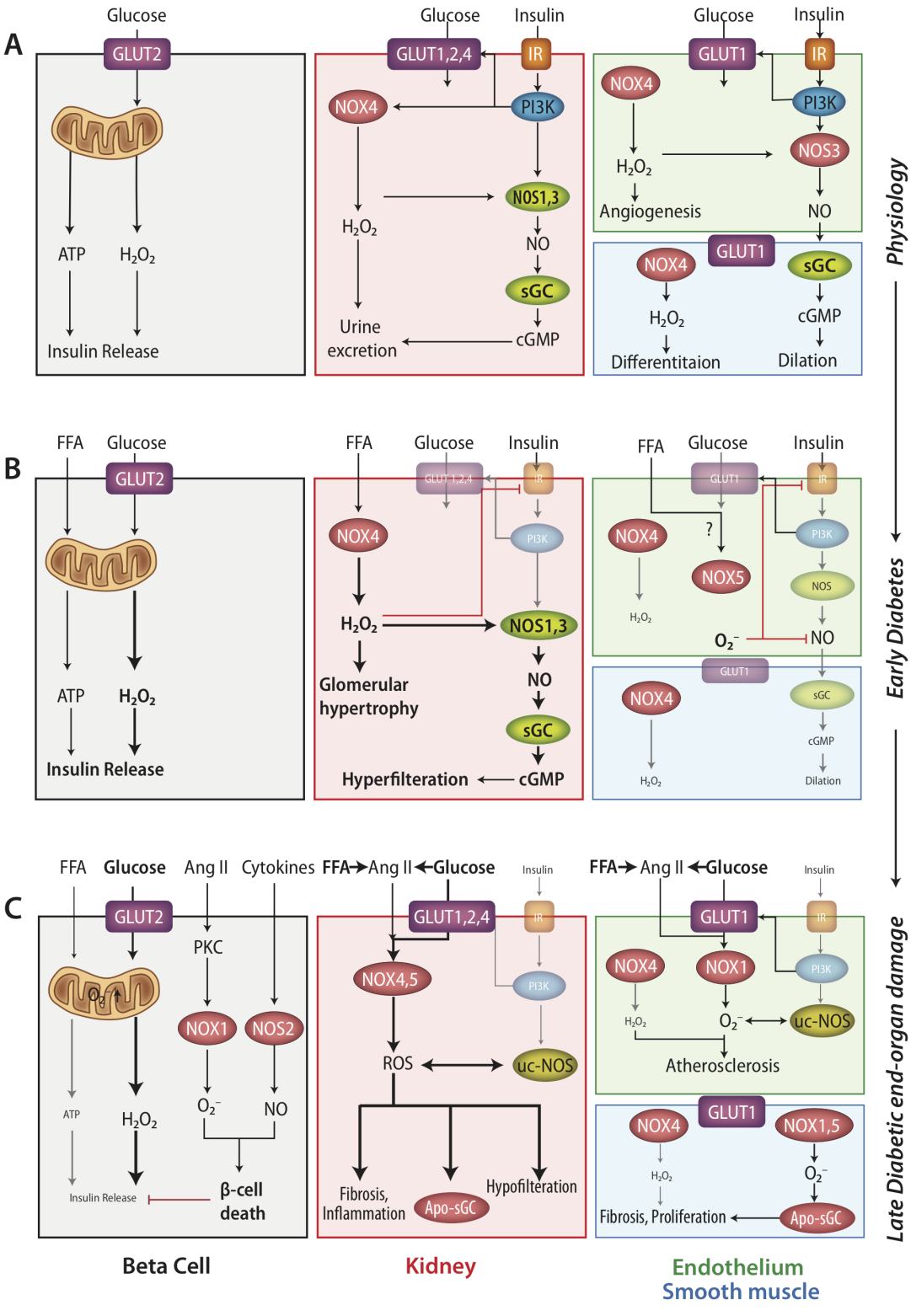

Figure 1. Key Figure: Differential Roles of ROS in Physiology and DM
Panels in (A) depict physiologic effects of ROS; (B), pathological changes in early DM; (C), late-stage DM end-organ damage. In each row, the black boxes on the left represent pancreatic β cells; red in the middle, renal cells; green and blue on the right, endothelial and vascular smooth muscle cells, respectively. Black arrows and red blocks represent stimulatory and inhibitory effects, respectively. ROS mediate both physiological and pathophysiological signaling. Mechanisms can be enhanced (bold black text and arrows) or diminished (small/transparent text and arrows) leading to pathological changes that are implicated in early and late stages of DM. Abbreviations: Ang II, angiotensin II; DM, diabetes mellitus; FFA, free fatty acids; GLUT, glucose transporter; H_2O_2, hydrogen peroxide; IR, insulin receptor; NO, nitric oxide; NOS, nitric oxide synthase; NOX, NADPH oxidase; , superoxide; PI3K, phosphatidylinositide 3-kinase; PKC, protein kinase C; ROS, reactive oxygen species; sGC, soluble guanylate cyclase.

Other End-Organ Complications

In diabetic retinopathy, H_2O_2 production is increased from an upregulated NOX4, resulting in increased VEGF expression and blood–retina barrier damage [45]. Moreover, NOX1 is activated to produce superoxide, which promotes cell death [46]. In chronic diabetic neuropathy, ROS from a yet undefined isoform of NADPH oxidase are associated with neuronal apoptosis [47]. In acute ischemic stroke [48], NOX4 is the main source of deleterious ROS and induces blood–brain barrier (BBB) damage and neuronal cell death [15, 49]. In the setting of DM, additional isoforms (e.g., NOX1 and NOX5) may come into play.

Mechanism and Network-Based Redox Therapies

Considering the failure of classic antioxidants in clinical trials focusing on diabetic complications [50, 51], new therapeutic approaches (i.e., mechanism-based redox therapies) are now state-of-the-art for future trials. These approaches include targeting specific ROS sources using pharmacological inhibitors, repairing ROS-induced damage, or upregulating endogenous antioxidant enzymes (Figure 2). The clinical status of these therapies is listed in Table 1. Importantly, targeting the ROS signaling network at multiple sites in a synergistic combinatorial manner enables a shift from single target approaches to network pharmacology, facilitating lower therapeutic doses with fewer side effects.

Table 1. Mechanism-Based Therapeutics and Their Clinical Status

Compound	Mechanism of action	Pathology	Clinical status
GKT137831	NOX1, NOX4, NOX5 inhibitor	T2DM nephropathy	Safe in phase I clinical trial Failed to reduce albuminuria in a short-term phase II trial (NCT02010242)
		T1DM nephropathy	Clinical trial ongoing (U1111-1187-2609)
		Primary Biliary Cirrhosis	Phase II clinical trial ongoing (NCT03226067)
Ronopterin (VAS203)	NOS2 inhibitor	Traumatic brain injury	Phase III clinical trial (NCT02794168)
		Renal function in Healthy volunteers	Safe in Phase I clinical trial (NCT02992236)
Allopurinol	XO inhibitor	T1DM nephropathy	Phase IV (NCT02829177)
AZD3241	MPO inhibitor	Multiple system atrophy	Phase II (NCT02388295)
AZD4831	MPO inhibitor	Heart failure	Phase II (NCT03756285)
MitoQ	Mitochondrial-targeted antioxidant	Chronic kidney disease	Declared as Dietary Supplement without indication or application in Phase IV (NCT02364648)

SkQ1	Mitochondrial-targeted antioxidant	Dry-eye syndrome	Phase III (NCT03764735)
Folic acid	NOS recoupling agent	T2DM nephropathy	Failed to improve renal endothelial function or reduce albuminuria in a phase III clinical trial (NCT00136188)
L-citrulline	NOS recoupling agent	Vascular dysfunction in T2DM	Clinical trial ongoing (NCT03358264)
		Peripheral artery disease	Phase III clinical trial ongoing (NCT02521220)
		Sickle cell disease	Phase I trial ongoing (NCT02697240)
Riociguat	sGC stimulator	Pulmonary hypertension	In the clinic
		Scleroderma	Phase II trial ongoing (NCT02915835)
		Sickle cell disease	Phase II trial ongoing (NCT02633397)
Vericiguat	sGC stimulator	Heart failure	Phase III clinical trial (NCT02861534)
Olinciguat (IW-1701)	sGC stimulator	Type I or II Achalasia	Phase II clinical trial ongoing (NCT02931565)
		Sickle cell disease	Phase II clinical trial ongoing (NCT03285178)

Praliciguat (IW-1973)	sGC stimulator	Heart failure with preserved ejection fraction	Phase II trial ongoing (NCT03254485)
		T2DM and hypertension	Phase II trial completed (NCT03091920)
Nelociguat (BAY60-4552)	sGC stimulator	Chronic heart failure	Phase I completed (NCT00565565)
Ataciguat	sGC activator	Aortic valve calcification	Phase II clinical trial (NCT02481258)
Bardoxolone methyl	NRF2 activator	T2DM and stage 4 CKD	Increased estimated GFR, but did not improve proteinuria and was associated with cardiovascular toxicity in phase III clinical trial (NCT01351675).
		T2DM and CKD	Increased measured GFR with no heart failure events due to fluid retention in phase II clinical trial (NCT02316821)
		CKD associated with T1DM	Phase II clinical trial (NCT03366337)
CXA-10	NRF2 activator	Pulmonary arterial hypertension	Phase II clinical trial ongoing (NCT03449524)
		Primary focal segmental glomerulosclerosis	Phase II clinical trial ongoing (NCT03422510)

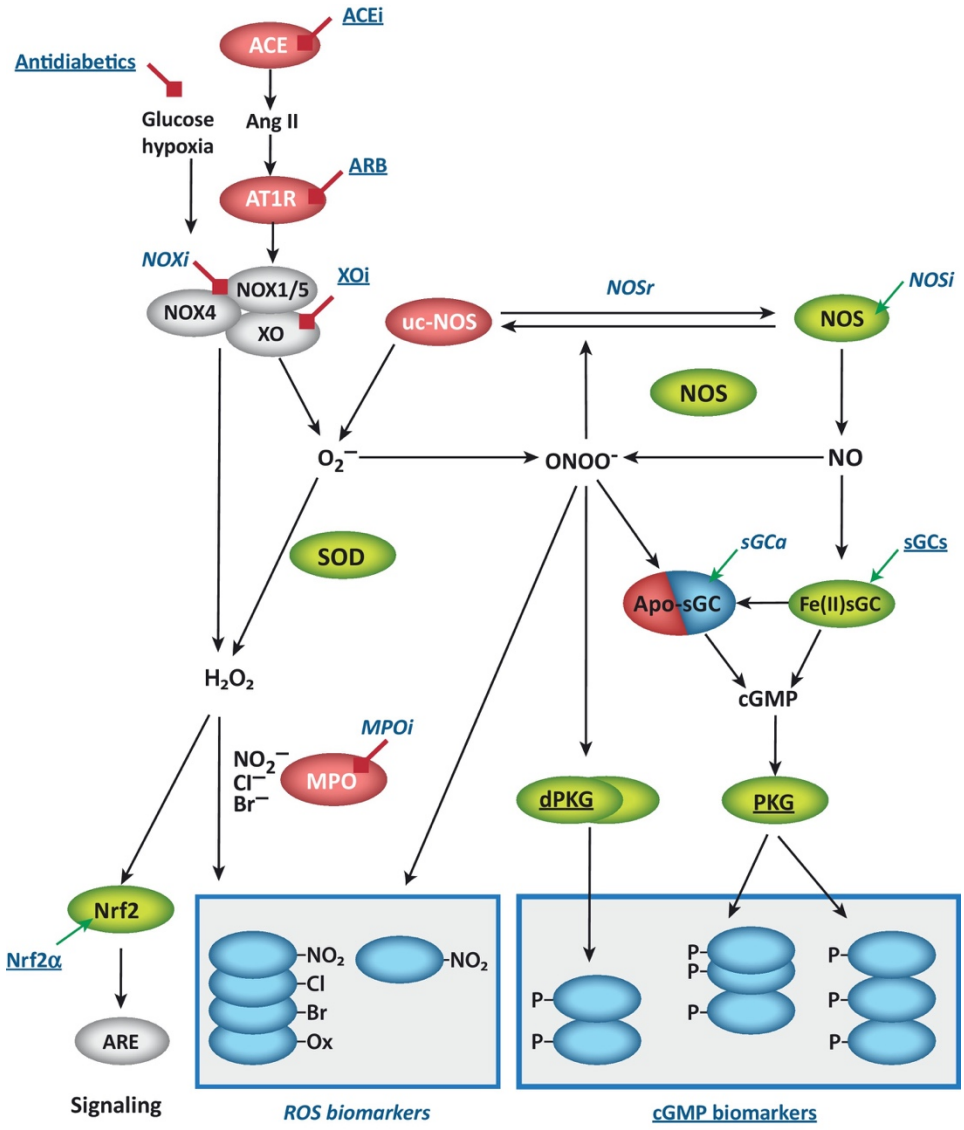

Figure 2. Network Pharmacology for ROS-Mediated Disease States.
In DM, high glucose and activated renin-angiotensin system (ACE/Ang II/AT1R) lead to the production of superoxide from NOXs and XO, and H_2O_2 from NOX4. Superoxide interferes with NO/cGMP/PKG signaling by: (i) scavenging NO to form highly reactive $ONOO^-$, (ii) uncoupling of NOS, and (iii) oxidation of sGC to form heme-free and NO-unresponsive apo-sGC. Proteins can be nitrated by $ONOO^-$ or MPO/nitrite/H_2O_2. Via NRF2, ROS can activate ARE genes leading to the expression of antioxidant enzymes such as SOD, which dismutates superoxide to H_2O_2. Several drugs (in blue and underlined when already registered; in italic when in advanced clinical development) act within this network at different sites by either activating/stimulating (green arrow) or inhibiting their target (red blocks) to either activate physiological and inhibit pathophysiological signaling, respectively. At the bottom, proteins (in blue) indicate targets and biomarkers of ROS and cGMP signaling potentially suitable for diagnosing ROS-related disease states and patient stratification. Abbreviations: ACE, angiotensin converting enzyme; Ang II, angiotensin II, ARB, angiotensin receptor blockers; ARE, antioxidant responsive element; AT1R, angiotensin II receptor type 1; DM, diabetes mellitus; H_2O_2, hydrogen peroxide; MPO, myeloperoxidase; MPOi, MPO inhibitors;

NO, nitric oxide; NOS, nitric oxide synthase; NOSi, NOS inhibitors; NOSr, NOS recoupling agents; NOX, NADPH oxidase, NOXi, NOX inhibitors; NRF2, nuclear factor (erythroid-derived 2)-like 2; NRF2a, NRF2 activators; $O_2^{\cdot-}$, superoxide; $ONOO^-$, peroxynitrite; PKG, protein kinase G; ROS, reactive oxygen species; sGC, soluble guanylyl cyclase; sGCa, sGC activators; sGCs, sGC stimulators; ucNOS, uncoupled endothelial NOS; SOD, superoxide dismutase; XO, xanthine oxidase; XOi, XO inhibitors.

Drugs Targeting ROS Sources

NOX Inhibitors

Several NOX inhibitors exist [3]. However, none of them are isoform specific. The NOX1/4 inhibitors, GKT137831 and GKT136901, have shown beneficial effects in several preclinical studies addressing diabetic complications [13, 36]. GKT137831 is currently the only NOX inhibitor in clinical trials focusing on diabetic nephropathy. It was safe in a Phase I trial, however failed to reduce albuminuria in a short-term Phase II trial in patients with T2DM and advanced nephropathy on maximal RAS blockade. Yet, there were positive signals on reduction of systemic inflammatory markers. Another trial is currently investigating the antialbuminuric effect of GKT137831 in type 1 diabetic nephropathy. This compound is also being tested in a clinical trial for primary biliary cirrhosis (Table 1).

In addition to GKT137831, other NOX inhibitors showed promising results in preclinical studies well, the pan-NOX inhibitor, APX-115, protects against nephropathy in a mouse T2DM model and was superior to GKT137831 in preserving renal function [52]. VAS2870, another pan-NOX inhibitor, reduces aortic contractility in diabetic rats by improving endothelial function [53] and, in stroke, stabilized the BBB, provided neuroprotection, improved neurological scores in mice [15], and inhibited reperfusion-induced hemorrhagic transformation in hyperglycemic rats [54]. Clearly, isoform-specific NOX inhibitors together with further testing in clinical trials focusing on diabetic complications are needed.

NOS Inhibitors

Despite its many beneficial actions, NO may also have detrimental effects when overproduced. After ischemic stroke, for example, overproduction of NO by NOS1 induces cell death and BBB hyperpermeability and in preclinical studies both nonselective NOS inhibitors or selective NOS1/2 inhibitors improved post-stroke

outcome [55]. Thus far, however, no clinical trial has tested NOS inhibitors in a stroke setting. VAS203, a pan-NOS inhibitor, is currently in a Phase III clinical trial (NOSTRA-III) in a related, yet not diabetic indication (i.e., patients with traumatic brain injury).

Drugs Targeting Other ROS Sources

Selective inhibitors of XO and MPO and mitochondrial-targeted antioxidants represent promising drugs for treatment of DM-related organ injury. XO inhibitors such as allopurinol and febuxostat, which are used because of their uric acid-lowering effects for treatment of gout patients, are now also tested in clinical trials because of their ROS-lowering effects and are focused on DM [e.g., in diabetic nephropathy and diabetic coronary artery disease (ALLIENCE trial)]. In addition, MPO inhibitors, verdiperstat (AZD3241) and AZD4831, and mitochondrial-targeted antioxidants MitoQ and SkQ1 are being tested clinically, albeit in nondiabetic conditions (Table 1).

Drugs Targeting ROS Targets

NOS Recoupling

Uncoupling of homodimeric NOS enzymes occurs by multiple mechanisms, i.e., competition of the substrate arginine with asymmetric dimethyl-l-arginine (ADMA), reduced availability of the cofactor BH_4, or oxidative damage and monomerization [56]. All of these mechanisms can be triggered by ROS. Moreover, uncoupled NOS will produce superoxide instead of NO, leading to further ROS accumulation and cellular dysfunction and damage. Several NOS recoupling strategies reduce diabetic complications by improving endothelial dysfunction in humans and animals (reviewed in [56]). Recently however, high-dose folic acid, which increases BH_4 content, failed in a Phase III clinical trial to improve renal endothelial function or to reduce albuminuria in patients with DM (NCT00136188). Studies on l-arginine supplementation gave conflicting results, probably due to its low oral bioavailability (reviewed in [57]). l-citrulline supplementation could be a better alternative due to its ideal pharmacokinetics and is currently in a Phase II clinical trial (CIPER) for treatment of peripheral artery disease. Preclinically, 3 weeks of l-citrulline treatment protected from glomerular hyperfiltration and proteinuria in streptozotocin (STZ)-diabetic rats, whereas arginine did not [58].

sGC Stimulators and Activators

ROS can also damage the NO receptor, sGC [30], resulting in impaired responsiveness to NO in DM-associated organ injury [59]. This can be functionally repaired by two different classes of drugs, sGC stimulators and activators. The former can synergize with low levels of endogenous NO by allosterically binding to sGC, while the latter bind to oxidatively damaged, heme-free apo-sGC, which can no longer sense NO. sGC activators fully recover cGMP formation from apo-sGC and prevent its degradation [59, 60]. Preclinical studies of diabetic complications using sGC stimulators and activators, respectively, show promising results. In diabetic NOS3-deficient mice (a model of late-stage diabetic nephropathy) the sGC stimulator, riociguat, combined with an angiotensin receptor blocker (ARB) significantly reduced albuminuria when compared with treatment with ARB alone [61]. The sGC activators, Bl703704 and cinaciguat, showed beneficial outcomes on renal function and improved renal structure in diabetics, respectively [39, 59]. HMR1766 (ataciguat), another sGC activator, improved NO/cGMP signaling and attenuated platelet activation in diabetic rats [62]. In addition, in a stroke model, treatment with the sGC activator, BAY 60-2770, decreased mortality, increased cerebral blood flow, decreased infarct size, attenuated BBB damage and protected from neuronal apoptosis [63]. Recently, riociguat has been approved for treatment of pulmonary hypertension and together with other sGC stimulators and activators is being tested in clinical trials, albeit so far only in nondiabetic disease conditions (Table 1).

NRF2 Activators

Induction of endogenous ROS metabolizing/eliminating enzymes by activating NRF2 boosts the endogenous control of physiological ROS signaling. Hence, NRF2 activation may be a promising approach to treat ROS-associated diseases, despite the failure of systemically applied antioxidants, which by definition interfere with any ROS, physiological or pathophysiological, leading to neutral or even detrimental outcomes. In a Chinese cohort of T2DM patients, the AA allele of the rs6721961 polymorphism in the NRF2 gene is associated with lower total antioxidative capacity and pancreatic β cell function and increased risk of newly diagnosed T2DM [64]. Therefore, mild systemic activation of NRF2 may elicit protective effects against hyperglycemia and related end-organ damage. Several NRF2 activators, including sulforaphane and different synthetic

triterpenoids, have promising effects in preclinical models of diabetic complications (reviewed in [4, 65]). For instance, in ApoE-deficient mice rendered diabetic by STZ injections, a low dose of the potent triterpenoid, dh404, protected against atherosclerosis and improved both renal function and structure. The study also demonstrated target engagement of dh404 on NRF2 activation by reduced ROS and attenuated proinflammatory and profibrotic markers [66]. Another triterpenoid, RTA-405, improved renal function, serum glucose, and triglyceride levels in STZ-induced diabetic rats when compared with untreated diabetic rats [67]. Both dh404 and RTA-405 do not show adverse effects on kidney or liver in obese rats with T1DM [67]. The most developed triterpenoid for clinical use in DM is bardoxolone methyl. In a Phase II clinical trial (BEAM), bardoxolone methyl increased the estimated glomerular filtration rate (GFR) in patients with DM and moderate to severe CKD and this effect persisted for the whole treatment period of 52 weeks [68]. In a Phase III trial (BEACON), bardoxolone methyl increased estimated GFR in patients with T2DM and stage 4 CKD [69]. The trial was terminated prematurely after preliminary analyses showed that patients randomized to bardoxolone methyl experienced significantly higher rates of heart failure events in the first 4 weeks of the trial. Elevated brain natriuretic peptide and a history of congestive heart failure were identified as risk factors that led to fluid overload events in post-hoc analyses and have been used to mitigate risk in further clinical trials with bardoxolone methyl. The cardiovascular adverse effects of bardoxolone methyl may be associated with modulation of the endothelin pathway, leading to sodium and volume retention and to blood pressure elevation in this subset of at-risk individuals [70]. In fact, in the Phase 2 TSUBAKI trial assessing bardoxolone methyl in Japanese patients with stage 3 and 4 CKD associated with T2DM, no fluid retention-related adverse events were observed, indicating that the risk-mitigation criteria could be applied to future studies as well [71]. A new Phase 3 trial (AYAME) is being conducted in Japan to assess the efficacy of multiple doses of RTA 402, using time-to-onset of a ≥30% decrease in estimated GFR from baseline or end-stage renal disease.

Indirect ROS Modulation

The current standard treatment for DM and its complications involves normalizing glucose, blood pressure, and dyslipidemia. These interventions delay microvascular complications and are used for chronic treatment of the macrovascular complications

of DM. Some of these treatment principles possess redox components, which may contribute to their beneficial effects on diabetic complications.

RAS

Drugs that block the RAS, such as angiotensin-converting enzyme inhibitors and ARB, are currently used to delay the progression of diabetic nephropathy. These drugs inhibit ROS production in different DM-associated conditions by indirectly lowering NOX expression and/or activity [48, 72]. RAS blockers also improve endothelial dysfunction and repair the damage induced by ROS in DM via recoupling of NOS [72, 73]. In addition, ARB increase the endogenous antioxidant, superoxide dismutase (SOD), via inhibition of NOX and activation of NRF2 in kidneys of diabetic mice [74].

Statins

Statins as cholesterol-lowering and anti-inflammatory [75] drugs are frequently used as part of DM care to lower the risk of cardiovascular complications [76]. With respect to ROS, statins inhibit the activation of RAC1, which is required for the activation of NOX, and in DM improve endothelial dysfunction by also inducing recoupling of NOS3 [76, 77].

Glucose-Lowering Drugs

Antihyperglycemic medications are commonly used to normalize glucose levels and include biguanides (metformin), glitazones, dipeptidyl peptidase-4 (DDP-4) inhibitors, and glucagon-like peptide-1 (GLP-1) agonists. With respect to ROS, NOX inhibition, NOS recoupling, and activation of endogenous antioxidant enzymes are all suggested mechanisms of action of these drugs [78, 79, 80, 81]. Metformin is the first-line therapy for T2DM patients and is being tested in several clinical trials (more than 2000 on https://www.clinicaltrials.org) in diabetic and nondiabetic conditions, including cancer. Metformin indirectly inhibits NOX via activation of AMP-activated protein kinase (AMPK) and recouples NOS via upregulation of GTP cyclohydrolase 1 and thus BH_4 levels [82]. Metformin also activates the endogenous NRF2 antioxidant pathway via activation of AMPK [81]. Sodium-glucose cotransporter-2 (SGLT2) inhibitors, including empagliflozin, dapagliflozin, canagliflozin, and ipragliflozin, have been recently approved as antihyperglycemic therapies. These drugs possess several favorable effects in T2DM patients, such as improved insulin sensitivity, weight loss, uric acid lowering, and blood pressure reduction and show potentially direct cardiovascular and

kidney benefits [83]. In addition to their glycosuric and natriuretic effects, several mechanisms have been suggested to explain these benefits, such as indirect inhibition of ROS production by NOX, recoupling of NOS, and activation of cGMP signaling [84, 85, 86].

Concluding Remarks and Future Perspectives

Theoretical and experimental evidence suggests a fundamentally new approach towards the contribution of ROS to T2DM and its pharmacological targeting. Instead of viewing ROS primarily as a metabolic by-product or waste, they are in fact essential signaling molecules with physiological and, upon dysregulation, also pathological roles. This dual quality of ROS depends on: (i) the type of ROS, (ii) the ROS sources, (iii) the ROS targets, and (iv) different functional consequences over time. Importantly, given the failure of classic antioxidant regimes in clinical trials, the field of ROS needs to evolve towards mechanism-based, precision medicine. Given the apparent safety of NOX inhibitors, the high efficacy of NRF2 activators in Phase III clinical trials, and the recent discovery of sGC stimulators and activators, clinical approaches of these targets in DM are ongoing or foreseeable in the very near future. These may also include their combination in a mechanism-based network pharmacology approach. Moreover, a better understanding of the causative mechanisms related to ROS formation in the development and progression of DM and its complications will allow identification of susceptible patients and more precise prevention and treatment (see Clinician's Corner). Indeed, development of mechanism-based diagnostics will allow early disease detection before the development of complications. Existing ROS biomarkers need to be validated in larger sample sizes and compared with current clinical diagnostic tools to establish them clinically (see Outstanding Questions). In any case, lifestyle changes need to be the primary intervention; pharmacotherapy only the ultima ratio.

Clinician's Corner

- Apart from lifestyle changes, none of the current antidiabetic therapies are curative as they do not target a disease mechanism, but rather focus on normalizing surrogate parameters or risk factors such as blood glucose or hypertension.
- One proposed causal disease mechanism involves reactive oxygen species (ROS), but exogenous antioxidants have failed in clinical outcome trials possibly due to the fact that ROS also have physiological functions.
- New approaches, now in clinical development, include the activation of endogenous antioxidant responses, inhibition of disease-relevant enzymatic sources of ROS, or the (functional) repair of damage induced by ROS. This includes NRF2 activators, NADPH oxidase (NOX) inhibitors, and soluble guanyl ate cyclase (sGC) stimulators and activators, respectively.
- Moreover, targeting the ROS signaling network with several drugs at different sites concurrently (network pharmacology) may enable usage of lower doses of each drug and possible fewer adverse side effects.
- Ideally, new mechanism-based biomarkers will stratify patients that suffer from a dysfunction of ROS signaling to enable precision medicine.

Outstanding Questions

- Will network pharmacology of specific ROS sources and targets in different stages of diabetes improve patient-relevant outcomes?
- Are there additional sources and targets of ROS in diabetes for mechanism-based therapy?
- Is there clinical synergy between direct and indirect modulators of ROS in diabetes?
- Will most of the current glucose-lowering, symptomatic but not mechanism-based antidiabetics become obsolete in the not too far future?
- Would effective lifestyle management programs of diabetes make pharmacotherapy obsolete in 90% of all diabetes patients? Is pharmacotherapy effective and safe in patients who do not succeed in lifestyle changes?
- How can mechanism-based diagnostics help to stratify diabetes patients for early diagnosis, prevention, and curative therapy?

Acknowledgments

The authors wish to thank Dr Merlijn J Meens and Dr Hermann Mucke for critically reading the manuscript and/or helpful suggestions. H.H.H.W.S. wishes to gratefully acknowledge funding by an ERC Advanced Investigator Grant (294683 – RadMed), an ERC proof-of-concept grant (139-101052 – SAVEBRAIN), and the EU Horizon 2020 programme, REPO-TRIAL. K.J.D. is supported by a fellowship of the National Health and Medical Research Council. A.C. is the recipient of grant SAF2016-76520-R from the Spanish Ministry of Economy and Competitiveness, P_37_732/2016 REDBRAIN from the European Regional Development Fund, and the Competitiveness Operational Program 2014-2020.

Glossary

Atherosclerosis

the narrowing of arteries due to plaque build-up on the arterial wall, a chronic inflammatory condition of large- to medium-sized arteries and major cause of cardiovascular disease.

Glomerular hyperfiltration

a condition of abnormally high glomerular filtration rate in the kidney, which occurs as early manifestation of diabetic nephropathy.

Insulin resistance

a state when body cells do not respond sufficiently to insulin and a driving factor leading to T2DM.

NADPH oxidase

a membrane-bound enzyme family which consists of seven members, NOX1–5 and two dual oxidases (DUOX1 and 2). They are the only known dedicated source of ROS and have no other function.

Nitric oxide synthase (NOS)

a family of enzymes that consists of three isoforms; NOS1–3, catalyzing the formation of NO, an important cellular signaling molecule, from l-arginine.

Nuclear factor (erythroid-derived 2)-like 2 (NRF2)

a transcription factor that regulates the expression of cytoprotective and antioxidant proteins.

Oxidative stress

an outdated view of ROS as primarily toxic metabolic waste products that need to be controlled by antioxidant enzymes or antioxidant drugs.

Reactive oxygen species (ROS)

a collective term for compounds such as superoxide, hydrogen peroxide, hydroxyl radical, peroxynitrite, and nitric oxide, although reactivity varies greatly between individual members.

Redox balance hypothesis

an outdated hypothesis that was frequently used to describe a supposedly neutral steady-state level of ROS (i.e., balance between ROS formation and cellular antioxidant defense).

Renin-angiotensin system (RAS)

a hormone system which controls blood pressure and sodium homeostasis. Its effects are coordinated through integrated actions in the kidney, cardiovascular system, and the central nervous system.

Soluble guanylate cyclase (sGC)

a heme-containing enzyme that acts as a receptor for NO to produce the second messenger cGMP, which activates protein kinase G, causes vasodilation and is regulated by phosphodiesterases.

Tubuloglomerular feedback

an adaptive mechanism that links the rate of glomerular filtration to the concentration of salt in the distal tubules.

Uncoupled NOS

when NOS enzymatic activity is uncoupled to produce superoxide instead of NO. This state usually occurs under pathological conditions induced by ROS.

References

1. N. C. D. R. F. Collaboration, Worldwide trends in diabetes since 1980: a pooled analysis of 751 population-based studies with 4.4 million participants. *Lancet* **387**, 1513-1530 (2016).
2. H. H. Schmidt *et al.*, Antioxidants in Translational Medicine. *Antioxid Redox Signal* **23**, 1130-1143 (2015).
3. V. T. Dao *et al.*, Pharmacology and Clinical Drug Candidates in Redox Medicine. *Antioxid Redox Signal* **23**, 1113-1129 (2015).
4. J. A. David, W. J. Rifkin, P. S. Rabbani, D. J. Ceradini, The Nrf2/Keap1/ARE Pathway and Oxidative Stress as a Therapeutic Target in Type II Diabetes Mellitus. *J Diabetes Res* **2017**, 4826724 (2017).
5. A. I. Casas *et al.*, Reactive Oxygen-Related Diseases: Therapeutic Targets and Emerging Clinical Indications. *Antioxid Redox Signal* **23**, 1171-1185 (2015).
6. Z. Cai, L. J. Yan, Protein Oxidative Modifications: Beneficial Roles in Disease and Health. *J Biochem Pharmacol Res* **1**, 15-26 (2013).
7. J. Pi *et al.*, Reactive oxygen species as a signal in glucose-stimulated insulin secretion. *Diabetes* **56**, 1783-1791 (2007).
8. R. Ray *et al.*, Endothelial Nox4 NADPH oxidase enhances vasodilatation and reduces blood pressure in vivo. *Arterioscler Thromb Vasc Biol* **31**, 1368-1376 (2011).
9. J. Y. Youn, L. Gao, H. Cai, The p47phox- and NADPH oxidase organiser 1 (NOXO1)-dependent activation of NADPH oxidase 1 (NOX1) mediates endothelial nitric oxide synthase (eNOS) uncoupling and endothelial dysfunction in a streptozotocin-induced murine model of diabetes. *Diabetologia* **55**, 2069-2079 (2012).
10. D. B. Zorov, M. Juhaszova, S. J. Sollott, Mitochondrial reactive oxygen species (ROS) and ROS-induced ROS release. *Physiol Rev* **94**, 909-950 (2014).
11. F. Langhauser *et al.*, A diseasome cluster-based drug repurposing of soluble guanylate cyclase activators from smooth muscle relaxation to direct neuroprotection. *NPJ Syst Biol Appl* **4**, 8 (2018).
12. A. D. Deshpande, M. Harris-Hayes, M. Schootman, Epidemiology of diabetes and diabetes-related complications. *Phys Ther* **88**, 1254-1264 (2008).

13. S. P. Gray *et al.*, NADPH oxidase 1 plays a key role in diabetes mellitus-accelerated atherosclerosis. *Circulation* **127**, 1888-1902 (2013).
14. J. C. Jha, C. Banal, B. S. Chow, M. E. Cooper, K. Jandeleit-Dahm, Diabetes and Kidney Disease: Role of Oxidative Stress. *Antioxid Redox Signal* **25**, 657-684 (2016).
15. C. Kleinschnitz *et al.*, Post-stroke inhibition of induced NADPH oxidase type 4 prevents oxidative stress and neurodegeneration. *PLoS Biol* **8**, (2010).
16. A. American Diabetes, 10. Microvascular Complications and Foot Care: Standards of Medical Care in Diabetes-2018. *Diabetes Care* **41**, S105-S118 (2018).
17. D. V. Young, D. Serebryanik, D. R. Janero, S. W. Tam, Suppression of proliferation of human coronary artery smooth muscle cells by the nitric oxide donor, S-nitrosoglutathione, is cGMP-independent. *Mol Cell Biol Res Commun* **4**, 32-36 (2000).
18. R. De Caterina *et al.*, Nitric oxide decreases cytokine-induced endothelial activation. Nitric oxide selectively reduces endothelial expression of adhesion molecules and proinflammatory cytokines. *J Clin Invest* **96**, 60-68 (1995).
19. G. R. Drummond, H. Cai, M. E. Davis, S. Ramasamy, D. G. Harrison, Transcriptional and posttranscriptional regulation of endothelial nitric oxide synthase expression by hydrogen peroxide. *Circ Res* **86**, 347-354 (2000).
20. H. Cai *et al.*, Akt-dependent phosphorylation of serine 1179 and mitogen-activated protein kinase kinase/extracellular signal-regulated kinase 1/2 cooperatively mediate activation of the endothelial nitric-oxide synthase by hydrogen peroxide. *Mol Pharmacol* **63**, 325-331 (2003).
21. J. R. Burgoyne *et al.*, Cysteine redox sensor in PKGIa enables oxidant-induced activation. *Science* **317**, 1393-1397 (2007).
22. L. Chen *et al.*, Both hydrogen peroxide and transforming growth factor beta 1 contribute to endothelial Nox4 mediated angiogenesis in endothelial Nox4 transgenic mouse lines. *Biochim Biophys Acta* **1842**, 2489-2499 (2014).
23. S. R. Datla *et al.*, Important role of Nox4 type NADPH oxidase in angiogenic responses in human microvascular endothelial cells in vitro. *Arterioscler Thromb Vasc Biol* **27**, 2319-2324 (2007).

24. E. R. Duncan *et al.*, Accelerated endothelial dysfunction in mild prediabetic insulin resistance: the early role of reactive oxygen species. *Am J Physiol Endocrinol Metab* **293**, E1311-1319 (2007).
25. E. Di Marco *et al.*, NOX4-derived reactive oxygen species limit fibrosis and inhibit proliferation of vascular smooth muscle cells in diabetic atherosclerosis. *Free Radic Biol Med* **97**, 556-567 (2016).
26. T. J. Guzik *et al.*, Calcium-dependent NOX5 nicotinamide adenine dinucleotide phosphate oxidase contributes to vascular oxidative stress in human coronary artery disease. *J Am Coll Cardiol* **52**, 1803-1809 (2008).
27. J. Du, L. M. Fan, A. Mai, J. M. Li, Crucial roles of Nox2-derived oxidative stress in deteriorating the function of insulin receptors and endothelium in dietary obesity of middle-aged mice. *Br J Pharmacol* **170**, 1064-1077 (2013).
28. M. O. Andreas Daiber, Steffen Daub, Sebastian Steven, Alexandra Schuff, Swenja Kröller-Schön, Michael Hausding, Philip Wenzel, Eberhard Schulz, Tommaso Gori, Thomas Münzel, in *Systems Biology of Free Radicals and Antioxidants,* I. Laher, Ed. (Springer, Berlin Heidelberg, 2014).
29. V. O. Melichar *et al.*, Reduced cGMP signaling associated with neointimal proliferation and vascular dysfunction in late-stage atherosclerosis. *Proc Natl Acad Sci U S A* **101**, 16671-16676 (2004).
30. J. P. Stasch *et al.*, Targeting the heme-oxidized nitric oxide receptor for selective vasodilatation of diseased blood vessels. *J Clin Invest* **116**, 2552-2561 (2006).
31. X. Lu *et al.*, Activation of ENaC in collecting duct cells by prorenin and its receptor PRR: involvement of Nox4-derived hydrogen peroxide. *Am J Physiol Renal Physiol* **310**, F1243-1250 (2016).
32. M. Munoz *et al.*, Hydrogen peroxide derived from NADPH oxidase 4- and 2 contributes to the endothelium-dependent vasodilatation of intrarenal arteries. *Redox Biol* **19**, 92-104 (2018).
33. D. S. Majid, L. G. Navar, Nitric oxide in the control of renal hemodynamics and excretory function. *Am J Hypertens* **14**, 74S-82S (2001).
34. J. J. Reid, M. J. Rand, Renal vasoconstriction is modulated by nitric oxide. *Clin Exp Pharmacol Physiol* **19**, 376-379 (1992).

35. C. S. Wilcox *et al.*, Nitric oxide synthase in macula densa regulates glomerular capillary pressure. *Proc Natl Acad Sci U S A* **89**, 11993-11997 (1992).
36. J. C. Jha *et al.*, Genetic targeting or pharmacologic inhibition of NADPH oxidase nox4 provides renoprotection in long-term diabetic nephropathy. *J Am Soc Nephrol* **25**, 1237-1254 (2014).
37. J. C. Jha *et al.*, NADPH Oxidase-Nox5 Accelerates Renal Injury in Diabetic Nephropathy. *Diabetes*, (2017).
38. S. Graham *et al.*, Abundance of TRPC6 protein in glomerular mesangial cells is decreased by ROS and PKC in diabetes. *Am J Physiol Cell Physiol* **301**, C304-315 (2011).
39. C. M. Boustany-Kari *et al.*, A Soluble Guanylate Cyclase Activator Inhibits the Progression of Diabetic Nephropathy in the ZSF1 Rat. *J Pharmacol Exp Ther* **356**, 712-719 (2016).
40. I. M. Goldstein, P. Ostwald, S. Roth, Nitric oxide: a review of its role in retinal function and disease. *Vision Res* **36**, 2979-2994 (1996).
41. G. G. Reid, J. G. Edwards, G. E. Marshall, R. G. Sutcliffe, W. R. Lee, Hydrogen peroxide induces microvilli on human retinal pigment epithelial cells in culture. *Cell Biol Int* **19**, 91-101 (1995).
42. V. Calabrese *et al.*, Nitric oxide in the central nervous system: neuroprotection versus neurotoxicity. *Nat Rev Neurosci* **8**, 766-775 (2007).
43. D. A. Borquez *et al.*, Dissecting the role of redox signaling in neuronal development. *J Neurochem* **137**, 506-517 (2016).
44. F. Meda, A. Joliot, S. Vriz, Nerves and hydrogen peroxide: how old enemies become new friends. *Neural Regen Res* **12**, 568-569 (2017).
45. J. Li *et al.*, Inhibition of reactive oxygen species by Lovastatin downregulates vascular endothelial growth factor expression and ameliorates blood-retinal barrier breakdown in db/db mice: role of NADPH oxidase 4. *Diabetes* **59**, 1528-1538 (2010).
46. J. Hu *et al.*, SUMO1/UBC9decreased Nox1 activity inhibits reactive oxygen species generation and apoptosis in diabetic retinopathy. *Mol Med Rep* **17**, 1690-1698 (2018).

47. M. Chopra *et al.*, *Oxidative stress in diabetic neuropathy—source of reactive oxygen species*. (2012), vol. 2.
48. I. Kusaka *et al.*, Role of AT1 receptors and NAD(P)H oxidase in diabetes-aggravated ischemic brain injury. *Am J Physiol Heart Circ Physiol* **286**, H2442-2451 (2004).
49. A. I. Casas *et al.*, NOX4-dependent neuronal autotoxicity and BBB breakdown explain the superior sensitivity of the brain to ischemic damage. *Proc Natl Acad Sci U S A*, (2017).
50. M. G. Saklayen, J. Yap, V. Vallyathan, Effect of month-long treatment with oral N-acetylcysteine on the oxidative stress and proteinuria in patients with diabetic nephropathy: a pilot study. *J Investig Med* **58**, 28-31 (2010).
51. E. i. N. S. I. Vitamin *et al.*, Efficacy of Oral Mixed Tocotrienols in Diabetic Peripheral Neuropathy: A Randomized Clinical Trial. *JAMA Neurol* **75**, 444-452 (2018).
52. J. J. Cha *et al.*, APX-115, a first-in-class pan-NADPH oxidase (Nox) inhibitor, protects db/db mice from renal injury. *Lab Invest* **97**, 419-431 (2017).
53. A. U. Rehman, E. Dugic, C. Benham, L. Lione, L. S. Mackenzie, Selective inhibition of NADPH oxidase reverses the over contraction of diabetic rat aorta. *Redox Biol* **2**, 61-64 (2014).
54. Z. Liu *et al.*, NADPH oxidase inhibitor regulates microRNAs with improved outcome after mechanical reperfusion. *J Neurointerv Surg* **9**, 702-706 (2017).
55. X. M. Chen, H. S. Chen, M. J. Xu, J. G. Shen, Targeting reactive nitrogen species: a promising therapeutic strategy for cerebral ischemia-reperfusion injury. *Acta Pharmacol Sin* **34**, 67-77 (2013).
56. Y. Zhang, S. P. Janssens, K. Wingler, H. H. Schmidt, A. L. Moens, Modulating endothelial nitric oxide synthase: a new cardiovascular therapeutic strategy. *Am J Physiol Heart Circ Physiol* **301**, H634-646 (2011).
57. H. H. Hoang, S. V. Padgham, C. J. Meininger, L-arginine, tetrahydrobiopterin, nitric oxide and diabetes. *Curr Opin Clin Nutr Metab Care* **16**, 76-82 (2013).
58. P. Persson, A. Fasching, T. Teerlink, P. Hansell, F. Palm, L-Citrulline, but not L-arginine, prevents diabetes mellitus-induced glomerular hyperfiltration and proteinuria in rat. *Hypertension* **64**, 323-329 (2014).

59. J. P. Stasch, J. Schlossmann, B. Hocher, Renal effects of soluble guanylate cyclase stimulators and activators: a review of the preclinical evidence. *Curr Opin Pharmacol* **21**, 95-104 (2015).
60. S. Meurer *et al.*, Nitric oxide-independent vasodilator rescues heme-oxidized soluble guanylate cyclase from proteasomal degradation. *Circ Res* **105**, 33-41 (2009).
61. I. M. Ott *et al.*, Effects of stimulation of soluble guanylate cyclase on diabetic nephropathy in diabetic eNOS knockout mice on top of angiotensin II receptor blockade. *PLoS One* **7**, e42623 (2012).
62. A. Schafer *et al.*, Soluble guanylyl cyclase activation with HMR1766 attenuates platelet activation in diabetic rats. *Arterioscler Thromb Vasc Biol* **26**, 2813-2818 (2006).
63. F. Langhauser *et al.*, Increases survival by apo-sGC activation via post-stroke blood brain barrier stabilisation and anti-inflammation. *BMC Pharmacology & Toxicology* **14**, P36-P36 (2013).
64. X. Wang *et al.*, Association between the NF-E2 Related Factor 2 Gene Polymorphism and Oxidative Stress, Anti-Oxidative Status, and Newly-Diagnosed Type 2 Diabetes Mellitus in a Chinese Population. *Int J Mol Sci* **16**, 16483-16496 (2015).
65. S. M. Tan, J. B. de Haan, Combating oxidative stress in diabetic complications with Nrf2 activators: how much is too much? *Redox Rep* **19**, 107-117 (2014).
66. S. M. Tan *et al.*, Derivative of bardoxolone methyl, dh404, in an inverse dose-dependent manner lessens diabetes-associated atherosclerosis and improves diabetic kidney disease. *Diabetes* **63**, 3091-3103 (2014).
67. M. Chin *et al.*, Bardoxolone methyl analogs RTA 405 and dh404 are well tolerated and exhibit efficacy in rodent models of Type 2 diabetes and obesity. *Am J Physiol Renal Physiol* **304**, F1438-1446 (2013).
68. P. E. Pergola *et al.*, Bardoxolone methyl and kidney function in CKD with type 2 diabetes. *N Engl J Med* **365**, 327-336 (2011).
69. D. de Zeeuw *et al.*, Bardoxolone methyl in type 2 diabetes and stage 4 chronic kidney disease. *N Engl J Med* **369**, 2492-2503 (2013).

70. M. P. Chin *et al.*, Mechanisms contributing to adverse cardiovascular events in patients with type 2 diabetes mellitus and stage 4 chronic kidney disease treated with bardoxolone methyl. *Am J Nephrol* **39**, 499-508 (2014).
71. K. Yamawaki, H. Kanda, R. Shimazaki, Nrf2 activator for the treatment of kidney diseases. *Toxicol Appl Pharmacol* **360**, 30-37 (2018).
72. J. H. Oak, H. Cai, Attenuation of angiotensin II signaling recouples eNOS and inhibits nonendothelial NOX activity in diabetic mice. *Diabetes* **56**, 118-126 (2007).
73. M. Satoh *et al.*, Angiotensin II type 1 receptor blocker ameliorates uncoupled endothelial nitric oxide synthase in rats with experimental diabetic nephropathy. *Nephrol Dial Transplant* **23**, 3806-3813 (2008).
74. H. Fujita *et al.*, Modulation of renal superoxide dismutase by telmisartan therapy in C57BL/6-Ins2(Akita) diabetic mice. *Hypertens Res* **35**, 213-220 (2012).
75. M. K. Jain, P. M. Ridker, Anti-inflammatory effects of statins: clinical evidence and basic mechanisms. *Nat Rev Drug Discov* **4**, 977-987 (2005).
76. M. Endres, U. Laufs, Effects of statins on endothelium and signaling mechanisms. *Stroke* **35**, 2708-2711 (2004).
77. P. Wenzel *et al.*, Mechanisms underlying recoupling of eNOS by HMG-CoA reductase inhibition in a rat model of streptozotocin-induced diabetes mellitus. *Atherosclerosis* **198**, 65-76 (2008).
78. S. H. Choi *et al.*, Dipeptidyl peptidase-4 inhibition by gemigliptin prevents abnormal vascular remodeling via NF-E2-related factor 2 activation. *Vascul Pharmacol* **73**, 11-19 (2015).
79. Q. Li, Y. Lin, S. Wang, L. Zhang, L. Guo, GLP-1 Inhibits High-Glucose-Induced Oxidative Injury of Vascular Endothelial Cells. *Sci Rep* **7**, 8008 (2017).
80. S. Wang, S. D. Ye, W. J. Sun, Y. Y. Hu, Pioglitazone Inhibits the Expressions of p22(phox) and p47(phox) in Rat Mesangial Cells In Vitro. *ISRN Endocrinol* **2014**, 601352 (2014).
81. G. Ashabi, L. Khalaj, F. Khodagholi, M. Goudarzvand, A. Sarkaki, Pre-treatment with metformin activates Nrf2 antioxidant pathways and inhibits inflammatory responses through induction of AMPK after transient global cerebral ischemia. *Metab Brain Dis* **30**, 747-754 (2015).

82. H. An *et al.*, Metformin attenuates fluctuating glucose-induced endothelial dysfunction through enhancing GTPCH1-mediated eNOS recoupling and inhibiting NADPH oxidase. *J Diabetes Complications* **30**, 1017-1024 (2016).
83. H. J. Heerspink, B. A. Perkins, D. H. Fitchett, M. Husain, D. Z. Cherney, Sodium Glucose Cotransporter 2 Inhibitors in the Treatment of Diabetes Mellitus: Cardiovascular and Kidney Effects, Potential Mechanisms, and Clinical Applications. *Circulation* **134**, 752-772 (2016).
84. M. Oelze *et al.*, The sodium-glucose co-transporter 2 inhibitor empagliflozin improves diabetes-induced vascular dysfunction in the streptozotocin diabetes rat model by interfering with oxidative stress and glucotoxicity. *PLoS One* **9**, e112394 (2014).
85. N. Terami *et al.*, Long-term treatment with the sodium glucose cotransporter 2 inhibitor, dapagliflozin, ameliorates glucose homeostasis and diabetic nephropathy in db/db mice. *PLoS One* **9**, e100777 (2014).
86. M. Kamezaki *et al.*, Comprehensive renoprotective effects of ipragliflozin on early diabetic nephropathy in mice. *Sci Rep* **8**, 4029 (2018).
87. J. R. Weaver, A Taylor-Fishwick, David A., in *Islets of Langerhans, 2. ed.,* M. S. Islam, Ed. (Springer, Dordrecht, 2014).
88. P. W. Kleikers *et al.*, A combined pre-clinical meta-analysis and randomized confirmatory trial approach to improve data validity for therapeutic target validation. *Sci Rep* **5**, 13428 (2015).
89. P. Llanos *et al.*, Correction: Glucose-Dependent Insulin Secretion in Pancreatic beta-Cell Islets from Male Rats Requires Ca2+ Release via ROS-Stimulated Ryanodine Receptors [corrected]. *PLoS One* **10**, e0140198 (2015).
90. H. H. Schmidt, T. D. Warner, K. Ishii, H. Sheng, F. Murad, Insulin secretion from pancreatic B cells caused by L-arginine-derived nitrogen oxides. *Science* **255**, 721-723 (1992).
91. M. Prentki, C. J. Nolan, Islet beta cell failure in type 2 diabetes. *J Clin Invest* **116**, 1802-1812 (2006).
92. S. Krauss, C. Y. Zhang, B. B. Lowell, The mitochondrial uncoupling-protein homologues. *Nat Rev Mol Cell Biol* **6**, 248-261 (2005).

93. W. L. Suarez-Pinzon *et al.*, An inhibitor of inducible nitric oxide synthase and scavenger of peroxynitrite prevents diabetes development in NOD mice. *J Autoimmun* **16**, 449-455 (2001).

94. C. M. Taniguchi, B. Emanuelli, C. R. Kahn, Critical nodes in signalling pathways: insights into insulin action. *Nat Rev Mol Cell Biol* **7**, 85-96 (2006).

95. K. Mahadev *et al.*, The NAD(P)H oxidase homolog Nox4 modulates insulin-stimulated generation of H2O2 and plays an integral role in insulin signal transduction. *Mol Cell Biol* **24**, 1844-1854 (2004).

96. K. Schroder, K. Wandzioch, I. Helmcke, R. P. Brandes, Nox4 acts as a switch between differentiation and proliferation in preadipocytes. *Arterioscler Thromb Vasc Biol* **29**, 239-245 (2009).

97. L. J. Den Hartigh *et al.*, Adipocyte-Specific Deficiency of NADPH Oxidase 4 Delays the Onset of Insulin Resistance and Attenuates Adipose Tissue Inflammation in Obesity. *Arterioscler Thromb Vasc Biol* **37**, 466-475 (2017).

98. T. Tiganis, Reactive oxygen species and insulin resistance: the good, the bad and the ugly. *Trends Pharmacol Sci* **32**, 82-89 (2011).

99. Y. Wei *et al.*, Angiotensin II-induced skeletal muscle insulin resistance mediated by NF-kappaB activation via NADPH oxidase. *Am J Physiol Endocrinol Metab* **294**, E345-351 (2008).

100. N. Houstis, E. D. Rosen, E. S. Lander, Reactive oxygen species have a causal role in multiple forms of insulin resistance. *Nature* **440**, 944-948 (2006).

101. A. van der Vliet, J. P. Eiserich, B. Halliwell, C. E. Cross, Formation of reactive nitrogen species during peroxidase-catalyzed oxidation of nitrite. A potential additional mechanism of nitric oxide-dependent toxicity. *J Biol Chem* **272**, 7617-7625 (1997).

102. X. Li *et al.*, Elevated Serum Xanthine Oxidase Activity Is Associated With the Development of Type 2 Diabetes: A Prospective Cohort Study. *Diabetes Care* **41**, 884-890 (2018).

103. Y. Kataoka *et al.*, Myeloperoxidase levels predict accelerated progression of coronary atherosclerosis in diabetic patients: insights from intravascular ultrasound. *Atherosclerosis* **232**, 377-383 (2014).

104. R. Komers, B. Xu, J. Schneider, T. T. Oyama, Effects of xanthine oxidase inhibition with febuxostat on the development of nephropathy in experimental type 2 diabetes. *Br J Pharmacol* **173**, 2573-2588 (2016).
105. D. J. Miric *et al.*, Xanthine Oxidase Activity in Type 2 Diabetes Mellitus Patients with and without Diabetic Peripheral Neuropathy. *J Diabetes Res* **2016**, 4370490 (2016).
106. B. Chen, Y. Lu, Y. Chen, J. Cheng, The role of Nrf2 in oxidative stress-induced endothelial injuries. *J Endocrinol* **225**, R83-99 (2015).
107. Z. Ungvari *et al.*, Adaptive induction of NF-E2-related factor-2-driven antioxidant genes in endothelial cells in response to hyperglycemia. *Am J Physiol Heart Circ Physiol* **300**, H1133-1140 (2011).
108. T. S. Liu *et al.*, Oscillating high glucose enhances oxidative stress and apoptosis in human coronary artery endothelial cells. *J Endocrinol Invest* **37**, 645-651 (2014).
109. T. Jiang *et al.*, The protective role of Nrf2 in streptozotocin-induced diabetic nephropathy. *Diabetes* **59**, 850-860 (2010).
110. K. Huang *et al.*, Sirt1 resists advanced glycation end products-induced expressions of fibronectin and TGF-beta1 by activating the Nrf2/ARE pathway in glomerular mesangial cells. *Free Radic Biol Med* **65**, 528-540 (2013).
111. L. M. Pedruzzi *et al.*, Systemic inflammation and oxidative stress in hemodialysis patients are associated with down-regulation of Nrf2. *J Nephrol* **28**, 495-501 (2015).
112. Z. Xu *et al.*, NRF2 plays a protective role in diabetic retinopathy in mice. *Diabetologia* **57**, 204-213 (2014).
113. A. Kumar, R. Mittal, Nrf2: a potential therapeutic target for diabetic neuropathy. *Inflammopharmacology* **25**, 393-402 (2017).

3

ISOFORM-SELECTIVE NADPH OXIDASE INHIBITOR PANEL FOR PHARMACOLOGICAL TARGET VALIDATION

Dao VT*, **Elbatreek MH***, Altenhofer S, Casas AI, Pachado MP, Neullens CT, et al. Isoform-selective NADPH oxidase inhibitor panel for pharmacological target validation. Free Radic Biol Med. 2019.

Highlights

- ROS have been hypothesized as an important disease mechanism, although clinical applications are missing.
- Pharmacological inhibition of NOXs is a promising therapeutic approach.
- Target validation of NOXs relies mainly on gene deletion models.
- Here we show that selective pharmacological inhibition of these NOX isoforms is in principle possible.
- By testing different NOX inhibitors, the relevant isoform can be validated in a pharmacological manner.

Abstract

Dysfunctional reactive oxygen species (ROS) signaling is considered an important disease mechanism. Therapeutically, non-selective scavenging of ROS by antioxidants, however, has failed in multiple clinical trials to provide patient benefit. Instead, pharmacological modulation of disease-relevant, enzymatic sources of ROS appears to be an alternative, more promising and meanwhile successfully validated approach. With respect to targets, the family of NADPH oxidases (NOX) stands out as main and dedicated ROS sources. Validation of the different NOX isoforms has been mainly through genetically modified rodent models and is lagging behind in other species. It is unclear whether the different NOX isoforms are sufficiently distinct to allow selective pharmacological modulation. Here we show for five widely used NOX inhibitors that isoform selectivity can be achieved, although individual compound specificity is as yet insufficient. NOX1 was most potently (IC50) targeted by ML171 (0.1 μM); NOX2, by VAS2870 (0.7 μM); NOX4, by M13 (0.01 μM) and NOX5, by ML090 (0.01 μM). In addition, some non-specific antioxidant and assay artefacts may limit the interpretation of data, which included, surprisingly, the clinically advanced NOX inhibitor, GKT136901. In a human ischemic blood-brain barrier hyperpermeability model where genetic target validation is not an option, we provide proof-of-principle that pharmacological target validation for different NOX isoforms is possible by applying an inhibitor panel at IC50 concentrations. Moreover, our findings encourage further lead optimization and development efforts for isoform-selective NOX inhibitors in different indications.

Graphical Abstract

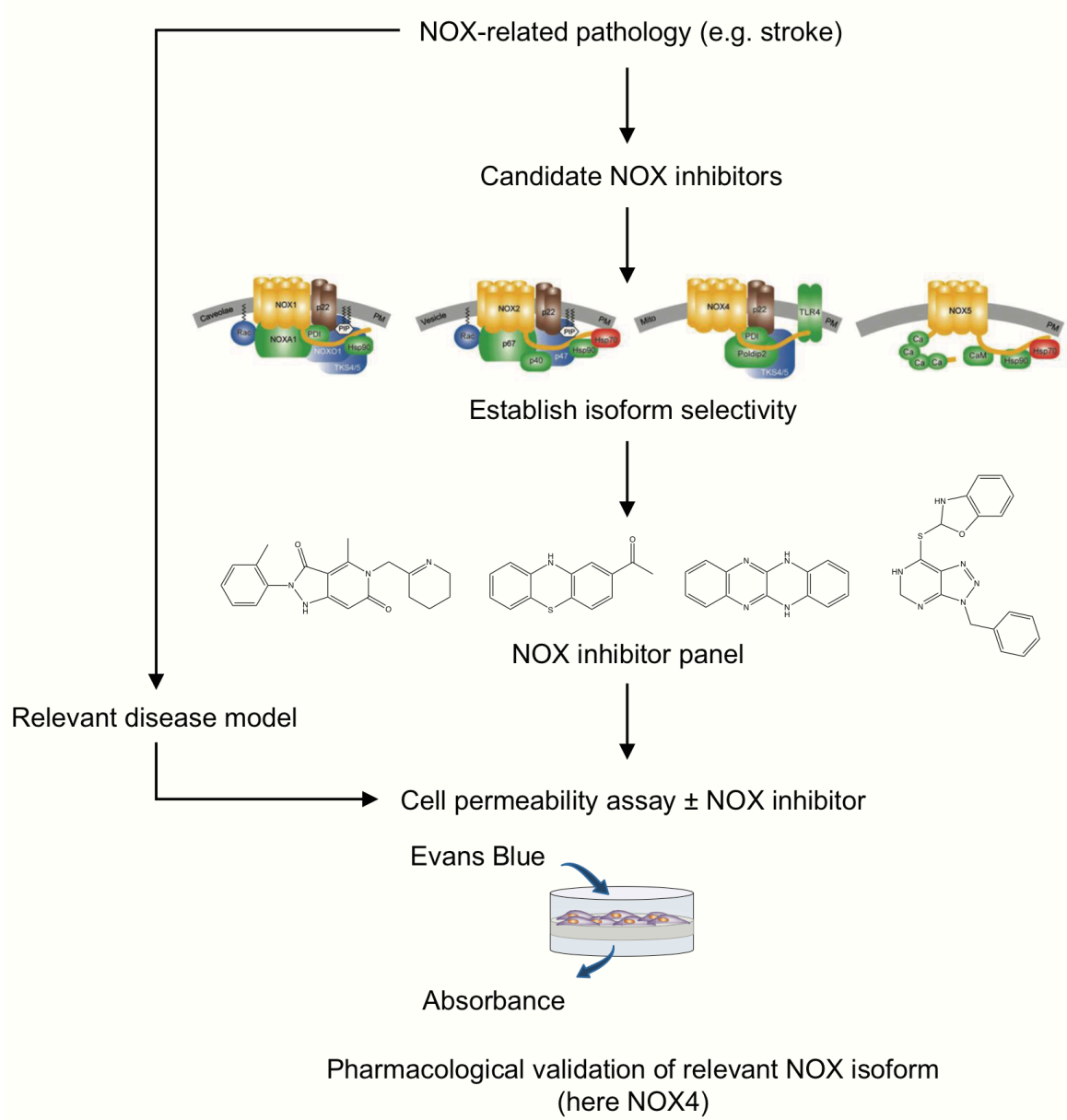

1. Introduction

Reactive oxygen species (ROS) signaling may become dysfunctional through (i) ROS formation in unphysiological high amounts, and/or (ii) at (sub)cellular locations, where normally no or only very low amounts of ROS are formed, and/or (iii) switch in the predominant ROS type, e.g. superoxide instead of hydrogen peroxide. Any of these mechanisms may lead to disease. The initial approach to translate of this hypothesis into therapeutic application by the use of antioxidants that scavenge ROS has consistently failed [1], in some cases even increasing mortality [[2], [3], [4]]. This paradox was initially explained by these compounds may have been underdosed [5], thereby not reaching efficacy. It is now understood, however, that ROS are not only harmful metabolic by-products, but also serve important protective, metabolic and signaling functions, such as the regulation of cell proliferation, differentiation, migration and survival, innate immune response, vascular tone, neuronal signaling as well as inflammation [[6], [7], [8], [9]]. Antioxidants obviously interfere with both qualities of ROS, the physiological and pathophysiological ones with overall neutral or even deleterious outcomes. Thus, ROS should not be modulated in a systemic, non-selective manner, but rather by identifying for each disease condition the relevant enzymatic source of ROS and inhibit this by selective pharmacological compounds without touching parallel physiological ROS-dependent processes [10].

ROS can be produced by several sources, dedicated ones and optional ones. These include mitochondrial ROS formation, xanthine oxidase, uncoupled nitric oxide synthase (uc-NOS) and NADPH oxidases (NOX) [11,12]. Of these, only NOX enzymes produce ROS as their sole and primary function; all others, only as a byproduct or upon damage. With respect to the different NOX isoforms, disease relevance has been suggested for NOX1 in diabetic atherosclerosis [13] and retinopathy [14]; NOX2, in neurodegeneration [15]; NOX4, in stroke [16], diabetic nephropathy [17] and neuropathic pain [18]; and NOX5, stroke [19], diabetic nephropathy [20,21], hypertension [22] and coronary artery disease [23]. Target validation in these cases, however, has been done primarily by gene knock-out (as reviewed in Ref. [24]) due to the lack of selective NOX inhibitors and, in the case of NOX5 [20], by knock-in technology. This approach has limiting target validation to mice and, in the case of NOX4, also to rat [16].

Source-specific pharmacological inhibition is important though. Similar to antioxidants, non-selective inhibition of NOX isoforms, i.e. inhibiting two or more NOX isoforms might be as ineffective or deleterious as antioxidants. For example, in diabetes-accelerated atherosclerosis, inhibition of NOX1 is protective [25], inhibition of NOX4 is detrimental [26,27] and inhibition of NOX2 is associated with increased mortality [25]. Therefore, for target validation in other species than mice and rats and clinical translation, isoform-selective NOX inhibitors are desirable. It is unclear, however, whether this is or will be achievable given the fact that all five NOX isoforms (NOX1, NOX2, NOX3, NOX4 and NOX5) are similarly structured transmembrane proteins containing highly conserved catalytic heme, FAD and NADPH binding sites. Some degree of variability derives from more (NOX1 and NOX2) or less (NOX4 and NOX5) binding partners or a unique regulation by calcium (NOX5) [28]. Furthermore, for each compound two potential sources of assay error or artifact need to be considered: (i) direct scavenging of ROS [29,30] instead of or in addition to NOX inhibition; and (ii) interference with the ROS detection probes [31,32]. We therefore here examine some of the best characterized and widely used NOX inhibitors, VAS2870, ML171, GKT136901, M13 and ML090 in a 'whole-cell' assay approach by analyzing isoform selectivity, possible assay interference and direct ROS-scavenging capacity.

2. Material and methods

2.1. Chemicals and reagents

Dulbecco's Modified Eagle Medium (DMEM) with GlutaMax, Roswell Park Memorial Institute (RPMI)-1640 medium with l-glutamine, Hanks' Buffered Salt Solution (HBSS) [Ingredients (mg/L); calcium chloride anhydrous (140), magnesium chloride hexahydrate (100), magnesium sulphate heptahydrate (100), potassium chloride (400), potassium phosphate monobasic (60), sodium bicarbonate (350), sodium chloride (8000), sodium phosphate dibasic anhydrous (48) and d-glucose (1000)] and phosphate buffered saline (PBS), pH 7.4 [Ingredients (mg/L); potassium phosphate monobasic (144), sodium chloride (9000), and sodium phosphate dibasic (795)] were purchased from GIBCO/Life Technologies. Krebs-Ringer Phosphate Glucose (KRPG) buffer, PH 7.35 [Ingredients (mg/L); sodium chloride (847.38), sodium dihydrogen phosphate

dihydrate (88.9), potassium chloride (36.23), calcium chloride dihydrate (7.939), magnesium sulphate heptahydrate (30) and d-glucose (109)] was prepared in house. Fetal bovine serum (FBS), fetal calf serum (FCS), 2-acetylphenothiazine (ML171), 5,12-dihydroquinoxalino(2,3-B)quinoxaline (ML090), phorbol 12-myristate 13-acetate (PMA), calcein, diphenyleneiodonium chloride (DPI), dextran sulphate, dimethyl sulfoxide (DMSO), Luminol, sodium salt, superoxide dismutase (SOD), Geneticin antibiotic (G418), ionomycin calcium salt ready to made solution and penicillin/streptomycin solution were purchased from Sigma–Aldrich. 3-benzyl-7-(2-benzoxazolyl) thio-1,2,3-triazolo [4,5-di] pyrimidine (VAS2870) was provided by Vasopharm; the pyrazolopyridine derivative GKT 136901, by GenKyoTex; M13, by Glucox Biotech. Amplex Red and horseradish peroxidase (HRP) were purchased from Invitrogen, CA, USA. The FuGENE® 6 transfection reagent was purchased from Promega. Endothelial growth medium (EGM-2 MV) [Ingredients (ml/500 ml medium); 500 ml of Endothelial Basal Medium-2 (EBMTM-2 Medium) and the following growth supplements: human Epidermal Growth Factor (hEGF), 0.5; Vascular Endothelial Growth Factor (VEGF), 0.5; R3-Insulin-like Growth Factor-1 (R3-IGF-1), 0.5 ml; Ascorbic Acid, 0.5; Hydrocortisone, 0.2; human Fibroblast Growth Factor-Beta (hFGF-β), 2.0; FBS, 25.0; Gentamicin/Amphotericin-B (GA), 0.5] was purchased from Lonza Bioscience.

2.2. Cell culture and transfections

Human embryonic kidney 293 (HEK293) cells cultured in DMEM medium containing 5% FBS were transfected with three plasmids [human NADPH oxidase organizer 1 (NOXO1), NADPH oxidase activator 1 (NOXA1) and NADPH oxidase 1 (NOX1)] to express active NOX1. However, to express active NOX4 or NOX5 in HEK293, it is sufficient to transfect the cells with only one plasmid, i.e. NOX4 or NOX5, respectively. All plasmids were confirmed by sequencing. Briefly, HEK293 cells were transfected with pcDNA control plasmid (vector control), NOX4 or NOX5 or triple transfected with NOX1, NOXO1 and NOXA1 using FuGENE6 transfection reagent (Promega) followed by ROS measurement after 48h. In all experiments, the NOX inhibitors were tested in the same preparation of transfected cells to ensure comparibility. To measure NOX2 activity, as described previously [32], superoxide was measured in human promyelocytic

leukemia (HL-60) cells (ATCC-No. CCL 240) that were cultured in RPMI-1640 medium with 5% FCS, penicillin (100 U•mL–1), streptomycin (100 µg•mL–1) and glutamine (2 mM). Cell suspensions (26 × 106 cells•mL–1) were incubated with 1.25% DMSO per 75 cm2 tissue culture flask (TCF-75) for 7 days to induce differentiation into granulocyte-like cells that were then centrifuged at 300xG, washed with HBSS and re-suspended in HBSS to the final seeding density needed for the experiment (5 × 105 cells/well in 96 well plate).

2.3. RNA extraction and cDNA synthesis

Briefly, HEK293 cells were trypsinized and collected in centrifuge tubes. Both HEK293 and HL-60 cells were then centrifuged for 5 min at 300xg and supernatants removed. Pelleted cells were lyzed by adding lysis buffer (provided with the kit) and then homogenized by passing the lysate 5 times through a blunt 20-gauge needle (0.9 mm diameter) fitted to an RNase-free syringe. RNA was extracted using RNeasy® Micro Kit (Qiagen) according to the manufacturer's kit manual.

cDNA was synthesized from 1 µg total RNA in 20 µl reactions using High Capacity cDNA Reverse Transcription Kit (Thermo Fisher Scientific). Briefly, reverse transcription master mix containing, reverse transcription buffer, deoxyribonucleotide triphosphate (dNTP) mix, reverse transcription random primers, MultiscribeTM reverse transcriptase, RNase inhibitor and nuclease-free water, was prepared. Then, 10 µl of the master mix and 10 µl RNA were pipetted in each well of 96-well plate. The plate was then sealed and centrifuged to spin down the contents and to eliminate any air bubbles. Afterwards, the plate was loaded into the thermal cycler. The PCR conditions were as follows: 10 min at 25 °C, followed by 120 min at 37 °C, followed by 5 min at 85 °C. After synthesis, the cDNA was stored at –20 °C.

2.4. Quantitative Real-Time PCR

RT-qPCR was performed on CFX96TM Real-Time PCR Detection System (Bio-Rad). All reactions were performed in triplicates in a total volume of 20 µl each using TaqMan® Universal PCR Master Mix (Applied Biosystems- Life Technologies) according to manufacturer's instructions. 3 µl cDNA was used as template and pre-designed TaqMan® primers of β-actin, Nox1, Nox2, Nox4 and Nox5 were used. The specific assay

ID for the primers used are shown in Supplementary Table S1. The standard PCR conditions were as follows: 10 min at 95 °C, followed by 15 s at 95 °C and 1 min at 60 °C, 59 repeats. The amount of mRNA was normalized to the measured expression of β-actin mRNA.

2.5. ROS measurement in intact cells

2.5.1. Luminol assay

To measure NOX1 activity, superoxide from vector-transfected or NOX1-transfected HEK293 cells was measured by luminol-enhanced chemiluminescence in white plates as follows. HEK293 cells were cultured in DMEM medium containing 5% FBS and then transfected with NOX1, NOXO1 and NOXA1 plasmids using FuGENE®6 transfection reagent. After 48 h, cells were detached by adding trypsin and then re-suspended in KRPG buffer. Each 50 µl of cell suspension consisted of 100,000 cells was added to each well (in triplicate) in a 96-well plate and incubated at 37 °C for 60 min. After 1 h of incubation, 50 µl reaction buffer (containing 6.4 U/ml HRP and 0.4 mM luminol in KRPG buffer) was added to the 50 µl cell suspension so that the total volume of assay was 100 µl. Cells were then stimulated by addition of 0.5 µM phorbol 12-myristate 13-acetate (PMA; PKC activator). Superoxide generation was detected by monitoring relative light units (RLU) with a Wallac luminometer Victor2 at 37 °C for 60 min. Superoxide dismutase (SOD) was added as control before PMA stimulation in selected wells.

2.5.2. Amplex Red assay

To measure the activity of NOX4 and NOX5, H_2O_2 production was measured in HEK293 cells by measuring Amplex Red fluorescence using Amplex™ Red Hydrogen Peroxide/Peroxidase Assay Kit (ThermoFiher Scientific). For the measurement, vector-transfected HEK293 cells or HEK293 cells transfected with NOX4 or NOX5 were trypsinized, counted, washed and re-suspended in KRPG buffer. NOX inhibitors dissolved in DMSO or solvent control (0.5% DMSO) were added to respective wells of a black 96-well plate and 50 µl of a reaction mixture containing 0.1 U·mL–1 HRP and 50 µM Amplex Red reagent was added to each well according to the kit manual and incubated at 37 °C for 10 min. Thereafter, 100,000 of respective HEK293 cells or solvent

control in 50 µl of KPRG buffer were added to each well. Amplex Red fluorescence was measured immediately at excitation (530–560 nm) and emission (~590 nm) at 37 °C for 60 min. HEK293 cells expressing NOX5 were activated by the Ca2+ ionophore ionomycin (40 µM).

2.5.3. Cytochrome C assay

To measure NOX2 activity, superoxide production in HL-60 cells was measured by cytochrome C reduction as described previously [32]. Briefly, HL-60 cells were cultured in RPMI-1640 medium with 5% FCS, penicillin (100 U•mL–1), streptomycin (100 µg•mL–1) and glutamine (2 mM). Cell suspensions (26 × 106 cells•mL–1) were incubated with 1.25% DMSO per TCF-75 for 7 days to induce differentiation into granulocyte-like cells that were then centrifuged at 300xG, washed with HBSS and re-suspended in HBSS to the final seeding density needed for the experiment (5 × 105 cells/well in 96 well plate). Cytochrome C (100 µM) and the inhibitors were added to the DMSO-differentiated HL-60 cell suspension then a basal reading was performed at 540 nm (isosbestic point of cytochrome C) and 550 nm (SpectraMax 340; Molecular Devices, Sunnyvale, CA, USA). Subsequently, the oxidative burst was initiated by the addition of 100 nM PMA. After incubation for 60 min at 37 °C the absorbance was measured. Signals were normalized to the basal readings. In addition, SOD was added as control before PMA stimulation in selected wells.

2.6. Superoxide measurement in cell-free assays

Xanthine (X; final concentration: 50 µm) and cytochrome C (final concentration: 100 µm) were dissolved in HBSS, and 100 µL aliquots of this solution were transferred to individual wells of a 96-well plate. After addition of the oxidase inhibitors, the mixtures were allowed to equilibrate for 20 min. The reaction was started by the addition of 100 µL xanthine oxidase (XO) (final concentration: 5 mU·mL–1), and absorbance at 540 and 550 nm was recorded 10 min after the start of the reaction. Superoxide production was calculated by normalization to the signals obtained at 540 nm. Similar experiments were performed with 0.4 mM luminol instead of cytochrome C. After 20 min equilibration, the reaction was started with XO (1 mU·mL–1), and chemiluminescence was subsequently recorded for 20 min in a Fluoroscan FL microplate reader. Signals were

calculated as area under curve (AUC) and normalized to the X/XO-derived control signal. Accordingly, a counter screen has been performed with cytochrome C or luminol without X/XO-generated superoxide.

2.7. H_2O_2 measurement in cell-free system

The fluorescence of Amplex Red was measured in the presence and absence of H_2O_2 (0.25 µM), reflecting NOX4 and NOX5 output. After addition of inhibitors and 50 µl Amplex Red reaction mixture containing 100 U·mL–1 HRP and 10 mM Amplex Red to each well, the plate was incubated at 37 °C for 10 min. Thereafter, the plate was read at excitation (530–560 nm) and emission (~590 nm) at 37 °C and for 60 min. Data was calculated as the AUC over 60 min and data were normalized to H_2O_2 output in the absence of inhibitor.

2.8. Cell permeability in HBMECs

For the passive dye diffusion assay, 2 × 104 human brain microvascular endothelial cells (HBMECs) were grown to confluence on membranes of transwell inserts (collagen-coated transwell pore polyester membrane insert; pore size = 3.0 µm (Corning, The Netherlands) Fig. 5A). After 6hrs of ischemia, cells were treated with 0.1 µM ML171, 0.6 µM VAS2870, 1 µM GKT136901, 0.2 µM M13 or 0.01 µM ML090 during 24hrs of re-oxygenation. Thereafter, cell permeability was assessed using Evans Blue (Sigma-Aldrich) (Fig. 5B). First, the medium was removed and previously warmed (37 °C) PBS (1.5 ml) was added to the abluminal side of the insert. Permeability buffer (0.5 ml) containing 4% bovine serum albumin (Sigma-Aldrich) and 0.67 mg/ml Evans blue dye in PBS was loaded on the luminal side of the insert followed by 15 min incubation at 37 °C. The concentration of Evans Blue in the abluminal chamber was measured by determining the absorbance of 200 µl buffer at 630 nm using a microplate reader.

2.9. Statistical analysis

Data analysis was performed using Prism 6.0g software package (GraphPad Software, San Diego, USA). IC50 values were calculated with a non-linear regression analysis using an algorithm for sigmoidal dose–response with variable slopes. Results are expressed as means ± SEM. Statistical differences between means were analyzed by one-way ANOVA

followed by Bonferroni correction for multiple comparisons. A value of $P < 0.05$ was considered statistically significant.

3. Results

3.1. Gene expression of NOX isoforms

To check the expression of the different NOX isoforms, we analyzed NOX1, 2, 4 and 5 mRNA expression in control vector-transfected HEK293 cells, HEK293 cells transfected with NOX1, 2, 4 and 5 and HL-60 cells. NOX isoforms mRNA expression was measured by RT-qPCR and mRNA levels were normalized to the expression of β-actin.

As reported previously [28,33], NOX1 was expressed in NOX1-transfected HEK293 cells (Fig. 1A), NOX2 in HL-60 (Fig. 1B), NOX4 in NOX4-transfected HEK293 (Fig. 1C) and NOX5 in NOX5-transfected HEK293 (Fig. 1D) and were below detection limit (defined as 100 times lower than in the respective NOX overexpressing cells) in all other cell preparations. Notably, the expression of NOX isoforms did not change after treatment with the respective assay conditions i.e. luminol for NOX1, cytochrome C for NOX2 and Amplex Red for NOX4 and NOX5 (Fig. 1A–1D).

3.2. NOX pharmacological isoform selectivity

To characterize the NOX isoform selectivity of the current second-generation NOX inhibitors we determined concentration-dependency and efficacy of GKT136901, ML171, VAS2870, M13 and ML090 on NOX1, 2, 4, and 5 (Fig. 2A). Our preference was for cell (lines) expressing a specific NOX isoform in a highly selective manner and ideally physiologically. The latter is only known for NOX2 and HL-60 cells [34,35]. For NOX1, NOX4 and NOX5, there is, to our knowledge, no such native human cell line. Therefore, for these three isoforms we used transiently transfected HEK-293 cells, using previously validated methodology [29]. One major limitation of this approach is that validation of the compounds on two different preparations i.e. transfected vs. constitutive expressing cells can affect the dose-response correlations and make it hard to extrapolate data to the real physiological scenarios.

NOX2 expressing HL-60 cells or HEK293 cells transfected with NOX1, NOX4 or NOX5 were incubated in presence of increasing concentrations of each compound. ROS

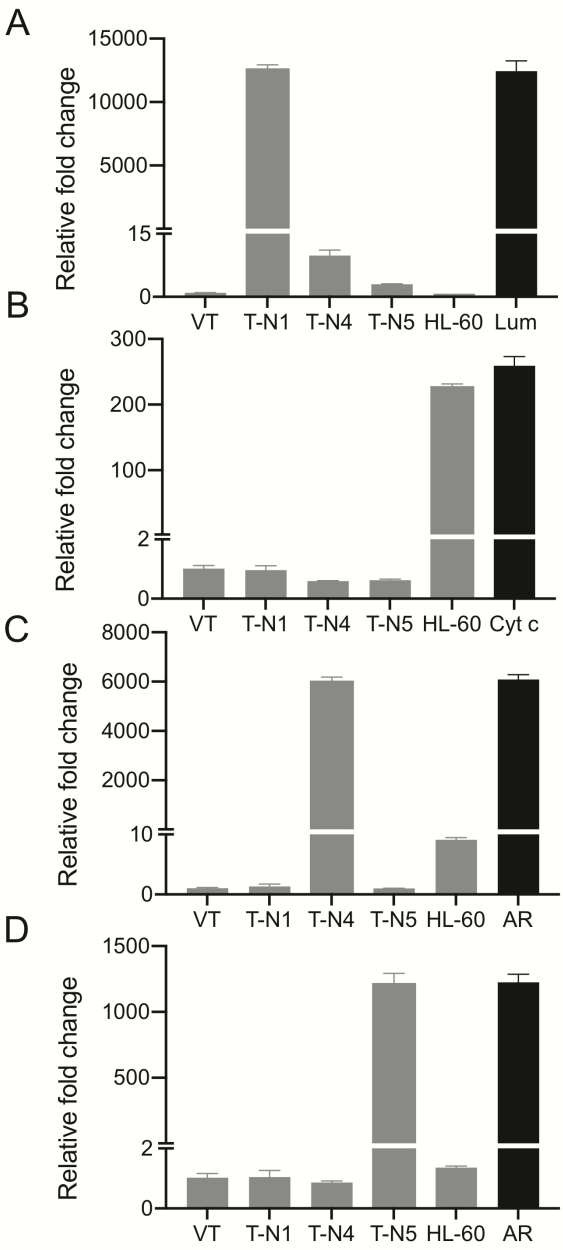

Fig. 1. **RT-qPCR of NOX isoforms mRNA expression in HEK293 and HL-60 cells**. NOX isoforms mRNA levels were measured and normalized to the expression of β-actin. Vector-transfected HEK293 cells (VT) were used as control. To check whether assay reagents interfere with NOXs gene expression, HEK293 cells transfected with NOX1 (T-N1) were treated with luminol (Lum), HL-60 cells were treated with cytochrome C (Cyt *c*) and HEK293 cells transfected with NOX4 (T-N4) or NOX5 (T-N5) were treated with Amplex Red (AR). A) mRNA levels of NOX1. B) mRNA levels of NOX2. C) mRNA levels of NOX4. D) mRNA levels of NOX5. Data are presented as the mean ± SEM of three experiments.

generation was subsequently induced by PMA to stimulate NOX1, NOX2 and NOX5, which was assayed in the presence of ionomycin. Thereafter, ROS production was assayed using a panel of cellular assays with structurally unrelated probes; i.e. Amplex Red, luminol or cytochrome C (Fig. 2B). Amplex Red was used to quantify extracellular H_2O_2 [36], while luminol-based chemiluminescence and cytochrome C-reduction were used to quantify superoxide generation. These probes were chosen based on previous data. Luminol assay has been validated to measure low superoxide-producing NOX1 activity [37,38], while cytochrome C is used for high superoxide-output NOX2 activity [34,39] and Amplex Red for testing hydrogen peroxide formation from NOX4 [[40], [41], [42]] and NOX5 [43,44] activities. As controls, medium, vector-transfected HEK293 cells and non-stimulated HL-60 cells were used (Fig. S1), in addition, PMA or PMA plus ionomycin did not stimulate cell controls i.e. vector-transfected HEK293 cells and non-stimulated HL-60 cells (Fig. S2).

NOX isoform concentration-response curves for GKT136901, ML171, VAS2870, M13 and ML090 were constructed (Fig. 3; see Table 1 for IC50 values). GKT136901 (Fig. 3A) showed selectivity for NOX1 over NOX4 and NOX5 inhibition while NOX2 inhibition was not observed. The same holds true for ML171 (Fig. 3B) which is more selective for NOX1 compared to NOX4 and NOX5. VAS2870 (Fig. 3C) displayed NOX2 over NOX1 and NOX4 selective inhibition and also slightly inhibited NOX5. The GlucoxBiotech compound M13 (Fig. 3D) showed almost selective NOX4 inhibition but NOX2 (with low Emax) and NOX1 (at high concentrations) inhibition was observed as well. Finally, ML090 (Fig. 3E) inhibited NOX5, NOX1 and NOX4 with comparable IC50 values but enhanced Emax for NOX5 inhibition. These data suggest that NOX inhibitors indeed display differential isoform targeting, albeit the single compound selectivity is yet not sufficient. Therefore, combined analysis of a NOX inhibitor panel with sufficient differential potencies and selectivities is suggested.

3.3. Non-specific antioxidant and assay artefacts

To screen for possible assay interference between GKT136901, ML171, VAS2870, M13 or ML090 and the NOX1 assay, a cell-free system was performed in which each inhibitor was screened in presence of luminol, 1mU/ml xanthine oxidase (XO) and 1 mg xanthine (X) generating superoxide. At concentration 1 μM, GKT136901 did not show interference

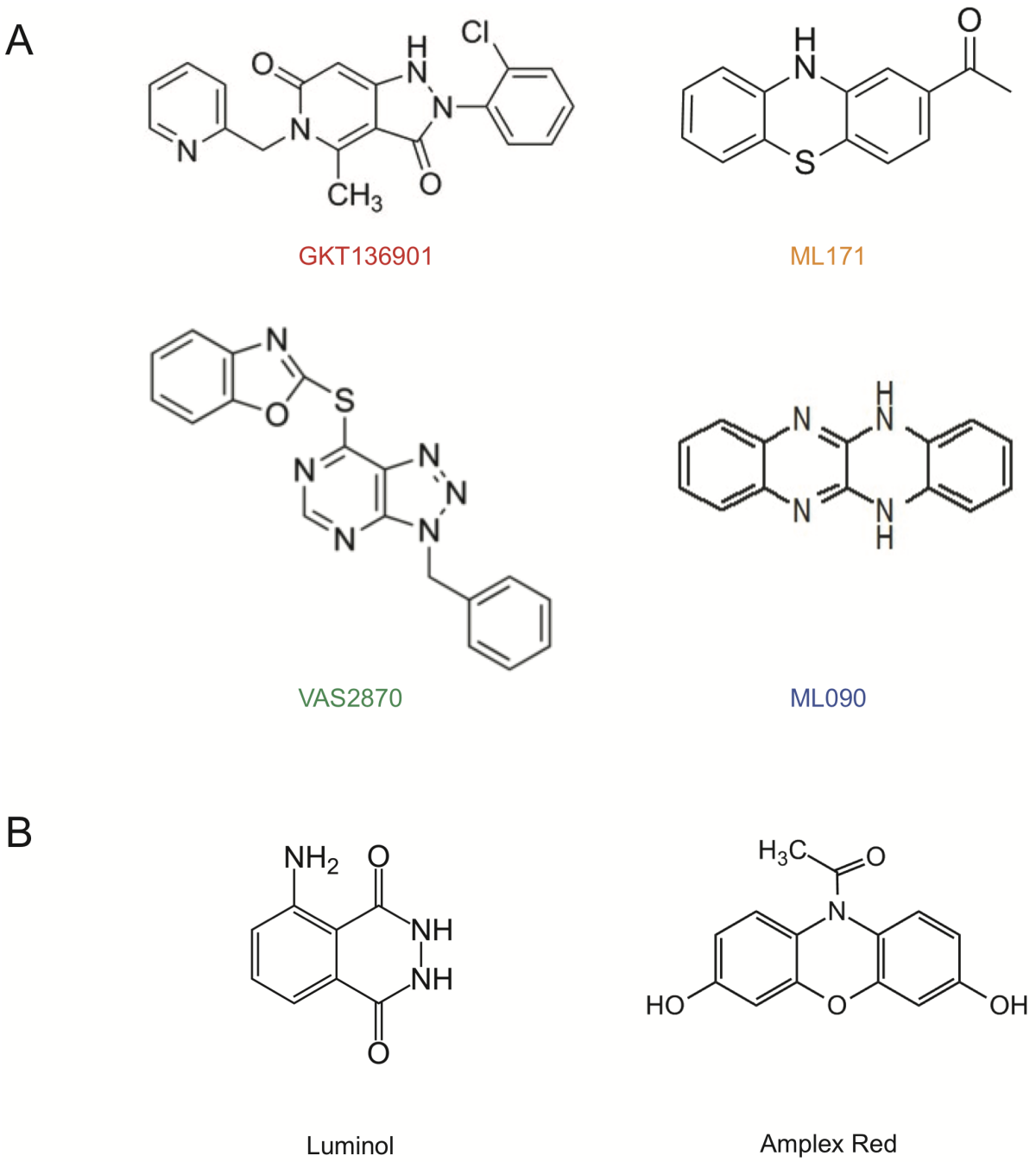

Fig. 2. **Chemical structures.** Chemical structure of (A) NOX inhibitors (red, orange, green and blue text) and (B) ROS detection probes (black text) used in the study. (For interpretation of the references to color in this figure legend, the reader is referred to the Web version of this article).

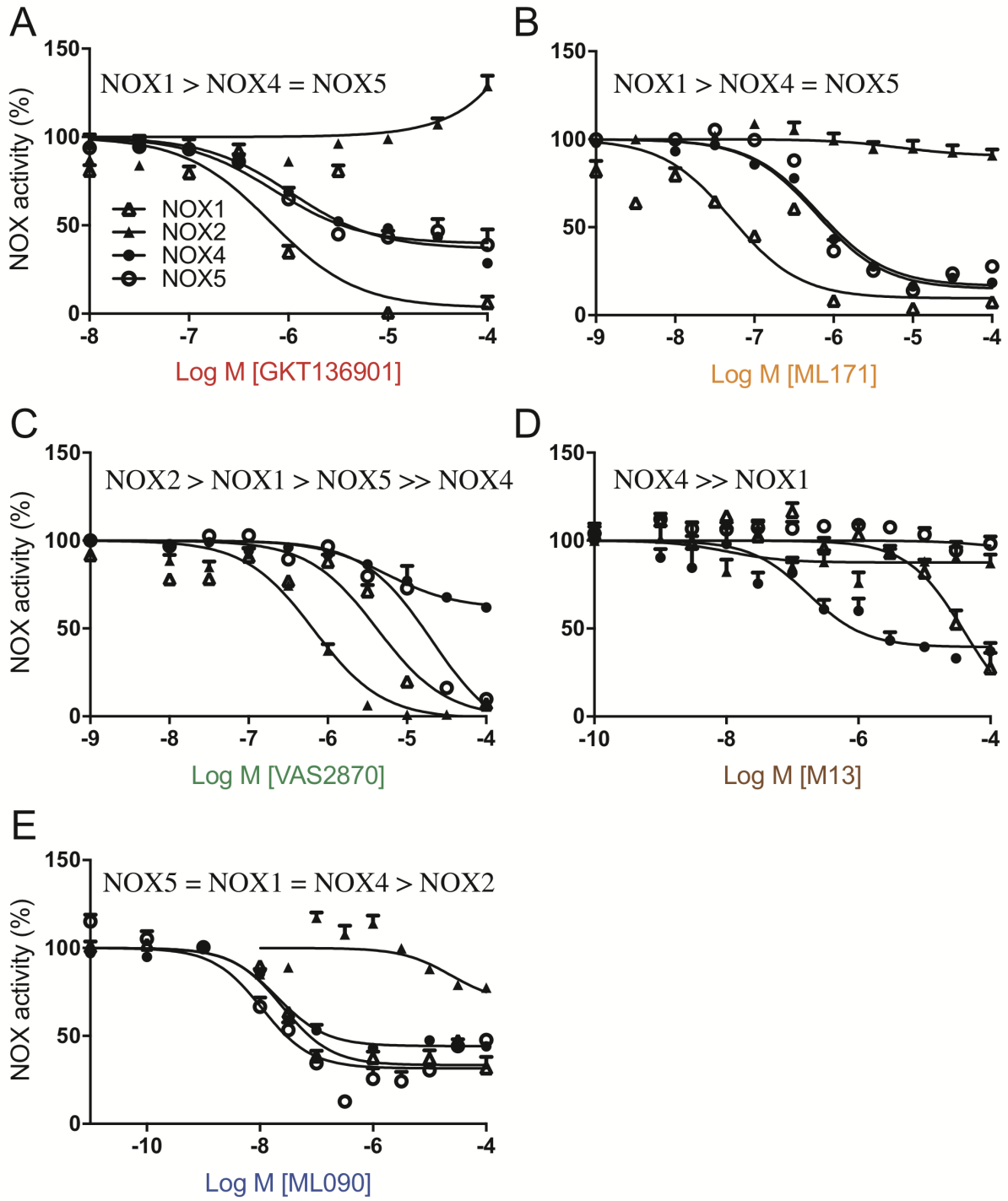

Fig. 3. **NOX inhibitors display isoform selectivity.** ROS production was assessed in whole cells using assays measuring superoxide production by NOX1 (luminol assay) or NOX2 (cytochrome C assay) and H_2O_2 production by NOX4 or NOX5 (Amplex Red assay). As illustrated in the figure (A–E), GKT136901 (A), ML171 (B), VAS2870 (C), M13 (D) or ML090 (E) inhibited ROS production with NOX isoform selective IC_{50}. Data are presented as the mean ± SEM of n = 3 independent experiments. 100% is the PMA-induced activation (PMA + ionomycin in case of NOX5) without inhibitors.

Table 1: Potency and efficacy of the five tested NOX inhibitors on different NOS isoforms.

NOX inhibitor		NOX1	NOX2	NOX4	NOX5
GKT136901	IC_{50}	-6.2	> -3	-6.0	-6.1
	E_{max}	**99**	N/A	**71**	61
ML171	IC_{50}	**-7.3**	N/A	-6.2	-6.2
	E_{max}	**96**	09	82	75
VAS2870	IC_{50}	-5.4	**-6.2**	N/A	-4.7
	E_{max}	93	**99**	38	90
M13	IC_{50}	-4.4	N/A	**-6.8**	N/A
	E_{max}	73	12.7	**67**	05
ML090	IC_{50}	-7.6	N/A	-7.7	**-8.0**
	E_{max}	68	23	57	**81**

Footnote: IC_{50}, concentration (log M) for half-maximal inhibition; E_{max}, maximal inhibition as % of control by each inhibitor per isoform. IC_{50} is written as not-applicable (N/A) when E_{max} is less than 50%. Predominant isoform in bold.

with either the molecular probe or with the X/XO system (Fig. 4A). Similar findings were obtained with 0.1 µM ML171, 10 µM VAS2870 and 30 nM ML090 (Fig. 4A). In contrast, 1 µM M13 enhanced chemiluminescence (Fig. 4A). To identify direct interactions between assay components and GKT136901, ML171, VAS2870, M13 or ML090 a cell-free counter screen was performed without X/XO-generated ROS. Indeed, ML171 and VAS2870 showed reduction of the luminol-based signal suggesting direct interference with luminol-based chemiluminescence (Fig. 4B). In contrast, in presence of ML090 the signal was enhanced (Fig. 4B).

To study non-specific antioxidant effects of VAS2870, the effect of 10 µM VAS2870 was studied in a cell-free system in presence of cytochrome C, and X/XO-derived ROS. In these assays, VAS2870 showed significant antioxidant effects (Fig. 4C).

To study whether the effects of GKT136901, ML171, VAS2870, M13 and ML090 on NOX4 and NOX5 are specific, a cell-free assay was performed with NOX4 or NOX5 effective concentrations of each inhibitor in presence of 0.25 µM H2O2 in an Amplex

Red assay. ML171, VAS2870, M13 and ML090 did not directly affect Amplex Red-based detection of H_2O_2 (Fig. 4D). However, GKT136901 reduced Amplex Red-based H_2O_2 signals suggesting assay interference. Hence, the assay was repeated without H_2O_2 to study potential direct assay component interference. Indeed, GKT136901, ML171, M13 and ML090 reduced the signal as compared to the control (Fig. 4E) whereas in the presence of VAS2870 the signal was enhanced (Fig. 4E).

Our data suggest that none of the current NOX inhibitors could be viewed as sufficiently isoform selective, but that a panel of NOX inhibitors may be feasible for pharmacological validation of a specific NOX isoforms in a (patho)physiological process. Because of the plethora of assay artefacts and direct ROS scavenging by GKT136901, this compound was thus excluded from the panel.

3.4. Target validation of NOX in ischemia-induced hyperpermeability model

We thus tested our NOX inhibitor panel in an in vitro human model of ischemia-induced hyperpermeability (Fig. 5A) where NOX4 is involved in subacute hypoxia-induced increases in cell permeability [16,45], whereas NOX1, NOX2 do not [45] and NOX5 only acutely [19]. Primary HBMEC cultures were subjected to 6h of hypoxia followed by 24h of re-oxygenation (Fig. 5B) in presence or absence of NOX inhibitors using the IC50 concentrations to target one NOX isoform in a relatively specific manner over the other isoforms, i.e. ML171 at 0.1 μM mainly targeting NOX1; VAS203 (0.6 μM, NOX2); M13 (0.2 μM, NOX4); or ML090 (0.01 μM, NOX5). Hypoxia increased cell permeability after 24hrs of re-oxygenation. As predicted from the inhibitor screen, M13 or ML171 protected against this detrimental effect (Fig. 5C), suggesting protection against hyperpermeability via NOX4 inhibition while, as expected given their respective IC50 values, VAS2870 or ML090 treatment showed no effect (Fig. 5C). These data provide a proof-of-concept for pharmacological target validation using NOX inhibitor panels.

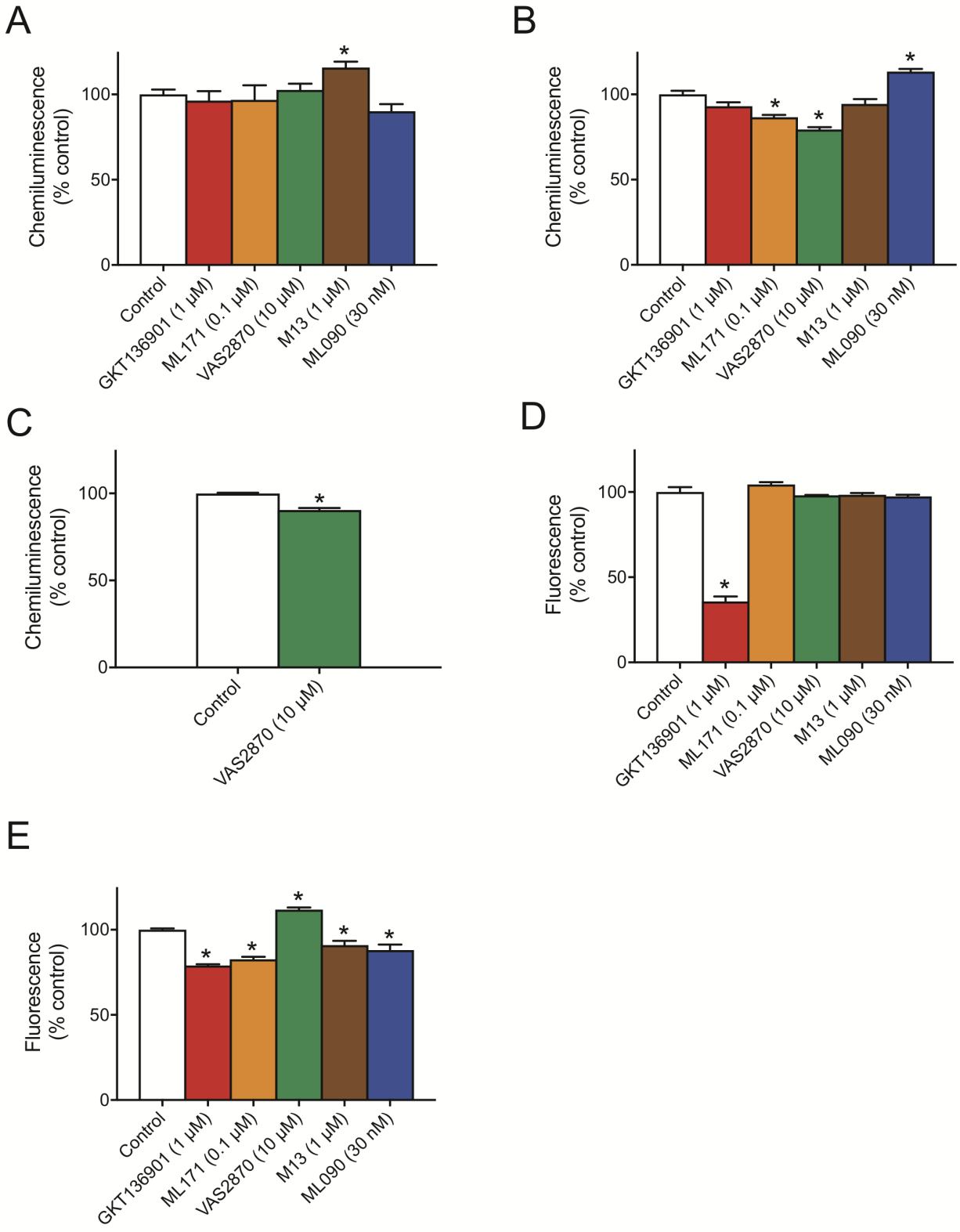

Fig. 4. **NOX inhibitors display interference with ROS assays.** A/B) To study possible interference of GKT136901, ML171, VAS2870, M13 or ML090 with luminol-based measurements cell-free luminol assays were used. In these assays, ROS production generated by X/XO was enhanced by M13 (A) but not by GKT136901, ML171, VAS2870 or ML090. Moreover, chemiluminescence produced by luminol only was inhibited by ML171 and VAS2870, enhanced by ML090 and not affected by GKT136901 or M13,

respectively (B). C) Possible assay interference by NOX2-specific VAS2870 was assessed by studying cytochrome C reduction in presence of X/XO-derived ROS in a cell-free system. Presence of VAS2870 slightly, but significantly reduced chemiluminescence. D/E) The possibility of interference between GKT136901, ML171, VAS2870, M13 or ML090 and Amplex Red-based assays was studied using cell-free Amplex Red assays. In these assays, Fluorescence generated by H_2O_2 was significantly inhibited by GKT136901 (D) but not by ML171, VAS2870, M13 or ML090 (D). Moreover, fluorescence produced by Amplex Red only was inhibited by GKT136901, ML171, M13 and ML090 while it was enhanced by VAS2870 (E). Data are presented as the mean ± SEM of three experiments. *P < 0.05.

4. Discussion

Here we present the isoform-selectivity of five widely used NOX inhibitors. Our results show that NOX-specific and isoform-selective pharmacological NOX inhibition is in principle achievable. Individual compound specificity, however, is as yet insufficient. None of the selected small molecule inhibitors were sufficiently 'isoform selective' to be used on their own. All compounds inhibited several NOX isoforms, yet with different potencies (IC50 values). In addition, (i) their mechanism of action and binding site is unclear, and (ii) assay interferences in addition to those that had been previously noted [46-48] needed to be taken into consideration. Nevertheless, when examining a human cell-based in-vitro model where NOX4 is a genetically validated causal ROS source, combining four NOX inhibitors into a panel NOX4 could be pharmacologically re-validated. Our data just provide also a proof-of-principle that similar approaches are now in principle possible for pharmacological target validation where gene KO is not an option.

With respect to the individual NOX inhibitor compounds in this study, VAS2870 has beneficial effects in several preclinical disease models such as stroke [45], Alzheimer's disease [49], thrombosis [50] and pulmonary hypertension [51]. This compound has been designated as a pan-NOX inhibitor [52] as inhibition of NOX1 [28,53], NOX2 [28,53,54], NOX4 [28,45] and NOX5 [28] has been observed. IC50 values for VAS2870 have been previously published for NOX2 [54,55] and recently for all the other NOX isoforms [48]. Based on the IC50 values reported in the present study, VAS2870 shows a slight preference for NOX2 (IC50 ~ 0.7 μM), over NOX1 and NOX4, which are inhibited in the lower micromolar range, and NOX5, in the higher micromolar range, in line with a recent study using two ROS assays, Amplex Red and

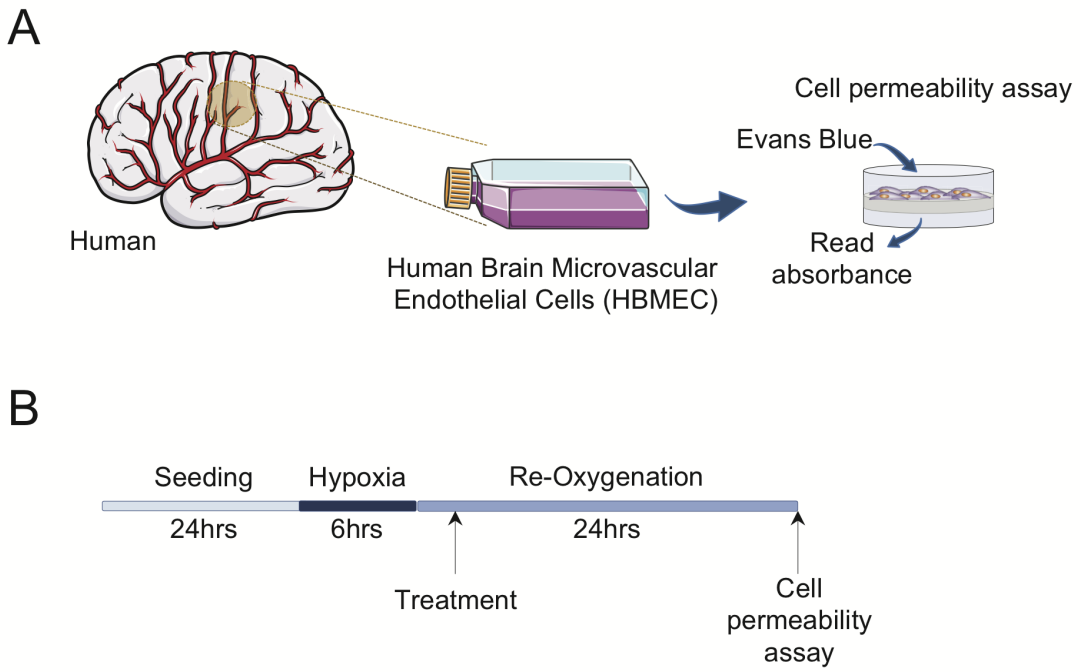

Fig. 5. **ML171 and M13 inhibit ischemia-induced hyperpermeability.** (A/B) HCMECs were subjected to 6hrs hypoxia followed by 24hrs re-oxygenation during which inhibitors were present. Cell permeability was subsequently assessed by measuring Evans Blue (EB) fluorescence. (C) Hypoxia caused hyperpermeability (open bar) which was significantly reduced in cells treated with ML171 (0.1 μM) or M13 (0.2 μM) while VAS2870 (0.6 μM) or ML090 (0.01 μM) treatment had no effect. Data are presented as the mean ± SEM of 4–6 experiments; *P < 0.05.

WST-1 [48]. With respect to non-specific effects, VAS2870 slightly interfered with luminol and Amplex Red and XO-generated ROS indicating antioxidant properties as has been reported previously [24]. The latter did, however, not preclude the interpretation of NOX inhibition because the interference with XO-generated ROS was 9.6% (see Fig. 4C), inhibition of the NOX2-dependent signal, 91.5% (see Fig. 3C).

M13, a previously unreported compound from Glucox Biotech, was identified here as a first-in-class relative NOX4 selective inhibitor, 200-times more potent in inhibiting NOX4 (IC50 ~ 0.01 μM) versus NOX1 (IC50 ~ 0.2 μM), negligible NOX2 inhibition and almost no effect on NOX5. Also, M13 interfered with the Amplex Red assay by 9% (see Fig. 4E), which again did not impair the interpretation of results, as this was less than the 40% reduction of the NOX4-dependent ROS signal (see Fig. 3D). Our findings thus support further lead optimization of this promising new pharmacophore as a potentially clinically important selective NOX4 inhibitor, e.g. in stroke [45,56].

ML090 was previously described as NOX1 selective [57]. In our hands, however, its IC50 values for NOX1, 4 and 5 were similar suggesting that this compound is rather pan NOX inhibitor. Again, two interferences were observed. ML090 lowered the Amplex Red signal 11.9% (see Fig. 4E); the NOX5 dependent ROS signal, however, was reduced by 46.8% (see Fig. 3E), suggesting a true inhibition. With respect to luminol, ML090 surprisingly increased the signal by 13.4% (see Fig. 4B); thus, the absolute 36.8% inhibition of the NOX1-dependent ROS signal (see Fig. 3D) appears to underestimate absolute efficacy for this isoform. Therapeutically, ML090 protects from vascular dysfunction in a rabbit model, an effect that has been attributed to NOX1 inhibition [58]. Based on the data presented here, however, an effect involving NOX4 and, in particular, NOX5 cannot be excluded as rabbits, unlike mice and rats, do express this isoform as well.

GKT136901, a chemical analogue and pharmacological sibling of the clinically most advanced NOX inhibitor, GKT831 (setanaxib), is widely referred to as a combined NOX1/NOX4-specific inhibitor. This compound presented, however, several problematic features and stood out amongst all compounds with respect to assay interference. GKT136901 interfered both with the Amplex Red assay for NOX4 and 5 and the luminol assay for NOX1. Moreover, it directly scavenged ROS. This latter antioxidant

effect has been observed also for H_2O_2 [47,48] and peroxynitrite [30]. These characteristics thus appear to limit the interpretability of results using GKT136901 as a NOX1/NOX4 inhibitor and structurally related compounds, which is why we decided not to include this compound into our NOX inhibitor panel.

Finally, the fifth compound tested, the phenothiazine derivative, ML171, had been published as being NOX1-specific [59] with beneficial effects in models of hypertension [60], diabetes [61] and cancer [62]. We also observed a potent NOX4 and NOX5 inhibition at slightly higher concentrations, suggesting only a relative but not absolute NOX1 selectivity. Again, also this compound presented assay interferences with both Amplex Red and luminol in line with a previous observation [63]. This is most likely due to the fact that phenothiazines are peroxidase substrates [64]. The latter did, however, not preclude the interpretation of NOX1 inhibition because the assay interference was 13.4% (see Fig. 4B), whereas the NOX1-dependent signal was inhibited by 55% (see Fig. 3B).

Thus, most ROS probes and the here examined NOX inhibitors are prone to artefacts (see also review in Ref. [65]). Results with NOX inhibitors on the quantification of NOX-derived ROS will need careful interpretation and require several reagent and assay controls. However, with the exception of GKT136901 this does not preclude the interpretability of functional experiments on the involvement of a given NOX isoform or not. For VAS2870, M13, ML090 and ML171 clear NOX-dependent effects were detectable in our cell-based assay.

With respect to the pharmacological validation of a specific NOX isoform, the lack of sufficient isoform selectivity of VAS2870, M13, ML090 and ML171 required to move to a NOX inhibitor panel. All compounds were used at cell based IC50 concentrations and tested in a genetically pre-validated model for NOX4 to investigate whether NOX4 could be re-validated pharmacologically. In this in-vitro blood brain barrier model, NOX4 causes a sub-acute increase in permeability. Indeed, we observed that subacute addition of M13 (NOX4) and ML171 (NOX1 > NOX4 = NOX5) were neuroprotective, in contrast to VAS2870 (NOX2 > NOX1 > NOX5) ML090 (NOX5 > NOX 1 = NOX4 > NOX2). These panel effects suggested that NOX4 is the responsible isoform in this subacute model in accordance with previous data that established the involvement of NOX4 in the same model using genetic approaches [16,45]. The

protective effect of ML171 here is attributed to inhibition of NOX4, which does, however, not exclude that inhibitory of effect of this compound in other models may be due to other isoforms such as NOX1. This, should, however, be tested using an inhibitor panel approach and not based on single compounds with limited selectivity. The inhibitor panel approach appears in principle to be feasible for pharmacological target validation of NOX in cell-based systems. Further validation in other in-vitro disease and models is needed.

In summary, all tested NOX inhibitor compounds displayed different apparent NOX isoform selectivity profiles suggesting differential chemical targeting of different NOX isoforms using small molecules is in principle possible. These and similar data [48] should stimulate focused library synthesis and structure-activity programs for further lead optimization to obtain eventually isoform selective small molecules for single compound target validation and potentially for clinical development. For now, we provide an immediately applicable inhibitor panel approach that allows target validation of NOXs under conditions where gene knock-out or knock-in are not feasible or, because of compensation mechanisms, not desirable.

Author contributions

H.H.H.W.S., V.T.D, S.A and M.H.E designed research; V.T.D., S.A, M.H.E, P.L, A.I.C, M.P.P, C.N and U.K performed research; V.T.D, S.A, A.I.C, M.H.E and H.H.H.W.S. analyzed and interpreted data; V.T.D and M.H.E contributed in writing and revised the final manuscript and figures; M.H.E, V.T.D. and H.H.H.W.S. wrote and edited figures and manuscript.

Declaration of competing interest

None to declare.

Acknowledgements

We wish to thank Dr. Per Wikström for providing M13, Dr. V. Jaquet for experimental advice and Dr. Merlijn J. Meens for reading the manuscript and helpful discussions. Technical assistance by P. Lijnen and J. Bost is gratefully acknowledged. Financial support (to HHHWS) by the ERC (AdG RadMed '294683' and PoC SAVEBRAIN '737586') and the Horizon 2020 programme (REPO-TRIAL '777111') is gratefully acknowledged.

Abbreviations

HBMEC: Human brain microvascular endothelial cells
HRP: Horseradish peroxidase
NOX: NADPH oxidase
PMA: Phorbol myristate acetate
ROS: Reactive oxygen species
XO: Xanthine oxidase

I. References

1. Y. Dotan, D. Lichtenberg, I. Pinchuk, No evidence supports vitamin E indiscriminate supplementation. *BioFactors (Oxford, England)* **35**, 469-473 (2009).

2. E. R. Miller *et al.*, Meta-analysis: high-dosage vitamin E supplementation may increase all-cause mortality. *Annals of internal medicine* **142**, 37-46 (2005).

3. G. Bjelakovic, D. Nikolova, L. L. Gluud, R. G. Simonetti, C. Gluud, Mortality in randomized trials of antioxidant supplements for primary and secondary prevention: systematic review and meta-analysis. *JAMA* **297**, 842-857 (2007).

4. H. O. P. E. S. Investigators *et al.*, Vitamin E supplementation and cardiovascular events in high-risk patients. *The New England journal of medicine* **342**, 154-160 (2000).

5. L. J. Roberts, 2nd *et al.*, The relationship between dose of vitamin E and suppression of oxidative stress in humans. *Free Radic Biol Med* **43**, 1388-1393 (2007).

6. K. Wingler *et al.*, NOX1, 2, 4, 5: counting out oxidative stress. *British journal of pharmacology* **164**, 866-883 (2011).

7. K. Bedard, K.-H. Krause, The NOX family of ROS-generating NADPH oxidases: physiology and pathophysiology. *Physiological reviews* **87**, 245-313 (2007).

8. P. D. Ray, B.-W. Huang, Y. Tsuji, Reactive oxygen species (ROS) homeostasis and redox regulation in cellular signaling. *Cellular signalling* **24**, 981-990 (2012).

9. T. Finkel, Signal transduction by reactive oxygen species. *The Journal of cell biology* **194**, 7-15 (2011).

10. V. T. Dao *et al.*, Pharmacology and Clinical Drug Candidates in Redox Medicine. *Antioxidants & redox signaling* **23**, 1113-1129 (2015).

11. M. H. Elbatreek, M. P. Pachado, A. Cuadrado, K. Jandeleit-Dahm, H. H. H. W. Schmidt, Reactive Oxygen Comes of Age: Mechanism-Based Therapy of Diabetic

End-Organ Damage. *Trends in endocrinology and metabolism: TEM* **30**, 312-327 (2019).

12. A. I. Casas *et al.*, Reactive Oxygen-Related Diseases: Therapeutic Targets and Emerging Clinical Indications. *Antioxidants & redox signaling* **23**, 1171-1185 (2015).

13. S. P. Gray *et al.*, NADPH oxidase 1 plays a key role in diabetes mellitus-accelerated atherosclerosis. *Circulation* **127**, 1888-1902 (2013).

14. J. L. Wilkinson-Berka *et al.*, NADPH Oxidase, NOX1, Mediates Vascular Injury in Ischemic Retinopathy. *Antioxidants & redox signaling*, (2013).

15. S. Sorce, K. H. Krause, NOX enzymes in the central nervous system: from signaling to disease. *Antioxidants & redox signaling* **11**, 2481-2504 (2009).

16. A. I. Casas *et al.*, NOX4-dependent neuronal autotoxicity and BBB breakdown explain the superior sensitivity of the brain to ischemic damage. *Proceedings of the National Academy of Sciences of the United States of America* **114**, 12315-12320 (2017).

17. J. C. Jha *et al.*, Genetic Targeting or Pharmacologic Inhibition of NADPH Oxidase Nox4 Provides Renoprotection in Long-Term Diabetic Nephropathy. *Journal of the American Society of Nephrology : JASN*, (2014).

18. C. Geis, E. Geuss, C. Sommer, H. H. H. W. Schmidt, C. Kleinschnitz, NOX4 is an early initiator of neuropathic pain. *Experimental neurology* **288**, 94-103 (2017).

19. A. I. Casas *et al.*, Calcium-dependent blood-brain barrier breakdown by NOX5 limits postreperfusion benefit in stroke. *The Journal of clinical investigation* **130**, 1772-1778 (2019).

20. C. E. Holterman *et al.*, Nephropathy and Elevated BP in Mice with Podocyte-Specific NADPH Oxidase 5 Expression. *Journal of the American Society of Nephrology : JASN*, ASN.2013040371 (2013).

21. J. C. Jha *et al.*, NADPH Oxidase Nox5 Accelerates Renal Injury in Diabetic Nephropathy. *Diabetes* **66**, 2691-2703 (2017).

22. D. Pandey *et al.*, Expression and functional significance of NADPH oxidase 5 (Nox5) and its splice variants in human blood vessels. *American journal of physiology. Heart and circulatory physiology* **302**, H1919-1928 (2012).

23. T. J. Guzik *et al.*, Calcium-dependent NOX5 nicotinamide adenine dinucleotide phosphate oxidase contributes to vascular oxidative stress in human coronary artery disease. *Journal of the American College of Cardiology* **52**, 1803-1809 (2008).

24. S. Altenhöfer, K. A. Radermacher, P. W. M. Kleikers, K. Wingler, H. H. H. W. Schmidt, Evolution of NADPH Oxidase Inhibitors: Selectivity and Mechanisms for Target Engagement. *Antioxidants & redox signaling* **23**, 406-427 (2015).

25. S. P. Gray *et al.*, NADPH oxidase 1 plays a key role in diabetes mellitus-accelerated atherosclerosis. *Circulation* **127**, 1888-1902 (2013).

26. S. P. Gray *et al.*, Reactive Oxygen Species Can Provide Atheroprotection via NOX4-Dependent Inhibition of Inflammation and Vascular Remodeling. *Arterioscler Thromb Vasc Biol* **36**, 295-307 (2016).

27. C. Schürmann *et al.*, The NADPH oxidase Nox4 has anti-atherosclerotic functions. *European heart journal* **36**, 3447-3456 (2015).

28. S. Altenhöfer *et al.*, The NOX toolbox: validating the role of NADPH oxidases in physiology and disease. *Cell Mol Life Sci* **69**, 2327-2343 (2012).

29. S. Heumüller *et al.*, Apocynin is not an inhibitor of vascular NADPH oxidases but an antioxidant. *Hypertension* **51**, 211-217 (2008).

30. S. Schildknecht *et al.*, The NOX1/4 inhibitor GKT136901 as selective and direct scavenger of peroxynitrite. *Current medicinal chemistry* **21**, 365-376 (2014).

31. J. Zielonka *et al.*, High-throughput assays for superoxide and hydrogen peroxide: design of a screening workflow to identify inhibitors of NADPH oxidases. *The Journal of biological chemistry* **289**, 16176-16189 (2014).

32. J. Zielonka, J. D. Lambeth, B. Kalyanaraman, On the use of L-012, a luminol-based chemiluminescent probe, for detecting superoxide and identifying inhibitors of

NADPH oxidase: a reevaluation. *Free radical biology & medicine* **65**, 1310-1314 (2013).

33. S. Wind *et al.*, Comparative pharmacology of chemically distinct NADPH oxidase inhibitors. *British journal of pharmacology* **161**, 885-898 (2010).

34. O. Teufelhofer *et al.*, Promyelocytic HL60 cells express NADPH oxidase and are excellent targets in a rapid spectrophotometric microplate assay for extracellular superoxide. *Toxicol Sci* **76**, 376-383 (2003).

35. K. Hirano *et al.*, Discovery of GSK2795039, a Novel Small Molecule NADPH Oxidase 2 Inhibitor. *Antioxid Redox Signal* **23**, 358-374 (2015).

36. G. J. Maghzal, K.-H. Krause, R. Stocker, V. Jaquet, Detection of reactive oxygen species derived from the family of NOX NADPH oxidases. *Free radical biology & medicine* **53**, 1903-1918 (2012).

37. D. Gianni *et al.*, A novel and specific NADPH oxidase-1 (Nox1) small-molecule inhibitor blocks the formation of functional invadopodia in human colon cancer cells. *ACS Chem Biol* **5**, 981-993 (2010).

38. D. Gianni *et al.*, in *Probe Reports from the NIH Molecular Libraries Program*. (Bethesda (MD), 2010).

39. S. Wind *et al.*, Comparative pharmacology of chemically distinct NADPH oxidase inhibitors. *Br J Pharmacol* **161**, 885-898 (2010).

40. X. Wang *et al.*, The novel NADPH oxidase 4 selective inhibitor GLX7013114 counteracts human islet cell death in vitro. *PLoS One* **13**, e0204271 (2018).

41. Y. Nisimoto, B. A. Diebold, D. Cosentino-Gomes, J. D. Lambeth, Nox4: a hydrogen peroxide-generating oxygen sensor. *Biochemistry* **53**, 5111-5120 (2014).

42. L. Serrander *et al.*, NOX4 activity is determined by mRNA levels and reveals a unique pattern of ROS generation. *Biochem J* **406**, 105-114 (2007).

43. L. Serrander *et al.*, NOX5 is expressed at the plasma membrane and generates superoxide in response to protein kinase C activation. *Biochimie* **89**, 1159-1167 (2007).

44. F. Chen *et al.*, Nox5 stability and superoxide production is regulated by C-terminal binding of Hsp90 and CO-chaperones. *Free Radic Biol Med* **89**, 793-805 (2015).

45. C. Kleinschnitz *et al.*, Post-stroke inhibition of induced NADPH oxidase type 4 prevents oxidative stress and neurodegeneration. *PLoS biology* **8**, (2010).

46. S. Altenhofer, K. A. Radermacher, P. W. Kleikers, K. Wingler, H. H. Schmidt, Evolution of NADPH Oxidase Inhibitors: Selectivity and Mechanisms for Target Engagement. *Antioxid Redox Signal* **23**, 406-427 (2015).

47. K. D. Martyn, L. M. Frederick, K. von Loehneysen, M. C. Dinauer, U. G. Knaus, Functional analysis of Nox4 reveals unique characteristics compared to other NADPH oxidases. *Cellular signalling* **18**, 69-82 (2006).

48. F. Augsburger *et al.*, Pharmacological characterization of the seven human NOX isoforms and their inhibitors. *Redox Biol* **26**, 101272 (2019).

49. A. A. Abubaker *et al.*, Amyloid Peptide beta1-42 Induces Integrin alphaIIbbeta3 Activation, Platelet Adhesion, and Thrombus Formation in a NADPH Oxidase-Dependent Manner. *Oxid Med Cell Longev* **2019**, 1050476 (2019).

50. P. V. Avdonin *et al.*, VAS2870 Inhibits Histamine-Induced Calcium Signaling and vWF Secretion in Human Umbilical Vein Endothelial Cells. *Cells* **8**, (2019).

51. T. Li *et al.*, Magnesium lithospermate B prevents phenotypic transformation of pulmonary arteries in rats with hypoxic pulmonary hypertension through suppression of NADPH oxidase. *Eur J Pharmacol* **847**, 32-41 (2019).

52. K. Wingler *et al.*, VAS2870 is a pan-NADPH oxidase inhibitor. *Cell Mol Life Sci* **69**, 3159-3160 (2012).

53. S. Wind *et al.*, Oxidative stress and endothelial dysfunction in aortas of aged spontaneously hypertensive rats by NOX1/2 is reversed by NADPH oxidase inhibition. *Hypertension* **56**, 490-497 (2010).

54. G. J. Gatto *et al.*, NADPH oxidase-dependent and -independent mechanisms of reported inhibitors of reactive oxygen generation. *Journal of enzyme inhibition and medicinal chemistry* **28**, 95-104 (2013).

55. H. ten Freyhaus *et al.*, Novel Nox inhibitor VAS2870 attenuates PDGF-dependent smooth muscle cell chemotaxis, but not proliferation. *Cardiovascular research* **71**, 331-341 (2006).

56. A. I. Casas *et al.*, NOX4-dependent neuronal autotoxicity and BBB breakdown explain the superior sensitivity of the brain to ischemic damage. *Proc Natl Acad Sci U S A*, (2017).

57. S. J. Brown *et al.*, Probe Report for NOX1 Inhibitors. (2010).

58. R. M. Smith, P. Kruzliak, Z. Adamcikova, A. Zulli, Role of Nox inhibitors plumbagin, ML090 and gp91ds-tat peptide on homocysteine thiolactone induced blood vessel dysfunction. *Clin Exp Pharmacol Physiol* **42**, 860-864 (2015).

59. D. Gianni *et al.*, A novel and specific NADPH oxidase-1 (Nox1) small-molecule inhibitor blocks the formation of functional invadopodia in human colon cancer cells. *ACS chemical biology* **5**, 981-993 (2010).

60. A. P. Harvey *et al.*, Vascular dysfunction and fibrosis in stroke-prone spontaneously hypertensive rats: The aldosterone-mineralocorticoid receptor-Nox1 axis. *Life Sci* **179**, 110-119 (2017).

61. J. R. Weaver, W. Grzesik, D. A. Taylor-Fishwick, Inhibition of NADPH oxidase-1 preserves beta cell function. *Diabetologia* **58**, 113-121 (2015).

62. S. Liang *et al.*, NADPH Oxidase 1 in Liver Macrophages Promotes Inflammation and Tumor Development in Mice. *Gastroenterology* **156**, 1156-1172 e1156 (2019).

63. T. Seredenina *et al.*, A subset of N-substituted phenothiazines inhibits NADPH oxidases. *Free radical biology & medicine* **86**, 239-249 (2015).

64. T. V. Rogozhina, V. V. Rogozhin, [Phenothiazines are slowly oxidizable substrates of horseradish peroxidase]. *Biomeditsinskaia khimiia* **57**, 544-553 (2011).

65. G. J. Maghzal, K. H. Krause, R. Stocker, V. Jaquet, Detection of reactive oxygen species derived from the family of NOX NADPH oxidases. *Free Radic Biol Med* **53**, 1903-1918 (2012).

Supplementary Materials

Table s1: qPCR Assays

Gene	Assay ID
β-actin	Hs99999903_m1
Nox1	Hs00246589_m1
Nox2	Hs00166163_m1
Nox4	Hs01558199_m1
Nox5	Hs00225846_m1

Figure S1:

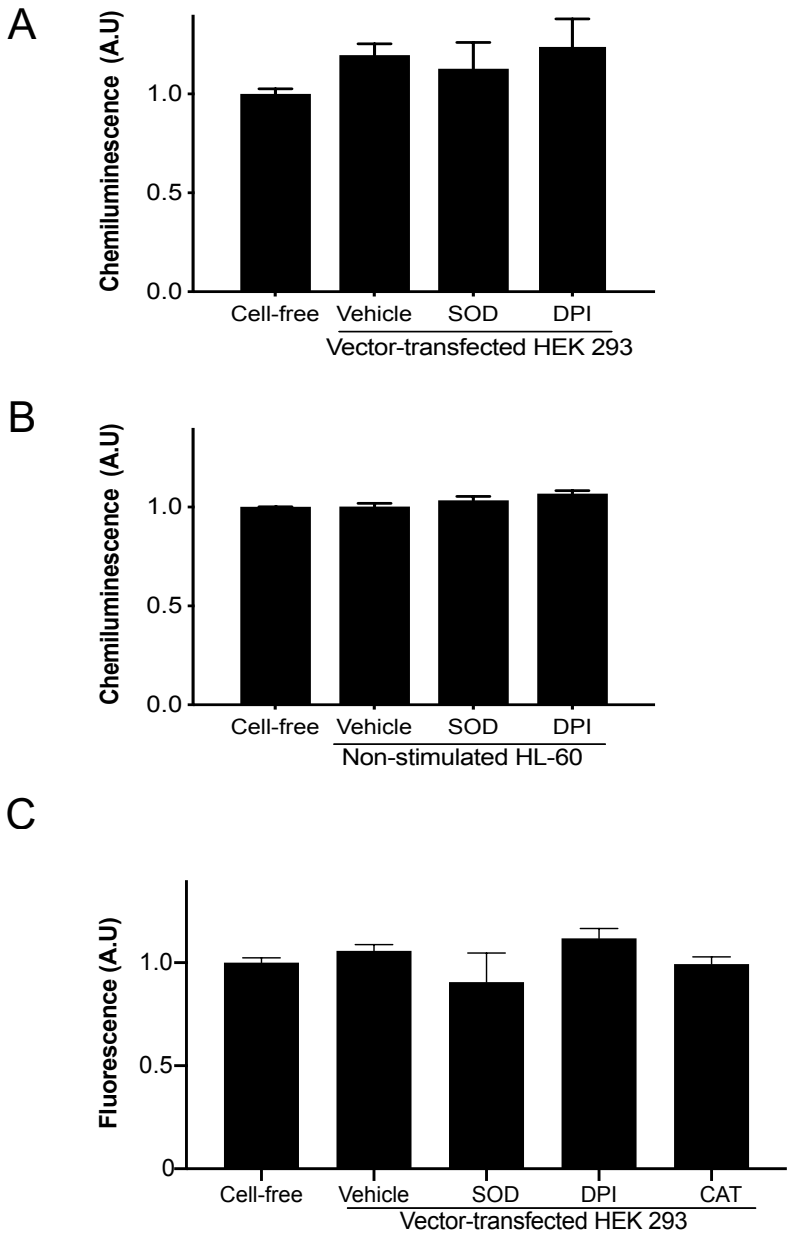

Figure S1: Controls for ROS production. Comparison of cell-free medium or control cells treated with the ROS inhibitors; SOD, catalase or diphenylene iodonium (DPI) in (A) Luminol assay, (B) Cytochrome C assay and (C) Amplex Red assay.

Figure S2:

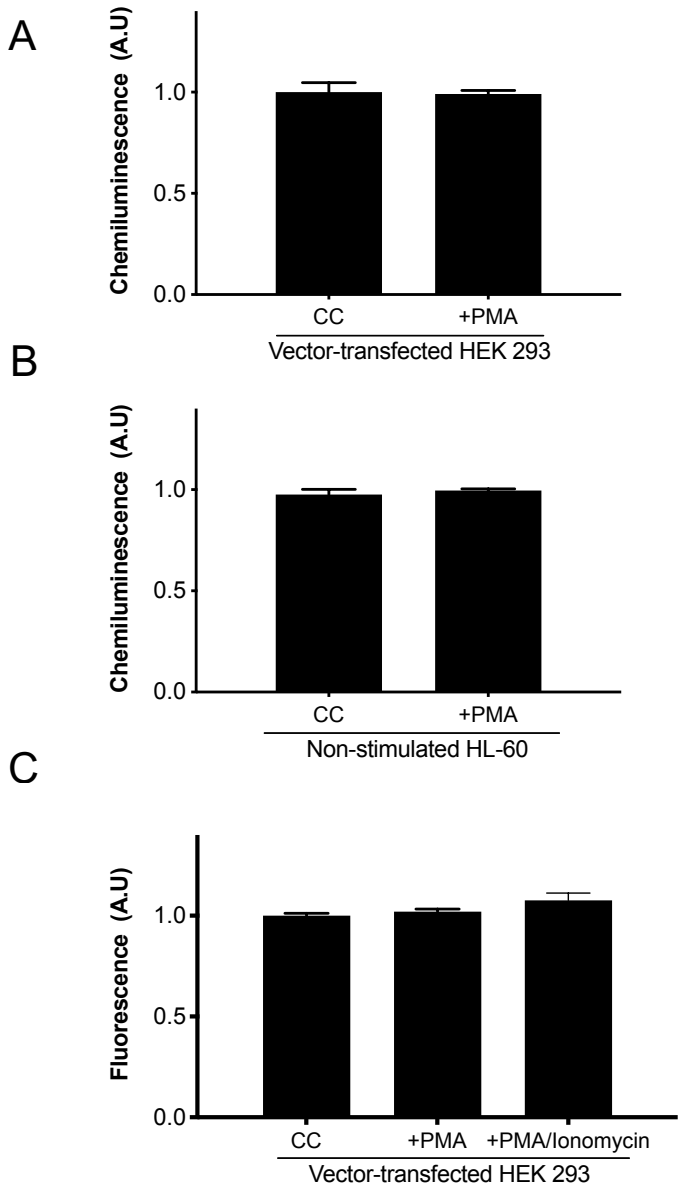

Figure S2: Controls for cells stimulation. Comparison of cell controls (CC) stimulated with PMA or PMA + ionomycin in (A) Luminol assay, (B) Cytochrome C assay and (C) Amplex Red assay.

4

NON-CANONICAL CHEMICAL FEEDBACK SELF-LIMITS NITRIC OXIDE-CYCLIC GMP SIGNALING IN HEALTH AND DISEASE

Dao VT*, **Elbatreek MH***, Deile M, Nedvetsky PI, Güldner A, Ibarra-Alvarado C, et al. Non-canonical chemical feedback self-limits nitric oxide-cyclic GMP signaling in health and disease. Scientific Reports. 2020.

Abstract

Nitric oxide (NO)-cyclic GMP (cGMP) signaling is a vasoprotective pathway therapeutically targeted for example in pulmonary hypertension. Its dysregulation in disease is incompletely understood. Here we show in pulmonary artery endothelial cells that feedback inhibition by NO of the NO receptor, the cGMP forming soluble guanylate cyclase (sGC), may contribute to this. Both endogenous NO from endothelial NO synthase or exogenous NO from NO donor compounds decreased sGC protein and activity. This was not mediated by cGMP as the NO-independent sGC stimulator or direct activation of cGMP-dependent protein kinase did not mimic it. Thiol-sensitive mechanisms were also not involved as the thiol-reducing agent, N-acetyl-L-cysteine did not prevent this feedback. Instead, both *in-vitro* and *in-vivo* and in health and acute respiratory lung disease, chronically elevated NO led to the inactivation and degradation of sGC whilst leaving the heme-free isoform, apo-sGC, intact or even increasing its levels. Thus, NO regulates sGC in a bimodal manner, acutely stimulating and chronically inhibiting, as part of self-limiting direct feedback that is cGMP-independent. In high NO disease conditions, this is aggravated but can be functionally recovered in a mechanism-based manner by apo-sGC activators that re-establish cGMP formation.

Introduction

The nitric oxide (NO)-cGMP signaling pathway plays several important roles in physiology including cardiopulmonary homeostasis [1, 2]. The main receptor and mediator of NO's actions is soluble guanylate cyclase (sGC), a heterodimeric heme protein. In its Fe(II)heme-containing state, sGC binds NO and is thereby activated to convert guanosine triphosphate (GTP) to the second messenger, cGMP, whose steady state levels are counter-regulated by different phosphodiesterases (PDEs) [3]. cGMP exerts its cardiopulmonary effects via activating cGMP-dependent protein kinase-I (PKG) [4]. This results in potent vasodilatory, anti-proliferative and anti-thrombotic effects [5]. In disease, heme loss, appearance of NO-insensitive apo-sGC and impaired NO-cGMP signaling have been described [6, 7].

In addition to sGC's acute activation, NO appears to have further roles in regulating sGC. During enzyme maturation, NO facilitates heme incorporation into sGC [8, 9], and activation of sGC by NO is followed by an acute and rapid desensitization involving protein S-nitrosylation [10, 11]. In addition, chronic exposure to NO donor drugs has been suggested to negatively affect sGC activity in a not fully reversible manner [12-14]. It is unclear, however, whether this effect pertains also to endogenously formed NO and has pathophysiological relevance.

Here, we examine this important knowledge gap in the (patho)biology of NO. As model systems we chose porcine pulmonary artery endothelial cells (PPAECs) as they relate to the clinical application of NO and cGMP modulating drugs in pulmonary hypertension [15, 16]. We investigate the effects of chronic exposure to both exogenous (from NO donor drugs) and endogenous NO on sGC protein and activity. In addition, we investigate in health and disease whether chronic effects of NO on sGC involve canonical cGMP signaling, thiol modulation, or formation of heme-free, apo-sGC. As disease model, we use again a condition related to pulmonary hypertension and chronically elevated levels of NO, porcine acute respiratory disease syndrome (ARDS) [17-19].

Results

NO chronically decreases vascular sGC protein and activity in-vivo and in-vitro.

To analyze the chronic effects of NO at a mechanistic level, we studied PPAECs. Cells were incubated for up to 72h in the presence of the NO synthase (NOS) inhibitor NG-nitro L-arginine methyl ester (L-NAME) and sGC expression and activity were measured. In the presence of L-NAME to eliminate endogenous NO formation, protein levels of the heme-binding sGCβ1 subunit were increased (Fig. 1A). This was associated also with increased sGC activity (Fig. 1B). Next we wanted to test the reverse, i.e. whether an increase of NO to supra-physiological concentrations [20-22] by chronic exposure to the long-acting NO donor compound, DETA/NO, would downregulate sGC. Indeed, pre-incubating cells with DETA/NO (100 μM) decreased both sGCα1 and sGCβ1 protein (Fig. 1C) and sGC activity (Fig. 1D). Thus, in-vitro in PPAECs, endogenous NO chronically downregulates sGC protein and activity in an L-NAME reversible manner, which is further aggravated by exogenous, pharmacologically applied NO in supra-physiological concentrations.

Next, we wanted to validate these in-vitro observations at an in-vivo level in eNOS knock-out mice (eNOS-/-), eliminating endogenous NO formation similar to the in-vitro L-NAME experiment, and in a porcine lung disease model (ARDS) characterized by NO overproduction, mimicking the exposure the supraphysiological NO concentration through the NO donor [17, 19, 23]. In line with our observations in PPAECs, eNOS-/- mice showed increased protein levels of sGCα1 and sGCβ1 (Fig. 1E) and increased sGC-activity (Fig. 1F), and in the high-NO pulmonary disease model, sGCα1 and sGCβ1 protein levels (Fig. 1G) and sGC activity were decreased (Fig. 1H). Collectively, these data suggest that both in-vitro and in-vivo lowering endogenous NO increases, and increasing endogenous NO lowers sGC protein subunit levels and sGC activity (Fig. 1I).

cGMP/PKG do not mediate the downregulation of sGC protein and activity by chronic NO.

Next, we aimed to clarify the mechanisms underlying the downregulation of sGC protein and activity by chronic NO. First, we tested whether cGMP/PKG signaling is involved as it had been shown previously to decrease both sGC activity [24] and expression [25]. Of experimental importance, cell passaging can cause downregulation of PKG and prevent the detection of PKG-dependent signaling [26-29]. Hence, we therefore restricted our studies to low passage number cells and ensured fully functional PKG signaling by validating the known autoregulation of PKG expression [30, 31]. Indeed, in our PPAEC system, both the PKG activator, 8-Br-cGMP, and the NO-independent sGC stimulator and PDE inhibitor, YC-1, [32] were able to reduce PKG expression (Supplementary Fig. S1 online) confirming the presence of fully functional PKG. We then studied whether the observed downregulation of sGC protein and activity by NO can be mimicked by cGMP or is prevented by inhibiting PKG. When we exposed PPAECs, however, for 72h with different concentrations of the sGC stimulator and PDE inhibitor, YC-1, to raise cGMP in an NO-independent manner, or to the direct PKG activator, 8-Br-cGMP, neither sGC protein nor activity were lowered (cf. to Fig. 1). In fact, we observed even a slight upregulation of sGC protein (Fig. 2, A and B). Consistent with this, the NO induced downregulation of sGC could not be prevented by co-incubation with the PKG inhibitor, Rp-8-Br-PET-cGMPS (Supplementary Fig. S2 online). To extend these in-vitro findings also to the in-vivo level, we subsequently studied sGC expression and activity in PKG knock-out mice (PKG-/-) [33]. Consistent with our in-vitro data, sGC protein levels (Fig. 2D) and sGC activity (Fig. 2E) were unchanged in PKG-/- as compared to wildtype mice. In conclusion, both our in-vivo and in-vitro data suggested that the downregulation of sGC protein and activity by chronic NO is cGMP- and PKG-independent and thus appeared to be due to a non-canonical mechanism (Fig. 2C). Two cGMP-independent effects on sGC have been reported, rapid desensitization [10, 20, 34] , which is reversible in a thiol-dependent manner [35,

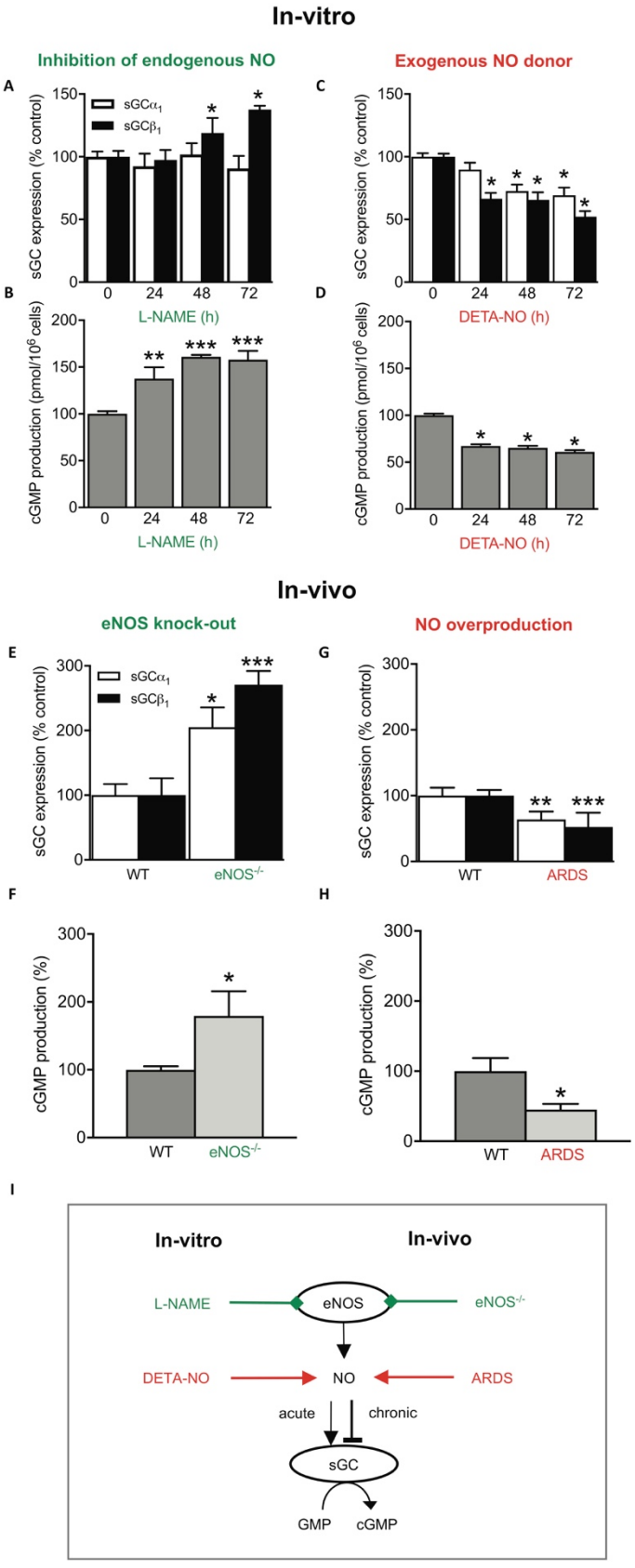
In-vitro
Inhibition of endogenous NO
Exogenous NO donor
A
B
C
D
sGC expression (% control)
cGMP production (pmol/10^6 cells)
sGCα1
sGCβ1
L-NAME (h)
DETA-NO (h)
In-vivo
eNOS knock-out
NO overproduction
E
F
G
H
cGMP production (%)
WT
eNOS-/-
ARDS
I
In-vitro
In-vivo
L-NAME
eNOS
eNOS-/-
DETA-NO
NO
ARDS
acute
chronic
sGC
GMP
cGMP

Fig. 1. Chronic NO decreases vascular sGC protein and activity *in-vivo* and *in-vitro*. **(A)** Inhibiting basal NO formation in PPAEC by L-NAME (100 µM) for up to 72h increased sGCβ_1 expression (N=6). **(B)** This upregulation was associated with increased sGC activity (N=3). Exposing cells to supra-physiological levels of NO by chronic exposure to the NO donor compound, DETA/NO (100 µM), for up to 72h decreased both sGCα_1 and sGCβ_1 protein **(C)** (N=6) and sGC activity **(D)** (N=5). *In-vivo* validation of the *in-vitro* observations showed in eNOS knock-out mice (eNOS$^{-/-}$) mice increased sGC protein **(E)** and activity levels **(F)** (N=9), and in a porcine lung disease model (ARDS) characterized by NO overproduction, decreased sGCα_1 and sGCβ_1 protein **(G)** (N=5) and sGC activity levels **(H)** (N=3). Data are expressed as mean ± SEM. *, **, ***: $p < 0.05$, 0.01 or 0.001 *vs.* control, respectively. **(I)** Schematic summary showing that both *in-vitro* (porcine lung endothelial cells) and *in-vivo* (the porcine lung disease model, ARDS) both endogenous and exogenous NO downregulate sGC protein and activity.

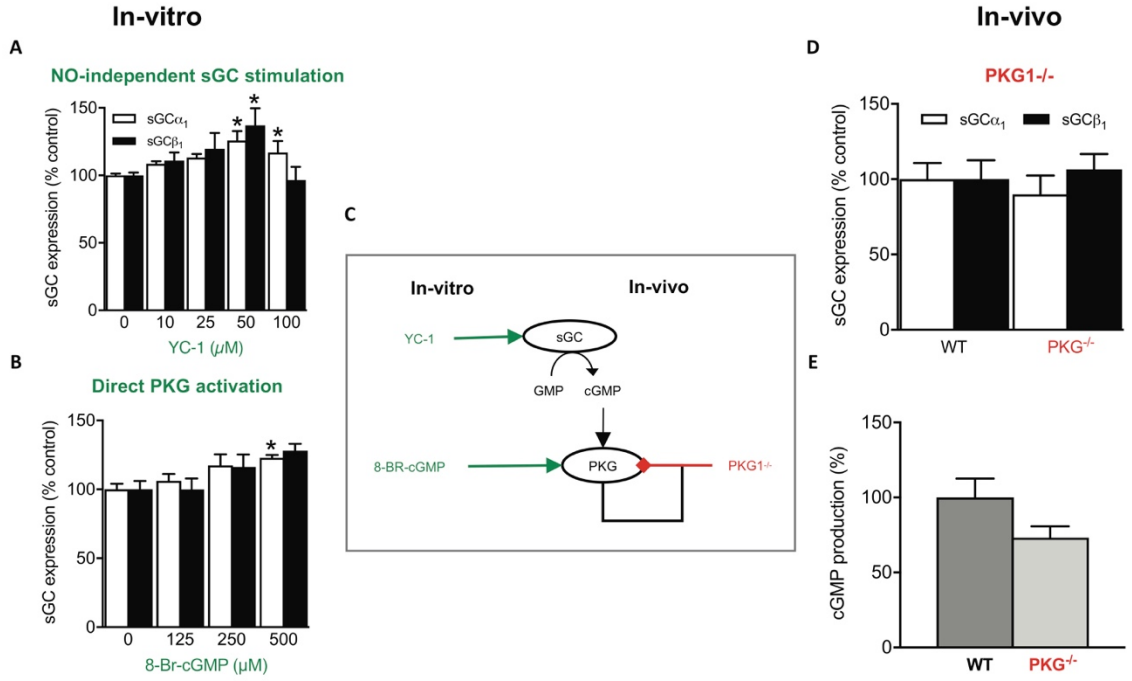

Fig. 2. PKG does not mediate the downregulation of sGC protein and activity by chronic NO. When PPAEC were incubated for 72 h in the absence or presence of increasing concentrations of **(A)** the NO-independent sGC stimulator, YC-1 (N=6), this did not cause a downregulation of sGCα_1 and sGCβ_1 expression but rather a small upregulation. Consistent with this, in **(B)** the direct PKG activator 8-Br-cGMP (N=6) lead to increased sGCα_1 protein expression. **(C)** The scheme summarizes the *in-vivo* and *in-vitro* data suggesting that the downregulation of sGC protein and activity by chronic NO is cGMP- and PKG-independent and thus appeared to be due to a non-canonical mechanism. **(D)** sGC protein expression (N=4) and **(E)** activity (N=4) are not altered in PKG$^{-/-}$ as

compared to wildtype mice. Data are expressed as mean ± SEM. *,**,***: $p < 0.05$, 0.01 or 0.001 *vs.* control, respectively.

36], and oxidative heme-loss yielding the NO-insensitive apo-form of (apo-sGC) [7, 37]. These possibilities were tested in our two next sets of experiments.

NO-induced sGC downregulation is thiol-independent.

It has been shown previously, that thiol-sensitive mechanisms are involved in sGC regulation such as sGC maturation and airway pathologies such as asthma [20]. Therefore, we assessed whether NO-posttranslational modification of free-thiol cysteines i.e. S-nitrosylation contributes to the downregulation of sGC by high chronic NO incubation. For this approach, PPAECs were again exposed for 72 h to DETA-NO (100μM) in absence or presence, over the full-time frame, of the membrane-permeable thiol-reducing agent, N-acetyl-L-cysteine (NAC; 1mM). NAC is a membrane-permeable de-nitrosylating agent and glutathione precursor that has been shown to protect from sGC nitrosylation [38, 39]. Although some studies had used higher concentration of NAC, 1 mM is sufficient to induce de-nitrosylation [40, 41]. The presence of NAC, however, neither affected sGC protein levels (Fig. 3A) nor sGC activity (Fig. 3B). This set of experiments suggested that it is unlikely that a thiol-reversible mechanism similar to the acute desensitization is involved in the chronic NO-induced downregulation of sGC protein and activity. This left oxidative heme-loss yielding the NO-insensitive apo-form of (apo-sGC) [7, 37] as only known cGMP-independent effect on sGC.

NO-induced sGC downregulation generates NO-insensitive sGC.

We therefore examined whether chronic NO converts sGC to the NO-insensitive, heme-free form of sGC, i.e. apo-sGC. To assay for the presence of apo-sGC, we took advantage of the apo-sGC activator drug, BAY 58-2667 (cinaciguat), which specifically binds to the empty heme binding pocket of apo-sGC and re-activates cGMP formation in an NO-independent manner [42]. Indeed, up to 72 h exposure of PPAECs to DETA-NO (100 μM) increased apo-sGC activity, measured as BAY 58-2667-induced cGMP formation (Fig. 3C), and reduced sGC activity (Fig. 1D). To validate this mechanistic finding in-vivo, we re-examined the above already

mentioned and utilized high-NO porcine ARDS model in which we had observed lower sGC protein levels and activity (see Fig. 1G, H). Consistent with our above in-vitro findings, apo-sGC activity was also increased in the high-NO porcine ARDS model (Fig. 3D) and established apo-sGC formation as one possible chronic mechanism of chronic NO in addition to total sGC protein loss.

Discussion

Our findings close important gaps in our understanding of NO-cGMP signaling, in particular on the long-term effects of endogenously formed NO versus NO donors on sGC and the pathophysiological relevance of chronic NO for sGC regulation. We thus expand the previously observed notion that NO donors drugs can reduce sGC mRNA levels [43] to the protein level and importantly from pharmacology to endogenous NO. Previously, sGC protein levels were not consistently investigated or with antibodies of unclear specificity [12, 44]. Moreover, the functional consequences of PKG on cGMP levels were investigated only in some cases [43, 45] or in relation to cGMP metabolism rather than its formation [43, 46, 47].

Surprisingly, not only pathological high levels of NO, as in our porcine ARDS model, but already low chronic endogenous NOS activity suppressed sGC protein and activity in an L-NAME reversible manner. These findings establish a previously not recognized delicate steady state in the interactions between NO and sGC, acutely stimulating and chronically limiting its expression and activity. On a positive note, under conditions of diminished NO synthesis, this may in turn rapidly upregulate sGC protein and activity as we have observed in the presence of the NOS inhibitor, L-NAME and in-vivo in eNOS-/- mice. In this regard, previous data are controversial. For example, sGC activity was increased in eNOS-/- mice [13, 48] which agrees with our findings. However, other studies showed that neither sGC expression nor activity were changed in eNOS-/- mice [49, 50], or upon treatment with high dose NO donors [51]. The reasons for this discrepancy are unclear.

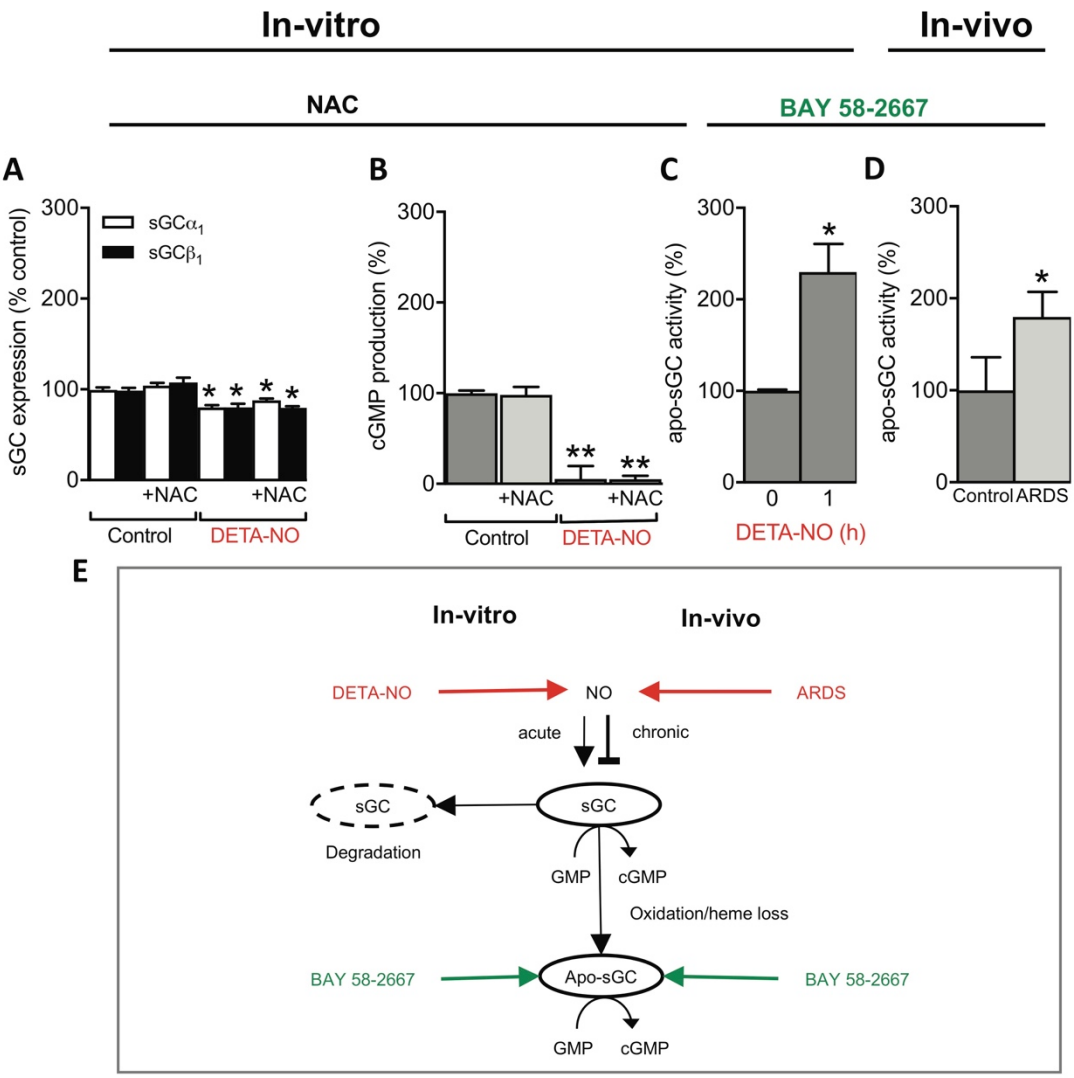

Fig. 3. NO-induced sGC downregulation is thiol-independent but involves sGC loss and a shift towards apo-sGC. When PPAECs were exposed for 72 h to DETA-NO (100µM) in the absence and presence of N-acetyl-L-cysteine (NAC; 1mM), NAC neither affected sGC protein levels (N=5) (**A**) nor activity (N=4) (**B**). Exposure of PPAECs for 72h to DETA-NO (100 µM) increased apo-sGC activity, measured as BAY 58-2667-induced cGMP formation (BAY 58-2667, 10 µM) (N=3) (**C**). Validation of the above *in-vitro* mechanistic findings *in-vivo* in the porcine high-NO ARDS model showing also increased apo-sGC activity (N=3) **(D)**. **(E)** A scheme summarizing both our *in-vitro* and *in-vivo* data that both endogenous NO or pharmacological NO donor compounds that acutely stimulate sGC, chronically decreased both sGC protein and activity leading to inactivation of sGC and an apparent net shift towards NO-insensitive apo-sGC. Data are expressed as mean ± SEM. *,**: $p < 0.05$ or 0.01 *vs.* control, respectively.

Of therapeutic importance is also the previously not recognized risk of chronic use of NO donor drugs as they will lead to a downregulation of both sGC protein and activity. Together with the problematic pharmacokinetics and known, but entirely different phenomenon of pharmacokinetic tolerance due to lack of NO donor drug conversion to NO [52-54], this adds to the limitations of this widely used drug class. With the introduction of NO-independent sGC stimulators and cGMP elevating agents into clinical practice [55] there is now an alternative. Indeed, we show that the prototypic sGC stimulator and PDE inhibitor, YC-1, does not lead to sGC downregulation.

With respect to the underlying mechanisms, we initially considered two known mechanisms in NO-cGMP physiology, i.e. cGMP/PKG and thiol modification [9, 10]. Surprisingly, both could be excluded, which was reminiscent of an earlier observation where long-term exposure to an exogenous NO donor also reduced sGC activity in a manner that could not be recovered with thiol treatment [14]. Instead, our findings suggest that endogenous and exogenous NO chronically induce a net shift from sGC to apo-sGC and that this is not only a pathophysiological mechanism but pertains to NO-cGMP physiology. This explains why apo-sGC activator-induced cGMP formation and functional effects are enhanced in but not exclusive to disease conditions [7]. Nevertheless, the availability of sGC activator compounds allows now to overcome such conditions in which sGC protein and activity is diminished in favor of apo-sGC and still induce cGMP formation. As a limitation, other potential underlying mechanisms such as decreased mRNA [43] or increased degradation of sGC have not been addressed by our study [56] and cannot be excluded.

Our findings also add to our understanding of apo-sGC as a therapeutic target. Hitherto apo-sGC has been mainly studied by using the heme oxidant, ODQ, or by expressing enzyme where the proximal heme ligating histidine had been deleted [57]. The mechanisms by which apo-sGC forms in pathophysiology were less clear. Now chronic exposure to (high) levels of NO can be considered one of these conditions. Whether this involves additional interactions with for example reactive oxygen species and from which source remains to be

investigated. Certainly, intermediate compounds such as peroxynitrite would be candidate molecule to potentiate NO's oxidative potential [58]. Of note, the shift from sGC to apo-sGC is not 1-to-1. Some sGC appears to be lost due to inactivation beyond recovery by apo-sGC activators, e.g. by channeling into the ubiquitylation-proteasome pathway [59]. Nevertheless, an apparent net shift from sGC to apo-sGC as main source of cGMP formation is a common denominator and has recently also been observed by us in another high NO model of ischemic stroke [6] and by others in an asthma model [20]. In contrast to other observations, in our settings chronic NO incubation for 72 h unlike others for overnight [20], did have an effect on sGC β1 expression independent of S-nitrosylation.

In conclusion, our data suggest that both in-vitro and in-vivo, and both under physiological conditions and in disease NO self-limits its ability to induce cGMP formation via a chemical redox feedback which causes inactivation of sGC and an apparent net shift towards NO-insensitive apo-sGC. Our findings are of direct therapeutic importance as a pathological sGC/apo-sGC ratio can be treated with sGC activator compounds such as BAY58-2667 [59] thereby reinstalling cGMP synthesis and PKG signaling [7, 37]. Moreover, with respect to the long-established class of NO donor drugs and the use of inhaled NO a cautionary note needs to be added. Not only do they cause reversible tolerance, but, as we now find, also irreversible downregulation of sGC and apo-sGC formation. This explains the superiority of the novel, NO-independent sGC stimulators, at least in indications such as pulmonary hypertension [15].

Materials and Methods

Chemicals

Polyclonal antibodies specific for sGCα1 and sGCβ1 have been described elsewhere (30). Actin monoclonal antibody (Oncogene Research Products, Boston, USA); collagenase type CLS II (Merck, Netherlands); 8-bromo-cGMP (BIOLOG, Germany); L-NAME, DETA/NO, DEA/NO , IBMX and GTP (Enzo Life Sciences, Netherlands); BAY 58-2667 was synthesized as described [60]. All other chemicals were of the highest purity grade available and obtained from Sigma or Merck (Netherlands). DETA/NO and DEA/NO were dissolved in 10 mM NaOH, BAY 58-2667 and YC-1 in DMSO.

Tissue isolation

Tissues from i) 6- to 8-months old male PKG-/- and age-matched control mice were obtained from Prof. Franz Hofmann, Department of Pharmacology and Toxicology at the Technical University Munich (genetic background 129/Sv) [33], and ii) 6- to 8-months old male eNOS-/- mice and age-matched control were obtained from the Department of Physiology at Heinrich-Heine-Universität Düsseldorf (genetic background C57BL/6) [36]. Animals' care was in accordance with guidelines of Technical University Munich and Heinrich-Heine-Universität Düsseldorf.

Preparation of pulmonary arteries from a porcine ARDS model

Pulmonary arteries were removed immediately after death from an experimental porcine model of ARDS, as previously described [35]. Pulmonary arteries were snap-frozen in liquid nitrogen and stored at minus 80°C or otherwise processed immediately to tissue powder and subsequently suspended in homogenization-buffer and homogenized in an Ultra Turrax at 4°C. These samples were then used further for protein determination, protein immune blots and sGC activity assays.

PPAECs

Fresh porcine pulmonary arteries were obtained from a local slaughterhouse and maintained in phosphate-buffered saline (PBS; 10mM Na2HPO4, 1.8mM KH2PO4, 140mM NaCl, 2.7mM KCl, pH 7.4) at 37°C. PPAECs were isolated enzymatically by incubation of the aorta inner surface with collagenase type CLS

II (0.5 mg/mL for 10 min at room temperature) and then collected in HEPES-buffered medium 199. After centrifugation (250 x g, 10 min) the pellet was re-suspended in growth medium (medium 199 supplemented with 10% fetal calf serum, 100 U/mL penicillin, 100 µg/mL streptomycin) and cells were propagated in coated plastic flasks and incubated (37°C, 6% CO_2). Upon confluence, endothelial cell monolayers were sub-cultured in 35-mm (for Western blot) or 60-mm (for cGMP determination) gelatin coated dishes. Confluent cell monolayers from the second passage were used for experiments. The growth medium was replaced either every 12 or 24 hours if applicable containing the indicated compounds. After incubation time cells were subsequently used for sGC activity measurements or western blot analysis.

Detection and quantification of sGC protein

Western blotting procedures were described previously [61]. Briefly, cells were lysed in 250 µL Roti-Load sample buffer (ROTH, Karlsruhe, Germany), preheated to 95°C and then boiled for additional 10 min prior loading on SDS gel electrophoresis. Primary antibodies were diluted 1:4000 for anti-sGCα1 and 1:2000 for anti-sGCβ1 antibody in 3% dry milk in TBST and incubated with nitrocellulose membranes at 4°C over-night following challenge of membranes with secondary goat anti-rabbit antibody (1:2000 in 3% milk in TBST) conjugated to horseradish peroxidase (Dako A/S, Denmark). Immuno-complexes were visualized using an enhanced chemiluminescence kit (Amersham Pharmacia Biotech, Freiburg). Samples were quantified with a Kodak Imager Station 440 CF and with the NIH 1.6 software. All blots are standardized to ß-actin or GAPDH expression that was not affected by the treatments. Representative western blot examples are shown in Supplementary Fig. S3 online.

Determination of sGC activity

To measure sGC activity, cells were stimulated with 250 µM DEA/NO or 10 µM BAY 58-2667 for 3 min at 37°C. Thereafter, cells were immediately lysed in 80 % ethanol. Cells were scraped and, after evaporation of ethanol, re-suspended in assay buffer and sonicated. Measurement of sGC activity in crude homogenates of porcine tissue was performed as previously described [61]. Briefly, all samples

were measured as the formation of cGMP at 37 °C during 10 min in a total incubation volume of 100 ml containing 50 mM triethanolamine-HCl (pH 7.4), 3 mM MgCl2, 3 mM glutathione, 1mM IBMX, 100mM zaprinast, 5 mM creatine phosphate, 0.25 mg/ml creatine kinase and 1mM or 0.5 mM GTP. The reaction was started by simultaneous addition of the sample and either DEA/NO or BAY 58-2667, respectively. After incubation of each sample for 10 min the reaction was stopped by boiling for 10 min at 95°C. Thereafter the amount of cGMP was subsequently determined by a commercial enzyme immunoassay kit (Enzo Life Sciences, Netherlands).

Statistics

For comparisons students´ t-test or multiple comparisons one-way analysis of variance (ANOVA) was followed by Bonferroni's test. Calculations were performed using GraphPad Prism 6.0 (GraphPad Software, San Diego, USA). All data are expressed as mean ± SEM. P-value < 0.05 was considered significant.

References

1. K. Bian, M.-F. Doursout, F. Murad, Vascular system: role of nitric oxide in cardiovascular diseases. *Journal of clinical hypertension (Greenwich, Conn.)* **10**, 304-310 (2008).

2. L. J. Ignarro, Nitric oxide as a unique signaling molecule in the vascular system: a historical overview. *Journal of physiology and pharmacology : an official journal of the Polish Physiological Society* **53**, 503-514 (2002).

3. S. P. L. Cary, J. A. Winger, M. A. Marletta, Tonic and acute nitric oxide signaling through soluble guanylate cyclase is mediated by nonheme nitric oxide, ATP, and GTP. *Proceedings of the National Academy of Sciences of the United States of America* **102**, 13064-13069 (2005).

4. E. J. Tsai, D. A. Kass, Cyclic GMP signaling in cardiovascular pathophysiology and therapeutics. *Pharmacology & therapeutics* **122**, 216-238 (2009).

5. U. Förstermann, N. Xia, H. Li, Roles of Vascular Oxidative Stress and Nitric Oxide in the Pathogenesis of Atherosclerosis. *Circulation research* **120**, 713-735 (2017).

6. F. Langhauser *et al.*, A diseasome cluster-based drug repurposing of soluble guanylate cyclase activators from smooth muscle relaxation to direct neuroprotection. *NPJ systems biology and applications* **4**, 8 (2018).

7. J.-P. Stasch *et al.*, Targeting the heme-oxidized nitric oxide receptor for selective vasodilatation of diseased blood vessels. *The Journal of clinical investigation* **116**, 2552-2561 (2006).

8. A. Ghosh, J.-P. Stasch, A. Papapetropoulos, D. J. Stuehr, Nitric oxide and heat shock protein 90 activate soluble guanylate cyclase by driving rapid change in its subunit interactions and heme content. *The Journal of biological chemistry* **289**, 15259-15271 (2014).

9. A. Ghosh, D. J. Stuehr, Soluble guanylyl cyclase requires heat shock protein 90 for heme insertion during maturation of the NO-active enzyme. *Proceedings of the National Academy of Sciences of the United States of America* **109**, 12998-13003 (2012).

10. A. Beuve, Thiol-Based Redox Modulation of Soluble Guanylyl Cyclase, the Nitric Oxide Receptor. *Antioxidants & redox signaling*, ars.2015.6591 (2016).

11. B. Mayer *et al.*, Inactivation of soluble guanylate cyclase by stoichiometric S-nitrosation. *Mol Pharmacol* **75**, 886-891 (2009).

12. R. P. Brandes *et al.*, Increased nitrovasodilator sensitivity in endothelial nitric oxide synthase knockout mice: role of soluble guanylyl cyclase. *Hypertension* **35**, 231-236 (2000).

13. F. M. Faraci, C. D. Sigmund, E. G. Shesely, N. Maeda, D. D. Heistad, Responses of carotid artery in mice deficient in expression of the gene for endothelial NO synthase. *The American journal of physiology* **274**, H564-570 (1998).

14. T. Sardón, M. A. Baltrons, A. García, Nitric oxide-dependent and independent down-regulation of NO-sensitive guanylyl cyclase in neural cells. *Toxicology letters* **149**, 75-83 (2004).

15. W. R. Auger, S. W. Jamieson, S. D. Pulmonary Thromboendarterectomy Program at University of California, Riociguat for pulmonary hypertension. *The New England journal of medicine* **369**, 2266-2268 (2013).

16. S. Prasad, J. Wilkinson, M. A. Gatzoulis, Sildenafil in primary pulmonary hypertension. *The New England journal of medicine* **343**, 1342-1342 (2000).

17. M. Lange, P. Enkhbaatar, Y. Nakano, D. L. Traber, Role of nitric oxide in shock: the large animal perspective. *Frontiers in bioscience (Landmark edition)* **14**, 1979-1989 (2009).

18. S. Muzaffar, J. Y. Jeremy, G. D. Angelini, K. Stuart-Smith, N. Shukla, Role of the endothelium and nitric oxide synthases in modulating superoxide formation induced by endotoxin and cytokines in porcine pulmonary arteries. *Thorax* **58**, 598-604 (2003).

19. C. Sittipunt *et al.*, Nitric oxide and nitrotyrosine in the lungs of patients with acute respiratory distress syndrome. *Am J Respir Crit Care Med* **163**, 503-510 (2001).

20. A. Ghosh *et al.*, Soluble guanylate cyclase as an alternative target for bronchodilator therapy in asthma. *Proc Natl Acad Sci U S A* **113**, E2355-2362 (2016).

21. L. A. Ridnour *et al.*, Nitric oxide regulates angiogenesis through a functional switch involving thrombospondin-1. *Proc Natl Acad Sci U S A* **102**, 13147-13152 (2005).

22. A. Cheung, P. L. Newland, M. Zaben, G. S. Attard, W. P. Gray, Intracellular nitric oxide mediates neuroproliferative effect of neuropeptide y on postnatal hippocampal precursor cells. *J Biol Chem* **287**, 20187-20196 (2012).

23. P. L. Silva *et al.*, Effects of intravascular volume replacement on lung and kidney function and damage in nonseptic experimental lung injury. *Anesthesiology* **118**, 395-408 (2013).

24. Z. Zhou *et al.*, Protein kinase G phosphorylates soluble guanylyl cyclase on serine 64 and inhibits its activity. *Arterioscler Thromb Vasc Biol* **28**, 1803-1810 (2008).

25. N. C. Browner, N. B. Dey, K. D. Bloch, T. M. Lincoln, Regulation of cGMP-dependent protein kinase expression by soluble guanylyl cyclase in vascular smooth muscle cells. *J Biol Chem* **279**, 46631-46636 (2004).

26. N. C. Browner, N. B. Dey, K. D. Bloch, T. M. Lincoln, Regulation of cGMP-dependent protein kinase expression by soluble guanylyl cyclase in

vascular smooth muscle cells. *The Journal of biological chemistry* **279**, 46631-46636 (2004).

27. T. L. Cornwell, T. M. Lincoln, Regulation of intracellular Ca2+ levels in cultured vascular smooth muscle cells. Reduction of Ca2+ by atriopeptin and 8-bromo-cyclic GMP is mediated by cyclic GMP-dependent protein kinase. *The Journal of biological chemistry* **264**, 1146-1155 (1989).

28. R. Draijer, D. E. Atsma, A. van der Laarse, V. W. van Hinsbergh, cGMP and nitric oxide modulate thrombin-induced endothelial permeability. Regulation via different pathways in human aortic and umbilical vein endothelial cells. *Circulation research* **76**, 199-208 (1995).

29. R. Draijer *et al.*, Expression of cGMP-dependent protein kinase I and phosphorylation of its substrate, vasodilator-stimulated phosphoprotein, in human endothelial cells of different origin. *Circulation research* **77**, 897-905 (1995).

30. Z. Zhou *et al.*, Protein kinase G phosphorylates soluble guanylyl cyclase on serine 64 and inhibits its activity. *Arteriosclerosis, Thrombosis, and Vascular Biology* **28**, 1803-1810 (2008).

31. H. Sellak, C.-s. Choi, N. B. Dey, T. M. Lincoln, Transcriptional and post-transcriptional regulation of cGMP-dependent protein kinase (PKG-I): pathophysiological significance. *Cardiovascular research* **97**, 200-207 (2013).

32. J. Galle *et al.*, Effects of the soluble guanylyl cyclase activator, YC-1, on vascular tone, cyclic GMP levels and phosphodiesterase activity. *Br J Pharmacol* **127**, 195-203 (1999).

33. A. Pfeifer *et al.*, Defective smooth muscle regulation in cGMP kinase I-deficient mice. *The EMBO journal* **17**, 3045-3051 (1998).

34. N. B. Fernhoff, E. R. Derbyshire, E. S. Underbakke, M. A. Marletta, Heme-assisted S-nitrosation desensitizes ferric soluble guanylate cyclase to nitric oxide. *The Journal of biological chemistry* **287**, 43053-43062 (2012).

35. N. Sayed, P. Baskaran, X. Ma, F. van den Akker, A. Beuve, Desensitization of soluble guanylyl cyclase, the NO receptor, by S-nitrosylation. *Proceedings of the National Academy of Sciences of the United States of America* **104**, 12312-12317 (2007).

36. N. Sayed *et al.*, Nitroglycerin-induced S-nitrosylation and desensitization of soluble guanylyl cyclase contribute to nitrate tolerance. *Circulation research* **103**, 606-614 (2008).

37. O. V. Evgenov *et al.*, NO-independent stimulators and activators of soluble guanylate cyclase: discovery and therapeutic potential. *Nature reviews. Drug discovery* **5**, 755-768 (2006).

38. N. Sayed *et al.*, Nitroglycerin-induced S-nitrosylation and desensitization of soluble guanylyl cyclase contribute to nitrate tolerance. *Circ Res* **103**, 606-614 (2008).

39. N. Sayed, P. Baskaran, X. Ma, F. van den Akker, A. Beuve, Desensitization of soluble guanylyl cyclase, the NO receptor, by S-nitrosylation. *Proc Natl Acad Sci U S A* **104**, 12312-12317 (2007).

40. N. L. Parinandi, W. M. Scribner, S. Vepa, S. Shi, V. Natarajan, Phospholipase D activation in endothelial cells is redox sensitive. *Antioxid Redox Signal* **1**, 193-210 (1999).

41. C. N. Morrell *et al.*, Regulation of platelet granule exocytosis by S-nitrosylation. *Proc Natl Acad Sci U S A* **102**, 3782-3787 (2005).

42. P. Schmidt, M. Schramm, H. Schröder, J.-P. Stasch, Mechanisms of nitric oxide independent activation of soluble guanylyl cyclase. *European journal of pharmacology* **468**, 167-174 (2003).

43. K. Ujiie *et al.*, Homologous and heterologous desensitization of a guanylyl cyclase-linked nitric oxide receptor in cultured rat medullary interstitial cells. *The Journal of pharmacology and experimental therapeutics* **270**, 761-767 (1994).

44. P. S. Yuen, L. K. Doolittle, D. L. Garbers, Dominant negative mutants of nitric oxide-sensitive guanylyl cyclase. *The Journal of biological chemistry* **269**, 791-793 (1994).

45. G. Filippov, D. B. Bloch, K. D. Bloch, Nitric oxide decreases stability of mRNAs encoding soluble guanylate cyclase subunits in rat pulmonary artery smooth muscle cells. *The Journal of clinical investigation* **100**, 942-948 (1997).

46. R. Ferrero, M. Torres, Prolonged exposure of chromaffin cells to nitric oxide down-regulates the activity of soluble guanylyl cyclase and corresponding mRNA and protein levels. *BMC biochemistry* **3**, 26 (2002).

47. A. Papapetropoulos, C. Y. Go, F. Murad, J. D. Catravas, Mechanisms of tolerance to sodium nitroprusside in rat cultured aortic smooth muscle cells. *British journal of pharmacology* **117**, 147-155 (1996).

48. M. B. Hussain, A. J. Hobbs, R. J. MacAllister, Autoregulation of nitric oxide-soluble guanylate cyclase-cyclic GMP signalling in mouse thoracic aorta. *Br J Pharmacol* **128**, 1082-1088 (1999).

49. R. P. Brandes *et al.*, Increased nitrovasodilator sensitivity in endothelial nitric oxide synthase knockout mice: role of soluble guanylyl cyclase. *Hypertension* **35**, 231-236 (2000).

50. M. M. Cortese-Krott *et al.*, Identification of a soluble guanylate cyclase in RBCs: preserved activity in patients with coronary artery disease. *Redox Biol* **14**, 328-337 (2018).

51. M. Oppermann, V. T. Dao, T. Suvorava, M. Bas, G. Kojda, Effect of oral organic nitrates on expression and activity of vascular soluble guanylyl cyclase. *Br J Pharmacol* **155**, 335-342 (2008).

52. T. Munzel, A. Daiber, A. Mulsch, Explaining the phenomenon of nitrate tolerance. *Circ Res* **97**, 618-628 (2005).

53. B. Mayer, M. Beretta, The enigma of nitroglycerin bioactivation and nitrate tolerance: news, views and troubles. *Br J Pharmacol* **155**, 170-184 (2008).

54. M. Oelze *et al.*, Chronic therapy with isosorbide-5-mononitrate causes endothelial dysfunction, oxidative stress, and a marked increase in vascular endothelin-1 expression. *Eur Heart J* **34**, 3206-3216 (2013).

55. H. A. Ghofrani *et al.*, Riociguat for the treatment of pulmonary arterial hypertension. *N Engl J Med* **369**, 330-340 (2013).

56. P. I. Nedvetsky *et al.*, Heat shock protein 90 regulates stabilization rather than activation of soluble guanylate cyclase. *FEBS Lett* **582**, 327-331 (2008).

57. R. Thoonen *et al.*, Cardiovascular and pharmacological implications of haem-deficient NO-unresponsive soluble guanylate cyclase knock-in mice. *Nature communications* **6**, 8482 (2015).

58. M. E. Armitage, K. Wingler, H. H. Schmidt, M. La, Translating the oxidative stress hypothesis into the clinic: NOX versus NOS. *Journal of molecular medicine (Berlin, Germany)* **87**, 1071-1076 (2009).

59. S. Meurer *et al.*, Nitric oxide-independent vasodilator rescues heme-oxidized soluble guanylate cyclase from proteasomal degradation. *Circulation research* **105**, 33-41 (2009).

60. J.-P. Stasch *et al.*, NO- and haem-independent activation of soluble guanylyl cyclase: molecular basis and cardiovascular implications of a new pharmacological principle. *British journal of pharmacology* **136**, 773-783 (2002).

61. P. I. Nedvetsky, C. Kleinschnitz, H. H. H. W. Schmidt, Regional distribution of protein and activity of the nitric oxide receptor, soluble guanylyl cyclase, in rat brain suggests multiple mechanisms of regulation. *Brain research* **950**, 148-154 (2002).

Acknowledgements: We thank Prof. Hofmann for providing the $PKG^{-/-}$ mice tissues; Helmut Müller, for expert technical assistance; Kirstin Wingler, Rob Hermans, Sabine Meurer and Merlijn Meens, for carefully reading and editing earlier versions of this manuscript.
Funding: This study was supported by a European Research Council Advanced Grant (RadMed).

Author contributions: H.H.H.W.S. designed research; V.T.D., M.E., M.D., P.I.N., A.Gü., C.I.A performed research; A.Gü. and A.Gö. contributed new reagents/analytic tools; V.T.D., M.E., M.D., P.I.N., C.I.A. and H.H.H.W.S. analyzed data; and V.T.D., M.E., A.Gö. and H.H.H.W.S. wrote the paper.

Competing interests: The authors declare no competing interests.

Data availability: All data needed to evaluate the conclusions in the paper are present in the paper or the Supplementary Materials.

SUPPLEMENTARY FIGURES

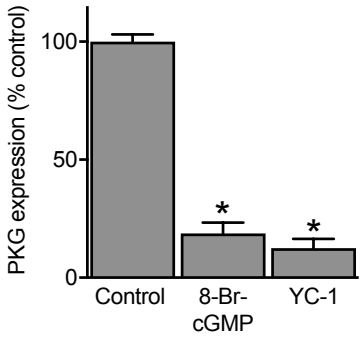

Supplementary Fig. S1. PPAECs display intact NO-cGMP-PKG signaling since treatment with 8-Br-cGMP (500 μM), or YC-1 for 72hrs reduced PKG expression (N=6-9). *P< 0.05 by one-way analysis of variance (ANOVA), data represent means ± SEM.

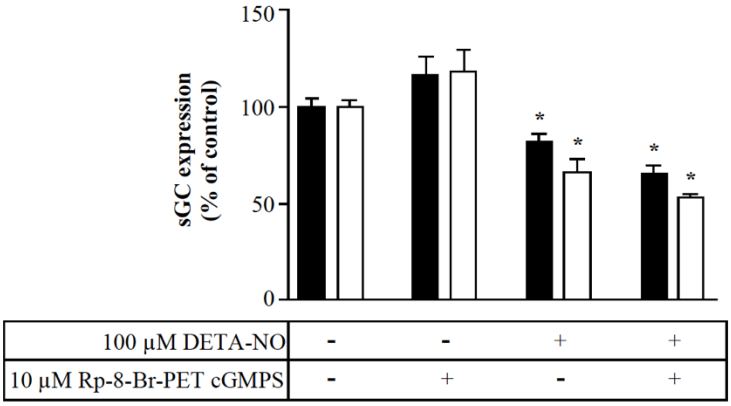

Supplementary Fig. S2. Inhibition of PKG does not prevent DETA-NO induced downregulation of sGCα_1 and sGC β_1. Treatment of PPAECs for 72h with either 100 μM DETA-NO, or with the PKG inhibitor Rp-8-Br-PET-cGMPS (10 μM), or a combination thereof resulted in down regulation of sGCα_1 (solid bars) and sGCβ_1 (open bars) level that could not be reversed by Rp-8-Br-PET-cGMPS. *P< 0.05 by one-way analysis of variance (ANOVA), data represent means ± SEM

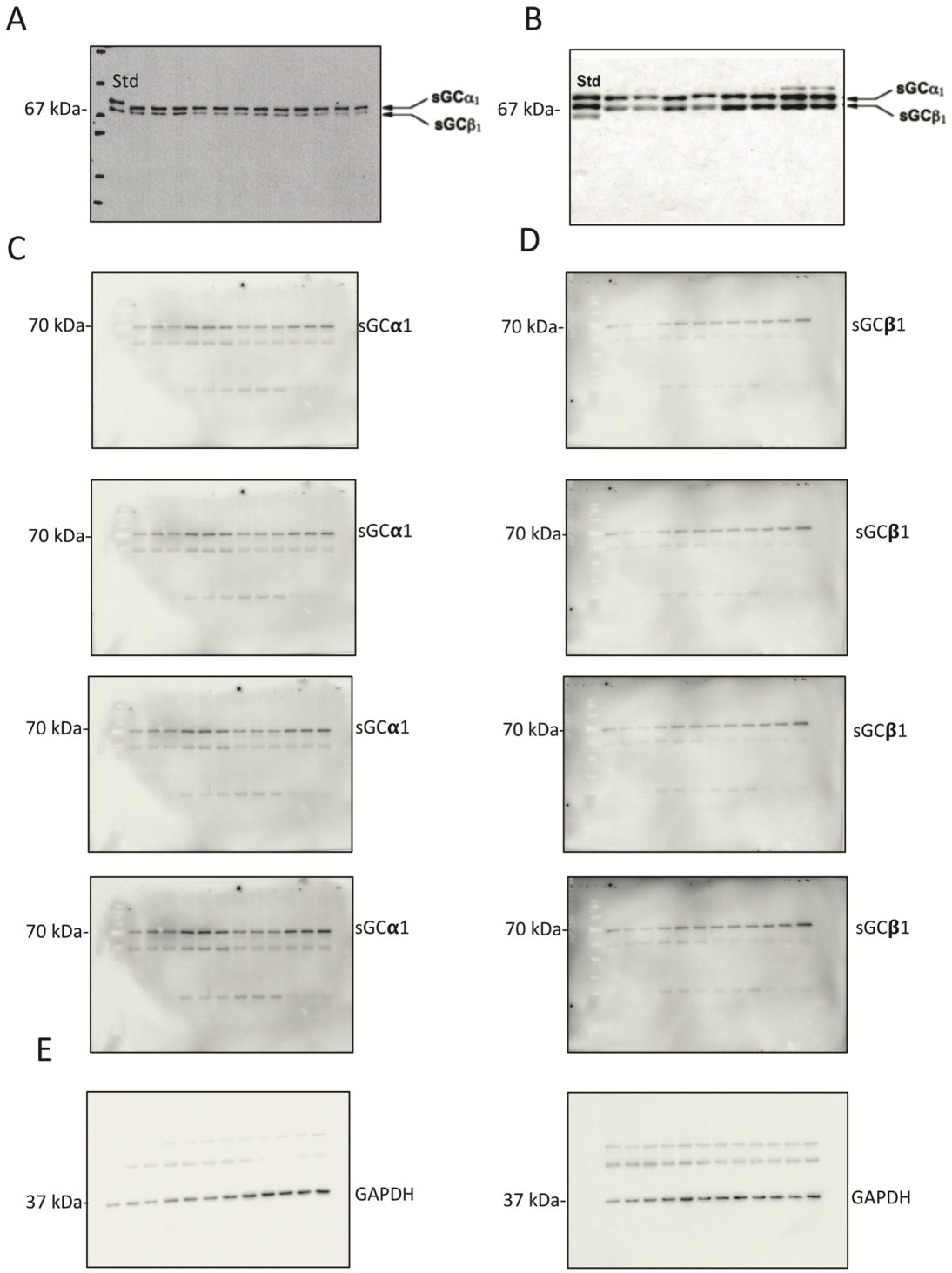

Supplementary Fig. S3. Representative Immune detection blots of controls, $sGC\alpha_1$ and $sGC\beta_1$. A. PPAECs. B. Mouse. C-E. ARDS (Multiple exposures).

5

FROM SINGLE DRUG TARGETS TO SYNERGISTIC NETWORK PHARMACOLOGY IN ISCHEMIC STROKE

Casas AI, Hassan AA, Larsen SJ, Gomez-Rangel V, **Elbatreek M**, Kleikers PWM, et al. From single drug targets to synergistic network pharmacology in ischemic stroke. Proc Natl Acad Sci U S A. 2019.

Significance

Current one drug–one target–one disease approaches in drug discovery have become increasingly inefficient. Network pharmacology defines disease mechanisms as networks best targeted by multiple, synergistic drugs. Using the high unmet medical need indication stroke, we here develop an integrative in silico approach based on a primary target, NADPH oxidase type 4, to identify a mechanistically related cotarget, NO synthase, for network pharmacology. Indeed, we validate both in vivo and in vitro, including humans, that both NOX4 and NOS inhibition is highly synergistic, leading to a significant reduction of infarct volume, direct neuroprotection, and blood–brain-barrier stabilization. This systems medicine approach provides a ground plan to decrease current failure in the field by being implemented in other complex indications.

Abstract

Drug discovery faces an efficacy crisis to which ineffective mainly single-target and symptom-based rather than mechanistic approaches have contributed. We here explore a mechanism-based disease definition for network pharmacology. Beginning with a primary causal target, we extend this to a second using guilt-by-association analysis. We then validate our prediction and explore synergy using both cellular in vitro and mouse in vivo models. As a disease model we chose ischemic stroke, one of the highest unmet medical need indications in medicine, and reactive oxygen species forming NADPH oxidase type 4 (Nox4) as a primary causal therapeutic target. For network analysis, we use classical protein–protein interactions but also metabolite-dependent interactions. Based on this protein–metabolite network, we conduct a gene ontology-based semantic similarity ranking to find suitable synergistic cotargets for network pharmacology. We identify the nitric oxide synthase (Nos1 to 3) gene family as the closest target to Nox4. Indeed, when combining a NOS and a NOX inhibitor at subthreshold concentrations, we observe pharmacological synergy as evidenced by reduced cell death, reduced infarct size, stabilized blood–brain barrier, reduced reoxygenation-induced leakage, and preserved neuromotor function, all in a supraadditive manner. Thus, protein–metabolite network analysis, for example guilt by association, can predict and pair synergistic mechanistic disease targets for systems medicine-driven network pharmacology. Such approaches may in the future reduce the risk of failure in single-target and symptom-based drug discovery and therapy.

In drug discovery, a “one disease–one target–one drug” approach is common practice, primarily to simplify compound screening, reduce unwanted side effects, and simplify registration (1). This approach, however, oversimplifies disease mechanisms, which are in fact complex subnetworks within the interactome (2, 3). Moreover, disease definitions are mostly symptom- rather than mechanism-based, and hence the therapeutics are likewise. Not surprisingly, drug discovery has thus become increasingly inefficient (4). Conversely, systems medicine and network pharmacology define diseases according to causal mechanisms (5, 6). Moreover, network pharmacology aims to further enhance this by targeting not only a single component within such a network but by combining drugs within these networks with the aim of achieving synergy and dose reduction (7). However, most network databases are curated (8); the de novo identification of such networks is only in its beginning. De novo network enrichment from a single primary validated target toward at least one secondary target holds high promise for systems medicine (9) but is currently not possible.

To address this challenge, we designed an approach that (i) is integrative, (ii) is based on the network pharmacology paradigm, (iii) predicts targets instead of drugs, (iv) is validated through experiment, and (v) is readily applicable by a broad range of biomedical scientists. In fact, our approach can be established as a powerful tool and therefore implemented in novel, complex, and frequently unexpected indications where already-marketed drugs can be repurposed, leading to new therapies. Our strategy amends the limitations of previous approaches, for example, simple pairwise combination of drugs as opposed to targeting networks (10, 11), or combining drugs, which may have different off-target effects, rather than drug targets (10⇓–12). Furthermore, most proposed computational methods have not been validated experimentally for de novo predictions (10⇓⇓⇓–14). Moreover, most of these methods rely on drug similarity signatures extracted from chemical structures, targets, and side effect profiles, introducing a potential bias toward the pharmacological classes currently represented in knowledge bases (15) and limiting their applicability to de novo candidate discovery (16).

We therefore here develop a simple and integrative in silico approach to pair an existing validated primary causal therapeutic target with a synergistic cotarget within a network pharmacology strategy. We importantly validate our prediction both in vitro

and in vivo, including a suitable in vitro human model. As a disease model for this we chose ischemic stroke, a multifactorial high unmet medical need indication for which no neuroprotective therapy is currently available. As a mechanistic starting point (node), we selected the reactive oxygen-forming enzyme NADPH oxidase type 4 (NOX4), a preclinically highly validated target directly involved in neurotoxicity and poststroke blood–brain barrier dysfunction (17, 18).

Results

Guilt-by-Association Analysis and Network Construction.

To identify synergistic and mechanistically related cotargets for NOX4, we employed a guilt-by-association analysis on a multilayered molecular interaction network. Since many signaling events are governed by intermediate metabolites rather than protein–protein interactions (19), we considered this approach alone as insufficient to search for secondary targets. We therefore combined protein–protein interactions with protein–metabolite interactions to overcome such a potential bias or limitation.

We adopted a bottom-up approach consisting of three interacting computational modules starting from a well-known clinical target in stroke, NOX4 (17), as our primary target protein and seed node (Fig. 1). In module 1, we expanded from this seed node to obtain a network of candidate targets and related metabolites, resulting in five metabolites which were extended to their interactors, yielding 537 proteins. The main product of Nox4 (20), hydrogen peroxide (H_2O_2), and the substrate, oxygen (O_2), were manually added due to their absence from the Human Metabolome Database (HMDB), and a curation request was sent to the database. As a filtering step for narrowing down the interactions search space, drug–target interactions were used, resulting in 166 potential druggable target proteins. In module 2, a protein–protein interaction network was constructed based on the previously obtained druggable target proteins (Fig. 1). Subsequently, networks from modules 1 and 2 were combined to obtain a two-layered network determining the closest interaction partners of our primary target by means of guilt by association (21). Hence, several levels of connectedness to NOX4 were observed, via direct protein interactions or indirect metabolic interactions (Fig. 2A), of which we consider the highest level, including nine proteins, as suitable

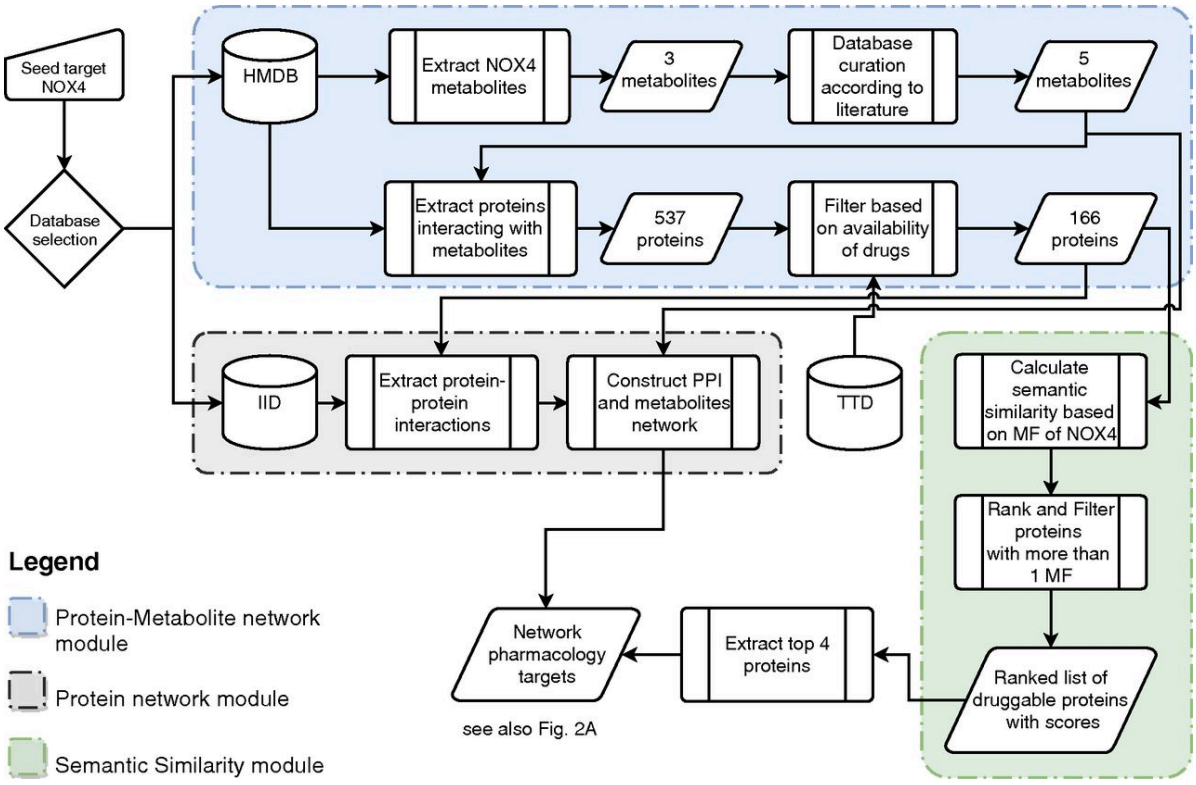

Fig. 1.
Computational workflow for target prioritization via network pharmacology. The computational target prioritization pipeline consists of three interdependent modules. The blue module extracts the metabolites interacting with the protein NOX4 from the Human Metabolome Database, performs curation of the metabolites, extracts the proteins interacting with them, and filters them based on the availability of drugs from the Therapeutic Target Database (TTD). The gray module uses the Integrated Interaction Database (IID) to extract protein–protein interactions of the proteins yielded by the blue module and constructs a network out of them. The green module calculates gene ontology-based semantic similarity scores of the output of the blue module compared with NOX4 using molecular function (MF) annotations, ranks the proteins based on their similarity scores, and excludes proteins with less than one molecular function. The output of the green module is used to annotate the network with the top four proteins.

NOX4-synergistic targets (Table 1). The full list of protein connectedness is reported in SI Appendix, Table S2.

Semantic Similarity of Gene Ontology Terms Affirms Network Analysis Results.

Semantic similarity quantifies the closeness or relatedness of two strings or terms, in our case the different gene ontology (GO) molecular function annotations (22). In module 3 of our approach (Fig. 1), we computed a single score measuring the similarity

of each GO term pair, which was then employed to compare the functional relatedness of two proteins. In brief, the functional relatedness score of two proteins was calculated by combining the similarity scores of every possible pair of GO terms annotating the two proteins. For scoring term pairs, we used the Wang et al. method (23) due to its ability to infer similarity according to the GO hierarchy, and not only the immediate terms in comparison. To combine these scores into the functional relatedness score of two proteins, we used the best average match strategy, as it accounts for both similar and dissimilar terms and is less affected by the number of terms available for comparison (22). Based on the assumption that functions of proteins act as a proxy for structural and biological similarity, we ranked the proteins according to their functional relatedness to NOX4 calculated based on GO similarity scores. Finally, the candidate proteins were filtered to extract the top 10 targets functionally most similar to NOX4 (Fig. 2B).

The intersection of the outcome of the semantic analysis with the list of the most connected targets from the network analysis narrowed down the candidate list of targets to only four: CYBB, NOS2, NOS3, and NOS1, which ranked as the topmost functionally similar drug targets, with similarity scores based on the molecular functions from the GO annotations of 0.87, 0.70, 0.67, and 0.67, respectively (Fig. 2 B and C). NOX1 also showed an equivalent score to NOS1; however, previous studies using a combined preclinical metaanalysis described that NOX1 plays no role in brain ischemia (24). Moreover, NOX4KO mice treated with a NOX inhibitor showed no additional effect, suggesting no additional NOX1-dependent mechanism in stroke (17). Having predicted a close connection between NOX4 and the NOS enzyme family by in silico hybrid protein–metabolic network analysis, we next wanted to validate our finding stepwise, first in vitro, then in vivo, with respect to mechanistic synergy and thus applicability for network pharmacology.

In Vitro Cotarget Validation and Drug Identification.

For in vitro validation, we used two models: an organotypic hippocampal culture (OHC) and human brain microvascular endothelial cells as a blood–brain barrier model. In the OHC model, oxygen and glucose deprivation (OGD) followed by reoxygenation (Fig. 3A) resulted in the increased expression of our primary target, NOX4 (17, 18) (Fig. 3B),

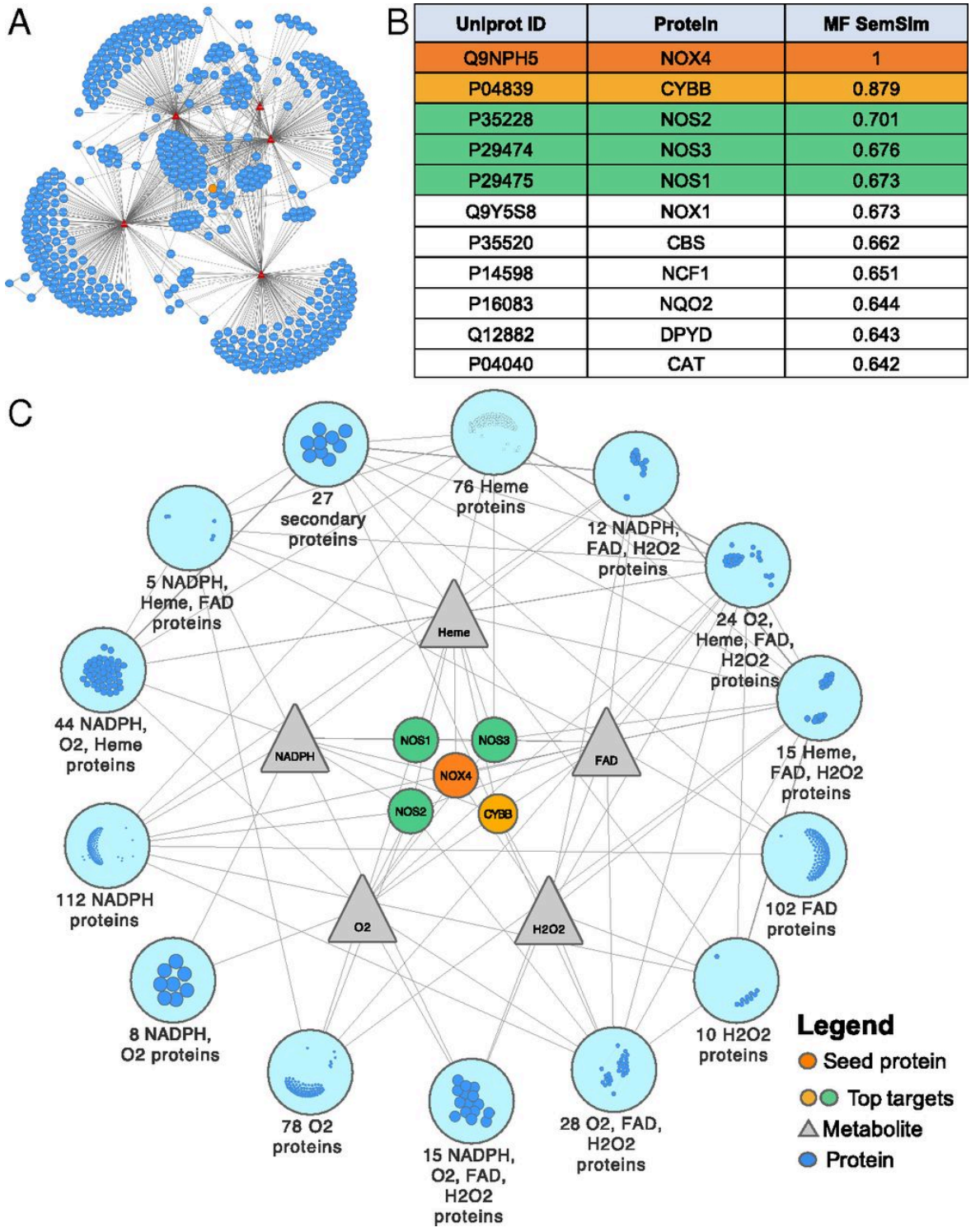

Uniprot ID	Protein	MF SemSim
Q9NPH5	NOX4	1
P04839	CYBB	0.879
P35228	NOS2	0.701
P29474	NOS3	0.676
P29475	NOS1	0.673
Q9Y5S8	NOX1	0.673
P35520	CBS	0.662
P14598	NCF1	0.651
P16083	NQO2	0.644
Q12882	DPYD	0.643
P04040	CAT	0.642

Fig. 2.
Integrated NOX4-extended multilayer network of biomolecular interactions used for candidate extraction and the involved protein semantic similarity ranking. (A) The full network constructed using the primary protein, NOX4 (orange node), connected to its direct metabolic interactors (red nodes), which have been linked to the proteins (blue nodes) interacting with them. We also show all protein–protein and metabolite–protein interactions (gray edges). (B) The semantic similarity ranking based on molecular functions (MF SemSim) of proteins with the top four similar proteins is highlighted. (C)

The simplified network with only the primary protein, and the top four similar proteins and metabolites shown individually, while the rest of the proteins are grouped as modules and their interactions are merged.

Table 1. Network proteins ranked according to their connectedness to NOX4 through its metabolites.

Protein symbol	Protein name	Uniprot ID	Connectedness to NOX4
NOS1	Nitric oxide synthase, brain	P29475	4
NOS2	Nitric oxide synthase, inducible	P35228	4
NOS3	Nitric oxide synthase, endothelial	P29474	4
HMOX1	Heme oxygenase 1	P09601	4
HMOX2	Heme oxygenase 2	P30519	4
DUOX1	Dual oxidase 1	Q9NRD9	4
DUOX2	Dual oxidase 2	Q9NRD8	4
PPOX	Protoporphyrinogen oxidase	P50336	4
AOX1	Aldehyde oxidase	Q06278	4
N=78	See supplemental material	-	3
N=70	See supplemental material	-	2
N=378	See supplemental material	-	1

Proteins n = 10 to n = 378 are included in SI Appendix, Table S1.

and all different NOS isoforms (Fig. 3C) within 2, 4, 8, 12, and 24 h post-OGD. Combinatory treatment with subthreshold concentrations of the NOX4 inhibitor GKT136901 (0.1 μM) and the NOS inhibitor L-NAME (0.3 μM) significantly reduced cell death (Fig. 3D) and formation of reactive oxygen and nitrogen species 24 h post-OGD,

while individual treatment with these subthreshold concentrations had no effect (Fig. 3E). Likewise, early kinetics (15-min) assessment of reactive oxygen species (ROS) formation postcotreatment reflected a significant reduction compared with single therapies (SI Appendix, Fig. S1). Similarly, in the human blood–brain barrier model, cotreatment with the same subthreshold concentrations of GKT136901 (0.1 μM) and L-NAME (0.3 μM) reduced cell death (Fig. 3F) and prevented the increase in permeability after hypoxia (Fig. 3G). These data validated both the mechanism-based nature of NOX4 and NOS as a target and their in silico predicted synergistic interaction, since chosen monotherapies were not significantly effective.

In Vivo Validation of Network Pharmacology for Clinical Translation.

To validate our network pharmacology approach in an in vivo model relevant for clinical translation, we used the mouse occlusion of the middle cerebral artery (MCAO) model in the absence or presence of GKT136901 (10 mg/kg) or L-NAME (3 mg/kg). Due to the many translational failures in stroke (25), the Stroke Treatment Academic Industry Roundtable (STAIR) established a set of guidelines to improve the success rate. Following these STAIR criteria, we assessed both a transient and permanent model, male and female, old and young mice. First, in transient MCAO, single subthreshold treatments showed no neuroprotection (Fig. 4A) but combinatory treatment significantly reduced brain infarctions compared with controls (Fig. 4A), both at 1 h and, importantly (26), 3 h poststroke (Fig. 4A), suggesting a wide therapeutic time window in agreement with our in vitro expression kinetics. Similar effects in a permanent MCAO model suggested therapeutic effect independent of reperfusion (Fig. 4A), and thus promise for patients where thrombolysis or/and thrombectomy is not recommended. In humans, stroke mostly occurs in the elderly population, and patient prognosis is

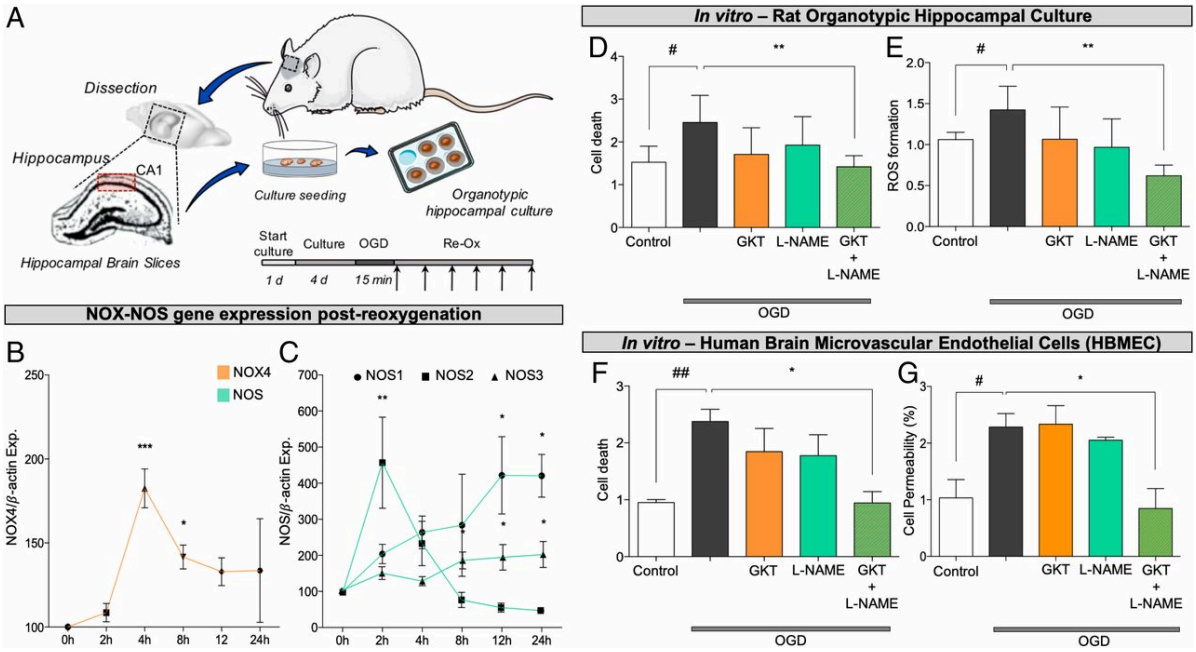

Fig. 3.
In vitro cotarget validation and drug identification of NOX4 and NOS inhibitors as a combinatory treatment. (A) Organotypic hippocampal cultures prepared from hippocampal slices were cultured for 4 d and subsequently subjected to 15 min of OGD period followed by 24-h treatment. Samples for gene expression detection were collected at 0, 2, 4, 8, 12, and 24 h post-OGD. (B) NOX4 expression was up-regulated at 4 and 8 h in comparison with the beginning of the ischemia period (*P < 0.05, ***P < 0.001; n = 3). (C) Inducible NOS (NOS2; square) was up-regulated only in the first 2 h post-OGD, while neuronal NOS (NOS1; circle) was up-regulated in the final 12 to 24 h after the OGD period. Similarly, endothelial NOS (NOS3; triangle) was also significantly up-regulated at 8, 12, and 24 h post-OGD (*P < 0.05, **P < 0.01; n = 4). Gene expression was normalized using β-actin as housekeeping gene. (D) Cell death was significantly reduced in OHCs treated with GKT136901 (0.01 μM) and L-NAME (0.3 μM) in combination (**P < 0.01; n = 8; green slashed bar) in comparison with control slices (#P < 0.05 with respect to basal; n = 8; gray bar). Individual treatments show no effect. (E) ROS formation was also significantly decreased in OHCs treated with the combination of GKT136901 (0.01 μM) and L-NAME (0.3 μM) in comparison with nontreated slices. Again, individual treatments show no effect on cell death. #P < 0.05 compared with basal conditions (gray bar; n = 5); **P < 0.01 with respect to nontreated slices (gray bar; n = 5). (F) Combinatory treatment of GKT136901 and L-NAME increases cell viability in human brain microvascular endothelial cells subjected to hypoxia/reoxygenation (Re-Ox). ##P < 0.01 with respect to basal conditions (n = 4; gray bar); *P < 0.05 with respect to nontreated cells (n = 4; green slashed bar). (G) Cell permeability was assessed by measuring Evans blue fluorescence post-OGD. Evans blue diffusion was significantly reduced in cells treated with GKT136901 (0.01 μM) and L-NAME (0.3 μM) in combination (#P < 0.05; n = 4; gray bar) in comparison with nontreated cells (*P < 0.05; n = 4; green slashed bar). Error bars are mean ± SD.

directly influenced by age (27). Thus, we confirmed these effects in aged female and male mice (Fig. 4A). Although smaller infarct sizes poststroke is an important readout, neurofunctional outcome and quality of life postischemia are the main clinical parameters. Hence, we additionally assessed three independent neuromotor functioning tests in the adult mice treated 1 and 3 h poststroke together with the aged mice model: the Bederson score (Fig. 4B), elevated body swing test (Fig. 4C), and four-limb hanging wire test (Fig. 4D), which all were significantly improved 1 h postoperation (PO), and Bederson and the four-limb test also 3 h PO (Fig. 4 C–E). Monotherapies were only assessed 1 h poststroke treatment in adult mice due to ethical restrictions (Material and Methods). Thus, dual NOX/NOS inhibition poststroke leads to a potent synergistic, mechanism-based, and neuroprotective effect, further confirming that both targets are causally linked in a clinically translatable manner.

Prevention of Blood–Brain Barrier Disruption and ROS Formation upon Stroke Treatment.

The cerebral vasculature, which is critical for the maintenance of the blood–brain barrier (BBB), is particularly susceptible to oxidative stress (28, 29). To test whether dual inhibition of NOX/NOS leads to the blood–brain barrier phenotype, we assessed the integrity of the blood–brain barrier after ischemic stroke. In line with previous findings, combinatory treatment significantly reduced blood–brain barrier disruption upon stroke compared with nontreated mice (Fig. 4E).

To link the neuroprotective effect on the enzymatic activity of both ROS sources, we measured oxidative stress and N-Tyr formation in brain tissue cryosections. ROS generation and N-Tyr formation were dramatically reduced in treated mice (Fig. 4F) after 24 h of cotreatment (Fig. 4G), demonstrating a direct link in ROS reduction and a broad neuroprotective effect (SI Appendix, Figs. S2 and S3).

Discussion

We here report a proof of concept for an in silico discovery approach to pair a single validated therapeutic drug target with another mechanistically related one for synergistic network pharmacology. Our multilayered interactome analysis including metabolites coupled with semantic similarity ranking detects pathomechanistically

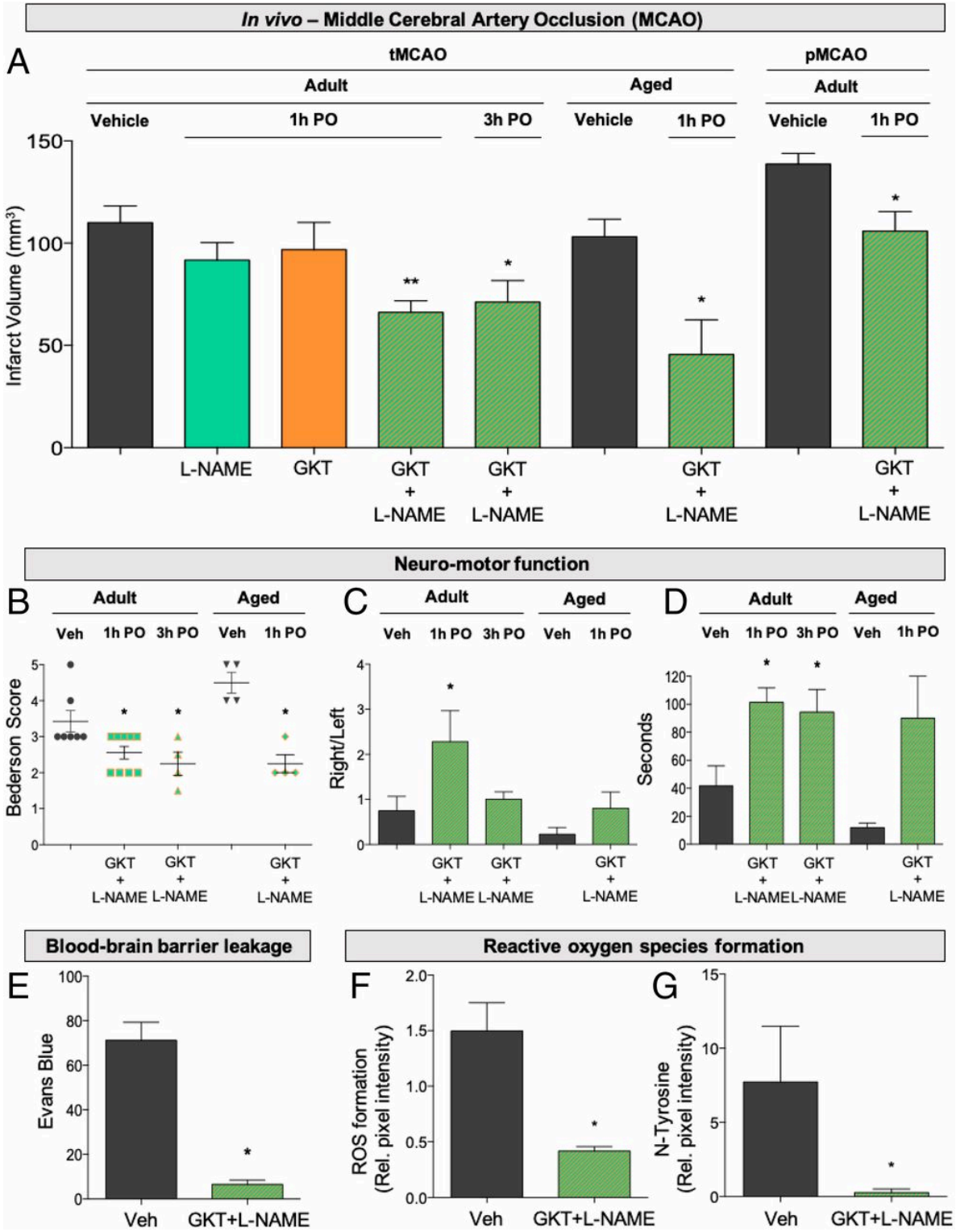

Fig. 4.
In vivo validation of network pharmacology for clinical translation. (A) Twenty-four hours after tMCAO infarct size was reduced in mice treated with GKT136901 (10 mg/kg) and L-NAME (3 mg/kg) in combination 1 h (**P < 0.01; n = 6) and 3 h poststroke (*P < 0.05; n = 5), while individual treatment showed no effect in reduction of infarct size. Infarct volume was also significantly reduced in aged animals treated with the combination (GKT+L-NAME) 1 h poststroke (**P < 0.01; n = 5). Similarly, combinatory

treatment decreased infarct volume after permanent occlusion of the MCA in adult mice (*P < 0.05; n = 5). (B) With respect to the neurological outcome of the combinatory treatment in surviving mice, neurological outcome (Bederson score) was improved in the adult mice treated 1 h poststroke (*P < 0.05; n = 9), 3 h poststroke (*P < 0.05; n = 5), and the aged model (*P < 0.05; n = 4). (C) Likewise, the elevated body swing test indicated a significant increase for the right swing number/total swing number ratio in adult mice treated 1 h PO (*P < 0.05; n = 9) but not in the other groups. (D) Significantly improved motor outcome was detected after four-limb hanging test in all groups: 1 h PO (*P < 0.05; n = 9), 3 h PO (*P < 0.05; n = 5), and aged animals (*P < 0.05; n = 4). (E) Blood–brain barrier integrity assessed by Evans blue extravasation was preserved in treated animals compared with nontreated mice at day 1 after 1 h of tMCAO (*P < 0.05; n = 4). (F) Treated mice showed decreased ROS formation compared with their respective nontreated animals (*P < 0.05; n = 4). (G) N-Tyr–positive cells were significantly reduced with the combinatory therapy compared with nontreated mice. (*P < 0.05; n = 4). Error bars are mean ± SD.

related proteins which can be cotargeted. Using this approach, we extend NOX4 to the closest functional neighbor gene, NOS.

In search for a secondary, synergistic, and causal network pharmacology target prediction, data-driven or modeling-based techniques have been developed. A data-driven approach integrated multiple sources of data on drugs such as target proteins and their pathways, medical indications, therapeutic effects, and side effects (30). DrugComboRanker prioritizes synergistic drug combinations (31) by constructing a functional drug network, although restricted to cancer drug–gene profiles. Here, community detection is performed via Bayesian nonnegative matrix factorization and, finally, similar drugs are inferred based on an adjacency matrix built from the drug–target network.

With respect to modeling, a network-based approach ranked combinations of proteins using a topological score calculated from an integrated protein–protein interaction (PPI) network constructed and enriched with gene expression data from a singular disease phenotype (13). Random forests were used to predict drug combinations by exploiting network features generated from PPI data, and drug chemical and pharmacogenomic features from drug-induced expression profiles (11). MASCOT is a model-driven machine-learning algorithm that leverages curated dynamic models of signaling networks and their disease states to predict synergistic targets of a desired therapeutic effect (14). In comparison with all these previous reports, our two-step approach utilized experimental databases on multilevel molecular

networks in a rather simple and generic manner, and our predictions were experimentally validated both in vitro and in vivo.

PPI networks or interactomes have been commonly used to understand complex disease mechanisms (32⇓⇓⇓–36). However, PPI networks are just one level of molecular interaction networks. Most signaling events are not due to wild-type PPIs but involve metabolites or metabolic protein modifications. We therefore used protein–metabolite networks in conjunction with PPI networks. In addition, this solved another issue of molecular interaction databases. Current databases suffer from selection and detection biases, high rates of false positives, and low rates of coverage (5, 37).

However, metabolome databases still have severe shortcomings. When querying the most comprehensive HMDB with seven additional key signaling enzymes, key metabolites were consistently missing, namely for soluble guanylate cyclase, the substrate, GTP, and the product, 2′,5′-cGMP, as well as GMP, cAMP, and 2′,3′-cGMP being wrongly listed. Thus, our approach will improve considerably once these or other metabolic databases are intensely curated and become more complete.

Although our method is generic and can be applied to other cases in concept, there are restrictions. For instance, the current computational pipeline supports one seed target; however, it is generally applicable to more than one seed target. For multiple seed targets, one would have to look for druggable candidates with the shortest average distance in the graph representation of the integrated network to all seeds.

In the network analysis step, the patchiness of the data sources may affect predictions, while for the semantic similarity, the availability and accuracy of GO annotations may impact on the ranking. In addition, we report only a single validated application of our method, and further use cases will be needed. In fact, NOX4-related targets, namely NCF1, NQO2, and DPYD, might also show potential. Targeting NCF1, also known as p47 (NOX subunit), may lead to indirect NOX4 activation. However, modulating NCF1 is so far not possible, since protein–protein interaction inhibitors proved noneffective and no further network pharmacology strategy could be achieved (38). Moreover, ribosyl dihydronicotinamide dehydrogenase (NQO2), a ROS-generating enzyme, shows a direct acetaminophen side effect, while this drug has been shown as protective in stroke, demonstrating a direct link (39). However, when weighing NQO2 and NOS as a cotarget of NOX4, we would still prefer NOS, because

with NOX4 and NQO2 we would both target ROS formation with possibly no synergy but rather additive effects.

We thus validated the therapeutic applicability of our in silico network pharmacology hypothesis both in vitro and in vivo by coadministering both a NOX inhibitor and NOS inhibitor, respectively, in three different species including a human BBB model. Of high translational relevance, combining a NOX and NOS inhibitor conveyed in direct neuroprotection in three different brain ischemia models, rat organotypic hippocampal culture, transient and permanent MCAO in mice, and human brain microvascular cells as a BBB model. Importantly, this was achieved at concentrations and doses, respectively, that on their own were ineffective. This will allow extension of the clinical translation of NOX4 inhibition in stroke to be enhanced in efficacy and safety by lowering in risk of any potential side effects, increasing mechanistic-based synergy and reducing the number needed to treat. Thus, our multitargeted approach therefore focuses on NOX4 inhibition coadministered with a NOS inhibitor while, due to synergy, reducing the doses/concentrations of both drugs to individual subthreshold levels.

On a mechanistic level, interaction between reactive oxygen species and NO, for example, to toxify NO via intermediate peroxynitrite formation, has been shown before (40). The source of ROS, however, has not always been identified (41⇓–43). Also, the signaling networks of NOS/NO on the one side and ROS formation and ROS targets on the other have been annotated as rather independent. Here, we show that, at least in disease, both networks represent subnetworks of the same common mechanism that involves both NOS and NOX4. At least NOX4 is one relevant ROS source interacting with NO, or NO's downstream signaling and online pathways have been suggested for curation, as far as possible. Importantly, this does not imply that all ROS sources will interact as well with NOS. Such assumptions represent a shortcoming of the current curated NOS and ROS pathways, as they combine, for example, all ROS sources and all ROS targets into one scheme. With respect to the relevant NOS isoform, the best characterized and validated is NOS1 (44), whereas NOS3 is rather protective (45) and NOS2 expression commences only 12 h after the onset of the stroke in an in vivo rat model (46), while our findings suggest different expression in mice primarily due to model and species differences.

With respect to clinical application there are two other NOS inhibitors worth being considered apart from L-NAME, which has been tested for the longest time. First, Vasopharm is developing VAS203 as a NOS common inhibitor currently entering phase III clinical trials for traumatic brain injury. Since it is a NOS common inhibitor like L-NAME it has a similar spectrum, but concerns have arisen with respect to covalent off-target effects (47, 48) and depression of kidney function (49). Second, S-methyl-L-thiocitrulline has also been tested in humans but appears to have only a limited spectrum, possibly limited to NOS1 (1), while our in silico prediction ranked NOS2 > NOS3 > NOS1. Such isoform-selective inhibitors will certainly be of interest in future studies aiming at deciphering the contribution of individual NOS isoforms in ROS–NO interaction.

Clearly, more de novo generated pathways as subgraphs of the interactome are necessary to eliminate such assumptions. Also, NOX4 generates H_2O_2, whereas typically superoxide, O_2^{-}, is considered the key interfering molecule with respect to NO. Moreover, NOX4 has also been identified as a positive indirect transcriptional regulator of the major H_2S-producing enzyme, cystathionine β-synthase (50), which plays a key role in the central nervous system and circulation linked to worse poststroke outcome (51). Thus, poststroke NOX4-dependent inhibition of the cystathionine β-synthase pathway may also result in at least additive effective effects in stroke within the same mechanistic network.

With respect to NOS1 to 3, the possibility exists that one of the isoforms may actually be protective. Importantly, the here-presented network approaches are by definition undirected, namely whether a cotarget needs to be inhibited or activated is not always immediately obvious. Chronically, NOS3 inhibition is certainly not of benefit (11); however, in an acute setting, even endothelial NOS-derived NO may for a time window where it interacts with NOX4-derived ROS be detrimental. Pan-NOS inhibition is almost as effective as NOS1 knockout. Thus, pharmacological validation will in many cases remain an essential component when interpreting and curating network pharmacology discovery results.

Thus, from a chemical point of view, the NOX4–NOS interaction that we predicted and validated was surprising, and may involve a hitherto underappreciated interaction of H_2O_2 with transition metal centers to form singlet oxygen (40, 52).

In conclusion, our present and other network pharmacology approaches (1, 53) provide a roadmap to reduce the risk of failure in single drug target development by moving toward multiple targeting of de novo causal networks to increase therapeutic efficacy and reduce individual drug dosing and possible side effects due to mechanism-based synergy (53, 54). We suggest extending our approach to other unmet medical need indications, where currently only single drug- or symptom-based approaches are available.

Material and Methods

Detailed experimental procedures are provided in SI Appendix, Material and Methods.

Study Design.

All animal experiments were performed after approval of the protocol by the Institutional Ethics Committee of the Autonomous University of Madrid according to European guidelines for the use and care of animals for research. The dropout rates were four mice in the vehicle groups [transient (t)MCAO, aged, permanent (p)MCAO, and Evans blue] versus three mice in different treatment groups (tMCAO and pMCAO) (SI Appendix, Table S2). Post hoc power analysis for adult mice is included in SI Appendix, Table S3.

Transient Occlusion of the Middle Cerebral Artery.

The model was previously described in ref. 17.

Human Brain Microvascular Endothelial Cells Subjected to Hypoxia.

Human brain microvascular endothelial cells (HBMECs) (Cell Systems) were cultured to ~90% confluence. Cell medium was replaced by non–FBS-containing medium (2 mL per well) following 6 h of hypoxia (94.8% N_2, 0.2% O_2, and 5% CO_2) and 24 h of reperfusion in the presence or absence of the pharmacological treatment (see SI Appendix for details).

Statistical Analysis.

All results obtained from the in vitro (hippocampal brain slices, OHCs, HBMECs) and in vivo (tMCAO) ischemia models were analyzed using Prism 5.0 software (GraphPad Software). Data were expressed as the means ± SEM of separate experiments. Statistical comparisons between groups were performed using one-way ANOVA, followed by a Newman–Keuls multiple-comparison test. Differences between two groups were considered significant at $P < 0.05$. Numbers of animals necessary to detect a standardized effect size on infarct volumes ≥0.2 (vehicle-treated control mice vs. treated mice) were determined via a priori sample size calculation with the following assumptions: $\alpha = 0.05$; $\beta = 0.2$; 20% SD of the mean. In each case, when only two groups were compared, the unpaired two-tailed Student's t test was applied followed by a Mann–Whitney U test, where significance was considered at $P < 0.05$.

Acknowledgments

This study was supported by the ERC (Advanced Investigator Grant 294683/RadMed and Proof-of-Concept Grant 737586/SAVEBRAIN, both to H.H.H.W.S.), Spanish Ministry of Economy and Competence (SAF2015-63935R to M.G.L.), Fondo de Investigaciones Sanitarias (Instituto de Salud Carlos III/Fondo Europeo de Desarrollo Regional) (Programa Miguel Servet: CP14/00008, PI16/00735), Fundación Mutua Madrileña (J.E.), short-term scientific missions by the COST Actions EU-ROS and OpenMultiMed, and Kootstra Talented Fellowship (UM) (to A.I.C.). J.B.'s work was financially supported by VILLUM Young Investigator Grant 13154. J.B. and H.H.H.W.S. also received support from H2020 Project 777111-REPO-TRIAL.

Author contributions: A.I.C., M.G.L., J.B., and H.H.H.W.S. designed research; A.I.C., A.A.H., S.J.L., V.G.-R., and M.E. performed research; J.E., M.G.L., and J.B. contributed new reagents/analytic tools; A.I.C., A.A.H., S.J.L., P.W.M.K., E.G., and J.B. analyzed data; and A.I.C., A.A.H., S.J.L., E.G., J.E., M.G.L., J.B., and H.H.H.W.S. wrote the paper.

Conflict of interest statement: H.H.H.W.S. is a cofounder of a biotech company, Vasopharm, engaged in the development of small-molecule NOS inhibitors, currently in stage III clinical development. However, H.H.H.W.S. has no operative role in the company and holds less than 1% of shares.

References

1. Yildirim MA, Goh K-I, Cusick ME, Barabási A-L, Vidal M (2007) Drug-target network. *Nat Biotechnol* 25(10):1119–1126.

2. Aguirre-Plans J, et al. (2018) Proximal Pathway Enrichment Analysis for Targeting Comorbid Diseases via Network Endopharmacology. *Pharmaceuticals (Basel)* 11(3):61.

3. Hopkins AL (2007) Network pharmacology. *Nat Biotechnol* 25(10):1110–1111.

4. Scannell JW, Blanckley A, Boldon H, Warrington B (2012) Diagnosing the decline in pharmaceutical R&D efficiency. *Nat Rev Drug Discov* 11(3):191–200.

5. Menche J, et al. (2015) Disease networks. Uncovering disease-disease relationships through the incomplete interactome. *Science* 347(6224):1257601–1257601.

6. Langhauser F, et al. (2018) A diseasome cluster-based drug repurposing of soluble guanylate cyclase activators from smooth muscle relaxation to direct neuroprotection. *NPJ Syst Biol Appl* 4(1):8.

7. Barabási A-L, Oltvai ZN (2004) Network biology: understanding the cell's functional organization. *Nat Rev Genet* 5(2):101–113.

8. Batra R, et al. (2017) On the performance of de novo pathway enrichment. *NPJ Syst Biol Appl* 3(1):6.

9. Alcaraz N, et al. (2017) De novo pathway-based biomarker identification. *Nucleic Acids Res* 45(16):e151–e151.

10. Koduru P, Chaganti R (1988) Congenital chromosome breakage clusters within Giemsa-light bands and identifies sites of chromatin instability. *Cytogenet Cell Genet* 49(4):269–274.

11. Li X, et al. (2017) Prediction of synergistic anti-cancer drug combinations based on drug target network and drug induced gene expression profiles. *Artif Intell Med* 83:35–43.

12. Meladze VG (1985) [Temporal characteristics of the autoregulation process of local cerebral blood flow in hypo- and hypertension]. *Patol Fiziol Eksp Ter* (4):29–32.

13. Vitali F, Mulas F, Marini P, Bellazzi R (2013) Network-based target ranking for polypharmacological therapies. *J Biomed Inform* 46(5):876–881.

14. Chua HE, Bhowmick SS, Tucker-Kellogg L (2017) Synergistic target combination prediction from curated signaling networks: Machine learning meets systems biology and pharmacology. *Methods* 129:60–80.

15. Vilar S, Hripcsak G (2017) The role of drug profiles as similarity metrics: applications to repurposing, adverse effects detection and drug-drug interactions. *Brief Bioinformatics* 18(4):670–681.

16. Guney E (2017) Reproducible drug repurposing: when similarity does not suffice. *Pac Symp Biocomput* 22:132–143.

17. Casas AI, et al. (2017) NOX4-dependent neuronal autotoxicity and BBB breakdown explain the superior sensitivity of the brain to ischemic damage. *Proc Natl Acad Sci USA* 114(46):12315–12320.

18. Kleinschnitz C, et al. (2010) Post-stroke inhibition of induced NADPH oxidase type 4 prevents oxidative stress and neurodegeneration. *PLoS Biol* 8(9):e1000479.

19. Li F, Xu W, Zhao S (2013) Regulatory roles of metabolites in cell signaling networks. *J Genet Genomics* 40(7):367–374.

20. Nisimoto Y, Diebold BA, Cosentino-Gomes D, Constentino-Gomes D, Lambeth JD (2014) Nox4: a hydrogen peroxide-generating oxygen sensor. *Biochemistry* 53(31):5111–5120.

21. Piovesan D, Giollo M, Ferrari C, Tosatto SCE (2015) Protein function prediction using guilty by association from interaction networks. *Amino Acids* 47(12):2583–2592.

22. Wang JZ, Du Z, Payattakool R, Yu PS, Chen C-F (2007) A new method to measure the semantic similarity of GO terms. *Bioinformatics* 23(10):1274–1281.

23. Pesquita C, et al. (2008) Metrics for GO based protein semantic similarity: a systematic evaluation. *BMC Bioinformatics* 9 Suppl 5(Suppl 5):S4.

24. Kleikers PWM, et al. (2015) A combined pre-clinical meta-analysis and randomized confirmatory trial approach to improve data validity for therapeutic target validation. *Sci Rep* 5(1):13428.

25. O'Collins VE, et al. (2006) 1,026 experimental treatments in acute stroke. *Ann Neurol* 59(3):467–477.

26. Peña ID, Borlongan C, Shen G, Davis W (2017) Strategies to Extend Thrombolytic Time Window for Ischemic Stroke Treatment: An Unmet Clinical Need. *J Stroke* 19(1):50–60.

27. Chen R-L, Balami JS, Esiri MM, Chen L-K, Buchan AM (2010) Ischemic stroke in the elderly: an overview of evidence. *Nat Rev Neurol* 6(5):256–265.

28. Lehner C, et al. (2011) Oxidative stress and blood-brain barrier dysfunction under particular consideration of matrix metalloproteinases. *Antioxid Redox Signal* 15(5):1305–1323.

29. Enciu A-M, Gherghiceanu M, Popescu BO (2013) Triggers and effectors of oxidative stress at blood-brain barrier level: relevance for brain ageing and neurodegeneration. *Oxid Med Cell Longev* 2013(10):297512–12.

30. Zhao X-M, et al. (2011) Prediction of drug combinations by integrating molecular and pharmacological data. *PLoS Comput Biol* 7(12):e1002323.

31. Huang L, et al. (2014) DrugComboRanker: drug combination discovery based on target network analysis. *Bioinformatics* 30(12):i228–36.

32. Vidal M, Cusick ME, Barabási A-L (2011) Interactome networks and human disease. *Cell* 144(6):986–998.

33. Futschik ME, Chaurasia G, Herzel H (2007) Comparison of human protein-protein interaction maps. *Bioinformatics* 23(5):605–611.

34. Lehne B, Schlitt T (2009) Protein-protein interaction databases: keeping up with growing interactomes. *Hum Genomics* 3(3):291–297.

35. Rolland T, et al. (2014) A proteome-scale map of the human interactome network. *Cell* 159(5):1212–1226.

36. Mehta V, Trinkle-Mulcahy L (2016) Recent advances in large-scale protein interactome mapping. *F1000Res* 5:782.

37. Amaral LAN (2008) A truer measure of our ignorance. *Proc Natl Acad Sci USA* 105(19):6795–6796.

38. Altenhöfer S, Radermacher KA, Kleikers PWM, Wingler K, Schmidt HHHW (2015) Evolution of NADPH Oxidase Inhibitors: Selectivity and Mechanisms for Target Engagement. *Antioxid Redox Signal* 23(5):406–427.

39. Miettinen TP, Björklund M (2014) NQO2 is a reactive oxygen species generating off-target for acetaminophen. *Mol Pharm* 11(12):4395–4404.

40. Radi R (2018) Oxygen radicals, nitric oxide, and peroxynitrite: Redox pathways in molecular medicine. *Proc Natl Acad Sci USA* 115(23):5839–5848.

41. Geiszt M (2006) NADPH oxidases: new kids on the block. *Cardiovasc Res* 71(2):289–299.

42. Espey MG, et al. (2002) A chemical perspective on the interplay between NO, reactive oxygen species, and reactive nitrogen oxide species. *Ann N Y Acad Sci* 962:195–206.

43. Ghezzi P, Jaquet V, Marcucci F, Schmidt HHHW (2017) The oxidative stress theory of disease: levels of evidence and epistemological aspects. *Br J Pharmacol* 174(12):1784–1796.

44. Kleinschnitz C, et al. (2016) NOS knockout or inhibition but not disrupting PSD-

95-NOS interaction protect against ischemic brain damage. *J Cereb Blood Flow Metab* 36(9):1508–1512.

45. Endres M, Laufs U, Liao JK, Moskowitz MA (2004) Targeting eNOS for stroke protection. *Trends Neurosci* 27(5):283–289.

46. Niwa M, et al. (2001) Time course of expression of three nitric oxide synthase isoforms after transient middle cerebral artery occlusion in rats. *Neurol Med Chir (Tokyo)* 41(2):63–72– discussion 72–3.

47. Dao VT-V, et al. (2015) Pharmacology and Clinical Drug Candidates in Redox Medicine. *Antioxid Redox Signal* 23(14):1113–1129.

48. Sun Q-A, Hess DT, Wang B, Miyagi M, Stamler JS (2012) Off-target thiol alkylation by the NADPH oxidase inhibitor 3-benzyl-7-(2-benzoxazolyl)thio-1,2,3-triazolo[4,5-d]pyrimidine (VAS2870). *Free Radic Biol Med* 52(9):1897–1902.

49. Ott C, et al. (2019) Effects of the nitric oxide synthase inhibitor ronopterin (VAS203) on renal function in healthy volunteers. *Br J Clin Pharmacol*. doi:10.1111/bcp.13870.

50. Mistry RK, et al. (2016) Transcriptional Regulation of Cystathionine-γ-Lyase in Endothelial Cells by NADPH Oxidase 4-Dependent Signaling. *J Biol Chem* 291(4):1774–1788.

51. Chan SJ, et al. (2015) Cystathionine β-synthase inhibition is a potential therapeutic approach to treatment of ischemic injury. *ASN Neuro* 7(2):175909141557871.

52. Noronha-Dutra AA, Epperlein MM, Woolf N (1993) Reaction of nitric oxide with hydrogen peroxide to produce potentially cytotoxic singlet oxygen as a model for nitric oxide-mediated killing. *FEBS Lett* 321(1):59–62.

53. Hopkins AL (2008) Network pharmacology: the next paradigm in drug discovery. *Nat Chem Biol* 4(11):682–690.

54. Tang J, Aittokallio T (2014) Network pharmacology strategies toward multi-target anticancer therapies: from computational models to experimental design principles. *Curr Pharm Des* 20(1):23–36.

Supplemental Material and Methods

Network analysis and semantic ranking

NOX4 was considered as initial stroke related target and primary protein. The goal is to identify more related targets *in silico* using publicly available molecular interaction databases. Since associated proteins can interact directly (physical protein-protein interactions) or indirectly (through downstream reactions through metabolites), we opted to cover the two data sources. Therefore, we integrated two databases: i) the Integrated Interactions Database (IID) (1) for protein-protein interactions, and ii) the Human Metabolome Database (HMDB) (2) for protein-metabolite interactions (See SI Appendix, **Table S4** for details on database versions, access dates, interactions, and evidence levels). Since IID is an integrated PPI database with experimentally detected interactions from several other PPI databases, predicted interactions and orthologous interactions; we chose to focus only on the experimentally detected interactions to limit the noise in our data. Integrating IID and HMDB gave rise to a two-layered network, which we constructed as follows: We first extracted the metabolites interacting with our primary target, NOX4, and using expert curation, we added important metabolites interactions that were missing from the HMDB database, namely oxygen (O_2) and hydrogen peroxide (H_2O_2). We subsequently extracted all proteins interacting with those metabolites yielding a two-layered NOX4-centric protein/metabolite-network. Since we are interested in identifying immediately clinically relevant targets, we filtered all proteins in the network to identify those annotated as targets of known drugs. To this end we utilized the Therapeutic Target Database (TTD) (See SI Appendix, **Table S4**) to obtain a list of druggable proteins, and we extracted the direct molecular interactions between them and thereby constructed the final, filtered network of potential targets. However, this network provides only a means of assessing the connectedness of proteins to our primary protein and not a quantitative measure to assess the functional similarity of candidate synergistic targets. Thus, we used a sematic analysis pipeline to rank the connected proteins. We utilized a strategy of scoring the similarity of molecular functions in the Gene Ontology terms of each of the proteins as opposed to those of NOX4 using the semantic the GOSim R software package (3). We used the Wang (4) method to compute the semantic similarity which yields a score in the range of 0 to 1, with 1 being identical to the primary protein. The Wang method is

an ontology-based approach where the sematic similarities of the GO terms are calculated based on their locations in the directed acyclic graph (DAG) representing the GO ontology. It defines the semantic value of each term based on the sum of the weighted contributions of all its ancestors, where closer ancestor terms have higher contribution, and which is used to calculate the semantic similarity between GO term pairs. The similarity between two proteins is then derived from the semantic similarities of all GO terms annotating both proteins. Finally, we used Cytoscape to visualize both the expanded and the reduced network with top targets annotated.

Study design

All animal experiments were performed after approval of the protocol by the institutional Ethics Committee of Autonomous University of Madrid (Madrid, Spain) according to the European Guidelines for the use and care of animals for research. All efforts were made to minimize animal suffering and to reduce the number of animals used in the experiments. Animals were housed under controlled conditions (22 ± 1°C, 55–65% humidity, 12h light-dark cycle), and have been given free access to water and standard laboratory chow. 8-16 week adult male and female mice and 1-year old mice (aged) were used for the *in vivo* animal study. Animals were excluded from end-point analyses if death occurred within 24h after tMCAO or pMCAO and if intracerebral haemorrhage occurred as macroscopically assessed during brain sampling. The drop-out rates were 4 mice in the vehicle groups (tMCAO, aged, pMCAO and Evans Blue) versus 3 mice in different treatment groups (tMCAO and pMCAO) (See SI Appendix, **Table S2**). Post-hoc power analysis for adult mice is included in SI Appendix, **Table S3**. 2-3 months old Sprague-Dawley rats were used for the i*n vitro* studies.

***Ex-vivo* acute model: Preparation of hippocampal brain slices and induction of oxygen and glucose deprivation**

Experiments were performed using hippocampal brain slices (HBS) from adult Sprague-Dawley rats (2-3 months) as previously described in (5, 6). Rats were decapitated and forebrains were rapidly removed from the skull and placed into ice-cold Krebs bicarbonate dissection buffer (pH 7.4), containing: NaCl 120 mM, KCl 2 mM, $CaCl_2$ 0.5 mM, $NaHCO_3$ 26 mM, $MgSO_4$ 10 mM, KH_2PO_4 1.18 mM, glucose 11 mM and sucrose 200 mM. The hippocampus was quickly dissected and subsequently cut into transverse

slices 300µm-thick using a Tissue Chopper Mcllwain. To help the tissue to recover from the slicing trauma, slices were incubated in Krebs buffer for 45 min at 34°C (stabilization period). Then, oxygen and glucose deprivation (OGD) was induced by incubating the slices during 15 min in a Krebs-bicarbonate solution where glucose was replaced by 2-deoxyglucose (OGD solution). In parallel, control slices were incubated during 15 min in a Krebs-bicarbonate solution without sucrose (control solution). At least 15 minutes before starting the experiment, both control and OGD solutions were bubbled with either 95% O_2/5% CO_2 or 95% N_2/5% CO_2 gas mixture to ensure O_2 and N_2 saturation respectively. After the OGD period, slices were returned to an oxygenated Krebs-bicarbonate solution containing glucose for 120 min (Re-oxygenation period). During this period, the slices were treated with 0.1, 0.3, 1 and 3µM GKT136901 and 0.3, 1 and 3µM L-NAME. Non-treated slices were used as 100% viability control.

Sinergy between compounds was considered since mono-therapies using sub-threshold concentrations/doses of both compounds were not therapeutically effective and effect size can be provided.

Cell viability of hippocampal brain slices

Hippocampal slices were collected immediately after the re-oxygenation period and subsequently incubated with 3-(4,5-dimethylthiazol-2-yl)-2,5-diphenyltetrazolium bromide (MTT, Sigma-Aldrich, Spain) in Krebs bicarbonate solution (0.5 mg/ml) for 30 min at 37°C. The tetrazolium ring of MTT is cleaved by active dehydrogenases in viable cells, producing a precipitated formazan derivative (7). This formazan derivative was solubilized by adding 200µM DMSO. The optical density was measured spectrophotometrically at 540 nm using a micro plate reader. Absorbance values obtained in control slices were set to 100% viability and experimental variables were normalized with respect to this value.

Preparation of Organotypic Hippocampal Slices and induction of oxygen and glucose deprivation

Hippocampal brain slices for organotypic cultures (OHC) were obtained from brains of 7-10-days-old Sprague Dawley rats. Organotypic cultures were prepared based on the methods previously described in (8, 9). Pups were quickly decapitated and forebrains removed from the skull and dissected. Hippocampus was cut into 300µm-thick slices

using a Tissue Chopper Mcllwain. Slices were separated in sterile ice-cold Hank's balanced salt solution (HBSS, Biowest, Madrid, Spain). Six slices were placed on each Millicell-0.4µm culture inserts (Millipore, Madrid, Spain). Each Millicell culture insert was placed in a well within a six-well culture plate. Neurobasal medium (Invitrogen, Madrid, Spain) enriched with 10% of fetal bovine serum (Sigma-Aldrich, Madrid, Spain) was used for the next 24h (1 ml/well). After 24h, B27 supplement and antioxidants were added to the culture medium. Slices were in culture for 4 days before inducing the OGD period. On day 6, neurobasal medium was replaced by 1 ml/well of OGD solution composed of (in mM): NaCl 137.93 mM, KCl 5.36 mM, $CaCl_2$ 2 mM, $MgSO_4$ 1.19 mM, $NaHCO_3$ 26 mM, KH_2PO_4 1.18 mM, and 2-deoxyglucose 11 mM (Sigma-Aldrich, Madrid, Spain). The cultures were then placed in a partially open airtight chamber (Billups and Rothenberg) exposed within 3 min to 95% N_2/5% CO_2 gas flow to ensure oxygen removal. After that, the chamber was sealed for 15 min at 37°C (OGD period). At the same time, control cultures were maintained under normoxic conditions in a solution with the same composition as previously described but containing normal glucose 15 mM (Sigma-Aldrich, Madrid, Spain) instead of 2-deoxyglucose. Afterwards, slice cultures were pharmacologically treated with 0.01 µM GKT136901 and 0.3 µM L-NAME separately or in combination before returning them to normal oxygen and glucose concentrations for 24h (re-oxygenation period). Non-treated slices were used as internal control.

Quantification of cell death in organotypic hippocampal cultures

Cell death was determined in the CA1 region by staining the OHCs with Propidium iodide (PI) (Invitrogen, Madrid, Spain). Slices were incubated with PI (1 µg/ml) and Hoechst (5 µg/ml) during 30 min. Fluorescence was measured in a fluorescence-inverted NIKON Eclipse T2000-U microscope at 10X magnification. Wavelengths of excitation and emission for PI and Hoechst were 530/350, and 580/460 nm, respectively. Fluorescence analysis was performed using the Metamorph software version 7.0. Hoechst staining was used to normalize PI fluorescence with respect to the number of nuclei as described in (10). Data were normalized with respect to the control values that were considered as 1.

ROS measurement in Organotypic Hippocampal Culture

To determine ROS/RNS production in OHCs, we used the fluorescent probe H_2DCFDA

as has been previously described in *(29)*. Organotypic hippocampal slices were loaded with 10μM H_2DCFDA, which diffuses through the cell membrane and is hydrolyzed by intracellular esterases to the non-fluorescent form dichlorofluorescein (DCFH). DCFH reacts with intracellular H_2O_2 to form the green fluorescent signal. Fluorescence was measured in a fluorescence-inverted NIKON Eclipse T2000-U microscope. Wavelengths of excitation and emission were 485 and 520 nm, respectively. All variables were normalized with respect to the control values (considered as 1).

ROS kinetics: DHE

***Ex-vivo* acute model: Hippocampal brain slices:** ROS production was evaluated in real-time by the fluorescence dye DHE method (10, 11). Stock solution of DHE (3.2 mM) was dissolved in previously oxygenated Krebs solution and added to the hippocampal brain slices. The average fluorescence intensity was monitored using a 10X objective in the CA1 region of the hippocampus every 30 sec during the first 10 min of the re-oxygenation period. Excitation and emission wavelength were 485 nm, and >580 nm, respectively. Fluorescence analysis was performed using the Metamorph software version 7.0. Each value was divided by the initial fluorescence value for normalization.

***Ex-vivo* chronic model: Organotypic hippocampal culture:** Similarly, a stock solution of DHE (3.2 mM) was dissolved in Krebs solution and added to the culture insert. Fluorescence measurements were performed at 0, 2, 4, 8 and 12h after the OGD period using a 10X objective in the CA1 region of the hippocampus. Same emission and excitation wavelength were used. Fluorescence analysis was performed using the Metamorph software version 7.0.

RNA extraction, quantification and reverse transcription

Hippocampal brain slices from organotypic culture were crushed and homogenized using TRI Reagent® (Sigma-Aldrich, The Netherlands). 100 μl of chloroform was added to the samples followed by 15 min centrifugation at 11.000 rpm and 4°C. After centrifugation, the upper phase was preserved (mRNA). 250 μl isopropanol was added to the upper phase and incubated during 1h at -20°C or overnight at -80°C. After incubation, samples were centrifuged during 10 min at 13.000 rpm and 4°C. 200 μl ethanol 80% was added to the supernatant (pellet discarded) followed by 10 min centrifugation at 13.000 rpm. After removal of the ethanol, mRNA was dissolved in 10 μl

RNAse free water. mRNA was quantified spectrophotometrically using the Nanodrop 2000 device. Later, 0.08 µg of total mRNA was reverse transcribed to cDNA with the High Capacity Reverse Transcription Kit (Applied Biosystems, The Netherlands) according to manufacturer's protocol.

Real-time PCR

mRNA levels of *Nox4*, *neuronal NOS (NOS1), inducible NOS (NOS2)* and *endothelial NOS (NOS3),* were quantified using the fluorescent Taqman® technology. We used TaqMan® gene expression arrays (TaqMan® Universal PCR Master Mix, ThermoFisher Scientific, The Netherlands) specific for rat: *Nox4* (Rn01506793_m1, ThermoFisher Scientific, The Netherlands), *NOS1* (Rn00694747_m1, ThermoFisher Scientific, The Netherlands), *NOS2* (Rn00561646_m1, ThermoFisher Scientific, The Netherlands), *NOS3* (Rn02132634_s1, ThermoFisher Scientific, The Netherlands). *β-actin* (Rn00667869_m1, ThermoFisher Scientific, The Netherlands) was used as a house-keeping gene. Water controls were included to ensure specificity and the comparative $2^{-\Delta\Delta Ct}$ method was used for relative quantification of gene expression.

***In vivo* MCAO ischemia model**

The model was conducted as described in (12). C57Bl6/J mice were anesthetized with isoflurane (0.6% in oxygen). The animal was placed on a heating-pad, and rectal temperature was maintained at 37.0°C using a servo-controlled rectal probe-heating pad (Cibertec, Spain). Transient cerebral ischemia was induced using an intraluminal filament technique. Using a surgical microscope (Tecnoscopio OPMI pico, Carl Zeiss, Meditec Iberia SA, Spain), a midline neck incision was made and the right common and external carotid arteries were isolated and permanently ligated. A microvascular temporarily ligature was placed on the internal carotid artery to temporarily stop the blood flow. A silicon rubber-coated monofilament (6023910PK10, Doccol Corporation, Sharon, MA, USA) was inserted through a small incision into the common carotid artery and advanced into the internal carotid artery until a resistance is felt. The tip of the monofilament is then precisely located at the origin of the right middle cerebral artery and thus interrupting blood flow. The filament was held in place by a tourniquet suture on the common carotid artery to prevent filament relocation during the ischemia period. Animals were maintained under anaesthesia during 1h occlusion period followed by the reperfusion period just started when the monofilament is removed.

After the surgery, wounds were carefully sutured and animals could recover from surgery in a temperature-controlled cupboard. For permanent MCAO (pMCAO) the occluding filament was left *in situ* until sacrificing the animals *(11)*. Operation time per animal did not exceed 20 minutes.

Treatment with NO synthase and NADPH oxidase inhibitors

L-NAME was dissolved in saline. GKT136901 was dissolved in a mixture of DMSO/saline in a ratio of 1/99. L-NAME (3 mg/kg), GKT136901 (10 mg/kg) or vehicle (DMSO/saline in a ratio of 1/99) was injected i.p. 1h and 3h after reperfusion, i.e. 1h or 3h after removal of the filament. Stroke outcome in mono therapies were only assessed 1h post-reperfusion due to ethical limitations. Our current ethical proposal is focused on go/no-go decisions to further reduce number of animals as much as possible. Therefore, testing already validated non-effective therapeutic strategy in different animal groups was explicitly not allowed. Therefore, only the combination therapy (effective) was validated in long-term treatment, aged animals, permanent occlusion brain ischemia model and different post-stroke outcomes.

Determination of infarct size

After sacrificing the mice, brains were quickly removed and cut in four 2-mm thick coronal sections using a mouse brain slice matrix (Harvard Apparatus, Spain). Brain slices were stained for 15 min at room temperature with 2% 2,3,5-triphenyltetrazolium chloride (TTC; Sigma-Aldrich, The Netherlands) in PBS to visualize the infarctions (13). Indirect infarct volumes were calculated by volumetry (ImageJ software, National Institutes of Health, USA) according to the following equation: $V_{indirect}$ (mm^3) = $V_{infarct}$ x (1-(V_{ih} – V_{ch})/V_{ch}), where the term (V_{ih} – V_{ch}) represents the volume difference between the ischemic hemisphere and the control hemisphere and (V_{ih} – V_{ch})/V_{ch} expresses this difference as a percentage of the control hemisphere.

Assessment of neuro-motor functional outcomes

Three different neuro-motor functional tests were assessed in all mice groups (adult male, female and aged) treated 1h after filament removal. The Bederson Score *(13)* is defined by: Score 0, no apparent neurological deficits; 1, body torsion and forelimb flexion; 2, right side weakness and thus decreased resistance to lateral push; 3, unidirectional circling behavior; 4, longitudinal spinning; 5, no movement. Within the elevated body swing test, the mice were held ~1 cm from the base of its tail and then

elevated above the surface in the vertical axis around 20 cm. We considered a swing whenever the animal moved its head out of the vertical axis to either the left or the right side (more than 10 degrees). Ratio of right/left swings were subsequently analyzed. Finally, to directly evaluate strength, the four-limbs hanging wire test was performed. The mouse was placed on the center of the wire with a diameter of 10 cm. Later, the wire was slowly inverted and placed at ~40 cm above a paper towel bedding. The time until the mouse fell from the wire was recorded considering as maximum time 120s.

Determination of blood-brain-barrier leakage and brain oedema

To determine the permeability of the cerebral vasculature and brain oedema formation after 1h occlusion of the middle cerebral artery (tMCAO), 2% Evans blue tracer (Sigma Aldrich, The Netherlands) was diluted in 0.9% NaCl and then injected intraperitoneally just after removing the filament. Measurement of Evans Blue extravasation was performed as described in (12).

Oxidative stress: DHE staining

ROS production formation *in vivo* brain tissue was determined using the florescence dye dihydroethidium (Thermo Scientific Technology, The Netherlands). Frozen brain cryosections were fixated in 4% paraformaldehyde (PFA) in PBS and then incubated with 2 µM DHE (2mM stock solution) for 30 minutes at 37°C. After three washing steps with PBS, slices were incubated with Hoechst (Hoechst 33342, Sigma-Aldrich, The Netherlands) 2 ng/ml for 10 min at 37°C. The relative pixel intensity was measured in identical regions with (ImageJ software, National Institutes of Health, USA.

Immunohistochemistry: N-Tyr staining

Brain tissue cryosections (10 µm) were fixed with 4% PFA in PBS. After fixation, sections were incubated for 1h at room temperature with a rabbit polyclonal anti-nitrotyrosine antibody (1:100; ThermoFisher Scientific, A-21285) in blocking buffer. After three washes in PBS, sections were incubated with the secondary antibody, Alexa Fluor 488 donkey anti-rabbit (1:100; ThermoFisher Scientific, A-21206) for 45 min at room temperature. Then, the fluorescent Hoechst33342 dye (2 ng/ml; ThermoFisher Scientific, The Netherlands) was added for 10 min at room temperature. Sections were washed in PBS and then mounted using a Dako Fluorescence Mounting Medium (S3023, Agilent Technologies). Immunofluorescent signals were viewed using a Leica DMI3000 B

fluorescence microscope. Quantitative analysis of nitro-tyrosine fluorescence was performed with (ImageJ software, National Institute of Health, USA).

Human brain microvascular endothelial cell (HBMEC) cultures subjected to hypoxia

HBMEC (Cell systems, USA) between passage 3 and 9 were cultured to approximately 95% confluence using specialized cell medium (EGM-2 MV BulletKit, Lonza, The Netherlands) enriched with 5% fetal bovine serum (FBS; Sigma-Aldrich, The Netherlands) before starting the hypoxia period. For hypoxia studies, HBMECs were seeded at specific density ($6x10^4$ cells/ml) in 12 wells-plate and incubated during 24h at 37°C. Then, cell medium was replaced with non-FBS containing medium (2 ml/well) following by 6h of hypoxia (94,8% N_2, 0.2% O_2 and 5% CO_2) at 37°C using hypoxia workstations (Ruskin Invivo2 400 station, The Netherlands). The hypoxia period was followed by 24h of reperfusion in the presence or absence of 0,1 µM GKT136901 (Genkyotech, Switzerland) and 0,3 µM L-NAME, incubated separately or in combination. Control cells were exposed to normoxia (75% N_2, 20% O_2 and 5% CO_2) and enriched medium during the hypoxia period. All flasks and well plates were pre-treated with fibronectin (Sigma-Aldrich, The Netherlands) solution (1:100 in PBS).

Assessment of cell viability in HBMEC

After 24h of re-oxygenation period, cell viability was assessed using the colorimetric MTT assay *(14)*. MTT solution (5 mg/ml) was added to each well (100 µl/ml) and incubated for 2h at 37°C. The formazan salt formed was solubilized by adding 350 µl/well DMSO. The optical density was measured spectrophotometrically at 540 nm using a micro plate reader. Absorbance values obtained in control cells were set to 100% viability.

Assessment of cell permeability in HBMEC

2×10^4 HBMECs were grown to confluence on membranes of Transwell inserts (collagen-coated Transwell Pore Polyester Membrane Insert; pore size = 3.0 µm, Corning, The Netherlands) 24h before inducing 6h of ischemic conditions followed by 24h re-oxygenation period where cells were treated with 1 µM GKT136901. Cell permeability was assessed using the Evans Blue dye (Sigma-Aldrich, The Netherlands). Before the diffusion experiment, medium was removed and cells were washed once with assay

buffer. The same buffer (1.5 ml) was added to the abluminal side of the insert. Permeability buffer (0.5 ml) containing 4% bovine serum albumin (Sigma-Aldrich, The Netherlands) and 0.67 mg/ml Evans blue dye was loaded on the luminal side of the insert followed by 15 min incubation at 37°C. The concentration of Evans Blue in the abluminal chamber was measured by determining the absorbance of 150 µl buffer at 630 nm using a microplate reader.

Transient occlusion of the middle cerebral artery (tMCAO). Model previously described in (17).

Supplementary Figures

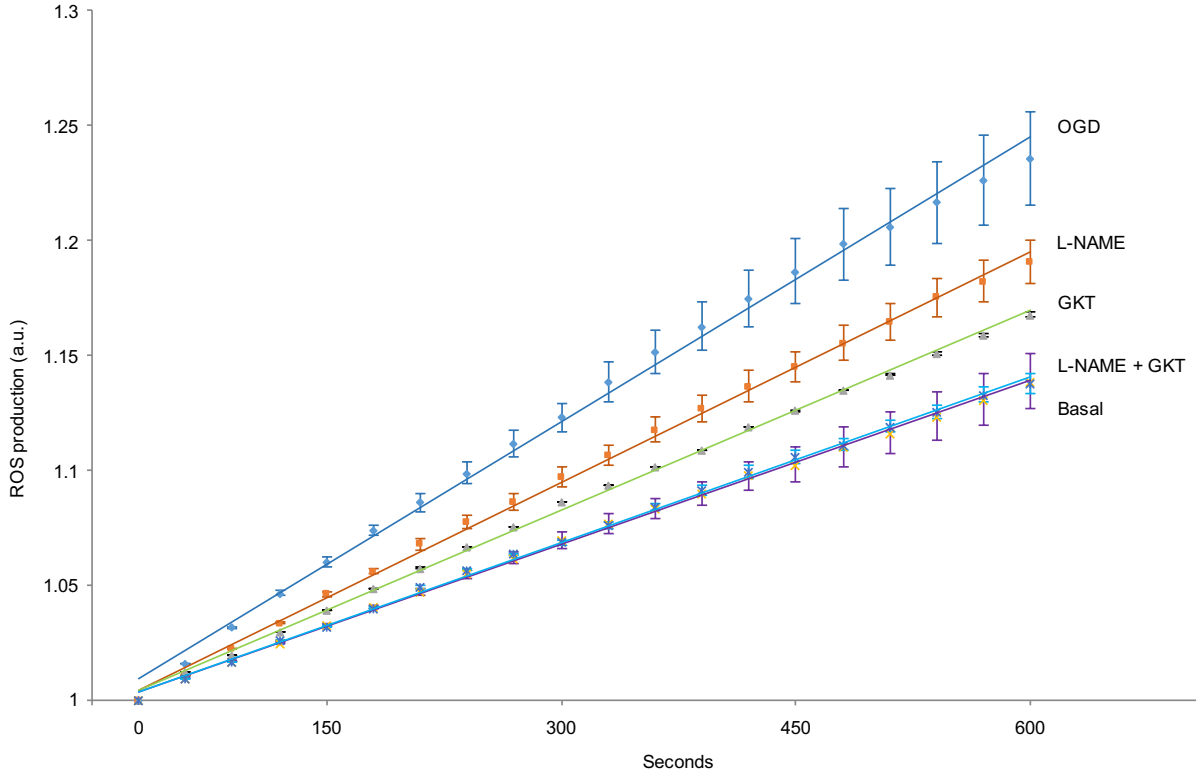

Figure S1. GKT136901 and L-NAME combinatory therapy inhibits ROS production in hippocampal brain slices (HBS) subjected to OGD. To define kinetics of ROS formation, fluorescence change was measured every 30s after the OGD period within the first 10 min after OGD. HBS treated with GKT (0,01 μM) and L-NAME (0,3 μM) in combination reduced ROS production to basal levels while individual treatments showed no significant effect.

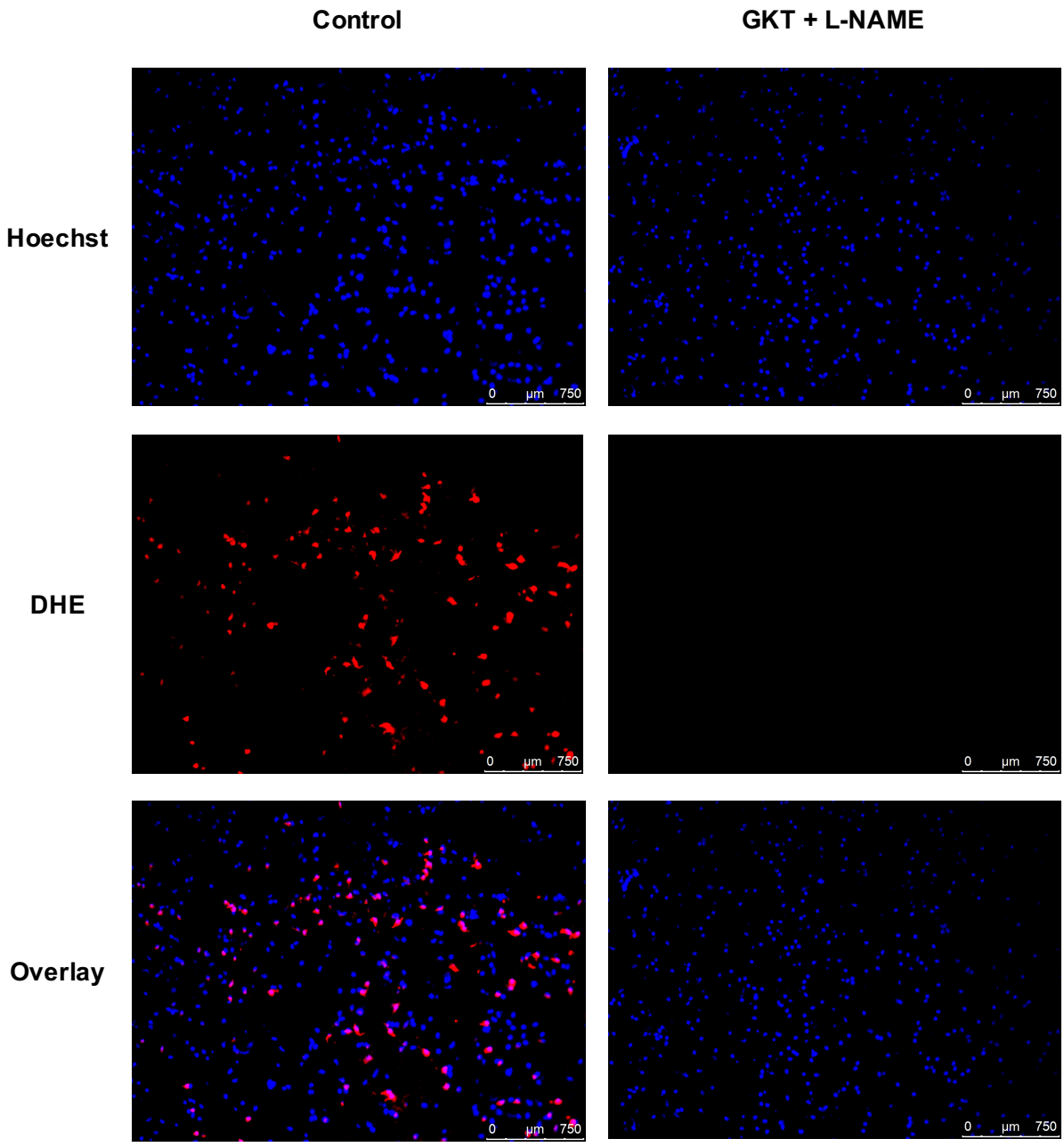

Figure S2. Representative DHE staining images. ROS production (red) was detected using cryosections from ipsilateral brain tissue after 1h occlusion of the middle cerebral artery (tMCAO) using treated (GKT+L-NAME) and non-treated (Control) animals. Combinatory treatment dramatically reduced ROS formation (DHE, GKT+L-NAME) in comparison with control conditions (DHE, Control). Same findings are shown in the overlay. Nuclei were detected using the fluorescence dye Hoescht (blue).

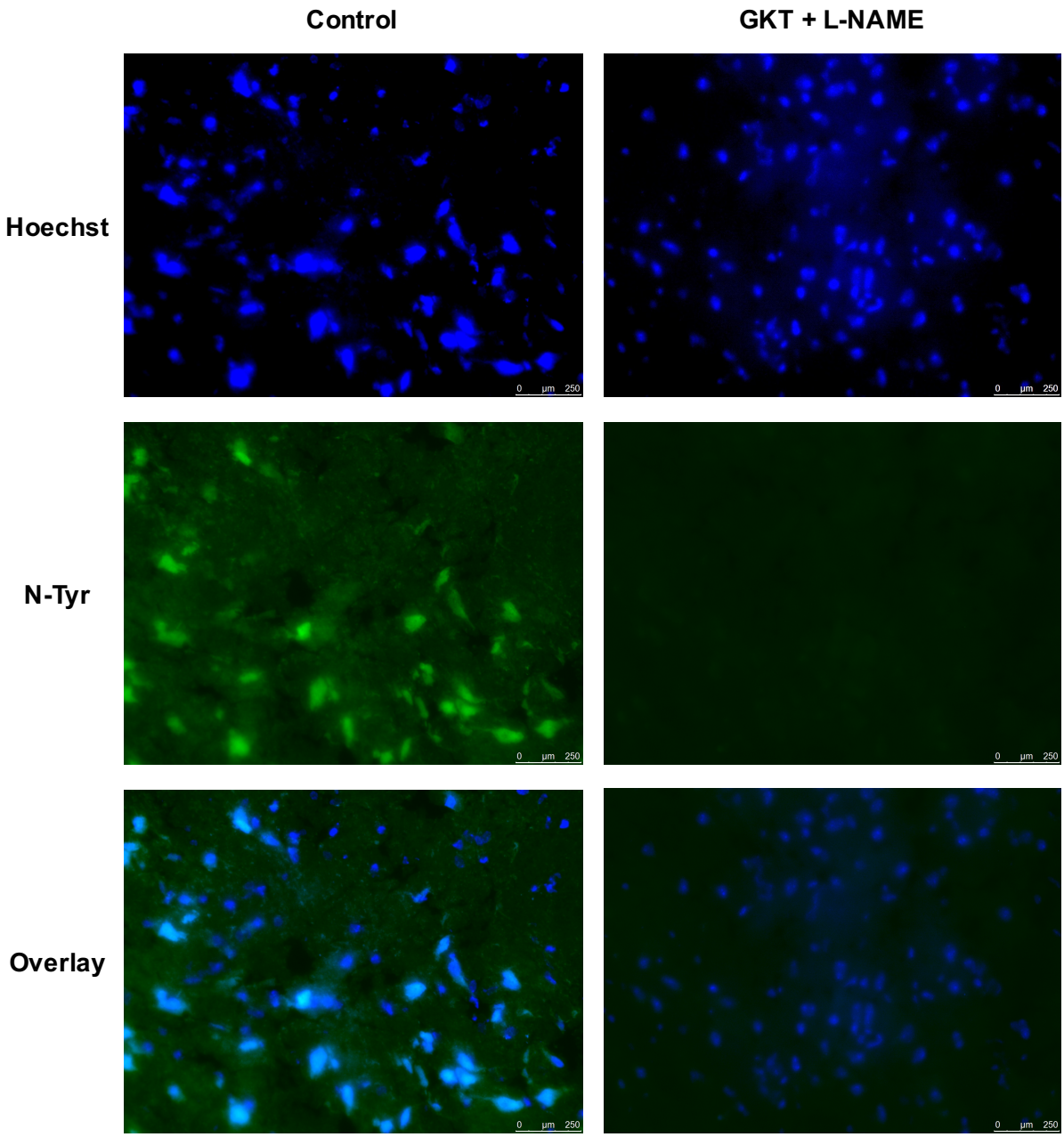

Figure S3. Representative N-Tyrosine staining images. Nitrated tyrosine formation (green) was detected using cryosections from ipsilateral brain tissue after 1h occlusion of the middle cerebral artery (tMCAO) using treated (GKT+L-NAME) and non-treated (Control) animals. Combinatory treatment dramatically reduced N-Tyrosine formation (N-Tyr, GKT+L-NAME) in comparison with control conditions (N-Tyr, Control). Same findings are shown in the overlay. Nuclei were detected using the fluorescence dye Hoescht (blue).

Supplementary Tables

Table S1. Network proteins and their connectedness to NOX4

Protein_symbol	Uniprot_id	Connectedness_to_NOX4	Protein_symbol	Uniprot_id	Connectedness_to_NOX4
NAXD	Q8IW45	1	RAC2	P15153	1
DHFR2	Q86XF0	1	GLRX	P35754	1
AKR1E2	Q96JD6	1	NCF4	Q15080	1
AKR1B10	O60218	1	NCF2	P19878	1
AASDHPPT	Q9NRN7	1	DECR2	Q9NUI1	1
TECR	Q9NZ01	1	CRYZ	Q08257	1
SRD5A3	Q9H8P0	1	DECR1	Q16698	1
NCF1C	A8MVU1	1	PGD	P52209	1
NCF1B	A6NI72	1	PECR	Q9BY49	1
HTATIP2	Q9BUP3	1	MECR	Q9BV79	1
DHRS3	O75911	1	ALDH1L1	O75891	1
PTGR2	Q8N8N7	1	TSTA3	Q13630	1
HSD17B12	Q53GQ0	1	MTHFD1	P11586	1
NUDT7	P0C024	1	NNT	Q13423	1
IYD	Q6PHW0	1	HMGCR	P04035	1
A9Z1X1	A9Z1X1	1	IDH1	O75874	1
AASS	A4D0W4	1	IDH2	P48735	1
AASDH	Q4L235	1	ME2	P23368	1
MTHFD1L	Q6UB35	1	ME3	Q16798	1
DHFR	B0YJ76	1	ME1	P48163	1
FAR2	Q96K12	1	ALDH18A1	P54886	1
FAR1	Q8WVX9	1	AASS	Q9UDR5	1
ALDH1L2	Q3SY69	1	HSD17B1	P14061	1
RDH10	Q8IZV5	1	HSD17B3	P37058	1
RDH11	Q8TC12	1	DHFR	P00374	1
RDH14	Q9HBH5	1	ADH1C	P00326	1
RDH8	Q9NYR8	1	ADH6	P28332	1
HSD3B2	P26439	1	ADH1A	P07327	1
AKR7A2	O43488	1	ADH7	P40394	1
KDSR	Q06136	1	ADH1B	P00325	1
RDH12	Q96NR8	1	ADH5	P11766	1
PYCR3	Q53H96	1	HSD11B1	P28845	1
HSD17B6	O14756	1	HSD11B2	P80365	1
DHRS9	Q9BPW9	1	SRD5A1	P18405	1
NCF1	P14598	1	SRD5A2	P31213	1
GAPDH	P04406	1	PGRMC2	O15173	1
GLUD1	P00367	1	PGRMC1	O00264	1

GAPDHS	O14556	1	NRF1	Q16656	1
GMPR	P36959	1	NFE2L1	Q14494	1
GMPR2	Q9P2T1	1	NENF	Q9UMX5	1
GLUD2	P49448	1	SLC25A28	Q96A46	1
AKR1D1	P51857	1	SLC25A37	Q9NYZ2	1
DHCR7	Q9UBM7	1	SLC48A1	Q6P1K1	1
QDPR	P09417	1	HERC2	O95714	1
ALDH3B1	P43353	1	HEBP2	Q9Y5Z4	1
ALDH3B2	P48448	1	HEBP1	Q9NRV9	1
AKR1A1	P14550	1	HBM	Q6B0K9	1
DHDH	Q9UQ10	1	HBE1	P02100	1
HSD17B8	Q92506	1	HBZ	P02008	1
HSD17B2	P37059	1	HBQ1	P09105	1
SPR	P35270	1	FRRS1	Q6ZNA5	1
GRHPR	Q9UBQ7	1	FADS3	Q9Y5Q0	1
AKR1C2	P52895	1	FADS2P1	A8MWK0	1
AKR1C1	Q04828	1	FA2H	Q7L5A8	1
AKR1C3	P42330	1	EIF2AK1	Q9BQI3	1
H6PD	O95479	1	CYB5B	O43169	1
G6PD	P11413	1	CYP4V2	Q6ZWL3	1
DCXR	Q7Z4W1	1	CYP2W1	Q8TAV3	1
PYCR2	Q96C36	1	CYP26C1	Q6V0L0	1
PYCR1	P32322	1	CYP26B1	Q9NR63	1
ALDH1B1	P30837	1	COX15	Q7KZN9	1
ALDH3A2	P51648	1	CDC37	Q16543	1
ALDH2	P05091	1	CYB5D2	Q8WUJ1	1
ALDH1A3	P47895	1	CYB5D1	Q6P9G0	1
ALDH7A1	P49419	1	CYB561D1	Q8N8Q1	1
ALDH3A1	P30838	1	CYP27C1	Q4G0S4	1
ALDH9A1	P49189	1	ABCB10	Q9NRK6	1
TM7SF2	O76062	1	ABCB7	O75027	1
FDFT1	P37268	1	ABCB6	Q9NP58	1
ALDH4A1	P30038	1	CD163	Q86VB7	1
AKR1B1	P15121	1	FADS2	O95864	1
CBR3	O75828	1	COX5A	P20674	1
DHRS4	Q9BTZ2	1	CYBRD1	Q53TN4	1
CBR1	P16152	1	SLC46A1	Q96NT5	1
AKR1C4	P17516	1	CYB5A	P00167	1
ALDH6A1	Q02252	1	HRG	P04196	1
FASN	P49327	1	TSPO	P30536	1
RSAD2	Q8WXG1	1	FADS1	O60427	1
CYBA	P13498	2	CYP21A2	P08686	2
NFE2	Q16621	1	AGMO	Q6ZNB7	1

FLVCR1	Q9Y5Y0	1	ALKBH1	Q13686	1
TF	P02787	1	ADI1	Q9BV57	1
CYP26A1	O43174	1	NOS1	B3VK56	2
PRDM2	Q13029	1	CP	A5PL27	1
HCCS	P53701	1	CYP2D6	Q6NWU0	3
CYCS	P99999	1	CYP21A2	Q08AG9	3
CYB561	P49447	1	P4HTM	Q9NXG6	1
CYB561D2	O14569	1	EGLN3	Q9H6Z9	1
KCNMA1	Q12791	1	EGLN2	Q96KS0	1
AMBP	P02760	1	EGLN1	Q9GZT9	1
HFE	Q30201	1	DOHH	Q9BU89	1
COX10	Q12887	1	KDM2B	Q8NHM5	1
HPX	P02790	1	KDM2A	Q9Y2K7	1
HBG1	P69891	1	P4HA3	Q7Z4N8	1
TBXAS1	P24557	1	P3H3	Q8IVL6	1
PTGIS	Q16647	1	P3H2	Q8IVL5	1
GUCY1B2	O75343	1	P3H1	Q32P28	1
GUCY1B3	Q02153	1	FTH1	P02794	1
ALAD	P13716	1	BCO2	Q9BYV7	1
FECH	P22830	1	ALKBH2	Q6NS38	1
UQCRH	P07919	1	ADO	Q96SZ5	1
CYC1	P08574	1	NGB	Q9NPG2	2
MT-CYB	P00156	1	HBD	P02042	2
UQCR10	Q9UDW1	1	CYGB	Q8WWM9	2
SUCLA2	Q9P2R7	1	CYP4F22	Q6NT55	3
CBS	P35520	1	CYP2U1	Q7Z449	2
BLVRA	P53004	2	CYP20A1	Q6UW02	2
HMBS	P08397	1	CYP1A1	A0N0X8	3
UROS	P10746	1	IDO2	Q6ZQW0	2
UROD	P06132	1	SCD5	Q86SK9	1
ALAS1	P13196	1	CYP4A22	Q5TCH4	3
ALAS2	P22557	1	COX4I2	Q96KJ9	1
TET3	O43151	1	COX6A1	P12074	1
TET2	Q6N021	1	MT-CO2	P00403	1
TET1	Q8NFU7	1	CYP8B1	Q9UNU6	3
PIR	O00625	1	CYP39A1	Q9NYL5	3
PHF8	Q9UPP1	1	TDO2	P48775	1
RIOX1	Q9H6W3	1	CYP11B2	P19099	1
RIOX2	Q8IUF8	1	CYP46A1	Q9Y6A2	3
KDM8	Q8N371	1	TMLHE	Q9NVH6	1
FAXDC2	Q96IV6	2	COX8C	Q7Z4L0	1
COX7A2L	O14548	1	CYP4F12	Q9HCS2	2
COX6C	P09669	1	CYP2C18	P33260	3

COX8A	P10176	1	CYP2D6	P10635	2
COX6B2	Q6YFQ2	1	CYP1B1	Q16678	3
COX4I1	P13073	1	CYP3A43	Q9HB55	3
COX7B2	Q8TF08	1	CYP4F11	Q9HBI6	3
COX6B1	P14854	1	CYP2E1	P05181	3
COX5B	P10606	1	HAAO	P46952	1
COX7C	P15954	1	CYP17A1	P05093	3
COX7B	P24311	1	CYP27B1	O15528	3
COX6A2	Q02221	1	CYP2C19	P33261	3
CH25H	O95992	1	CYP27A1	Q02318	3
COX7A2	P14406	1	CYP2C9	P11712	3
FXN	Q16595	2	HIF1AN	Q9NWT6	1
HBG2	P69892	2	ASPH	Q12797	1
CYP2R1	Q6VVX0	3	CYP3A4	P08684	3
MB	P02144	2	CYP4F3	Q08477	3
COX7A1	P24310	1	CYP4F2	P78329	3
CYP24A1	Q07973	3	ALOX15	P16050	1
COQ7	Q99807	2	PTGS1	P23219	2
GGCX	P38435	1	PTGS2	P35354	2
MT-CO1	P00395	2	ALOX12	P18054	1
CYP7B1	O75881	3	ALOX15B	O15296	1
HBA1	P69905	2	ALOX5	P09917	1
HBB	P68871	2	CDO1	Q16878	2
BCO1	Q9HAY6	1	HSD17B7	P56937	2
CYP2A6	P11509	3	HGD	Q93099	1
CYP2A7	P20853	3	HPD	P32754	1
CYP2J2	P51589	3	MIOX	Q9UGB7	1
CYP4F8	P98187	3	CYP11A1	P05108	2
CYP2S1	Q96SQ9	3	CYP7A1	P22680	3
CYP2C8	P10632	3	CP	P00450	1
CYP19A1	P11511	3	TPH2	Q8IWU9	1
CYP1A2	P05177	3	FTMT	Q8N4E7	1
CYP4Z1	Q86W10	3	TPH1	P17752	1
CYP4B1	P13584	3	PLOD3	O60568	1
CYP3A7	P24462	3	PLOD2	O00469	1
CYP2A13	Q16696	3	PLOD1	Q02809	1
CYP1A1	P04798	3	CYP11B1	P15538	2
CYP3A5	P20815	3	IDO1	P14902	2
CYP2B6	P20813	3	CYP4A11	Q02928	3
CYP4X1	Q8N118	3	BBOX1	O75936	1
CYP2F1	P24903	3	SCD	O00767	1
P4HA1	P13674	1	NDUFB2	A4D1T5	1
P4HA2	O15460	1	STEAP4	Q687X5	2

PAH	P00439	1	STEAP2	Q8NFT2	2
TH	P07101	1	STEAP1	Q9UHE8	2
PHYH	O14832	1	SQOR	Q9Y6N5	1
CYP51A1	Q16850	3	RETSAT	Q6NUM9	1
NSDHL	Q15738	2	RNLS	Q5VYX0	1
MSMO1	Q15800	2	QSOX2	Q6ZRP7	3
DBH	P09172	1	QSOX1	O00391	3
PAM	P19021	1	PYROXD1	Q8WU10	1
CPOX	P36551	2	PDP2	Q9P2J9	1
TYR	P14679	1	PCYOX1L	Q8NBM8	1
GPX8	Q8TED1	1	PCYOX1	Q9UHG3	3
NOXO1	Q8NFA2	1	OXNAD1	Q96HP4	1
NOXA1	Q86UR1	2	IL4I1	Q96RQ9	3
LOXL2	Q9Y4K0	2	NOX4	Q9NPH5	5
PXDNL	A1KZ92	2	NOX1	Q9Y5S8	2
PXDN	Q92626	2	NDOR1	Q9UHB4	1
SOD3	P08294	2	MTO1	Q9Y2Z2	1
PRDX5	P30044	1	MICAL3	Q7RTP6	3
SOD1	P00441	2	MICAL2	O94851	3
SOD2	P04179	2	MICAL1	Q8TDZ2	3
CAT	P04040	3	KDM1A	O60341	1
SUOX	P51687	3	FOXRED2	Q8IWF2	1
GPX2	P18283	1	FOXRED1	Q96CU9	1
GPX3	P22352	1	ERO1B	Q86YB8	1
GPX4	P36969	1	ERO1A	Q96HE7	1
GPX1	P07203	1	DUS4L	O95620	1
GPX6	P59796	1	DUS3L	Q96G46	1
GPX5	O75715	1	DUS1L	Q6P1R4	1
GPX7	Q96SL4	1	CRY2	Q49AN0	1
HAO2	Q9NYQ3	2	KDM1B	Q8NB78	1
HAO1	Q9UJM8	2	GFER	P55789	3
LOX	P28300	2	AIFM3	Q96NN9	1
PNPO	Q9NVS9	2	AIFM2	Q9BRQ8	1
AOC2	O75106	2	ACOXL	Q9NUZ1	1
AOC3	Q16853	2	ACADVL	P49748	1
AOC1	P19801	2	STEAP3	Q658P3	2
EPX	P11678	2	NOX3	Q9HBY0	2
MPO	P05164	2	NOX5	Q96PH1	3
PRDX6	P30041	2	COQ6	Q9Y2Z9	2
LPO	P22079	2	FLAD1	Q8NFF5	1
TPO	P07202	2	Q5HYI4	Q5HYI4	3
CYB5RL	Q6IPT4	1	CHDH	Q8NE62	1
CYB5R4	Q7L1T6	2	ALDH1A1	P00352	1

CYB5R2	Q6BCY4	1	HMOX1	P09601	4
CYB5R1	Q9UHQ9	1	GPD2	P43304	1
TXNRD3	Q86VQ6	2	GSR	P00390	2
DUOX1	Q9NRD9	4	ENPP3	O14638	1
PRODH2	Q9UF12	1	SDHB	P21912	1
ACAD9	Q9H845	1	ACOX3	O15254	3
ACAD8	Q9UKU7	1	NDUFS6	O75380	1
LDHD	Q86WU2	1	NDUFA13	Q9P0J0	1
DUOX2	Q9NRD8	4	MT-ND6	P03923	1
CRY1	Q16526	1	MTHFR	P42898	2
AIFM1	O95831	1	NDUFB9	Q9Y6M9	1
SMOX	Q9NWM0	3	NDUFV1	P49821	1
KMO	O15229	3	FMO1	Q01740	3
TKFC	Q3LXA3	1	DHODH	Q02127	3
L2HGDH	Q9H9P8	1	POR	P16435	3
D2HGDH	Q8N465	1	XDH	P47989	3
PRODH	O43272	1	NDUFS7	O75251	1
ETFB	P38117	1	SDHD	O14521	2
APP	P05067	2	MT-ND4	P03905	1
DHCR24	Q15392	2	NDUFA9	Q16795	1
FMO6P	O60774	3	ETFDH	Q16134	1
ETFA	P13804	1	NDUFA5	Q16718	1
CYBB	P04839	5	NDUFAB1	O14561	1
NQO1	P15559	2	NDUFB7	P17568	1
ACADSB	P45954	1	NDUFB3	O43676	1
AGPS	O00116	1	FMO3	P31513	3
NDUFB11	Q9NX14	1	NDUFC2	O95298	1
PPOX	P50336	4	MAOA	P21397	3
NOS3	P29474	4	IVD	P26440	1
NOS1	P29475	4	FMO4	P31512	3
NOS2	P35228	4	ACOX2	Q99424	1
SARDH	Q9UL12	1	NDUFB5	O43674	1
DPYD	Q12882	2	NDUFS1	P28331	1
BLVRB	P30043	3	MAOB	P27338	3
DUS2	Q9NX74	1	MTR	Q99707	1
MTRR	Q9UBK8	2	NDUFA2	O43678	1
DAO	P14920	3	TXNRD2	Q9NNW7	2
ALDH1A2	O94788	1	NDUFA7	O95182	1
FDXR	P22570	2	FMO2	Q99518	3
DMGDH	Q9UI17	1	MT-ND2	P03891	1
GCDH	Q92947	1	SQLE	Q14534	3
NDUFS8	O00217	1	NDUFA4	O00483	1

HMOX2	P30519	4
SDHA	P31040	1
NDUFB4	O95168	1
DDO	Q99489	3
ACOX1	Q15067	3
NDUFA6	P56556	1
NDUFA10	O95299	1
FMO5	P49326	3
NDUFV2	P19404	1
NDUFS5	O43920	1
NDUFS3	O75489	1
NQO2	P16083	1
NDUFS4	O43181	1
SC5D	O75845	3
TXNRD1	Q16881	2
NDUFA11	Q86Y39	1
MT-ND4L	P03901	1
NDUFA8	P51970	1
NDUFA3	O95167	1
NDUFA4L2	Q9NRX3	1
NDUFA1	O15239	1
AOX1	Q06278	4
CYB5R3	P00387	1
NDUFA12	Q9UI09	1
PAOX	Q6QHF9	3
PIPOX	Q9P0Z9	3
SDHC	Q99643	2
NDUFS2	O75306	1
ENPP1	P22413	1
NDUFB1	O75438	1
MT-ND1	P03886	1
ACADM	P11310	1
ACADS	P16219	1
ACADL	P28330	1
DLD	P09622	1

Table S2. Animals excluded from the statistical analysis after tMCAO

Animals	Ischemia model	Duration	Excluded Animals	Reason of exclusion
C57/Bl6J	Control (TTC)	24h	1 of 8	Dead within the first 24h
C57/Bl6J	L-NAME (TTC)	24h	1 of 6	Dead within the first 24h
C57/Bl6J	GKT136901 (TTC)	24h	1 of 5	Dead within the first 24h
C57/Bl6J	C. ther. 1h PO (TTC)	24h	0 of 6	-
C57/Bl6J	C. ther. 3h PO (TTC)	24h	0 of 6	-
C57/Bl6J	Control Aged (TTC)	24h	1 of 6	Dead during the surgery
C57/Bl6J	C. ther. Aged (TTC)	24h	0 of 5	-
C57/Bl6J	pMCAO Control (TTC)	24h	1 of 7	Dead during the surgery
C57/Bl6J	pMCAO C. ther. 1h PO (TTC)	24h	1 of 6	Dead within the first 24h
C57/Bl6J	Control (EB)	24h	1 of 6	Dead during the surgery
C57/Bl6J	C. ther. (EB)	24h	0 of 5	-
C57/Bl6J	Control (DHE)	24h	0 of 4	-
C57/Bl6J	C. ther. (DHE)	24h	0 of 4	-
C57/Bl6J	Control (N-Tyr)	24h	0 of 4	-
C57/Bl6J	C. ther. (N-Tyr)	24h	0 of 4	-

tMCAO, transient occlusion of the middle cerebral artery; TTC, 2,3,5-triphenyltetrazolium hydrochloride; C. ther., combinatory therapy; EB, Evans Blue. Animal exclusion procedures are described in the respective methods parts.

Table S3. Power analysis

Adult mice - tMCAO – GKT+L-NAME (10 mg/kg, 3 mg/kg)				
Infarct size (mm^3)				
	Mean	*SD*	*N*	*Power for measured difference (%)*
Vehicle	110,1	21,5	7	89,7
Treatment	66,2	13,9	6	
Four limb hanging				
	Mean	*SD*	*N*	*Power for measured difference (%)*
Vehicle	41,7	38,2	7	98,2
Treatment	101	31,1	5	
		Elevated body swing		
	Mean	*SD*	*N*	*Power for measured difference (%)*
Vehicle	0,8	0,8	7	96,1
Treatment	2,3	2,1	9	

Aged mice - tMCAO – GKT+L-NAME (10 mg/kg, 3 mg/kg)				
Infarct size (mm^3)				
	Mean	*SD*	*N*	*Power for measured difference (%)*
Vehicle	103,19	19,6	5	25,4
Treatment	45,61	37,85	5	

tMCAO, transient middle cerebral artery occlusion; SD, standard deviation; N, number of animals. We conducted a post hoc analysis of power in the different animal groups. For each animal treatment group, a pooled variance of the vehicle and treatment groups was calculated from mean, SD and n-number with n the size of the group and CV the coefficient of variation (SD/Mean) of the group. Power was calculated for the measured difference using Russ Lenth's power software with an alpha of 0.05, the measured effect (%) and the calculated pooled variances [(Lenth, R.V 2006-9, java Applets for Power and Sample Size [Computer Software],
Retrieved 02-17-2014, from http://www.stat.uiowa.edu/~rlenth/Power.

Table S4. Databases used and their details

Database Name	Version	Access date	Number of nodes/edges	Evidence level used
Human Metabolite Database (HMDB) (2)	4.0	2018-01-24	114,100/ 866,004	All
Integrated Interactions Database (IID) (1)	Human 2017-04	2017-12	18,627/ 923,913	exp
Therapeutic Target Database (TTD) (14)	Sep 15th, 2017	2018-02	2957/--	--

References

1. Kotlyar M, Pastrello C, Sheahan N, Jurisica I (2016) Integrated interactions database: tissue-specific view of the human and model organism interactomes. *Nucleic Acids Res* 44(D1):D536–41.

2. Wishart DS, et al. (2018) HMDB 4.0: the human metabolome database for 2018. *Nucleic Acids Res* 46(D1):D608–D617.

3. Fröhlich H, Speer N, Poustka A, Beissbarth T (2007) GOSim--an R-package for computation of information theoretic GO similarities between terms and gene products. *BMC Bioinformatics* 8(1):166.

4. Wang JZ, Du Z, Payattakool R, Yu PS, Chen C-F (2007) A new method to measure the semantic similarity of GO terms. *Bioinformatics* 23(10):1274–1281.

5. Egea J, et al. (2007) Neuroprotection afforded by nicotine against oxygen and glucose deprivation in hippocampal slices is lost in alpha7 nicotinic receptor knockout mice. *Neuroscience* 145(3):866–872.

6. Egea J, et al. (2014) Small synthetic hyaluronan disaccharides afford neuroprotection in brain ischemia-related models. *Neuroscience* 265:313–322.

7. Denizot F, Lang R (1986) Rapid colorimetric assay for cell growth and survival. Modifications to the tetrazolium dye procedure giving improved sensitivity and reliability. *J Immunol Methods* 89(2):271–277.

8. Huuskonen J, Suuronen T, Miettinen R, van Groen T, Salminen A (2005) A refined in vitro model to study inflammatory responses in organotypic membrane culture of postnatal rat hippocampal slices. *J Neuroinflammation* 2(1):25.

9. Egea J, et al. (2015) Melatonin-sulforaphane hybrid ITH12674 induces neuroprotection in oxidative stress conditions by a “drug-prodrug” mechanism of action. *Br J Pharmacol* 172(7):1807–1821.

10. Egea J, et al. (2012) Galantamine elicits neuroprotection by inhibiting iNOS, NADPH oxidase and ROS in hippocampal slices stressed with

anoxia/reoxygenation. *Neuropharmacology* 62(2):1082–1090.

11. Bindokas VP, Jordán J, Lee CC, Miller RJ (1996) Superoxide production in rat hippocampal neurons: selective imaging with hydroethidine. *J Neurosci* 16(4):1324–1336.

12. Kleinschnitz C, et al. (2010) Post-stroke inhibition of induced NADPH oxidase type 4 prevents oxidative stress and neurodegeneration. *PLoS Biol* 8(9):e1000479.

13. Bederson JB, et al. (1986) Evaluation of 2,3,5-triphenyltetrazolium chloride as a stain for detection and quantification of experimental cerebral infarction in rats. *Stroke* 17(6):1304–1308.

14. Li YH, et al. (2018) Therapeutic target database update 2018: enriched resource for facilitating bench-to-clinic research of targeted therapeutics. *Nucleic Acids Res* 46(D1):D1121–D1127.

6

ROS-CGMP DISEASE MODULE-BASED NETWORK PHARMACOLOGY PREVENTS HEMORRHAGIC TRANSFORMATION IN REAL-WORD STROKE-DIABETES COMORBIDITY

Casas AI, **Elbatreek MH**, Nogales C, Sadegh S, Anastasi E, Baumbach J, et al. ROS-cGMP disease module-based network pharmacology prevents hemorrhagic transformation in real-word stroke-diabetes comorbidity. In preparation.

Abstract

Translational stroke research has yielded only a single registered thrombolytic drug and no neuroprotective therapy. Two systematic errors contributed to this. First, mainly single drug targets are considered; second, stroke models often ignore real-world comorbidities such as diabetes. Diabetic patients are, however, excluded from thrombolysis because of a high risk of fatal hemorrhagic transformation. Here we address both shortcomings by in-silico multitarget discovery based on the multiscale network of human diseases and comorbidities linked to ischemic stroke and diabetes. Within the resulting disease cluster, genes related to, amongst others, reactive oxygen species (ROS) and cyclic GMP (cGMP) are located. We extend these by all known ROS and cGMP related clinical drug targets and conducted an interactome-based first neighbor analysis. This yielded a single ROS-cGMP module containing NOS1, NOS3, GUCYA1, GUCYB1, NOX5 and, through metabolites, NOX4 and NOS2. To validate this module in vivo, we applied network pharmacology, i.e. a triple combination therapy with a NOS inhibitor, a NOX inhibitor and an sGC activator, in a mouse stroke model with diabetes as comorbidity. This resulted in high synergy of subthreshold doses of each compound to decrease infarct size, stabilize blood-brain barrier, improve neuro-motor function and increase survival. Surprisingly, using a humanized mouse model, we identified NOX5 as the cause of diabetes-associated hemorrhagic transformation. Thus, a multi-target ROS-cGMP module defines an underlying molecular mechanism of ischemic stroke and its hemorrhagic transformation in diabetes, both of which can be effectively targeted by highly synergistic network pharmacology.

Introduction

1.5 million people are yearly diagnosed with stroke in the EU resulting in a gigantic economic burden which overall reaches €60 billion in health costs [1]. Despite classical studies revealed several potential targets for stroke therapy, all translational clinical trials failed leaving 85% of stroke patients without access to any pharmacotherapy [2]. The "one disease-one target" approach is still a common practice in the drug discovery field and could be consider a clear reason of failure [3]. This strategy overlooks complex disease pathomechanisms and underlying comorbidities while focusing on a symptom- rather than a mechanistic-based therapy [4]. Together with non-precise clinical trial design, the drug discovery field has recently become considerably ineffective where stroke therapy remains as a dramatic case of translational failure.

To address this challenge, we designed an approach focused on the interactome, a comprehensive map including all biologically relevant molecular interactions [5]. Here, proteins associated to specific diseases are not randomly spread but tend to interact forming connected subgraphs, the so-called disease modules [6]. Thus, *de novo* identification of mechanistic-related diseases genes clusters leads to promising target detection and future therapeutic options [7]. In fact, systems medicine and network pharmacology propose the same disease definition based on causal mechanisms. Network pharmacology suggests not targeting single components of a disease module but co-targeting these networks by combining drugs towards (i) maximal dose reduction, (ii) decreased potential side-effects, and (iii) an ultimate synergistic effect [8]. This approach is particularly powerful in complex diseases where mechanistically-related comorbidities worsen the prognosis.

High glucose levels lead to poor brain microvasculature, early endothelial aging and physiological dysfunction. Indeed, diabetic patients have been associated with increased brain edema, infarct size, risk of recurrent ischemic event (1.5-3-fold), worsen prognosis and elevated mortality rate post-stroke [9]. Thus, diabetes is one of the vital comorbidity risk factors of stroke [10] resulting in direct clinical exclusion of the only approved pharmacological treatment so far [11]. Despite this unmet medical need, preclinical experimentation rarely considers real-world stroke scenarios such as diabetes as a comorbidity and therefore frequently overlooks patients' characteristics.

Moreover, diabetes has also been identified as a clinical predictor of secondary hemorrhagic transformation in acute ischemic stroke patients [12, 13] directly correlated to increase in-hospital mortality rate, poor functional recovery and impaired overall prognosis [14]. Despite these strong clinical evidences, the specific underlying mechanisms have not yet been fully identified [13].

We therefore based our novel approach on an in-silico multitarget discovery focused on the multiscale network of human diseases. Within the diseasome, genes related to reactive oxygen species (ROS) and cyclic GMP (cGMP), amongst others, are located [15]. Genetic evidences pointed cGMP as the underlying mechanism of a validated disease cluster including highly prevalent diseases, i.e. diabetes and stroke [16]. Moreover, several ROS sources has been identified as key players of stroke pathomechanism and its comorbidities [17]. Therefore, we here extended these findings to all known ROS and cGMP related clinical drug targets and conducted an interactome-based first neighbor analysis. We identified a disease module for target prediction in stroke therapy by linking six mechanistically related stroke targets within a causal network pharmacology approach. We importantly validated our therapeutic prediction both *in vivo* and *in vitro*, including a translational human blood-brain barrier model and a stroke-diabetes comorbidity model while surprisingly identifying the cause of hemorrhagic transformation, the most detrimental diabetic-dependent event in stroke patients.

Results

In silico disease module target prediction for stroke. To identify the first mechanism-based disease module for stroke therapy, we implemented an *in silico* multitarget approach by extending all known ROS-cGMP clinically translational drug targets, followed by a first-neighbor network analysis. We built a protein-protein interaction (PPI) network using the Integrative Interactive Database (IID) and a list of clinically validated seed proteins. This list included (i) the three human nitric oxide synthase (NOS) isoforms, NOS1, NOS2 and NOS3; (ii) the NADPH oxidase (NOX) isoforms, NOX1, NOX2, NOX3, NOX4 and NOX5; (iii) the soluble guanylate cyclase (sGC) subunits GCYA1, GCYA2, GCYB1 and GCYB2; (iv) the two human monoamine oxidase, MAO-A and MAO-B; (v) xanthine oxidase, XO; and (vi) the ROS toxifier, i.e. myeloperoxidase, MPO. To correct for non-disease relevant but highly connected

proteins (hub nodes), a subnet participation-degree (SPD) score was calculated by normalizing the total PPIs in the subnetwork to the total PPIs in the interactome. The final SPD-pruned network (Fig. 1) highlights a disease-relevant module including NOX5, NOS1, NOS2, NOS3 and sGC. GCYB2 does not have any protein interactions (according to IID) and consequently does not appear in the final network. NOS2 belongs to a different disease module and NOX4 remains isolated. Nevertheless, this method is limited by PPI non considering formed metabolites, i.e. H_2O_2, $O_2^{\cdot-}$. Once including generated metabolites, NOX4 turned to be directly connected to NOS based on a previously described guilt-by-association analysis [4], finally resulting in a protein–metabolic disease module formed by NOX4, NOX5, NOS1, NOS2, NOS3 and sGC.

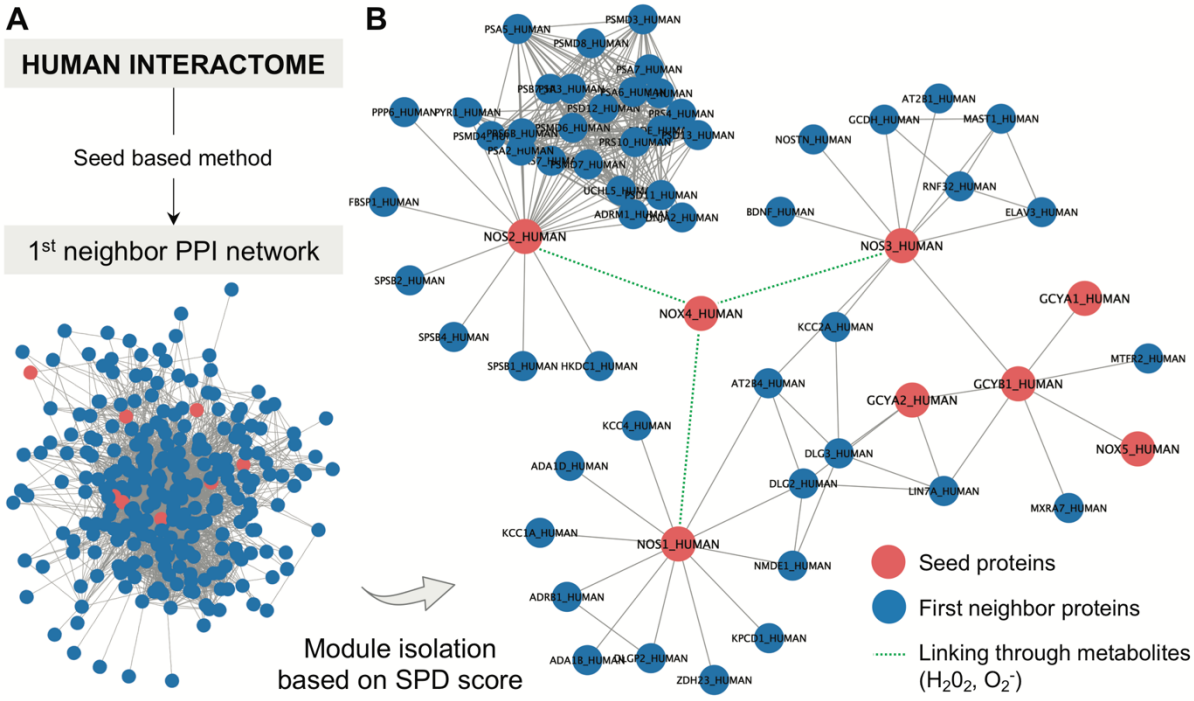

Fig. 1. In silico network pharmacology target prediction. (A) From a list of clinically validated seed proteins (red), a protein-protein interaction (PPI) subnetwork was constructed by expanding to their first neighbors (blue) PPI interactions in IID i.e. human interactome (B) A subnet participation degree score (SPD) score is calculated by the ratio of the degree of the nodes in the subnetwork to the degree of the nodes in the interactome and a 0.18 subnet participation degree score (SPD) was chosen to prune non-relevant protein interactions. By previous guilt-by-association analysis (4), NOX4 is connected to NOS1, NOS2 and NOS3 through metabolites (green dotted line).

Target engagement and ROS biomarker assessment. Having identified NOX, NOS and sGC as mechanistically related targets through an *in-silico* disease module

construction, we designed a network pharmacology based therapeutic approach. This strategy aims to treat diseases by tackling not only single nodes but multiple components of a common underline mechanism; altogether towards potential synergistic effects, dose reduction and decreased side-effects [18]. First, we examined the link of this therapeutic approach to the enzymatic activity, i.e. ROS formation and nitration pattern. Therefore, diabetic 12-to-24 week old mice were subjected to 45min of transient middle cerebral occlusion (tMCAO) followed by 23h of reperfusion in absence or presence of the network pharmacology based triple therapy (3Rx), i.e. GKT137831 (10 mg/kg), SMTC (1 mg/kg) and BAY58-2776 (0.03 mg/kg). ROS generation was assessed through dihydroethidium staining of stroked brain cryosections while the biomarker N-Tyr revealed nitration levels (Fig. 2A). Both ROS and N-Tyr formation were dramatically reduced in treated mice after 24h (Fig. 2B) demonstrating a direct link in ROS/RNS reduction and the pharmacological targeting of mechanistically related enzymes.

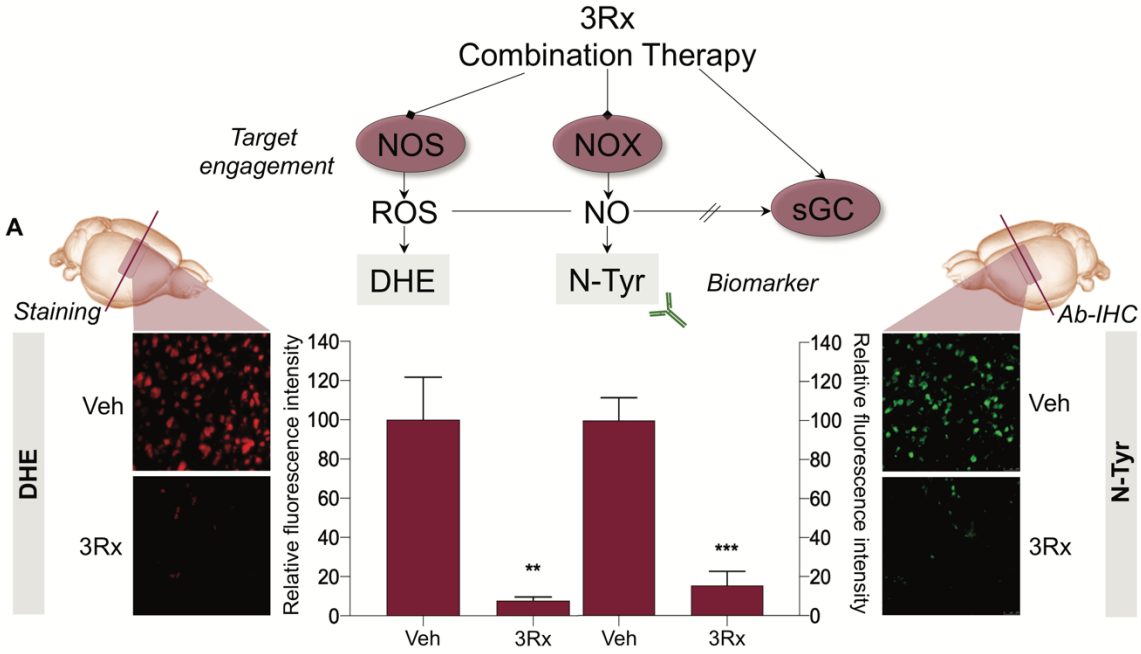

Fig. 2. Target engagement through ROS/RNS detection. (A) Network pharmacology based triple therapy (3Rx) focused on both NO synthase (NOS) and NADPH oxidase (NOX) inhibition together with sGC activation. ROS formation was assessed using the DHE staining while N-Tyr was used as nitration biomarker. (B) Treated (3Rx) diabetic mice showed decreased ROS formation compared to non-treated mice (Veh) (**p<0.01, n=4). Representative staining pictures are shown on the left side of the figure. (C) Nitration levels (N-Tyr) cells were significantly reduced in treated animals (3Rx) in

comparison with non-treated mice (Veh) (***p<0.001, n=4) Representative staining pictures are shown on the right side of the figure.

Network pharmacology based triple therapy validation in a stroke-diabetes comorbidity model. Hyperglycemia leads to endothelial dysfunction, systemic inflammation and thickening of the capillary membrane [19]. Thus, early endothelial aging linked to diabetes make these patients 2-6 times more prone to develop a stroke event also resulting in a dramatically worsen prognosis [20]. However, stroke pre-clinical research frequently ignores this comorbidity risk overlooking real-world clinical scenarios. Thus, to first validate our network pharmacology therapeutic strategy in an *in vivo* model, male and female non-diabetic mice were subjected to 45 min tMCAO in presence or absence of the triple therapy (Fig. 3A). Single subthreshold treatments showed no neuroprotective effect while the triple therapy synergistically reduced infarct volume 24h post-reperfusion (Fig. 3B). In fact, the proposed triple therapy approach showed an improved therapeutic effect compared with the dual therapy suggesting a supra-additive synergistic therapy and further re-conforming our network pharmacology strategy (Fig. S1). Moreover, significant reduction of therapeutic doses aims to maximally reduce possible side-effects towards a fully safe drug profile.

Similar to a clinical scenario, 45 min tMCAO in diabetic mice increased infarct volume in comparison with non-diabetic animals while the triple therapy completely prevented this diabetic-dependent worsen outcome (Fig. 3B). Although infarct volume remains the standard read-out, neuromotor sequelae and life expectancy post-stroke are currently consider the major challenge of stroke survivors [21]. Hence, we additionally assessed two neuro-motor functioning tests in diabetic and non-diabetic comorbid mice (i) the elevated body swing test (Fig. 3C) and (ii) Bederson score (Fig. 3D), which both showed significant neuro-motor impairment in diabetic animals compared to non-comorbid mice. Surprisingly, the 3Rx therapy improved the outcome post-stroke avoiding any worsening due to diabetes. Therefore, the network pharmacology-based therapy prevents neuro-motor dysfunction and increased infarct volume not exclusively on ischemic mice but also on diabetes-stroke comorbid animals.

Blood-brain barrier (BBB) disruption takes place in early ischemic stages being associated to endothelial dysfunction and inflammatory processes, altogether damaging

the neurovascular unit [22]. Indeed, high levels of matrix metalloproteinase-9 (MMP-9) is currently considered a BBB marker directly correlated to larger infarct volumes, stroke severity and impaired functional outcome [23]. To test whether the triple therapy, i.e inhibition/activation of mechanistically related targets results in a blood-brain barrier phenotype, we assessed MMP-9 levels post-stroke in diabetic animals subjected to stroke. In line with previous findings, triple therapy significantly reduced MMP-9 levels and subsequent blood-brain barrier leakage upon stroke compared to non-treated animals (Fig. 3E).

To link the neuroprotective effect of the 3Rx therapy to a possible improvement of life expectancy, we assessed acute mortality over the first 24h post-stroke. 1-day post-reperfusion 95% of treated animals survived while only 62% of non-treated diabetic animals remained alive 24h post-surgery (Fig. 3F). Thus, pharmacological targeting of NOX, NOS and sGC as part of the same disease module leads to the first potent, mechanism-based, neuroprotective and synergistic therapy for currently not treatable patients suffering from diabetes-related poor outcome after a stroke event.

Identification of NOX5 as the direct cause of diabetes associated hemorrhagic transformation. Ca^{2+}-dependent NOX5 has been recently identified as the mechanistic link between postreperfusion calcium overload and early BBB opening playing a key role in stroke pathomechanism [24]. However, this NOX isoform is missing from the mouse genome [25]. To examine the role of NOX5 in a clinical scenario, i.e. as part of a diabetes-stroke comorbidity, hyperglycemia was induced in humanized NOX5 mice later subjected to 1h tMCAO followed by 24h reperfusion (Fig. 4A). Surprisingly, NOX5KI diabetic mice developed hemorrhagic transformation upon stroke (Fig. S2) and no clear infarct volume was therefore detectable (Fig. 4B). Mechanical validation of the MCAO surgery in diabetic NOX5KI mice was conducted to discard any possible technical bias (Fig. S3).

Hemorrhagic transformation risk has been directly associated to diabetes patients excluding them from any therapeutic available option, being the ones who suffer the worst outcome from stroke, increased recurrence rate and terrible prognosis [26]. However, in our humanized *in vivo* model, hemorrhagic transformation was prevented by the triple therapy (Fig. 4B). Moreover, no hemorrhagic transformation

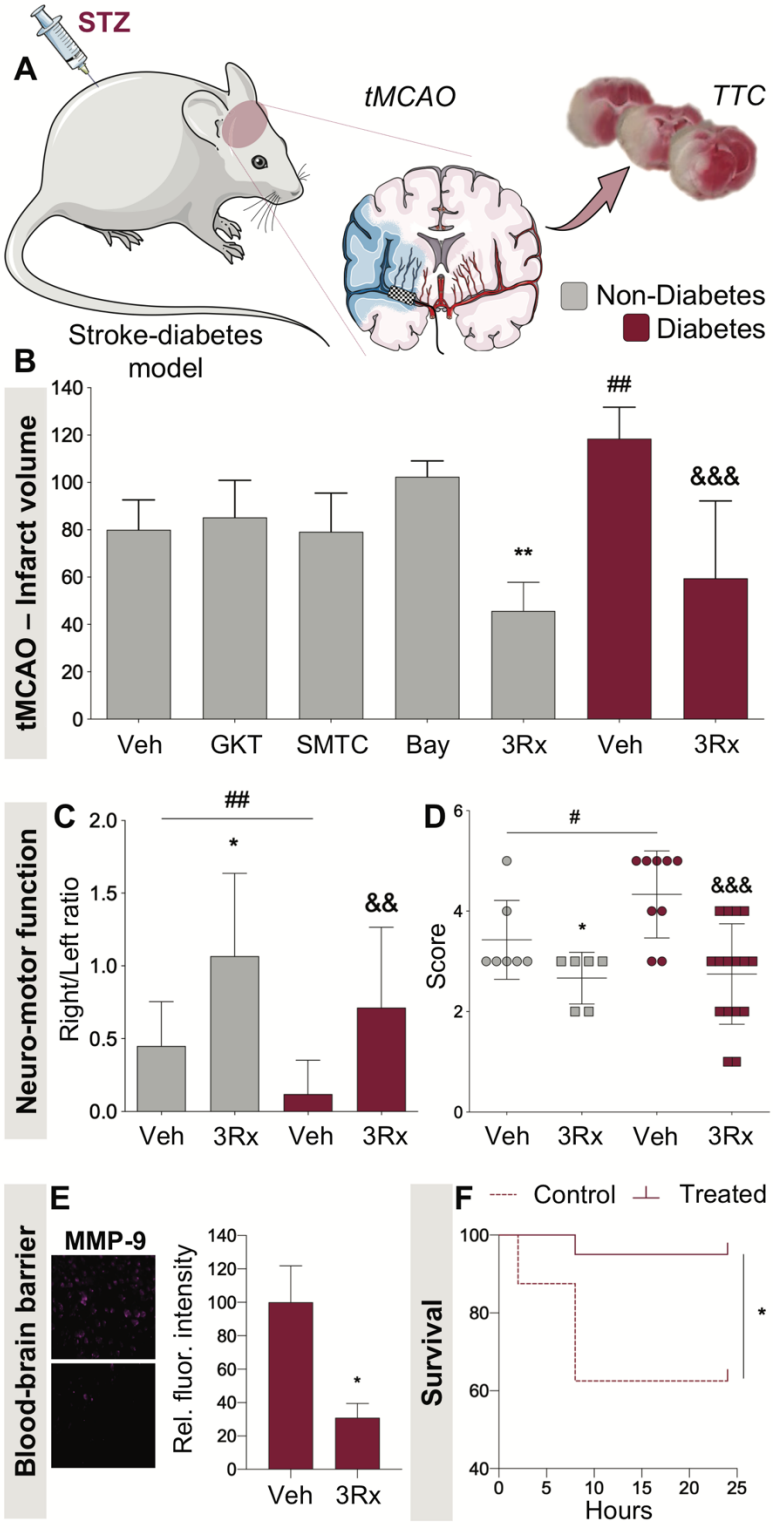

Fig. 3. Network pharmacology therapy reduced infarct size, stabilized blood-brain barrier and increases survival in a stroke model with diabetes as comorbidity. (A) Diabetes was induced by streptozotocin (STZ) administration in adult mice (6-9 weeks) which were later (12-24 weeks) subjected to 45 min transient

occlusion of the middle cerebral artery (tMCAO) followed by 24h reperfusion. Treatment was injected i.p. 1h post-reperfusion. (B) 24h post-stroke infarct size was reduced in non-diabetic mice treated with the combination therapy (3Rx), i.e. GKT137831 (10 mg/kg), SMTC (1 mg/kg) and BAY58-2667 (0.03 mg/kg), while no effect was detected in animals treated with single-compound subthreshold doses of the same drugs (**p<0.01, n=7). Moreover, 45 min tMCAO in diabetic mice increased infarct volume in comparison with non-diabetic animals (##p<0.01, n=7) being completely prevented by the triple therapy (&&&p<0.001, n=10). (C) Of clinical relevance, neurological outcome (elevated body swing test) was improved in diabetic (&&p<0.01, n=10) and non-diabetic (*p<0.05, n=6) mice under treatment (3Rx) compared to non-treated mice while diabetes significantly aggravated neuromotor functioning in basal (Veh) conditions (##p<0.01, n=10). (D) Similarly, the Bederson score showed a significant improvement in neuromotor functioning both in comorbid (*p<0.05, n=6) and non-comorbid (&&&p<0.001, n=10) conditions while worsening the outcome in diabetic animals (#p<0.05, n=10). (E) Blood-brain barrier disruption was indirectly assessed through measuring MMP-9 level. The triple therapy preserved BBB from leakage 1-day after reperfusion (*p<0.05, n=4). (F) Triple therapy increased survival in the acute reperfusion phase (first 24h) compared to non-treated mice.

events occurred in NOX5WT mice while 6 out of 7 humanized animals developed hemorrhagic transformation post-reperfusion (Fig. 4C). To evaluate the hemorrhagic extent, hemorrhagic transformation was macroscopically assessed and classified into 5 subtypes based on the severity and extension of the formed hematoma [27]. NOX5KI diabetic mice treated post-stroke showed either no hemorrhage or a small petechial hemorrhagic infarction (Fig. 4D). Of clinical relevance, we assessed acute survival upon stroke both in NOX5WT and NOX5KI diabetic mice. Indeed, the 3Rx combination therapy significantly increased survival both in NOX5WT (Fig. 4E) and NOX5KI (Fig. 4F) diabetic mice post-reperfusion. Hence, we identified NOX5 as the main cause of diabetes-associated hemorrhagic transformation which could be directly prevented by triple therapy while increasing acute survival.

In vitro human validation for clinical translation. Hyperglycemia is strongly associated to the alteration of BBB transporting functions, physiological integrity, i.e. tight junctions disruption and thickening of the capillary walls, followed by ROS/RNS induction [28]. Brain ischemia dramatically aggravates this pathological scenario. Therefore, to test the translatability of our findings into a future clinical setting, we used a primary culture of human brain microvascular endothelial cells (HBMECs) as an in vitro blood-brain barrier model (Fig. 5A). First, we subjected HBMECs expressing NOX5

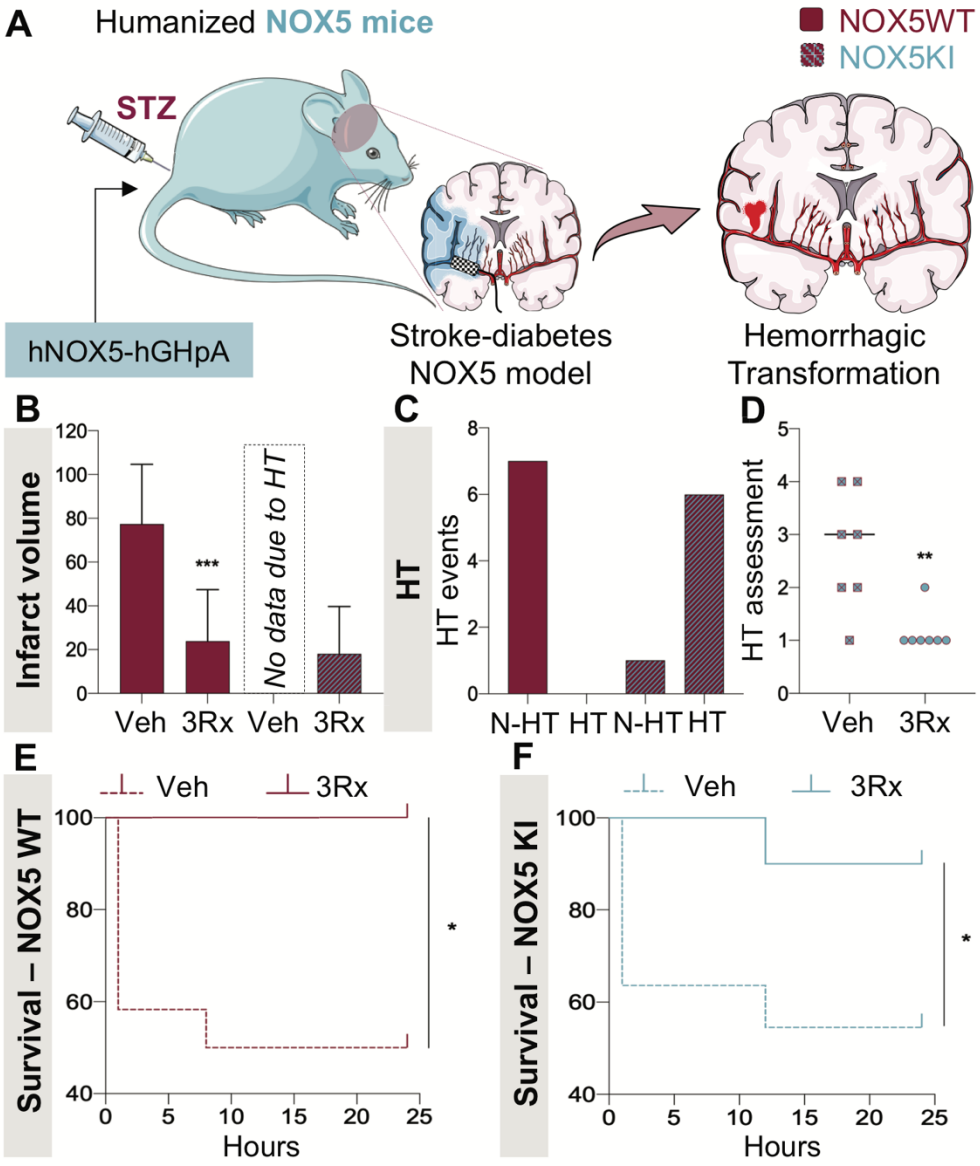

Fig. 4. Identification of NOX5 as the cause of diabetes-associated hemorrhagic transformation. (A) The humanized NOX5KI mice was generated as described in (21). Then, diabetes was induced by streptozotocin administration to NOX5KI/WT adult mice (6-9 weeks) which were later subjected to 45 min transient occlusion of the middle cerebral artery (tMCAO) followed by 24h reperfusion. Treatment was injected i.p. 1h post-reperfusion. (B) Infarct size was reduced in NOX5WT mice post-treatment (3Rx) 24h after reperfusion (***p<0.01, n=8). However, no clear infarct volume was detected in NOX5KI due to the development of hemorrhagic transformation (HT). Infarct assessment was again possible in NOX5KI treated mice due to a full prevention of HT. (C) No HT events occurred in non-treated NOX5WT mice while all NOX5KI animals (n=6) but 1 developed HT within the first 24h post-reperfusion under basal conditions (Veh). (D) Macroscopic evaluation of HT in NOX5KI mice showed a significant reduction in cerebral HT after the 3Rx treatment compared to non-treated (Veh) animals (*p<0.05, n=7). (E) In line with previous findings, the triple therapy increased

survival in NOX5WT mice (*p<0.05, n=6) and (F) NOX5KI animals within the acute phase post-stroke (*p<0.05, n=7).

endogenously to 6 hours of hypoxia under normal glucose conditions, followed by 24 hours of reoxygenation. Cell viability was increased in the presence or absence of the triple therapy compared to non-treated cultures while subthreshold concentrations of single-drug therapies remained non-effective (Fig. 5B). Similarly, the 3Rx therapy prevented the increase in permeability after hypoxia under normal glucose conditions (Fig. 5C). Importantly, hyperglycemia (25mM glucose) significantly reduced cell viability post-reoxygenation in comparison with normal glycemic conditions which could be prevented by the 3Rx (Fig. 5D). Thus, we validated our 3Rx therapy in a human in vitro translational model where the hyperglycemia-dependent aggravation of hypoxia could be directly treated. We therefore here propose the first mechanism-based, synergic and neuroprotective therapy for a currently non-treatable disease condition.

Discussion

Based on *in silico* prediction, we have identified a multi-target ROS-cGMP module which defines an underlying molecular mechanism of ischemic stroke and its hemorrhagic transformation in diabetes. We could validate this module *in vivo* and *in vitro* by applying a network pharmacology approach. Indeed, a triple combination therapy with a NOS inhibitor, a NOX inhibitor and an sGC activator was highly synergistic and resulted in decreased infarct size, stabilized blood-brain barrier, improved neuro-motor function and increased survival in a mouse stroke model with diabetes as comorbidity. In addition, we identified NOX5 as the cause of diabetes-associated hemorrhagic transformation.

On a broader level, disease module prediction using our metabolome/interactome-based approach can be applied to other complex diseases. Based on PPI networks, we have identified a disease relevant module including NOX5, NOS1, NOS2, NOS3 and sGC. However, PPI networks alone are just one level of molecular interaction networks and most signaling events also involve metabolites or metabolic protein modifications [4, 29, 30]. Therefore, we used protein-metabolite networks in conjunction with PPI networks. Accordingly, our module was expanded to include NOX4.

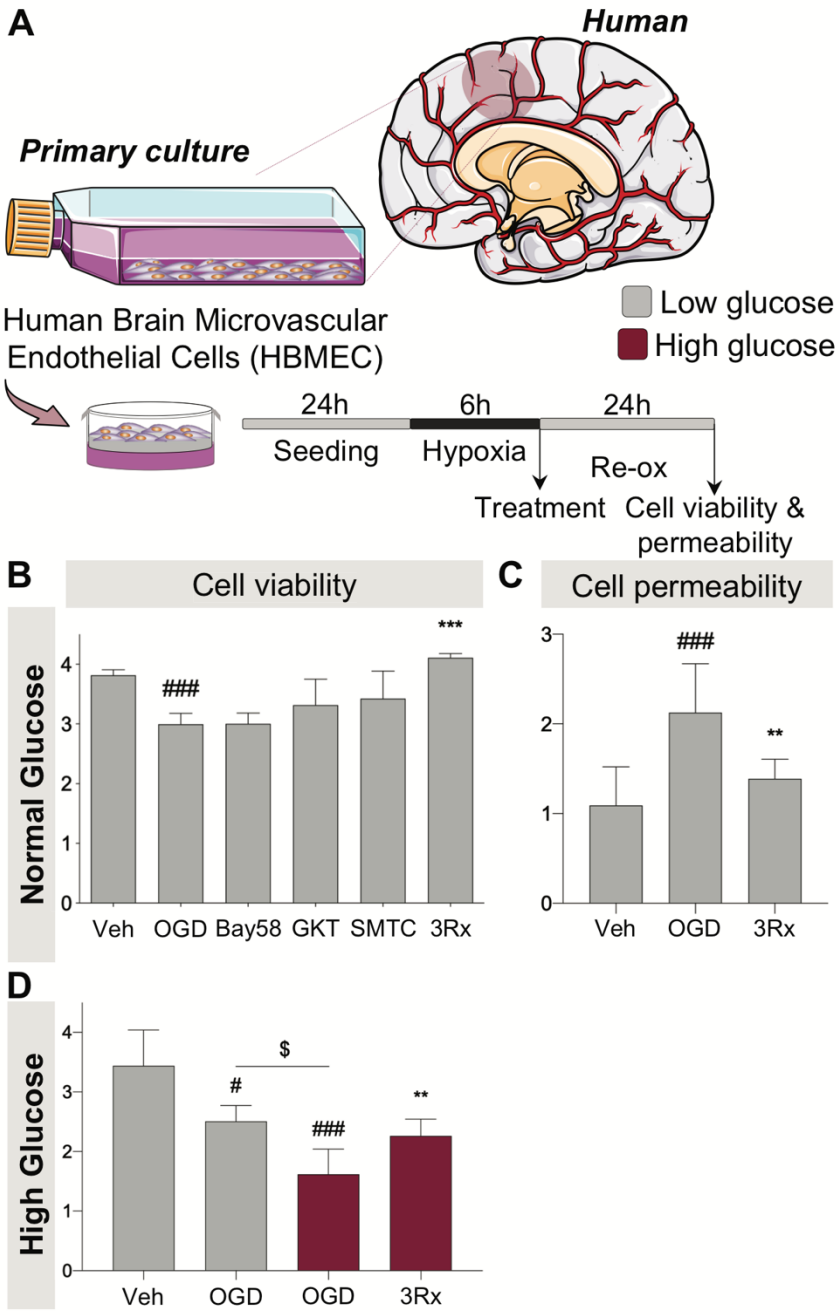

Fig. 5. Therapeutic translation to an in vitro human blood-brain barrier model. (A) Human Brain Microvascular Endothelial Cells (HBMECs) were incubated under physiological conditions until the optimal cell confluence was reached. Then, HBMECs were subjected to 6h hypoxia (Hyp) in presence of normal or hyperglycemic conditions followed by 24h reoxygenation. To mimic the clinical situation, therapy was added just after re-oxygenation. 1-day later both cell viability and permeability were assessed. (B) Under normal glucose conditions, cell viability significantly increased in cells treated with the combination therapy (3Rx) (***p<0.001, n=10) while no reduction was detected after single-drug treatments, i.e. GKT137831 (0,3µM), SMTC (0,1µM), and BAY 58-2667 (0,03µM) compared to non-treated cells (###p<0.001, n=6). (C) Similarly, cell permeability was reduced under the triple therapy (**p<0.01, n=6) in comparison with non-treated cells (###p<0.001, n=6). (D) To translate previous findings to an human in

vitro set-up, cells were subjected to hypoxia under hyperglycemic conditions. Presence of high glucose (25mM) significantly reduced cell viability compared to non-hyperglycemic cells ($p<0.05, n=5). This glucose-dependent detrimental effect was fully prevented by the triple therapy (**p<0.01, n=10).

Previous preclinical data in stroke showed that NOS1-3, NOX4 and NOX5 play detrimental roles [24, 31] possibly via formation of peroxynitrite and oxidation of sGC [16, 32]. However, most of these studies did not consider multiple targets or real-world stroke scenarios such as diabetes as a comorbidity. Therefore, we validated the therapeutic applicability of our *in-silico* network pharmacology hypothesis both *in vitro* and *in vivo* by co-administering a NOX inhibitor, NOS inhibitor and sGC activator under high glucose/diabetic conditions. Importantly for efficacy and safety, the combination therapy resulted in a neuroprotective effect using subthreshold concentrations or doses.

Diabetes is a main risk factor of post-stroke hemorrhagic transformation following recombinant tissue plasminogen activator (rt-PA) therapy and may attenuate the therapeutic benefit of rt-PA [13]. Previous data showed that these detrimental actions are attributed to hyperglycemia that is associated with increased ROS production from NOX during reperfusion [33, 34]. However, these studies used i) transient hyperglycemia model by glucose injection after stroke and not chronic diabetes, ii) animals that do not express NOX5, and iii) non-specific antioxidants (apocynin and VAS2870). Yet, here we identified NOX5 as a causal protein in diabetes-induced hemorrhagic transformation using chronic model of diabetes in humanized mice that express NOX5.

Overall, our findings using *in silico* metabolome/interactome network approach and further preclinical validation show ROS-cGMP dysfunction as a causal mechanism in stroke. Diabetic humanized NOX5 KI mice represent an interesting mechanism-based animal model of hemorrhagic transformation. Therapeutically, low-dose combination of a NOS inhibitor, a NOX inhibitor and an sGC activator represents a first-in-class mechanism-based approach for stroke treatment. Moreover, NOX5 inhibition could be used as adjunctive therapy with rt-PA after stroke.

Materials and Methods

In silico disease module prediction

A protein-protein interaction subnetwork with 278 proteins as nodes and 2791 protein-protein interactions was extracted from the Integrative Interaction Database (IID) [6] i.e. interactome. First, NOS1, NOS2, NOS3, GUCYA1, GUCYA2, GUCYB1, NOX4 and NOX5 were selected as seeds and all first neighbors' protein interactions were added. In order to emerge weighted disease modules, a subnet participation degree (SPD) score was calculated by normalizing the degree of the protein nodes in the subnetwork to the degree of the nodes in the interactome. A final subnetwork including 61 nodes and 313 protein protein interactions was extracted using a SPD score of 0.18. This score cutoff corresponds to 80% of the cumulative sum of the percentage of the nodes, removing non-specific interactions while including most module-specific interactions.

Study design

All animal experiments were performed according to the EU Directive 2010/63/EU for animal experiments and approved by the Dutch law on animal experiment and the Institutional Ethics Committee of Universidad Autónoma de Madrid, Madrid, Spain. Animals were socially housed under controlled conditions (22°C, 55– 65% humidity, 12h light-dark cycle), and had free access to water and standard laboratory chow. All efforts were made to minimize animal suffering and to reduce the number of animals used in the experiments. 8-20 weeks C57/BlJ, NOX5WT and NOX5KI adult male and female mice were used for the *in vivo* animal study. NOX5KI animals were compared to their respective matched WT line. Animals were excluded from end-point analyses if death occurred within 24h after tMCAO. Details regarding the study design and animal exclusion could be found in Table S1.

Generation of a diabetic mouse model

Diabetes was induced in mice (6-9 weeks old) by i.p. injections of streptozotocin (STZ) (Merck Millipore, The Netherlands) dissolved in 0.5M sodium citrate buffer with a final dose of 55 mg/kg during 5 consecutive days. Blood glucose was measured daily for 7 days after the last STZ injection using a glucometer (Contor XT, Ascensia Diabetes Care, The Netherlands). Blood glucose levels higher than 12mM 7 days after STZ injections were considered diabetic and therefore included in the study. Diabetic mice were

monitored daily for any signs of welfare discomfort and blood glucose levels were followed-up weekly (Table S2, Table S3).

In vivo stroke model: Transient occlusion of the middle cerebral artery (tMCAO)

C57Bl6/J mice were anesthetized with isoflurane (0.6% in oxygen). The animal was placed on a heating-pad, and rectal temperature was maintained at 37.0°C using an homeothermic monitoring system (Harvard Apparatus, Spain). The model was conducted as previously described in [4]. Transient cerebral ischemia was induced using the intraluminal filament technique. A midline neck incision was made, and the right common and external carotid arteries were isolated and permanently ligated, altogether using a surgical microscope (Tecnoscopio OPMI pico, Carl Zeiss, Meditec Iberia SA, Spain). A microvascular temporarily ligature was placed on the internal carotid artery to temporarily stop the blood flow. A silicon rubber-coated monofilament (6023910PK10, Doccol Corporation, Sharon, MA, USA) was inserted through a small incision into the common carotid artery and advanced into the internal carotid artery until the tip of the monofilament is then precisely located at the origin of the right middle cerebral artery and thus interrupting completely the blood flow. The filament was held in place by a tourniquet suture on the common carotid artery to prevent filament displacement during the ischemic period. Animals were maintained under anesthesia during 45min followed by 23h reperfusion period starting when the monofilament is removed. After the surgery, wounds were carefully sutured and animals could recover from surgery. Operation time per animal did not exceed 15 minutes.

In vivo network-pharmacology based combination therapy

Three different compounds were simultaneously used, i.e. S-Methyl-L-thiocitrulline (SMTC, SanBio bv, The Netherlands), GKT137831 (GKT, Genkyotech, Switzerland) and BAY 58-2667 (Bayer Pharmaceuticals, Germany). SMTC was directly dissolved in sterile saline while GKT and BAY 58-2667 were dissolved in a mixture of DMSO/saline in a ratio of 1/99. SMTC (1 mg/kg), GKT (10 mg/kg) and BAY (0.03 mg/kg), or vehicle (DMSO/saline in a ratio of 1/99) were injected i.p. 30 min after filament removal, i.e. reperfusion. Infarct size after monotherapy was only tested in non-diabetic animals due to ethical limitations. Indeed, our current ethical approval is focused on go/no-go decisions to further reduce unnecessary animal experimentation. Therefore, testing an

already validated, non-effective therapeutic strategy in diabetic animals would result in ethical concerns. Therefore, only the combination therapy was assessed.

Oxidative stress measurement: DHE staining

Assessing ROS production ex vivo in stroked brain tissue was determined using the florescence dye dihydroethidium (DHE, Thermo Fisher Scientific, The Netherlands). Frozen brain cryosections (10 µm) were fixated using 4% paraformaldehyde in PBS and then incubated under 2 µM DHE (2mM stock solution) for 30 minutes at 37°C. After three washing steps with PBS, slices were incubated with Hoechst 2 ng/ml (Hoechst 33342, Sigma-Aldrich, The Netherlands) for 10 min at 37°C. The relative pixel intensity was measured in identical regions using a Leica DMI3000 B fluorescence microscope (The Netherlands) and later analysed with the ImageJ software (National Institutes of Health, USA).

Assessment of nitrated proteins

Stroked brain tissue cryosections (10 µm) were fixed with 4% paraformaldehyde in PBS. After fixation, sections were incubated for 1h at room temperature using a rabbit polyclonal anti-nitrotyrosine antibody (1:100); (A-21285, Thermo Fisher Scientific, The Netherlands) in blocking buffer. After washing in PBS (3x), sections were incubated with the secondary antibody, Alexa Fluor 488 donkey anti-rabbit (1:100); (A-21206, Thermo Fisher Scientific, The Netherlands) for 45 min at room temperature. The fluorescent Hoechst33342 dye (ThermoFisher Scientific, The Netherlands) was added (2 ng/ml) for 10 min at room temperature. Sections were washed in PBS and then mounted using a Dako Fluorescence Mounting Medium (S3023, Agilent Technologies, The Netherlands). Immunofluorescent signal was assessed using a Leica DMI3000 B microscope (The Netherlands) and quantitative analysis of nitro-tyrosine fluorescence was performed with the ImageJ software (National Institute of Health, USA).

Infarct size determination

After animal sacrificing, brains were quickly removed and cut into four 2mm thick coronal sections using a mouse brain slicer matrix (Zivic Instruments, The Netherlands). Brain slices were kept at 4°C during 5 min and later stained using 2% 2,3,5-triphenyltetrazolium (TTC; Sigma-Aldrich, The Netherlands) for 15 min at room temperature in PBS to visualize the infarctions. Indirect infarct volumes were calculated

by volumetry (ImageJ software, National Institutes of Health, USA) according to the following equation:

Vindirect (mm3) = Vinfarct x (1-(Vih – Vch)/Vch)

where the term (Vih – Vch) represents the volume difference between the ischemic hemisphere and the control hemisphere and (Vih – Vch)/Vch expresses this difference as a percentage of the control hemisphere.

Neuro-motor functioning

Two different neuro-motor functional tests were assessed in both comorbid and non-comorbid animals in presence and absence of the combinatory therapy 24h post-reperfusion. Test 1. The Bederson Score [35] categorizes the animals based on: Score 0, no apparent neurological deficits; 1, body torsion and forelimb flexion; 2, right side weakness and thus decreased resistance to lateral push; 3, unidirectional circling behavior; 4, longitudinal spinning; 5, no movement. Test 2. During the elevated body swing test, the mice are held ~1 cm from the base of its tail and then elevated above the surface in the vertical axis around 20 cm. A swing was considered whenever the animal moved its head out of the vertical axis to either the left or the

right side (more than 10 degrees). Ratio of right/left swings were subsequently analyzed.

Determination of blood-brain barrier stability

Cryosections (10µm) from stroked mice were fixed in 4% paraformaldehyde (Sigma-Aldrich, The Netherlands) for 10 min followed by 1h blocking period in 1% bovine serum albumin. Brain sections were incubated overnight at 4°C with a rabbit polyclonal MMP9 antibody (1:100); (Thermo Fischer Scientific, The Netherlands). Subsequently, they were incubated for 45 min at room temperature with the secondary antibody, Alexa fluor 488 donkey anti-rabbit (1:200 in 1% BSA in PBS); (Thermo Fischer Scientific, The Netherlands). Brain sections were then incubated with 2µg/ml 4′,6-diamidino-2-phenylindole (DAPI) fluorescent dye (Thermo Fischer, The Netherlands) for 10 min and finally mounted using DAKO mounting medium (Agilent, US). Signal was assessed using a fluorescence microscope Leica DMI3000 B microscope (The Netherlands) and quantitative analysis was performed with the ImageJ software (National Institute of Health, USA).

Generation of the humanized NOX5KI mouse

Since both mice and rats genome naturally lacks the *NADPH oxidase 5* gene, we created a new mouse line expressing the human *NOX5* gene under the control of the *Tie2* promoter. Details concerning the generation process could be found in [24].

Hemorrhagic transformation: Events and assessment

A macroscopic score for hemorrhagic transformation based on human clinical studies classified brain hemorrhage into five types [27]: (0) no hemorrhage; (1) small petechial hemorrhagic infarction; (2) confluent petechial hemorrhagic infarction; (3) parenchymal hematoma type-1 (<30% of infarct); (4) parenchymal hematoma type-2 (>30% of infarct).

HEK culture and NOX5 transfections

Human embryonic kidney 293 (HEK293) cells cultured in DMEM medium containing 5% FBS were transfected with pcDNA control plasmid (vector control) or NOX5 plasmid using FuGENE6 transfection reagent (Promega) followed by ROS measurement after 48h.

ROS measurement by luminol assay

To measure NOX5 activity, superoxide from vector-transfected or NOX5-transfected HEK293 cells was measured by luminol-enhanced chemiluminescence in white plates as follows. HEK293 cells were cultured in DMEM medium containing 5% FBS and then transfected with pcDNA control or NOX5 plasmids using FuGENE® 6 transfection reagent. After 48 h, cells were detached by adding trypsin and then re-suspended in HBSS buffer. Each 50 µl of cell suspension consisted of 100,000 cells was added to each well (in triplicate) in a 96-well plate and incubated at 37 °C for 10 min with vehicle, superoxide dismutase (SOD), diphenyleneiodonium chloride (DPI) or GKT137831. After 10 min of incubation, 50 µl reaction buffer (containing 6.4 U/ml HRP and 0.4 mM luminol in KRPG buffer) was added to the 50 µl cell suspension so that the total volume of assay was 100 µl. Cells were then stimulated by addition of 1µM phorbol 12-myristate 13-acetate (PMA; PKC activator) and the Ca^{2+} ionophore ionomycin (40 µM). Superoxide generation was detected by monitoring relative light units (RLU) with a Wallac luminometer Victor2 at 37 °C for 20 min. Cell-free experiments were similarly performed using xanthine 50µM/xanthine oxidase 1mU/ml as the ROS source.

Human brain microvascular endothelial cells (HBMEC) under hypoxic conditions

HBME cells (Cell systems, USA) between passage 3 and 9 were cultured to ~95% confluence using a specialized cell medium and grow factors (EGM-2 MV BulletKit, Lonza, The Netherlands) enriched with 5% fetal bovine serum (FBS; Sigma-Aldrich, The Netherlands). Before being subjected to hypoxia, HBMECs were seeded at $6x10^4$ cells/ml in 12 wells-plate and incubated during 24h at 37°C. Then, cell medium was replaced with non-FBS containing medium (2 ml/well) followed by 6h of hypoxia (94,8% N_2, 0.2% O_2 and 5% CO_2) at 37°C using the hypoxia workstations (Ruskin Invivo2 400 station, The Netherlands). The hypoxia period was followed by 24h of reperfusion in the presence or absence of the combinatory therapy 0.3 µM GKT137831, 1 µM SMTC and 0,03 µM BAY 58-2667 under normal glucose conditions or hyperglycemia (25mM glucose). Control cells were exposed to normoxia (75% N_2, 20% O_2 and 5%CO_2) and enriched medium during the hypoxia period.

Assessment of cell viability in HBMEC

24h post-reoxygenation, cell viability was assessed using the colorimetric MTT (3-(4,5-dimethylthiazol-2-yl)-2,5-diphenyltetrazolium bromide) assay [36]. MTT solution (5 mg/ml) was added (100 µl/ml) and incubated for 2h at 37°C. The formazan salt formed was solubilized by adding DMSO (250 µl/well) for later measuring spectrophotometrically its optical density at 540 nm.

Assessment of cell permeability in HBMEC

$2x10^4$ HBME cells were seeded and grown to confluence on membranes of Transwell inserts (12mm Transwell®-COL Collagen-Coated 3.0µm Pore PTFE Membrane Insert, Corning, The Netherlands) 24h before inducing hypoxia. 6h of ischemic conditions were followed by a 24h re-oxygenation period in the presence or absence of the combinatory therapy 0.3 µM GKT137831, 1 µM SMTC and 0,03 µM BAY 58-2667. Cell permeability was assessed using the Evans Blue dye (Sigma-Aldrich, The Netherlands). Before the diffusion experiment, the assay buffer (4% bovine serum albumin in PBS, 1.5 ml) was added to the abluminal side of the insert. The permeability buffer (0.5 ml) containing 4% bovine serum albumin and 0.67 mg/ml Evans blue dye was loaded on the luminal side of the insert followed by 10 min incubation at 37°C. The concentration of Evans Blue in the abluminal chamber was measured by determining the absorbance of 150µl buffer at 630 nm using a microplate reader.

Statistical analysis

All results obtained from the *in vitro* (HBMECs), ex vivo (staining and immunohistochemistry) and *in vivo* (tMCAO) experimentation were analyzed using Prism 8.0 software. Data were expressed as the means ± SEM of separate experiments. Statistical comparisons between groups were performed using one-way ANOVA, followed by a Newman–Keuls multiple-comparison test. Differences between two groups were considered significant at $P<0.05$. In each case, when only two groups were compared, the unpaired two-tailed Student's t test was applied, where significance was considered at $P<0.05$. For comparison of survival curves the log-rank (Mantel-Cox) test was used. $P<0.05$ was considered statistically significant. Numbers of animals necessary to detect a standardized effect size on infarct volumes ≥0.2 (vehicle-treated control mice vs. treated mice) were determined via a priori sample size calculation with the following assumptions: $\alpha=0.05$; $\beta=0.2$; 20% SD of the mean.

Acknowledgments: Dr. Javier Egea is gratefully acknowledged for supporting NOX5KI mice breeding. **Funding**: This study was supported by the H2020 Project 777111-REPO-TRIAL, ERC PoC SAVEBRAIN (both to H.H.H.W.S.), short-term scientific missions by the COST Actions EU-ROS and Open-MultiMed, and Kootstra Talented Fellowship (UM) (to A.I.C.). J.B.'s work was financially supported by VILLUM Young Investigator Grant 13154. **Author contributions**: A.C.: design, acquisition, analysis and interpretation of the data, writing manuscript, figure design; M.E.: support immunohistochemistry, staining and animal studies; C.N., S.S., T.K. and J.B. provided all bioinformatic tools, data adquision and analysis; H.S. project conception, experimental design, data interpretation, writing manuscript, figure design. **Competing interests**: H.H.H.W.S. is a cofounder of Vasopharm, currently developing a small-molecule NOS inhibitor (phase III clinical trial). However, H.H.H.W.S. has no longer any operative role in the company and holds less than 1% of shares.

References

1. Luengo-Fernandez, R. et al. (2020) Economic burden of stroke across Europe: A population-based cost analysis. Eur Stroke J 5 (1), 17-25.

2. Zerna, C. et al. (2017) Towards Improved Translational Stroke Research: Progress and Perspectives of the Recent National Institute of Neurological Disorders and Stroke Consensus Group Meeting. Stroke 48 (9), 2341-2342.

3. Yildirim, M.A. et al. (2007) Drug-target network. Nat Biotechnol 25 (10), 1119-26.

4. Casas, A.I. et al. (2019) From single drug targets to synergistic network pharmacology in ischemic stroke. Proc Natl Acad Sci U S A 116 (14), 7129-7136.

5. Barabasi, A.L. et al. (2011) Network medicine: a network-based approach to human disease. Nat Rev Genet 12 (1), 56-68.

6. Menche, J. et al. (2015) Disease networks. Uncovering disease-disease relationships through the incomplete interactome. Science 347 (6224), 1257601.

7. Caldera, M. et al. (2017) Interactome-based approaches to human disease. Current Opinion in Systems Biology 3, 88-94.

8. Hopkins, A.L. (2008) Network pharmacology: the next paradigm in drug discovery. Nat Chem Biol 4 (11), 682-90.

9. Gaillard, T. and Miller, E. (2018) Guidelines for Stroke Survivors With Diabetes Mellitus. Stroke 49 (6), e215-e217.

10. Nayak, A.R. et al. (2016) Prediction of Outcome in Diabetic Acute Ischemic Stroke Patients: A Hospital-Based Pilot Study Report. Ann Neurosci 23 (4), 199-208.

11. Hafez, S. et al. (2014) Hyperglycemia, acute ischemic stroke, and thrombolytic therapy. Transl Stroke Res 5 (4), 442-453.

12. Paciaroni, M. et al. (2009) Acute hyperglycemia and early hemorrhagic transformation in ischemic stroke. Cerebrovasc Dis 28 (2), 119-23.

13. Mishiro, K. et al. (2014) Diabetes mellitus aggravates hemorrhagic transformation after ischemic stroke via mitochondrial defects leading to endothelial apoptosis. PLoS One 9 (8), e103818.

14. Mi, D. et al. (2018) Correlation of hyperglycemia with mortality after acute ischemic stroke. Ther Adv Neurol Disord 11, 1756285617731686.

15. Goh, K.I. et al. (2007) The human disease network. Proc Natl Acad Sci U S A 104 (21), 8685-90.

16. Langhauser, F. et al. (2018) A diseasome cluster-based drug repurposing of soluble guanylate cyclase activators from smooth muscle relaxation to direct neuroprotection. NPJ Syst Biol Appl 4, 8.

17. Tun, N.N. et al. (2017) Diabetes mellitus and stroke: A clinical update. World J Diabetes 8 (6), 235-248.

18. Barabasi, A.L. and Oltvai, Z.N. (2004) Network biology: understanding the cell's functional organization. Nat Rev Genet 5 (2), 101-13.

19. Chen, R. et al. (2016) Diabetes and Stroke: Epidemiology, Pathophysiology, Pharmaceuticals and Outcomes. Am J Med Sci 351 (4), 380-6.

20. Ergul, A. et al. (2012) Cerebrovascular complications of diabetes: focus on stroke. Endocr Metab Immune Disord Drug Targets 12 (2), 148-58.

21. Morone, G. et al. (2014) Advances in neuromotor stroke rehabilitation. Biomed Res Int 2014, 236043.

22. Hoffmann, A. et al. (2018) Early Blood-Brain Barrier Disruption in Ischemic Stroke Initiates Multifocally Around Capillaries/Venules. Stroke 49 (6), 1479-1487.

23. Ramos-Fernandez, M. et al. (2011) Matrix metalloproteinase-9 as a marker for acute ischemic stroke: a systematic review. J Stroke Cerebrovasc Dis 20 (1), 47-54.

24. Casas, A.I. et al. (2019) Calcium-dependent blood-brain barrier breakdown by NOX5 limits postreperfusion benefit in stroke. J Clin Invest 130, 1772-1778.

25. Holterman, C.E. et al. (2014) Nephropathy and elevated BP in mice with podocyte-specific NADPH oxidase 5 expression. J Am Soc Nephrol 25 (4), 784-97.

26. Kunte, H. et al. (2012) Hemorrhagic transformation of ischemic stroke in diabetics on sulfonylureas. Ann Neurol 72 (5), 799-806.

27. Couret, D. et al. (2018) A hemorrhagic transformation model of mechanical stroke therapy with acute hyperglycemia in mice. J Comp Neurol 526 (6), 1006-1016.

28. Prasad, S. et al. (2014) Diabetes Mellitus and Blood-Brain Barrier Dysfunction: An Overview. J Pharmacovigil 2 (2), 125.

29. Mehta, V. and Trinkle-Mulcahy, L. (2016) Recent advances in large-scale protein interactome mapping. F1000Res 5.

30. Vidal, M. et al. (2011) Interactome networks and human disease. Cell 144 (6), 986-98.

31. Kleinschnitz, C. et al. (2010) Post-stroke inhibition of induced NADPH oxidase type 4 prevents oxidative stress and neurodegeneration. PLoS biology 8 (9).

32. Pacher, P. et al. (2007) Nitric oxide and peroxynitrite in health and disease. Physiological reviews 87 (1), 315-424.

33. Tuo, Y.H. et al. (2017) NADPH oxidase inhibitor improves outcome of mechanical reperfusion by suppressing hemorrhagic transformation. J Neurointerv Surg 9 (5), 492-498.

34. Won, S.J. et al. (2011) Hyperglycemia promotes tissue plasminogen activator-induced hemorrhage by Increasing superoxide production. Ann Neurol 70 (4), 583-90.

35. Bederson, J.B. et al. (1986) Evaluation of 2,3,5-triphenyltetrazolium chloride as a stain for detection and quantification of experimental cerebral infarction in rats. Stroke 17 (6), 1304-8.

36. Denizot, F. and Lang, R. (1986) Rapid colorimetric assay for cell growth and survival. Modifications to the tetrazolium dye procedure giving improved sensitivity and reliability. J Immunol Methods 89 (2), 271-7.

Supplementary Tables

Table S1. Animals excluded from the statistical analysis after tMCAO

Animals	Glycemic status	Ischemia model	Excluded animals	Reason of exclusion
C57/Bl6	Non-diabetic	Veh (TTC)	0 of 7	-
C57/Bl6		GKT137831 (TTC)	0 of 5	-
C57/Bl6		SMTC (TTC)	0 of 5	-
C57/Bl6		BAY58-2667 (TTC)	0 of 5	-
C57/Bl6		3Rx (TTC)	0 of 7	-
C57/Bl6	Diabetic	Veh (TTC)	5 of 12	Dead within the first 24h
C57/Bl6		Veh (DHE)	1 of 5	Dead within the first 24h
C57/Bl6		Veh (N-Tyr)	0 of 4	-
C57/Bl6		Veh (MMP-9)	0 of 4	-
C57/Bl6		3Rx (TTC)	1 of 11	Dead within the first 24h
C57/Bl6		3Rx (DHE)	0 of 4	-
C57/Bl6		3Rx (N-Tyr	0 of 4	-
C57/Bl6		3Rx (MMP-9)	0 of 4	-
NOX5WT	Diabetic	Veh (TTC)	6 of 13	Dead due to surgical complications (2); Dead within the first 24h (4)
NOX5WT		3Rx (TTC)	0 of 8	-
NOX5KI		Veh (TTC)	5 of 12	Dead within the first 24h
NOX5KI		3Rx (TTC)	1 of 8	Dead due to surgical complications

TTC, 2,3,5- triphenyltetrazolium hydrochloride; Veh, vehicle; SMTC, S-methyl-L-thiocitrulline; N-Tyr, nitro-tyrosine; DHE, dihydroethidium; MMP-9, Matrix metallopeptidase 9; 3Rx., triple therapy. Animal exclusion procedures are described in the respective methods parts.

Table S2. Blood glucose measurements in C57/Bl6 mice

Animals	Experimentation	Blood glucose before MCAO
C57/Bl6	Veh (TTC)	(Dead)
C57/Bl6	Veh (TTC)	28.1
C57/Bl6	Veh (TTC)	21.2
C57/Bl6	Veh (TTC)	20.6
C57/Bl6	Veh (TTC)	21.1
C57/Bl6	Veh (TTC)	(Dead)
C57/Bl6	Veh (TTC)	31
C57/Bl6	Veh (TTC)	12.6
C57/Bl6	Veh (TTC)	10
C57/Bl6	Veh (TTC)	(Dead)
C57/Bl6	Veh (TTC)	(Dead)
C57/Bl6	Veh (TTC)	(Dead)
C57/Bl6	Veh (DHE)	12.6
C57/Bl6	Veh (DHE)	13.2
C57/Bl6	Veh (DHE)	13.6
C57/Bl6	Veh (DHE)	19.5
C57/Bl6	Veh (DHE)	(Dead)
C57/Bl6	Veh (N-Tyr)	12.6
C57/Bl6	Veh (N-Tyr)	13.2
C57/Bl6	Veh (N-Tyr)	13.6
C57/Bl6	Veh (N-Tyr)	19.5
C57/Bl6	Veh (MMP-9)	12.6
C57/Bl6	Veh (MMP-9)	13.2
C57/Bl6	Veh (MMP-9)	13.6
C57/Bl6	Veh (MMP-9)	19.5
C57/Bl6	3Rx (TTC)	17.7
C57/Bl6	3Rx (TTC)	12.9
C57/Bl6	3Rx (TTC)	21
C57/Bl6	3Rx (TTC)	(Dead)
C57/Bl6	3Rx (TTC)	20
C57/Bl6	3Rx (TTC)	18.1
C57/Bl6	3Rx (TTC)	20.8
C57/Bl6	3Rx (TTC)	29.4
C57/Bl6	3Rx (TTC)	21
C57/Bl6	3Rx (TTC)	17.2
C57/Bl6	3Rx (TTC)	30
C57/Bl6	3Rx (DHE)	12.4
C57/Bl6	3Rx (DHE)	12.2
C57/Bl6	3Rx (DHE)	30.1
C57/Bl6	3Rx (DHE)	15.7
C57/Bl6	3Rx (N-Tyr)	12.4
C57/Bl6	3Rx (N-Tyr)	12.2
C57/Bl6	3Rx (N-Tyr)	30.1

C57/Bl6	3Rx (N-Tyr)	15.7
C57/Bl6	3Rx (MMP-9)	12.4
C57/Bl6	3Rx (MMP-9)	12.2
C57/Bl6	3Rx (MMP-9)	30.1
C57/Bl6	3Rx (MMP-9)	15.7

TTC, 2,3,5- triphenyltetrazolium hydrochloride; Veh, vehicle; SMTC, S-methyl-L-thiocitrulline; N-Tyr, nitro-tyrosine; DHE, dihydroethidium; MMP-9, Matrix metallopeptidase 9; 3Rx., triple therapy.

Table S3. Blood glucose measurements in NOX5WT and NOX5KI mice

Genotype	Experimentation	Blood glucose before MCAO
NOX5WT	Veh (TTC)	(Dead)
NOX5WT	Veh (TTC)	16.3
NOX5WT	Veh (TTC)	15.2
NOX5WT	Veh (TTC)	(Dead)
NOX5WT	Veh (TTC)	(Dead)
NOX5WT	Veh (TTC)	19.1
NOX5WT	Veh (TTC)	(Dead)
NOX5WT	Veh (TTC)	23.2
NOX5WT	Veh (TTC)	(Dead)
NOX5WT	Veh (TTC)	17.1
NOX5WT	Veh (TTC)	(Dead)
NOX5WT	Veh (TTC)	13.2
NOX5WT	Veh (TTC)	17.9
NOX5WT	3Rx (TTC)	17.4
NOX5WT	3Rx (TTC)	12.4
NOX5WT	3Rx (TTC)	16.9
NOX5WT	3Rx (TTC)	18.6
NOX5WT	3Rx (TTC)	17.1
NOX5WT	3Rx (TTC)	19.1
NOX5WT	3Rx (TTC)	15.1
NOX5WT	3Rx (TTC)	13.1
NOX5KI	Veh (HT)	30
NOX5KI	Veh (HT)	16.8
NOX5KI	Veh (HT)	30.6
NOX5KI	Veh (HT)	24.1
NOX5KI	Veh (HT)	29.1
NOX5KI	Veh (HT)	28.8
NOX5KI	Veh (TTC)	(Dead)
NOX5KI	Veh (TTC)	(Dead)
NOX5KI	Veh (TTC)	(Dead)
NOX5KI	Veh (TTC)	(Dead)
NOX5KI	Veh (TTC)	(Dead)
NOX5KI	Veh (TTC)	17.9
NOX5KI	3Rx (TTC)	23.1
NOX5KI	3Rx (TTC)	12
NOX5KI	3Rx (TTC)	21.3
NOX5KI	3Rx (TTC)	20.3
NOX5KI	3Rx (TTC)	14.1
NOX5KI	3Rx (TTC)	20.2
NOX5KI	3Rx (TTC)	(Dead)
NOX5KI	3Rx (TTC)	16.9

TTC, 2,3,5- triphenyltetrazolium hydrochloride; Veh, vehicle; SMTC, S-methyl-L-thiocitrulline; N-Tyr, nitro-tyrosine; DHE, dihydroethidium; MMP-9, Matrix metallopeptidase 9; 3Rx., triple therapy.

Supplementary Figures

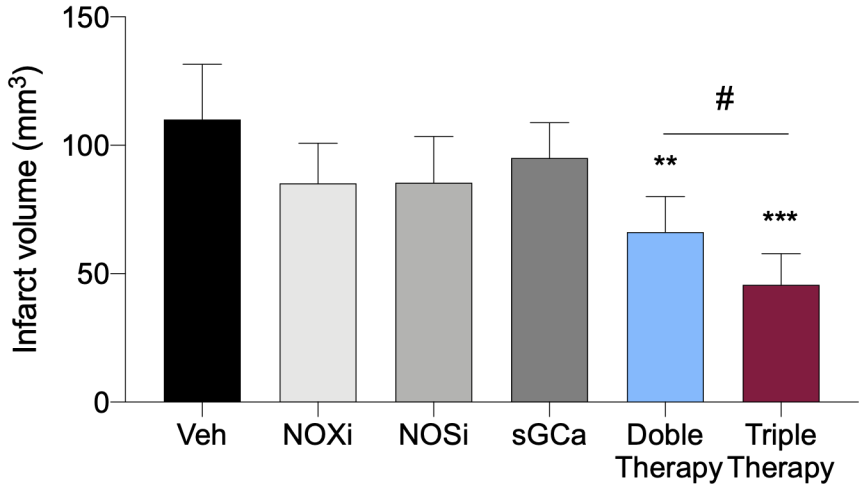

Fig. S1. Network pharmacology based therapeutic strategy. Comparison between double (blue) and triple (red) combinatory therapy post-stroke using infarct size as the main read-out parameter. Both double (NOXi+NOSi) and triple (NOXi+NOSi+sGCa) therapy significantly reduced infarct volume compared to non-treated animals (** *p<0,01*; *** *p<0,001; n=7)*. Escalating from a double to a triple therapy potentiates the synergistic effect of the treatment significantly reducing infarct size in comparison with the double therapy (# *p<0,05)*.

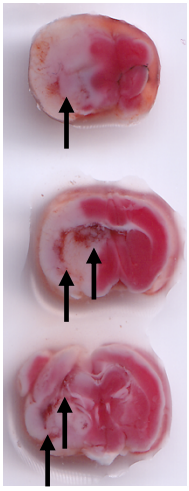

Fig. S2. Representative TTC staining pictures of hemorrhagic transformation in NOX5KI mice

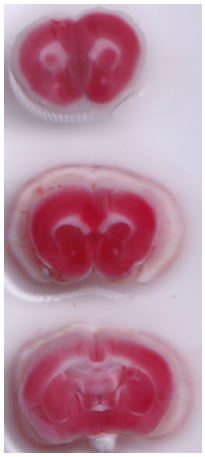

Fig. S3. Mechanical validation of the tMCAO model. NOX5KI mice (n=3) were subjected to the complete MCAO surgical procedure although no long-term occlusion was performed. The silicon coated filament was located and rapidly removed from the middle cerebral artery. No vascular disruption was observed.

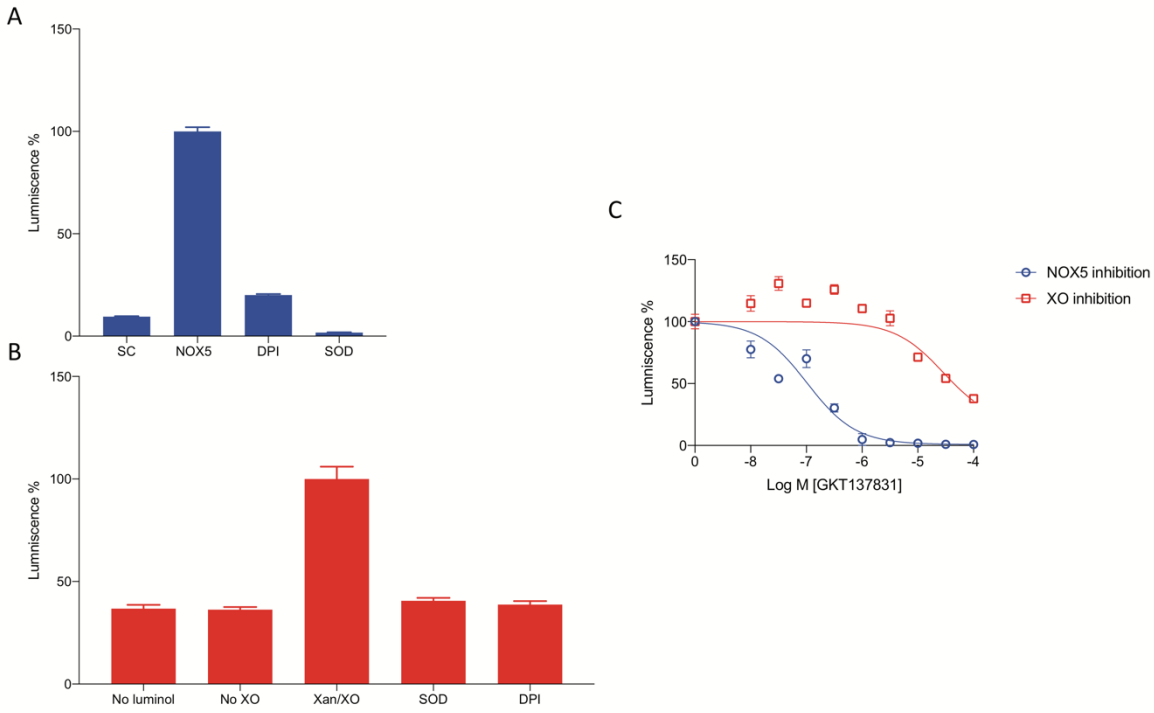

Fig. S4. GKT137831 inhibits NOX5. ROS production in presence and absence of GKT137831 was assessed using luminol assay to measure superoxide production by (**A**) HEK293 cells transfected with NOX5 and **(B)** Xanthine/xanthine oxidase cell-free system. **C.** Concentration response curves of GKT137831 on HEK293 cells transfected with NOX5 and Xanthine/xanthine oxidase cell-free system. Data are presented as the mean ± SEM.

7

ENDOTHELIAL NOX5 INDUCES AORTIC ANEURYSMS IN DIABETIC APOE$^{-/-}$ MICE

Ho F, **Elbatreek MH**, Kleikers P, Jha J, Watson A, Schmidt HHHW, et al. Endothelial Nox5 induces aortic aneurysms in diabetic ApoE$^{-/-}$ mice . In preparation.

Abstract

Atherosclerosis is a major cause of cardiovascular morbidity and death, further aggravated by diabetes mellitus as a comorbidity. The appearance of elevated levels of reactive oxygen species (ROS) and metabolites correlate with atherosclerosis, suggesting possible causality. NADPH oxidases (NOX) are the main dedicated source of ROS, and NOX5 has been suggested as a potential source of pro-atherosclerotic ROS in human atherosclerosis. The Nox5 gene is, however, not present in the mouse and rat genome. Here, we examine knock-in mice expressing human Nox5 in the physiological endothelial cell location either on a pro-atherosclerotic high fat diet or crossed with atherosclerosis prone ApoE$^{-/-}$ mice with and without streptozotocin induced diabetes. Aged hypertensive Nox5 KI mice fed a high cholesterol diet for 28 weeks did not develop atherosclerosis. ApoE$^{-/-}$ mice did develop atherosclerosis, which was accelerated in the context of diabetes but knock-in of the Nox5 neither changed plaque distribution nor area. Surprisingly, however, we found a significant Nox5-dependent increase in aortic aneurysm correlating with lower fibronectin gene expression. These findings suggest that Nox5 expression in endothelial cells does not promote atherosclerosis, neither with nor without diabetes, but may initiate aneurysm formation in the abdominal aorta by suppressing fibronectin levels.

Introduction

Atherosclerosis is a major cause of stroke, myocardial infarction and death. Several factors including diabetes mellitus further accelerate atherosclerosis and result in worse outcomes [1,2]. Apart from elevated cholesterol and a proinflammatory state the key pathomechanisms leading to atherosclerosis, and in particular diabetes-accelerated atherosclerosis, are not fully understood. One mechanism that has been suggested to play a causal role in atherogenesis is dysregulated reactive oxygen species (ROS) formation [3]. Here, in particular the type 5 NADPH oxidase (NOX5) appears to stand out in humans [4], whilst NOX1 has a minor role [5], NOX2 knock-out increases mortality and NOX4 is rather atheroprotective [6,7]. The functional role of NOX5 in atherosclerosis is, however, understudied, as this gene is absent from the mouse and rat genome [4].

To determine the functional role of NOX5 in atherosclerosis, we investigated humanized NOX5 knock-in (KI) mice, which express NOX5 in endothelial cells, the physiological location in humans. Mice are highly resistant to the induction of atherosclerosis, probably because they carry most of their cholesterol on high-density lipoprotein (HDL) which is atheroprotective in humans [8,9]. Mice deficient in apolipoprotein E ($ApoE^{-/-}$ mice), however, spontaneously develop atherosclerosis [8,9] and one line of NOX5 mice were thus crossed with $ApoE^{-/-}$ mice. Given the role of NOX5 in diabetic complications [10,11] and that atherosclerosis is accelerated in diabetes, we also test the role of NOX5 in the development of atherosclerosis in $ApoE^{-/-}$ diabetic mice. For this, we induced diabetes in NOX5 KI/$ApoE^{-/-}$ by injection of low-dose streptozotocin (STZ).

Methods

Animals and metabolic parameters

Humanized NOX5 Knock-in mice were generated and validated as previously described[12]. Briefly, the model was developed using the hypoxanthine phospho-ribosyl-transferase (Hprt) targeted transgenic approach under the control of the Tie2 promoter. Therefore, NOX5 is expressed mainly in endothelial cells ($eNOX5^{ki/ki}$). Expression of NOX5 in the KI mice tissues was validated by qPCR and compared to Wild Type (WT) mice [12]. Both WT and $eNOX5^{ki/ki}$ aged mice (56-64 weeks old) (total n=42) were fed a high cholesterol (Paigen) diet for 28 weeks to induce atherosclerosis. On the day of sacrifice, blood glucose was measured by using glucometer (Contour XT, Ascensia, Switzerland), mice were then anesthetized with 3-4% isoflurane. The abdominal cavity was opened, and blood was withdrawn via a heart puncture. Then, the mouse was flushed with 20 ml nitroprusside and organs were taken out and weighed. The blood collected from the mice was allowed to clot for 30 min to 1 hour. After 10 minutes centrifugation at 10.000rpm at 4°C, the supernatant (serum) was pipetted and aliquoted in 100µL portions to be stored at -20°C. Cholesterol levels were measured by Cholesterol FS 10` kit (DiaSys – Diagnostic Systems GmbH, Holzheim, Germany). Triglyceride levels were measured by Triglyceride FS 5` Ecoline kit (DiaSys – Diagnostic Systems GmbH, Holzheim, Germany).

For the experiments using $ApoE^{-/-}$ mice, non-diabetic and diabetic WT and NOX5 KI mice (six weeks old) were used. Thus, we had four groups; non-diabetic $ApoE^{-/-}$ x WT, non-diabetic $ApoE^{-/-}$ x $eNOX5^{ki/ki}$, diabetic $ApoE^{-/-}$ x WT and diabetic $ApoE^{-/-}$ x $eNOX5^{ki/ki}$. Mice were injected with a low-dose streptozotocin (STZ) (55 mg/kg) every day for 5 days to induce diabetes. All mice were allowed free access to water and food in a temperature-regulated room (22˚C) and placed in a 12 h light-dark cycle. Blood glucose, glycated hemoglobin, and systolic blood pressure were measured at 20 weeks after diabetes induction as previously described [13-15]. After 20 weeks of diabetes, mice were then sacrificed to collect blood and tissues. On the day of sacrifice, mice were anaesthetized by sodium pentobarbitone IP (100 mg/kg body weight; Euthatal, Sigma-Aldrich, Castle Hill, NSW, Australia) and organs were rapidly dissected. Aorta was visualized under the microscope during cull to check the presence of aneurysm.

All experimental procedures were carried out according to the guidelines of the Animal Ethics Committee of Faculty of Health, Medicine and Life Sciences, Maastricht University, Netherlands and the Alfred Medical Research and Education Precinct Animal Ethics Committee under the guidelines laid down by the National Health and Medical Research Council of Australia.

Atherosclerotic plaque area

Assessment of plaque area was undertaken using en-face analysis, after staining with Sudan IV-Herxheimer's solution (BDH, Poole UK) as previously described [16].

Hematoxylin and Eosin (H and E)

4um thick sections of paraffin embedded aortic arches and valvular heart region, were cut and stained with Hematoxylin and Eosin to detect fatty streaks and/or plaques in aortic arch and valvular heart region.

Quantitative RT-PCR

Total RNA was extracted after homogenising whole aorta (Polytron PT-MR2100; Kinematica, Littau/Lucerne, Switzerland) in TRIzol reagent (Invitrogen Australia, Mt Waverly, Vic, Australia) as previously described [14]. Gene expression were analyzed quantitatively as previously described [14].

Statistical analysis

Data were analyzed for normality using the D'Agostino-Pearson test before being analyzed. T-test was used to compare between two groups and one or two-way ANOVA followed by Tukey's multiple comparisons test to compare between more than two groups. $P<0.05$ was considered significant. Results are expressed as mean ± SEM. Data were analyzed using Prism GraphPad software.

Results

Metabolic parameters in aged mice

To test the metabolic effects induced by feeding a high cholesterol diet on aged hypertensive NOX5 KI, we measured the body and organ weights, blood glucose, triglycerides and cholesterol levels of aged WT and $eNOX5^{ki/ki}$ mice fed on Paigen diet for 28 weeks. Surprisingly, WT mice had higher body weights compared to KI mice,

however, there were no differences in kidney, liver and heart weights (Table 1). As expected, aged eNOX5$^{ki/ki}$ had higher systolic blood pressure compared to WT mice. Blood glucose levels, serum triglycerides and cholesterol levels were similar between aged WT and KI mice (Table 1). Having known that NOX5 does not affect the metabolic parameters in aged mice, we proceeded with checking whether NOX5 can induce vascular phenotype associated with atherosclerosis.

Table1. Metabolic parameters in aged WT and eNOX5$^{ki/ki}$ mice.

	Aged WT	**Aged eNOX5$^{ki/ki}$**
Body weight, g	40.5±1.9 (19)	35.8±1.1 (16)*
Systolic blood pressure, mmHg	126±2 (19)	141±4 (16)**
Blood glucose, mmol/L	5.0±0.2 (19)	4.6±0.2 (17)
Cholesterol, mmol/L	1.4±0.1 (19)	1.1±0.1 (17)
Triglycerides, mmol/L	0.13±0.02 (19)	0.15±0.06 (17)
Kidney weight, g	0.51±0.03 (19)	0.46±0.02 (17)
Heart weight, g	0.2±0.005 (19)	0.2±0.008 (16)
Liver weight, g	2.4±0.2 (18)	1.9±0.1 (17)

Data are mean±SEM (n). P<0.05 * compared with aged WT.

Knocking in NOX5 in endothelial cells is not sufficient to induce atherosclerosis in aged hypertensive mice

To check whether NOX5 can induce atherosclerosis in mice, we measured atherosclerotic plaque area in the whole aorta of both WT and KI mice by en-face analysis. There was no plaque formation in both mice groups (Supplementary Fig1. a) indicating no role for NOX5 in the development of advanced atherosclerotic lesions. We then thought that NOX5 might be only involved in early stages of atherosclerosis development i.e. fatty streak formation at valvular heart region (heart root) or aortic arch [17]. To test this hypothesis, we stained the aortic arch and heart root with H and E stain. We could not also detect any fatty streaks or plaques in WT and KI mice

(Supplementary Fig1. b). Our data show that knocking in NOX5 gene in the endothelium of mice does not overcome their resistance to atherosclerosis even in ageing/hypertension states. Therefore, we decided to check the role of NOX5 in atherosclerosis under both normal and diabetic conditions using ApoE$^{-/-}$ mice which develop atherosclerosis spontaneously.

Metabolic parameters in ApoE$^{-/-}$ mice

To examine the effect of NOX5 on atherosclerosis, first we checked whether it has an effect on metabolic parameters and blood pressure in ApoE$^{-/-}$ mice. Therefore, we measured body and organ weights, blood glucose, HbA1c and blood pressure of non-diabetic and diabetic WT and NOX5 KI mice after 20 weeks after induction of diabetes. As expected, all diabetic mice had lower body weights (Table 2), elevated glucose and HbA1c levels compared to their nondiabetic controls. There was no difference in systolic blood pressure among all groups. There was no difference between NOX5 KI and WT mice in all of the above-mentioned parameters, however, KI mice had slightly higher body weight. These data show that NOX5 has no effect on metabolic parameters and blood pressure in ApoE$^{-/-}$ mice with/without diabetes.

Table2. Baseline data including metabolic parameters for animals at 20 weeks of study

	Control ApoE$^{-/-}$ x WT	**Control ApoE$^{-/-}$ x eNOX5$^{ki/ki}$**	**Diabetic ApoE$^{-/-}$ x WT**	**Diabetic ApoE$^{-/-}$ x eNOX5$^{ki/ki}$**	*p-value: Effect of diabetes*	*p-value: Effect of NOX5*
Body weights (g)	30.6 ± 1.0	31.6 ± 1.1	25.1 ± 0.3 #†	28.8 ± 0.5 ‡	**<0.0001**	**0.0110**
24h urine output (mL)	1.0 ± 0.1	0.9 ± 0.2	16.0 ± 1.6 #†	16.8 ± 2.7 #†	**<0.0001**	0.8490
HbA1c (mmol/mol, %)	4.6 ± 0.2	4.4 ± 0.1	10.1 ± 0.6 #†	9.6 ± 0.3 #†	**<0.0001**	0.3560
Plasma glucose (mmol/L)	9.3 ± 0.8	9.8 ± 0.7	21.6 ± 2.2 #†	24.1 ± 2.8 #†	**<0.0001**	0.3957
Plasma cholesterol (mmol/L)	14.1 ± 0.5	11.5 ± 0.3	23.7 ± 4.6 #†	22.5 ± 1.7 #†	**<0.0001**	0.3516
Plasma triglycerides (mmol/L)	1.3 ± 0.1	0.8 ± 0.1	1.6 ± 0.3	1.3 ± 0.2	0.0947	**0.0448**

Plasma HDL (mmol/L)	1.6 ± 0.0	1.5 ± 0.1	1.0 ± 0.2 #†	0.8 ± 0.2 #†	**<0.0001**	0.3431
Plasma LDL (mmol/L)	21.1 ± 0.5	22.1 ± 0.2	9.9 ± 4.6 #†	12.0 ± 1.6 #†	**<0.0001**	0.4616
Tibia lengths (mm)	17.2 ± 0.2	17.6 ± 0.1	17.5 ± 0.1	17.4 ± 0.1	0.8589	0.4300
Blood pressure (mmHg)	105 ± 27	105 ± 27	94 ± 30	107 ± 36	0.3421	0.1783

Data shown as mean ± SEM. Two-way ANOVA statistics shown in columns. Post-hoc multiple comparisons test (Tukey's): # vs. Control ApoE$^{-/-}$ x WT group; † vs. Control ApoE$^{-/-}$ x eNOX5$^{ki/ki}$ group; ‡ vs. Diabetic ApoE$^{-/-}$ x WT group. n = 6-10/group for body weight, 24h urine output and HbA1c values; n = 7-9/group for plasma values; n = 8-18/group for tibia lengths; n = 9-15 for blood pressure measurements. ApoE$^{-/-}$ = Apolipoprotein E knockout; HDL = high density lipoprotein; LDL = low density lipoprotein NOX = NADPH oxidase

Endothelial NOX5 KI does not increase plaque formation, but aneurysm in diabetes

To assess whether NOX5 plays a role in diabetic atherosclerosis, we measured atherosclerotic plaque area in ApoE$^{-/-}$ x WT and ApoE$^{-/-}$ x eNOX5$^{ki/ki}$ mice with/without diabetes. After 20 weeks of diabetes, all diabetic mice showed a significant increase in atherosclerotic plaque areas compared to non-diabetic mice, yet there was no difference between WT and KI mice (Fig1). However, surprisingly diabetic ApoE$^{-/-}$ x eNOX5$^{ki/ki}$ mice had more frequent aneurysm formation than ApoE$^{-/-}$ x WT mice (Table 3). We then examined whether there was a difference between NOX5 KI mice and WT in inflammatory and fibrotic biomarkers. Indeed there was no difference between NOX5 KI mice and WT in gene expression of all inflammatory and fibrotic biomarkers, however, diabetic ApoE$^{-/-}$ x eNOX5$^{ki/ki}$ mice showed lower fibronectin expression compared to diabetic ApoE$^{-/-}$ x WT mice (Table 4).

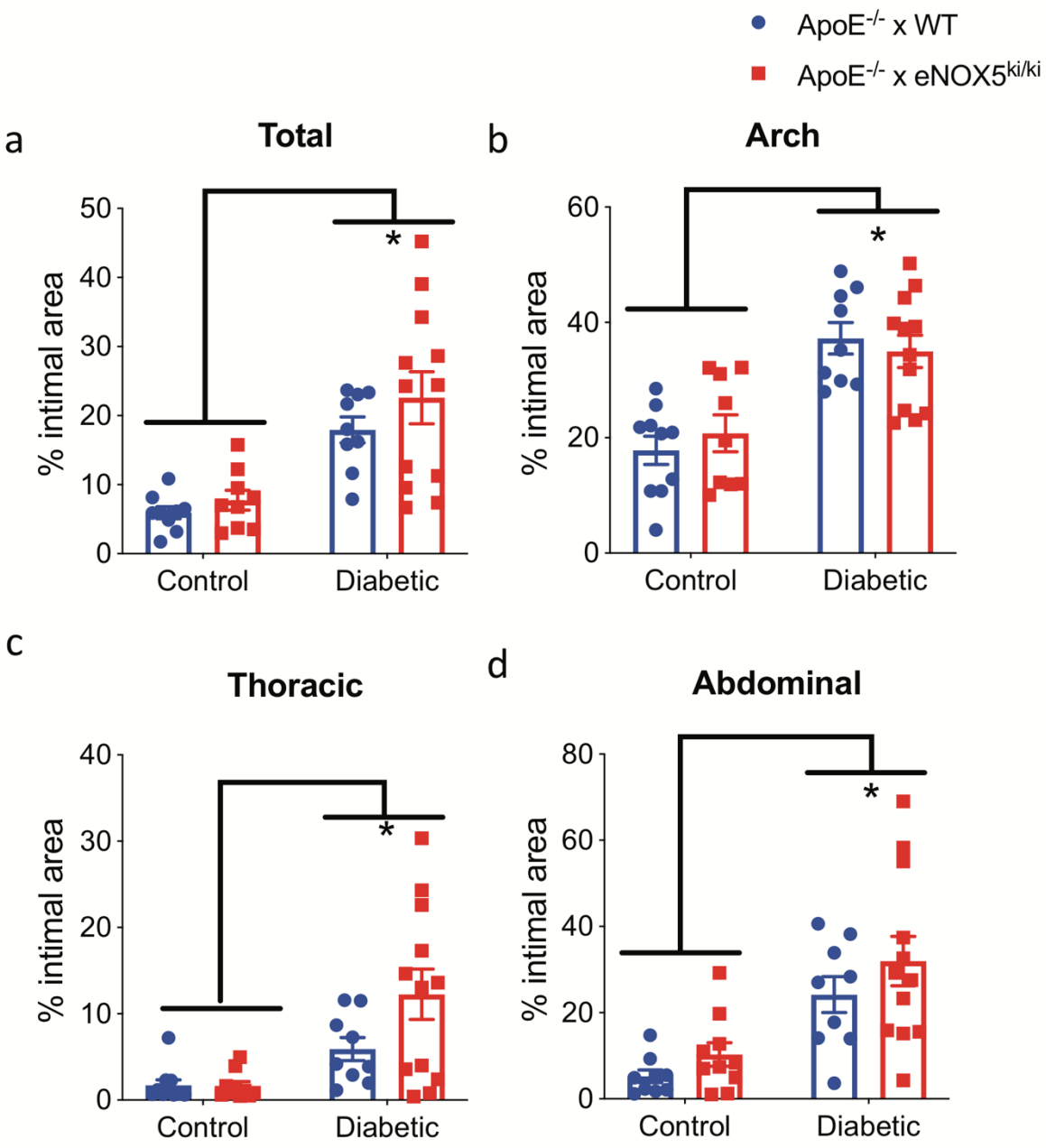

Fig1. NOX5 does not induce atherosclerosis in ApoE$^{-/-}$ mice. Atherosclerotic plaque area was measured at 20 weeks after induction of diabetes in total aorta (a), aortic arch (b), thoracic aorta (c) and abdominal aorta (d). Data shown as mean ± SEM. * P < 0.05.

Table3. Aneurysm formation in Diabetic ApoE$^{-/-}$ x NOX5$^{ki/ki}$ animals and their respective controls at 20 weeks of study

	Animals with aneurysms	Animals with aneurysms (%)
Non-diabetic ApoE$^{-/-}$ x WT	1/13	7.7%
Non-diabetic ApoE$^{-/-}$ x eNOX5$^{ki/ki}$	0/18	0.0%
Diabetic ApoE$^{-/-}$ x WT	1/10	10.0%
Diabetic ApoE$^{-/-}$ x eNOX5$^{ki/ki}$	7/21	33.3%

Data expressed as number of animals with aneurysms present, compared to the total number of animals assessed for aneurysm formation.

Table4. RT-PCR gene expression data for ApoE$^{-/-}$ x NOX5$^{ki/ki}$ animals and their respective controls at 20 weeks of study

Gene of interest	Control ApoE$^{-/-}$ x WT	Control ApoE$^{-/-}$ x eNOX5$^{ki/ki}$	Diabetic ApoE$^{-/-}$ x WT	Diabetic ApoE$^{-/-}$ x eNOX5$^{ki/ki}$	*p-value: Effect of diabetes*	*p-value: Effect of NOX5*
Inflammatory markers						
MCP-1	1.00 ± 0.41	0.94 ± 0.96	2.49 ± 0.45	5.21 ± 1.71 #†	**0.0031**	0.1458
VCAM-1	1.00 ± 0.41	0.43 ± 0.11	0.96 ± 0.27	1.99 ± 0.67	0.0816	0.5834
F4/80	1.00 ± 0.29	0.92 ± 0.18	4.95 ± 1.84 #†	2.22 ± 0.54	**0.0062**	0.1200
NFkB	1.00 ± 0.25	1.06 ± 0.16	1.00 ± 0.17	0.90 ± 0.33	0.7602	0.9980
NOX isoforms and antioxidants						
NOX2	1.00 ± 0.22	1.36 ± 0.21	9.71 ± 3.68 #†	3.81 ± 0.70	**0.0020**	0.0977
NOX4	1.00 ± 0.30	0.65 ± 0.12	0.58 ± 0.13	0.71 ± 0.35	0.4581	0.6650
HO1	1.00 ± 0.18	1.68 ± 0.22	3.52 ± 0.87 #	3.20 ± 0.70 #	**0.0005**	0.7158
GPx1	1.00 ± 0.12	1.03 ± 0.10	1.59 ± 0.36	0.95 ± 0.14	0.2097	0.1398
NRF2	1.00 ± 0.13	1.40 ± 0.19	1.79 ± 0.99	1.76 ± 0.78	0.2609	0.7159
Fibrotic and remodelling markers						
Collagen III	1.00 ± 0.26	1.15 ± 0.17	1.83 ± 0.50	1.09 ± 0.32	0.2300	0.3549
Collagen IV	1.00 ± 0.24	0.71 ± 0.05	1.10 ± 0.29	0.57 ± 0.18	0.9192	0.0692

Fibronectin	1.00 ± 0.23	0.92 ± 0.14	2.91 ± 0.96 †	0.71 ± 0.13 ‡	0.1074	**0.0347**
CTGF	1.00 ± 0.18	1.04 ± 0.17	0.84 ± 0.33	0.75 ± 0.38	0.3869	0.9190
MMP2	1.00 ± 0.27	1.18 ± 0.32	2.10 ± 0.65	1.38 ± 0.25	0.1202	0.5085
MMP9	1.00 ± 0.38	0.91 ± 0.11	0.61 ± 0.14	1.09 ± 0.58	0.7800	0.6144
PKCα	1.00 ± 0.13	1.07 ± 0.24	1.73 ± 0.35	1.14 ± 0.35	0.1539	0.3420
PDGF	1.00 ± 0.25	1.68 ± 0.21	2.29 ± 0.88	3.61 ± 1.26	**0.0379**	0.1818
Cholesterol uptake transporters						
CD36	1.00 ± 0.18	2.42 ± 0.64	4.36 ± 2.20	1.78 ± 0.38	0.1258	0.5060
ACAT1	1.00 ± 0.18	1.62 ± 0.28	1.35 ± 0.34	1.16 ± 0.17	0.8276	0.3746
ABCA1	1.00 ± 0.12	1.14 ± 0.26	2.80 ± 1.17	1.78 ± 0.25	**0.0272**	0.4053

Data shown as mean ± SEM, with all values expressed relative to non-diabetic NOX5- animals. Two-way ANOVA statistics shown in columns, in bold if $p<0.05$. Post-hoc multiple comparisons test (Tukey's): # vs. Control ApoE$^{-/-}$ x WT group; † vs. Control ApoE$^{-/-}$ x eNOX5$^{ki/ki}$ group; ‡ vs. Diabetic ApoE$^{-/-}$ x WT group. n = 6-9/group (except n=5 for diabetic NOX5- group for NRF2, n=5 for diabetic NOX5+ group for CTGF, n=5 for diabetic NOX5- group for MMP9, n=4-9 for cholesterol uptake transporters).

Discussion

The data that we have presented here show that endothelial NOX5 does not play a role in atherosclerosis but is a causal protein in aortic aneurysm. In this study, we have used a NOX5KI mouse model that expresses NOX5 in endothelial cells and develops hypertension spontaneously upon ageing. Feeding aged NOX5KI mice with an atherogenic diet for 28 weeks did not result in atherosclerotic lesion formation. Also, in a more severe model of diabetes-accelerated atherosclerosis i.e. STZ-injected ApoE$^{-/-}$ mice, endothelial NOX5 did not aggravate atherosclerosis after 20 weeks of diabetes. However, surprisingly, endothelial NOX5 induced aortic aneurysm.

Previously, NOX5 was shown to be expressed in the endothelium in the early lesions and in vascular smooth muscle cells in the advanced coronary lesions in vessels of coronary artery disease patients [4]. Yet our data argue against a causal role of endothelial NOX5 in atherosclerosis despite its role in atherosclerosis-related comorbidities i.e. diabetes [11,18], hypertension, stroke [12] and myocardial infarction [19]. NOX5 expressed in vascular smooth muscle cells [20-22] may be more relevant in atherosclerosis and its role needs to be explored. In addition, other vascular NOXs;

NOX1 and NOX2 seem to be the major isoforms involved in atherosclerosis [23,24] while NOX4 is atheroprotective [6,7].

Reactive oxygen species production is a common phenomenon in aortic aneurysm. Previous findings suggest that superoxide formation is increased in human aortic aneurysm and is much higher in patients with high overall mortality risk [25,26]. However, the sources of ROS in aortic aneurysm have not been extensively studied. Interestingly, our data show that endothelial NOX5 is a causal protein in aortic aneurysm. Indeed, NOX, cyclooxygenase, iNOS and uncoupled NOS have been suggested as the major enzymatic sources of ROS in human and animal aortic aneurysm [25,27]. Previous study showed that mRNA levels for NOX2 and NOX5 are significantly increased in human aortic aneurysm while NOX4 mRNA expression is decreased [25]. In addition, deletion of p47phox (NOX2 organizer protein) or NOX1 attenuated angiotensin II-induced aortic aneurysm formation in mice [28,29]. Also, using genetic animal models, NOS uncoupling was shown to lie downstream of NOX1, NOX2 and NOX4 and induced aortic aneurysm in $ApoE^{-/-}$ mice [25,30] which was attenuated by folic acid treatment [31,32]. The role of NOX5 has not been studied in previous preclinical studies due to the absence of NOX5 in the rodent genome. Thus, it would be also possible that NOX5 causes aneurysm by uncoupling of NOS.

Diabetes is a negative risk factor of aortic aneurysm. Protection against aortic aneurysm in diabetes is a function of diabetes-mediated changes in the vascular extracellular matrix biology [33,34]. There is also support for the idea that the treatment regimens used in diabetes may afford protection against aortic aneurysm [35]. Here, we showed that endothelial NOX5 can induce aortic aneurysm in diabetic atherosclerosis model by reducing fibronectin expression. In contrast, previous studies showed that NOX5 is involved in fibrotic diseases. NOX5 expressed in endothelial cells or smooth muscle cells of mice is associated with increased kidney extracellular matrix proteins in diabetic nephropathy [11,18]. NOX5 also promotes fibrosis in human hepatic stellate cells [36]. Therefore, the role of NOX5 on fibrosis, could be cell type-, tissue-, or disease-specific.

In conclusion, our findings show that endothelial NOX5 is not a causal protein in atherosclerosis or diabetes-accelerated atherosclerosis. Yet, it can induce aneurysm even under diabetic conditions. Future studies on NOX5 in aortic aneurysm should

focus on diabetes comorbidities such as hypertension to check whether a NOX5-induced aneurysm endotype is present in diabetes. Of therapeutic interest, given the antifibrotic effect of non-selective NOX inhibitors, selective NOX5 inhibitors should be tested in aortic aneurysm.

References

1. Libby, P. et al. Atherosclerosis. Nat Rev Dis Primers 5, 56 (2019).
2. Kanter, J. E. & Bornfeldt, K. E. Inflammation and diabetes-accelerated atherosclerosis: myeloid cell mediators. Trends Endocrinol. Metab. 24, 137–144 (2013).
3. Kattoor, A. J., Pothineni, N. V. K., Palagiri, D. & Mehta, J. L. Oxidative Stress in Atherosclerosis. Curr. Atheroscler. Rep. 19, 42 (2017).
4. Guzik, T. J. et al. Calcium-dependent NOX5 nicotinamide adenine dinucleotide phosphate oxidase contributes to vascular oxidative stress in human coronary artery disease. J. Am. Coll. Cardiol. 52, 1803–1809 (2008).
5. Sheehan, A. L. et al. Role for Nox1 NADPH oxidase in atherosclerosis. Atherosclerosis vol. 216 321–326 (2011).
6. Gray, S. P. et al. Reactive Oxygen Species Can Provide Atheroprotection via NOX4-Dependent Inhibition of Inflammation and Vascular Remodeling. Arterioscler. Thromb. Vasc. Biol. 36, 295–307 (2016).
7. Schröder, K. et al. Nox4 is a protective reactive oxygen species generating vascular NADPH oxidase. Circ. Res. 110, 1217–1225 (2012).
8. Jawien, J. Mouse Models of Experimental Atherosclerosis as a Tool for Checking a Putative Anti-Atherogenic Action of Drugs. Atherogenesis (2012) doi:10.5772/26071.
9. Emini Veseli, B. et al. Animal models of atherosclerosis. Eur. J. Pharmacol. 816, 3–13 (2017).
10. Holterman, C. E. et al. Nephropathy and elevated BP in mice with podocyte-specific NADPH oxidase 5 expression. J. Am. Soc. Nephrol. 25, 784–797 (2014).
11. Jha, J. C. et al. NADPH Oxidase Nox5 Accelerates Renal Injury in Diabetic Nephropathy. Diabetes 66, 2691–2703 (2017).
12. Casas, A. I. et al. Calcium-dependent blood-brain barrier breakdown by NOX5 limits postreperfusion benefit in stroke. J. Clin. Invest. 130, 1772–1778 (2019).
13. Krege, J. H., Hodgin, J. B., Hagaman, J. R. & Smithies, O. A noninvasive computerized tail-cuff system for measuring blood pressure in mice. Hypertension 25, 1111–1115 (1995).

14. Watson, A. M. D. et al. The endothelin receptor antagonist avosentan ameliorates nephropathy and atherosclerosis in diabetic apolipoprotein E knockout mice. Diabetologia 53, 192–203 (2010).
15. Jha, J. C. et al. Genetic Targeting or Pharmacologic Inhibition of NADPH Oxidase Nox4 Provides Renoprotection in Long-Term Diabetic Nephropathy. Journal of the American Society of Nephrology vol. 25 1237–1254 (2014).
16. Candido, R. et al. Irbesartan but Not Amlodipine Suppresses Diabetes-Associated Atherosclerosis. Circulation vol. 109 1536–1542 (2004).
17. Li, Y., Gilbert, T. R., Matsumoto, A. H. & Shi, W. Effect of Aging on Fatty Streak Formation in a Diet-Induced Mouse Model of Atherosclerosis. Journal of Vascular Research vol. 45 205–210 (2008).
18. Jha, J. C. et al. Endothelial or vascular smooth muscle cell-specific expression of human NOX5 exacerbates renal inflammation, fibrosis and albuminuria in the Akita mouse. Diabetologia vol. 62 1712–1726 (2019).
19. Hahn, N. E. et al. NOX5 expression is increased in intramyocardial blood vessels and cardiomyocytes after acute myocardial infarction in humans. Am. J. Pathol. 180, 2222–2229 (2012).
20. Manea, S.-A., Todirita, A., Raicu, M. & Manea, A. C/EBP transcription factors regulate NADPH oxidase in human aortic smooth muscle cells. J. Cell. Mol. Med. 18, 1467–1477 (2014).
21. Furmanik, G. et al. Nox5 Regulates Vascular Smooth Muscle Cell Phenotype. Atherosclerosis vol. 287 e27 (2019).
22. Montezano, A. C. et al. NADPH Oxidase 5 Is a Pro-Contractile Nox Isoform and a Point of Cross-Talk for Calcium and Redox Signaling-Implications in Vascular Function. Journal of the American Heart Association vol. 7 (2018).
23. Sukumar, P. et al. Nox2 NADPH Oxidase Has a Critical Role in Insulin Resistance-Related Endothelial Cell Dysfunction. Diabetes vol. 62 2130–2134 (2013).
24. Gray, S. P. et al. NADPH Oxidase 1 Plays a Key Role in Diabetes Mellitus–Accelerated Atherosclerosis. Circulation vol. 127 1888–1902 (2013).
25. Guzik, B. et al. Mechanisms of oxidative stress in human aortic aneurysms — Association with clinical risk factors for atherosclerosis and disease severity. International Journal of Cardiology vol. 168 2389–2396 (2013).

26. Miller, F. J., Jr et al. Oxidative stress in human abdominal aortic aneurysms: a potential mediator of aneurysmal remodeling. Arterioscler. Thromb. Vasc. Biol. 22, 560–565 (2002).
27. Xiong, W. et al. Inhibition of reactive oxygen species attenuates aneurysm formation in a murine model. Atherosclerosis 202, 128–134 (2009).
28. Thomas, M. et al. Deletion of p47phox attenuates angiotensin II-induced abdominal aortic aneurysm formation in apolipoprotein E-deficient mice. Circulation 114, 404–413 (2006).
29. Gavazzi, G. et al. NOX1 deficiency protects from aortic dissection in response to angiotensin II. Hypertension 50, 189–196 (2007).
30. Siu, K. L. et al. NOX isoforms in the development of abdominal aortic aneurysm. Redox Biol 11, 118–125 (2017).
31. Gao, L. et al. Role of uncoupled endothelial nitric oxide synthase in abdominal aortic aneurysm formation: treatment with folic acid. Hypertension 59, 158–166 (2012).
32. Siu, K. L., Miao, X. N. & Cai, H. Recoupling of eNOS with folic acid prevents abdominal aortic aneurysm formation in angiotensin II-infused apolipoprotein E null mice. PLoS One 9, e88899 (2014).
33. Patel, K., Zafar, M. A., Ziganshin, B. A. & Elefteriades, J. A. Diabetes Mellitus: Is It Protective against Aneurysm? A Narrative Review. Cardiology 141, 107–122 (2018).
34. Raffort, J. et al. Diabetes and aortic aneurysm: current state of the art. Cardiovasc. Res. 114, 1702–1713 (2018).
35. Torsney, E., Pirianov, G. & Cockerill, G. W. Diabetes as a Negative Risk Factor for Abdominal Aortic Aneurysm – Does the Disease Aetiology or the Treatment Provide the Mechanism of Protection? Current Vascular Pharmacology vol. 11 293–298 (2013).
36. Andueza, A. et al. NADPH oxidase 5 promotes proliferation and fibrosis in human hepatic stellate cells. Free Radic. Biol. Med. 126, 15–26 (2018).

Supplementary Figure 1

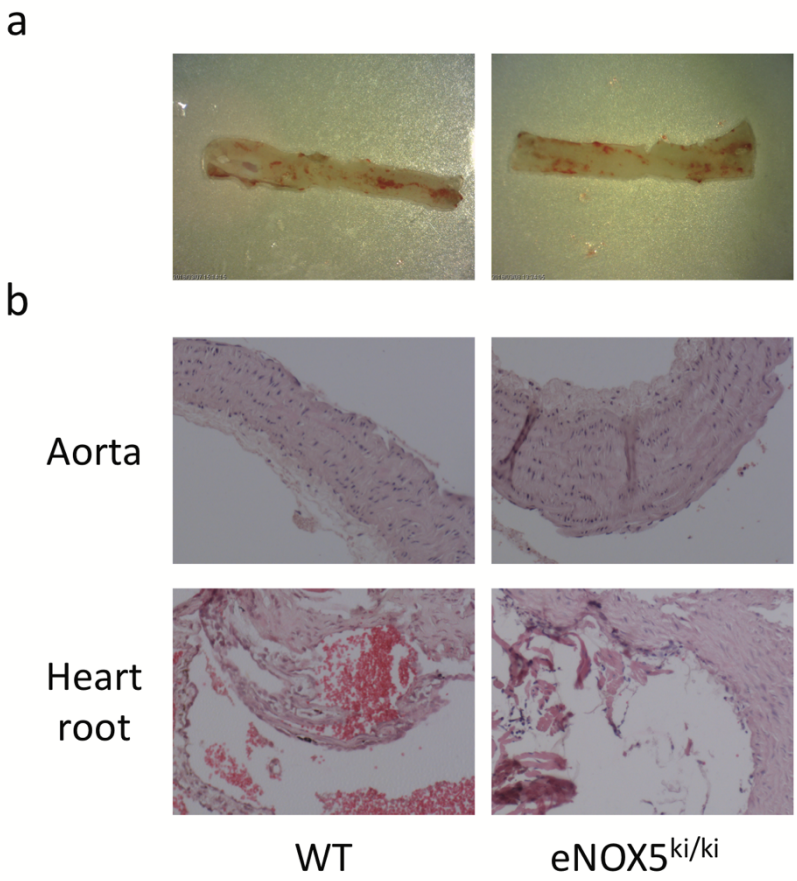

Supplementary Fig 1. Representative images of aorta and heart root of aged WT and eNOX5$^{ki/ki}$ mice stained with Sudan stain (a) and H/E stain (b).

8

NOX5-INDUCED UNCOUPLING OF ENDOTHELIAL NO SYNTHASE IS A CAUSAL MECHANISM AND THERAGNOSTIC TARGET OF AN AGE-RELATED HYPERTENSION ENDOTYPE

Elbatreek MH, Sadegh S, Anastasi E, Guney E, Kacprowski T, Hassan AA, et al. NOX5-induced uncoupling of endothelial NO synthase is a causal mechanism and theragnostic target of an age-related hypertension endotype validation. PLOS Biology. 2020.

Abstract

Hypertension is the most important cause of death and disability in the elderly. In nine of ten cases the molecular cause, however, is unknown. One mechanistic hypothesis involves impaired endothelium-dependent vasodilation through reactive oxygen (ROS) formation. Indeed, ROS forming Nox genes associate with hypertension; yet target validation has been negative. We re-investigate this association by molecular network analysis and identify Nox5, not present in rodents, as sole neighbor to human vasodilatory endothelial nitric oxide (NO) signaling. In hypertensive patients, endothelial microparticles contained, indeed, higher levels of NOX5 with a bimodal distribution correlating with disease severity. Mechanistically, mice expressing human Nox5 in endothelial cells, developed, upon aging, severe systolic hypertension and impaired endothelium-dependent vasodilation due to uncoupled NO synthase. We conclude that NOX5-induced uncoupling of endothelial NO synthase is a causal mechanism and theragnostic target of an age-related hypertension endotype; Nox5 knock-in mice represent the first mechanism-based animal model of hypertension.

Introduction

Hypertension is of major medical relevance as a risk factor for myocardial infarction, stroke and other chronic conditions and death [1]. With the exception of 5% of patients with renal hypertension (due to an anatomically evident renal artery occlusion), in the remaining 95% of all cases the cause of hypertension is not known. In these cases of so-called 'essential hypertension', treatments have to focus on symptomatic vasodilatory drug therapy and lifestyle management. Consequently, antihypertensive therapy is neither curative nor effective, needing high numbers to treat with many patients still experiencing adverse outcomes [2].

One molecular mechanism of hypertension that has been suggested for decades is oxidative stress, i.e. an unphysiological production of reactive oxygen species (ROS), which in blood vessels interferes with vasodilation by the endothelium-derived relaxing factor, nitric oxide (NO) [3]. No hypertension-relevant cellular source of ROS, however, has been identified to either prove this hypothesis or exploit it for a mechanism-based or even curative clinical therapy.

Recent genome-wide association studies (GWAS) [4] in search for hypertension risk genes point towards NADPH oxidases (NOX), the only known enzyme family dedicated to ROS formation, in particular the genes *Nox4* and *Nox5*. From preclinical studies, NOX4, although widely expressed, appears irrelevant for blood pressure or hypertension [5]; and NOX5, which is expressed in vascular endothelial cells in human blood vessels, may be associated with diabetic nephropathy [6-8], but mice expressing human NOX5 in vascular smooth muscle cells are normotensive [9].

Network medicine [10] predicts that for most diseases not single genes but modules, i.e. sub- graphs of the interactome, are relevant [11-13]. Therefore, we set out to re-investigate the association of NOX with hypertension and NO-dependent vasodilation using three complementing unbiased *in-silico* approaches and to validate any prediction both in mice and, if possible, also human patient samples.

Results

NOX5 is the only direct neighbor of endothelial NO-cyclic GMP signaling

To explore the possible link between NOX isoforms and hypertension and NO-dependent vasodilation, we constructed a pruned molecular subnetwork from the first neighbors of NOX family members and nitric oxide-cyclic GMP related proteins as seed nodes in the experimentally validated interactome obtained from the IID [14] interactome database. These included NOX1, NOX3, NOX4, NOX5, NOS1, NOS3, GUCYA1, GUCYA2, GUCYB1, PDE5A, PDE9A and PRKG1, but not NOX2 and NOS2. The resulting subnetwork was further pruned according to the subnetwork-participation-degree (SPD) to correct for hub nodes (i.e. proteins that occurred mainly because of their high number of interactions in the whole network). This resulted in a disease module consisting of several connected components, which revealed that all NOX isoforms but NOX5 were excluded as close neighbor of endothelial NO-cyclic GMP signaling. NOX5 fell into the same connected component with the genes encoding the NO receptor, GUCYA1, GUCYA2 and GUCYB1, and with endothelial NOS (NOS3) (Fig. 1A). From IID, this connection is based on a physical interaction suggested by high-throughput affinity chromatography [15].

To cross-check our *in-silico* findings of a NOX disease module, we employed two additional computational network module identification methods, global modularity optimization and agglomerative local search, both of which have been top-performers in the recent Module Identification DREAM Challenge [16]. In brief, the global modularity optimization approach combines multiple module detection algorithms to avoid suboptimal partitions resulting from individual algorithms [17]. The agglomerative local method uses the SPICi algorithm [18] to optimize local density of modules around seed nodes. With all three *in-silico* methods we reached the same conclusion: Exclusion of all NOX genes, except NOX5, as a direct neighbor of endothelial nitric oxide-cyclic GMP signaling (Fig. 1A).

NOX5 protein levels are increased in hypertensive patients

To test this causal endothelial NOX5 hypothesis for human hypertension, we enrolled consecutive outpatients with essential hypertension and a baseline estimated

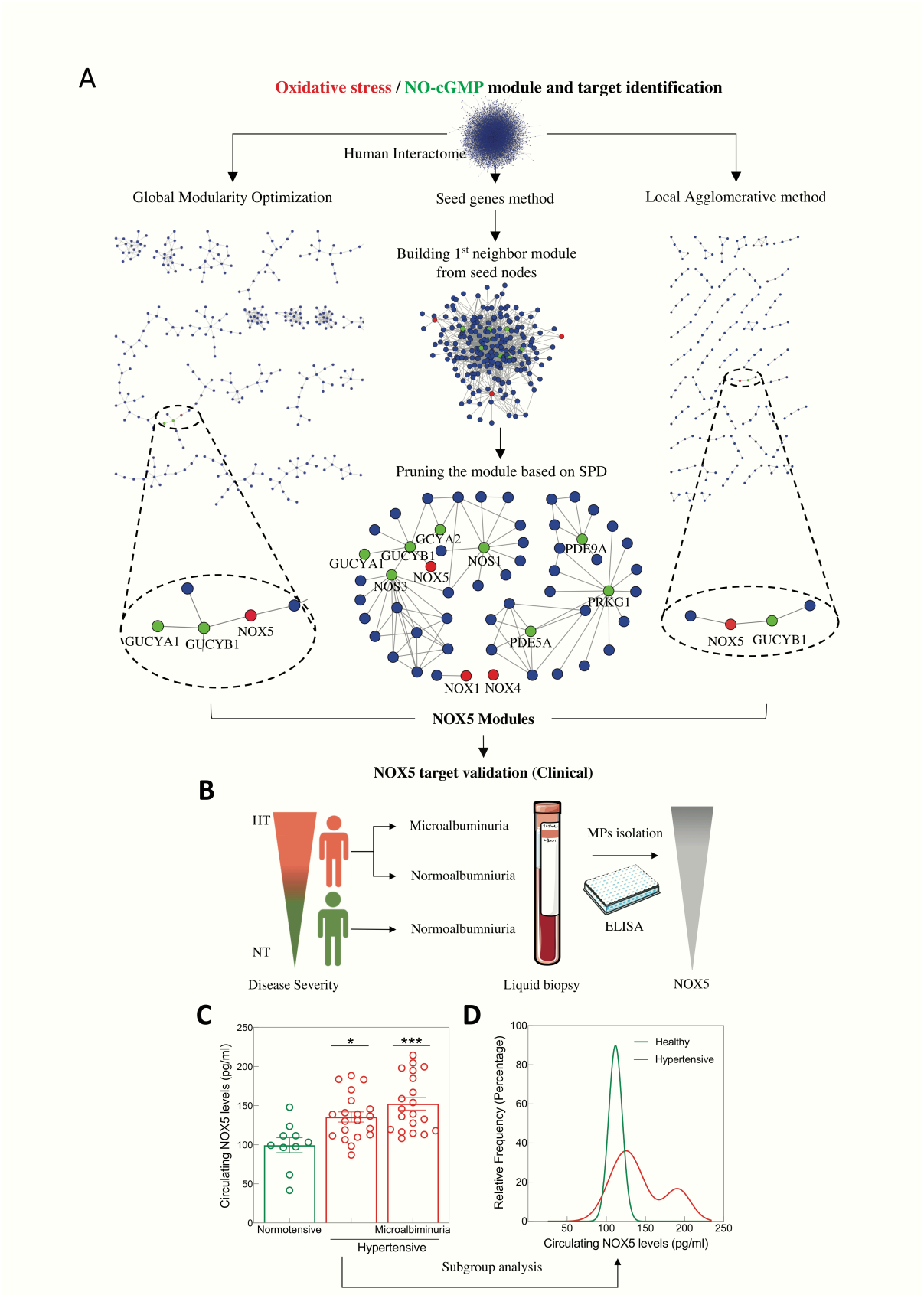

Fig. 1. Identification of NOX5 as direct neighbor of endothelial NO-cGMP signaling and clinical validation in hypertension. **A.** NOX module was constructed by 1st neighbor

subnetwork pruned based on SPD (the middle panel) where NOX isoforms (red nodes) and NO-cGMP related proteins (green nodes) were used as seed nodes. The resulting NOX module was confirmed with two disease module identification methods, global modularity optimization (the left panel) and the agglomerative local method (the right panel). All the methods identified NOX5 as the closest link to NO-cGMP signaling and excluded NOX1-4 and all other known ROS sources (not shown). **B.** NOX5 levels in endothelial microparticles (MPs) isolated from plasma of normotensive (NT), normoalbuminuric subjects and hypertensive (HT) normoalbuminuric and microalbuminuric patients were measured by ELISA. **C.** NOX5 levels were increased in hypertensive patients with normoalbuminuria (n=20) compared to normotensive subjects (n=10). NOX5 levels were even higher in hypertensive patients with microalbuminuria (n=20). Comparison between groups was done by one-way ANOVA followed by Tukey's multiple comparisons test. **D.** Subgroup analysis of all hypertensive patients shows bimodal distribution (p=0.0007, two-tailed F-test, adjusted r-squared=0.9973). All data are represented as mean ± S.E.M. of n independent experiments *P < 0.05, ***P < 0.001.

glomerular filtration rate (eGFR) ≥30 mL/min/1.73 m^2. Study subjects were divided into 3 groups, healthy (n=10), hypertensive patients with normoalbuminuria (n=20) and hypertensive patients with moderately increased albuminuria (previously termed microalbuminuria) (n=20). The baseline characteristics of the patients are listed in Table 1. To measure NOX5 protein levels, circulating endothelial microparticles, i.e. membrane vesicles that are released from endothelial cells upon cellular activation or cell death and carry endothelial proteins [19], were isolated from plasma of the participants (Fig. 1B). We observed higher NOX5 protein levels in endothelial microparticles of hypertensive *versus* normotensive subjects and within hypertensive subjects, patients with microalbuminuria showed even higher NOX5 protein levels (Fig. 1C). These data suggest that NOX5 levels are associated with hypertension and correlate with disease severity. Hypertension is rather an umbrella term that may involve different molecular mechanisms all resulting in a similar phenotype, i.e. elevated blood pressure. NOX5-dependent hypertension may be such an endotype but apply only to a subset of patients [20-22]. We, therefore, performed a subgroup analysis of all hypertensive patients and, indeed, NOX5 levels showed a bimodal distribution (Fig. 1D). Based on this, approximately every fourth hypertensive patient would fall into a high NOX5 mechanotype, which according to the PPI interaction would cause NO-cGMP signaling dysfunction. We therefore aimed to test this hypothesis *in-vivo*.

Table 1. Baseline characteristics in healthy subjects and hypertensive patients

	Healthy subjects (n = 10)	HTN patients without albuminuria (n = 20)	HTN patients with microalbuminuria (n = 20)	p value
Age (yrs)	44 ± 4	56 ± 3	60 ± 3	0.012
Men	7 (70%)	12 (60%)	13 (65%)	0.859
Diabetes	0 (0%)	3 (15%)	6 (30%)	0.118
BMI	24.1 ± 0.94	26.1 ± 0.76	26.9 ± 0.73	0.096
Smoking	0 (0%)	7 (35%)	9 (32%)	0.042
T. Chol	178 ± 11	193 ± 9	199 ± 8	0.358
Triglyceride	158 ± 42	146 ± 19	214 ± 27	0.139
HDL	50 ± 3	47 ± 3	41 ± 2	0.081
LDL	97 ± 11	117 ± 8	115 ± 9	0.360
Fasting glucose	96 ± 6	104 ± 8	120 ± 7	0.107
Serum Cr	0.81 ± 0.07	0.91 ± 0.05	1.01 ± 0.07	0.144
Uric acid	6.2 ± 0.53	6.1 ± 0.31	6.5 ± 0.29	0.656
GFR	87.0 ± 5.69	83.2 ± 3.57	79.3 ± 5.52	0.606
FRS	5.2 ± 1.73	8.2 ± 1.78	10.9 ± 1.9	0.168
ACR	0.008 ± 0.0009	0.010 ± 0.0001	0.059 ± 0.0008	< 0.001
hsCRP	0.56 ± 0.33	0.25 ± 0.03	0.52 ± 0.09	0.188
Adiponectin	16.0 ± 2.75	20.4 ± 3.08	18.5 ± 2.99	0.671
NT-pro-BNP	75.1 ± 11.95	80.9 ± 8.76	95.8 ± 16.9	0.572
Medications				
ACE-I	0 (0%)	4 (20%)	1 (5%)	0.143
ARB	0 (0%)	14 (70%)	16 (80%)	< 0.001
CCB	0 (0%)	13 (65%)	14 (70%)	< 0.001
Beta-blocker	0 (0%)	2 (10%)	9 (45%)	0.005
Thiazides	0 (0%)	6 (30%)	8 (40%)	0.069
Statin	1 (10%)	3 (15%)	7 (35%)	0.185

Values are mean ± SEM or number (%). HTN, hypertension; BMI, body mass index; T. Chol, total cholesterol (mg/dL); HDL, high-density lipoprotein (mg/dL); LDL, low-density lipoprotein (mg/dL); Cr, creatinine (mg/dL); GFR, glomerular filtration rate (mL/min/1.73 m^2/year); FRS, Framingham risk score (%);ACR, albumin/creatinine ratio; hsCRP, high-sensitivity C-reactive protein (mg/dL); T-pro-BNP, N terminal pro- brain natriuretic peptide (pg/mL); ACE-I, angiotensin-converting enzyme inhibitor; ARB, angiotensin II receptor blocker; CCB, calcium channel blocker.

Endothelial NOX5 induces age-related hypertension

In the absence of NOX5 specific inhibitors, we tested the possible role of NOX5 in endothelial NO-cGMP signaling dysfunction and hypertension in mice. Mice, however, lack the *Nox5* gene. We therefore analyzed a knock-in mouse model expressing human *Nox5* in its physiological endothelial cell location [23] (Fig. 2A). In young (9 – 15 weeks old) NOX5 KI mice of both genders (n = 19-20), systolic blood pressure and diastolic blood pressure were, however, not different from age- and sex-matched wild type (WT) mice (Fig. 2B, C). Upon aging (68 – 87 weeks), though, systolic blood pressure was significantly elevated throughout the day in KI (n = 33) compared to age- and sex-matched WT mice (n = 31) (Fig. 2D). Diastolic blood pressure remained unmodified (Fig. 2E) as was heart to body weight ratio (Fig. S1A) indicating that there was no cardiac hypertrophy in KI mice. These observations indicate that in mice, expression of NOX5 in the endothelium leads, upon aging, to a selective elevation of systolic arterial blood pressure. Having established the potential of NOX5 to induce a hypertensive phenotype, we wanted to test the mechanistic link to vascular NO-cGMP signaling as suggested from the *in-silico* network analysis

Endothelial NOX5 causes endothelial dysfunction by uncoupling NOS

In thoracic aorta, femoral artery and saphenous artery isolated from aged KI and WT mice of both genders (n = 9), we analyzed the structural, smooth muscle and endothelial vasomotor properties. Collectively, these blood vessels cover the entire range of large elastic conduit, muscular conduit and small muscular resistance-sized arteries, respectively. In thoracic aorta, femoral artery and saphenous artery of the aged animals, the relation between resting wall tension and arterial lumen diameter did not differ between KI and WT mice (Fig. S2A-C). It is therefore unlikely that the blood pressure

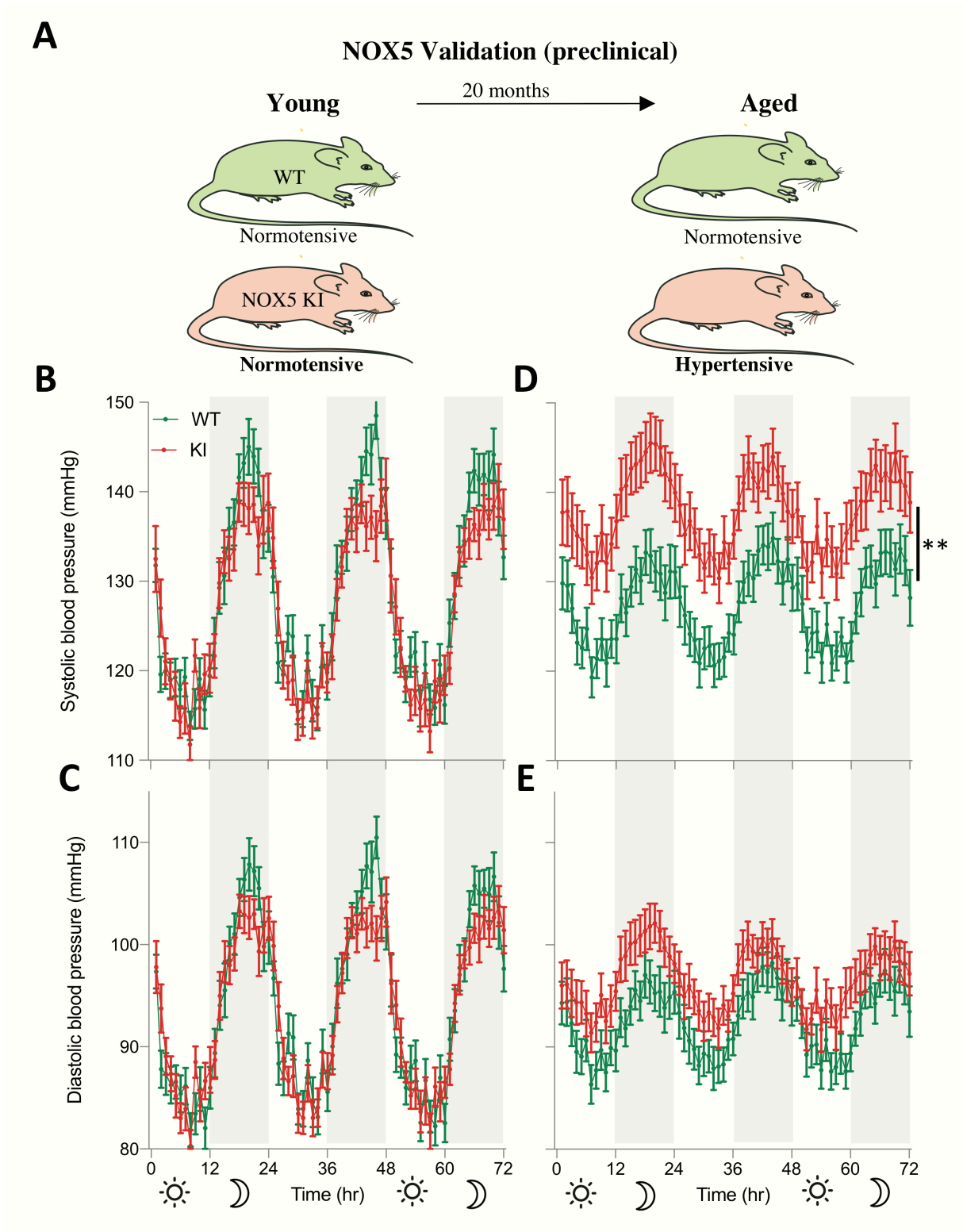

Fig. 2. Preclinical validation of NOX5 in hypertension. **A.** Both young WT and NOX5 KI mice were normotensive however only KI mice become hypertensive upon ageing. **B and C.** There was no significant difference in systolic (B) and diastolic (C) blood pressure between young WT (n=19) and KI (n=20). **D and E.** Aged KI mice (n=33) had higher systolic (D) but similar diastolic (E) blood pressure compared to WT (n=31). Telemetry data were analyzed by two-way repeated measures ANOVA followed by

Sidak's multiple comparisons test. All data are represented as mean ± S.E.M. of n individual animals **P < 0.01.

phenotype of the KI mice resulted from stiffening or inward remodeling of the conduit or resistance arteries.

To test the effect of endothelial NOX5 on endothelium-dependent, NO-cGMP mediated relaxation, arterial segments were pre-contracted by either depolarization (K^+), α_1-adrenergic activation (phenylephrine), or endothelin-1; vasorelaxation was then induced by acetylcholine (Ach) the classical endothelium-derived relaxing factor stimulant [24]. In femoral arteries, irrespective whether pre-contracted with K^+, phenylephrine or endothelin-1, the amplitudes of Ach-induced relaxing responses were significantly smaller in KI compared to WT mice (Fig. 3A) (Fig. S3A, D). Conversely, in saphenous artery (Fig. 3B) (Fig. S3B, E) and thoracic aorta (Fig. S3C, F, G), Ach-induced relaxing responses did not differ between KI and WT mice. To check whether this caliber specific effect on vasomotor function was due to differential expression of NOX5 along the systemic arterial tree, we measured NOX5 gene expression by quantitative PCR. There was, however, no difference in NOX5 gene expression between thoracic aorta, femoral arteries and saphenous arteries of NOX5 KI mice (Fig. S4). These data suggest an ageing-dependent dysfunction of endothelial NO-cGMP signaling due to NOX5 and that this effect is not uniformly distributed along the systemic arterial tree.

We next tested whether, alternatively, chronic changes in the underlying arterial smooth muscle layer could have contributed to the observed blood pressure and vasomotor phenotypes in aged NOX5 KI mice. Contractile responses to K^+ and the sensitivity and maximal responsiveness to phenylephrine and endothelin-1 did, however, not differ between KI and WT mice in all arterial segments (Fig. S5A-I). Also, the blunting of agonist-induced contractile responses by indomethacin was similar in the thoracic aorta of the KI and WT mice (Fig. S5G-I).

To test which component of NO-cGMP signaling was most likely affected, we tested an uncoupling effect on endothelial NO synthase [25] or an oxidative damage of the NO receptor, soluble guanylate cyclase yielding oxidized or heme-free apo-sGC [26, 27]. To test for sGC/apo-sGC, relaxing responses to the NO donor compound and sGC stimulator, PAPA/NO [28], and to the apo-sGC activator, BAY 60-2770 [26], were

analyzed. Neither the PAPA/NO (Fig. S6A-C) nor the BAY 60-2770 response (Fig. S6D) differed between WT and KI mice. These observations suggested that sGC was not dysfunctional in aged NOX5 KI mice. Uncoupling of endothelial NOS is considered a major cause of endothelial dysfunction characterized by decreased NO formation and increased superoxide production and occurs mainly when ROS oxidize the NOS cofactor tetrahydrobiopterin (H_4Bip) [29]. When we incubated femoral arteries of aged NOX5 KI mice, precontracted with phenylephrine, with the H_4Bip precursor sepiapterin, Ach-induced relaxations were greatly improved and became indistinguishable from those in WT (Fig. 3A). Collectively, these data suggest that endothelial NOX5 induces endothelial dysfunction by uncoupling of endothelial NOS leading to impaired endothelium-dependent relaxation of muscular conduit arteries and thus systolic hypertension (Fig. 3C).

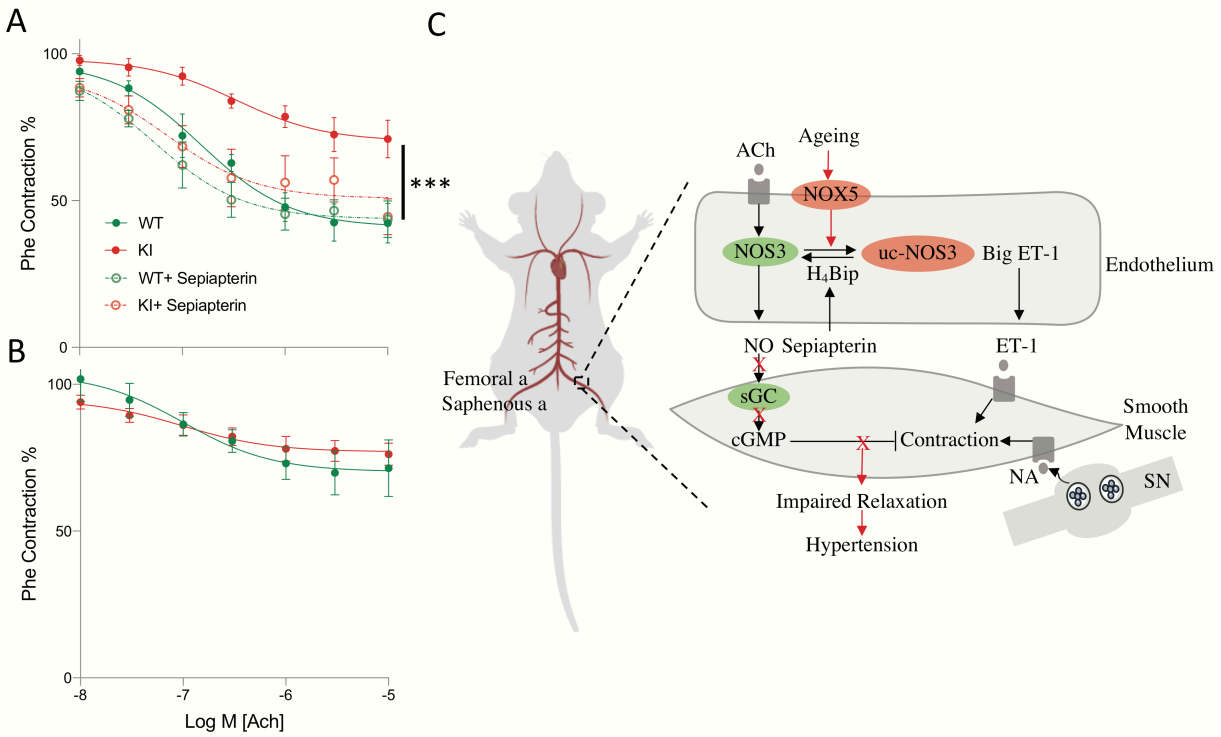

Fig. 3. Endothelial NOX5 induces endothelial dysfunction and hypertension by uncoupling NOS. **A.** Femoral arteries of aged KI mice (n=9) precontracted with phenylephrine (Phe) had less responsiveness to acetylcholine (Ach)-induced relaxation compared to WT (n=9) while pretreatment with sepiapterin improved relaxation in KI (n=4) which was not different from WT (n=3). **B.** Saphenous arteries of aged KI mice (n=9) precontracted with Phe showed no difference in Ach-induced relaxation compared to WT (n=8). Myograph data were analyzed by two-way ANOVA followed by

Sidak's multiple comparisons test. **C.** Schematic representation of NOX5-induced age-dependent hypertension. In ageing, endothelial NOX5 is activated and interferes with normal NO-cGMP signaling which results in impaired vascular smooth muscle relaxations and raised blood pressure. Abbreviations: EC, endothelial cell; ET-1, endothelin-1; H_4Bip, tetrahydrobiopterin; NA, noradrenaline; NOS3, endothelial nitric oxide synthase; SMC, smooth muscle cell; sGC, soluble guanylate cyclase; SN, sympathetic nerve. All data are represented as mean ± S.E.M. of n individual animals ***P < 0.001.

Discussion

Based on human genetic, human clinical, and genetic pre-clinical mechanistic validation, we here report the first identified causal molecular mechanism of human systolic hypertension associated with ageing. This endotype affects approximately one in four patients and molecularly consists of a NOX5-induced uncoupling of endothelial NO synthase followed by an impaired endothelium-dependent vasodilation in muscular conduit arteries. Detection of elevated levels of NOX5 in circulating microparticles appears to serve as a mechanism-based liquid biopsy marker to stratify patients for therapeutic intervention. Based on our in-vivo validation such an intervention may include the H_4Bpi precursor and NOS recoupling agent, sepiapterin and, once such compounds should become clinically available [30-33], a NOX5 inhibitor.

Endothelial expression of human NOX5 in mice led with ageing to severe systolic hypertension. This was not due to stiffening, structural remodeling or increased sensitivity to vasoconstrictor stimuli in the systemic arterial tree. It rather resulted from a regionally selective and specific attenuation of NO-mediated endothelium-dependent relaxation in medium-sized muscular conduit arteries via uncoupling of NOS.

Collectively, our data warrant clinical proof-of-concept trials aiming at a theragnostic [34] strategy in carefully stratified hypertensive patients based on the detection of elevated NOX5, ROS overproduction, e.g. by oxidatively modified proteins, and mechanism-based functional repair by a network pharmacology approach that inhibits NOX5 and recouples NOS. If successful, this will be the first case of a molecular redefinition of the phenotypic disease definition, essential hypertension, and a first step towards precision medicine in a currently high number-needed-to-treat indication. This may be the case for about a fourth of all hypertensives. Our estimate, though significant,

is limited by the relatively small number of patients in the present study and needs to be validated in larger and international hypertension cohort.

The fact that NOX5 is also involved in a worse outcome in stroke [23], for which hypertension is a major risk factor [35], and correlates with atherosclerosis [36], this approach may not only lower blood pressure, but also two major consequences of hypertension, stroke and myocardial infarction.

On a broader scale, our present three-fold interactome-based approach for disease module discovery, pre-clinical and clinal validation appears to be applicable to a wide range of common or complex diseases. We here identify NOX5 as the missing link between ROS and impaired NO signaling. The full module consists of NOX5, NOS3, the different subunits of the NO receptor sGC and the phosphodiesterases, PDE5 and PDE9, as well as the cGMP dependent protein kinase, PKG1. Dysregulation of such a module may be best treated by multiple drugs targeting different protein components. In the present case, the WT mice mimic pharmacological NOX5 inhibition (not yet available) and the treatment with sepiapterin, NOS recoupling.

Disease module construction is a young research field at the interface of biomedicine and bioinformatics. We began with a seed gene-based approach, based on clinically validated proteins. NOX were suggested by GWAS in old [4] but not in younger patients [37] and are the only known enzyme family solely dedicated to ROS formation [38]. The NO-cGMP pathway is important for blood pressure regulation and its dysfunction a hallmark of hypertension [39]. Our approach yielded a module containing a sufficient set of NO-cGMP signaling components and, importantly, with *Nox5* as sole ROS source. We confirmed our findings independently by two complementing *in-silico* network module detection approaches.

Our clinical data are yet still correlative. Endothelial microparticles are, however, well established surrogate biomarkers associated with hypertension and its progression [40, 41]. They produce ROS, contain NOX, induce endothelial dysfunction and impair endothelium-dependent relaxation [42]. In human endothelial cells, angiotensin II, the target of clinically used angiotensin type 1 receptor blockers and angiotensin converting enzyme inhibitors, and the pro-hypertensive autacoid, ET-1, increase NOX5 expression (gene and protein) and activity [43]. In addition to its physiological vascular expression

in endothelial cells, NOX5 is also increased (gene, protein, and activity) to higher levels in human renal proximal tubule cells of hypertensive patients [44], which may contribute to the observed correlation of NOX5, blood pressure and microalbuminuria. Induction of NOX5 in smooth muscle cells does not cause hypertension per se, but correlates with advanced atherosclerotic lesions and diseased coronary arteries show high NOX5 expression and activity [36]. Hypertension is rather an umbrella term for different blood pressure-elevating mechanisms. Some of these may be related to worse clinical outcome, some not. NOX5-dependent hypertension, however, appears to be disease-relevant as this molecular mechanism also leads to or aggravates hypertension-associated clinical outcomes, stroke [23], myocardial infarction [45] and renal failure [44, 46].

GWAS had delivered two NOX candidate genes, *Nox4* and *Nox5*. Knocking out *Nox4* is without a blood pressure phenotype [5, 47]; in many models, *Nox4* was rather vasoprotective [48-50]. The enzymatic product of NOX4, H_2O_2, activates NOS [51] and is an alternative endothelium-derived relaxing factor in its own right [52-54]. This left *Nox5* as candidate gene, which was confirmed by first neighbor analysis linked to NO-cGMP signaling. Unlike NOX4, NOX5 produces superoxide which can uncouple endothelial NO synthase in hypertension by oxidation of H_4Bpi [55, 56] in a sepiapterin-reversible manner [57]. The mechanistic validation of this role of NOX5 in hypertension was performed in a pre-clinical mouse KI model expressing NOX5, not present in the mouse genome, in the physiological cell type, endothelial cells. Here NOX5 is important for endothelial migration and angiogenesis [58]. In mice expressing NOX5 non-physiologically in smooth muscle cells, blood pressure is normal and angiotensin II-induced pressure effects are not augmented [9]. Of particular interest is the regionally selective effect of NOX5, which was reminiscent of the vascular heterogeneity in age-related endothelial dysfunction [59, 60]. It was present in muscular femoral conduit arteries but not in the small resistance-sized saphenous arteries of the KI mice and could, thus, selectively result in systolic hypertension with accompanying elevation of arterial pulse pressure.

Overall, our findings using *in-silico* network approaches as well as further clinical and preclinical validation explain the long-observed correlation between oxidative

stress, endothelial dysfunction and systolic hypertension. Humanized endothelial cell NOX5 KI mice represent the first mechanism-based animal model of human age-related hypertension and endothelial dysfunction. Therapeutically, NOX5 inhibition and NOS recoupling, ideally in combination with mechanistic biomarker stratification, e.g. based on endothelial microparticle liquid biopsies, represents a first-in-class mechanism-based approach for curative antihypertensive therapy obviating the need for symptomatic vasodilators.

Materials and Methods

Study design

Human subjects sample size was determined by G*Power software. For mice, we used a power analysis according to the formula n=2x s2x (Za/2+Zb)2/D2 (L. Sachs, Angewandte Statistik, Springer, 1983, Berlijn, Springer Verlag). Human subjects with history or clinical evidence of angina, myocardial infarction, congestive heart failure, peripheral vascular disease, inflammatory disease, or any disease predisposing to vasculitis were excluded. Causes of secondary hypertension were excluded by appropriate investigations. Patients with stage 4 and 5 chronic kidney disease (GFR <30 mL/min/1.73 m2) were also excluded. Human samples were allocated to different group based on blood pressure and albuminuria values. Mice were allocated to experimental groups according to genotypes. Investigators were blinded to the experimental groups. Replicate experiments were successful. All experiments were reproduced at least three times with independent biological samples.

In-silico methods

We extracted a molecular subnetwork from experimentally validated protein-protein interactions from the IID[13] database (interactome) using NOX family members and nitric oxide-cyclic GMP related proteins as seed nodes. This set of seeds comprises NOX1, NOX3, NOX4, NOX5, NOS1, NOS3, GUCYA1, GUCYA2, GUCYB1, PDE5A, PDE9A and PRKG1. We obtained the subnetwork induced by all first neighbors of the seed genes from the interactome. The induced subnetwork was then pruned according to the subnetwork-participation-degree (SPD), defined as the degree of the node (protein) inside the subnetwork normalized by the degree of the node in the full interactome.

The SPD quantifies how enriched the interactions of a given protein are in a given subnetwork. This way, we emerged a weighted disease module, which is represented by a set of connected components and some single nodes. We selected an SPD cutoff corresponding to 80% of the cumulative sum of the percentage of the nodes as a cutoff value in the pruning step, as this includes most module-specific interactions while excluding most non-specific nodes. The final subnetwork consisted of 56 proteins and 83 protein-protein interactions.

Moreover, we applied the two top-ranked disease network module identification methods from the Module Identification DREAM Challenge [16] to the interactome. We selected these methods from two complementary categories of methods, global and local. The main difference between these two methods is that global methods exploit the global structure information of PPI networks, while the local methods considers only local neighbor information. The global modularity optimization method (M1) of the DREAM challenge bundled in the MONET tool and the agglomerative local method (L1) from SPICi tool [18] have been selected (as best performers in their categories) and applied to find disease modules in the interactome. Note that M1 is an ensemble approach combining multiple module detection algorithms to avoid suboptimal partitions resulting from individual algorithms [17], which notably works without any seed nodes in this tool. The agglomerative L1 method clusters the network greedily, starting from automatically selected local seeds with high weighted degree. This algorithm improves local density of modules in the neighboring region of seed nodes.

Human study participants

The study was approved by the research ethics committee of Taipei Veterans General Hospital (Taipei Veterans General Hospital Institutional Review Board, No: 96-12-42A), and all participants provided their written informed consent. We designed the current study on the basis of a previous study in which we had enrolled consecutive outpatients with essential hypertension and a baseline estimated GFR ≥30 mL/min/1.73 m^2 at Taipei Veterans General Hospital between April 2008 and December 2008 [61, 62]. Hypertension was defined as a systolic blood pressure ≥140 mmHg, a diastolic blood pressure ≥90 mmHg, or use of antihypertensive drugs. Subjects with history or clinical evidence of angina, myocardial infarction, congestive heart failure, peripheral vascular

disease, inflammatory disease, or any disease predisposing to vasculitis were excluded. Causes of secondary hypertension were excluded by appropriate investigations. Patients with stage 4 and 5 chronic kidney disease (GFR <30 mL/min/1.73 m^2) were also excluded. Medical history, including cardiovascular risk factors, previous and present cardiovascular events, and current medication regimen, was obtained during a personal interview and from medical files. Weight, height, and waist circumference were measured and body mass index (BMI) was calculated. Brachial blood pressure was measured by a physician with a mercury sphygmomanometer after patients sat for 15 minutes or longer. The average of 3 measurements was used for the analysis.

Blood and urine measurements

Venous blood samples were collected from all patients after 8 hours of overnight fasting for measurement. The blood samples were centrifuged at 3000 rpm for 10 minutes immediately after collection, and the plasma samples were kept frozen at -70°C until analysis. Each standard and plasma sample was analyzed twice, and the mean value was used in all subsequent analyses. The plasma high-sensitivity C-reactive protein (hs-CRP) level was determined using a latex-enhanced immunonephelometric assay (Dade Behring, Marburg, Germany). Plasma N-terminal pro b-type natriuretic peptide (NT-proBNP) was determined by a sandwich immunoassay (EIMA) with two antibodies (Cortez Diagnostics, Calabasas, CA, USA). Overnight urine samples were obtained for measurement of the albumin excretion rate. Normoalbuminuria was defined as albumin excretion rate of less than 20mg/min, moderately increased albuminuria (previously known as microalbuminuria) was defined as albumin excretion rate of 20–200mg/min, and severely increased albuminuria (previously known as macroalbuminuria) was defined as albumin excretion rate more than 200 mg/min.

Endothelial microparticles extraction and measurement of NOX5

CD144+ microparticles were isolated as described with modifications [63, 64]. Briefly, Dynabeads G (Invitrogen, Carlsbad, CA) were washed with PBS containing 0.1% BSA and then reconstituted with PBS. Anti-CD144 antibody (Santa Cruz Biotechnology, Dallas, TX) was mixed with prewashed Dynabeads G for 2 hours and then incubated with serum samples at 1:200 dilution overnight at 4°C. After precipitation, Dynabeads G were washed with PBS and 1% Tween-20 three times. The purity of CD144+ MPs, determined by FACS analysis, was 70%±5.6%. With the use of FITC-conjugated beads

as size references, the size of such particles was assessed to be <0.5 μm in diameter. Human NADPH oxidase 5 (NOX5) levels were measured using commercially available enzyme-linked immunosorbent assay (ELISA, Cusabio Technology LLC, Houston, Texas) kit according to the manufacturer's instructions. Samples were stored at –70°C from date of collection in 2008 until testing for NOX5 in 2014 (totally 50 samples were available). The intra-assay and inter-assay variation coefficients of the tests were <8% and <10%, respectively.

Animals

Mice naturally do not express the NOX5 gene, therefore, we have generated and validated humanized NOX5 Knock-in (KI) mice as previously described [23]. Briefly, the model was developed using the hypoxanthine phospho-ribosyl-transferase (Hprt) targeted transgenic approach under the control of the Tie2 promoter. Therefore, our NOX5 KI mice express the NOX5 in endothelial and hematopoietic cells which mimic the physiological human expression of NOX5. Expression of NOX5 in the KI mice tissues was previously validated by quantitative real-time PCR and compared to Wild Type (WT) mice [23].

Age- and gender-matched groups of male and female mice (9-15 weeks old, n = 19-20) and (68-87 weeks old, n = 31-33) were used. All mice were allowed free access to water and food in a temperature-regulated room (22˚C) and placed in a 12 h light-dark cycle. All experimental procedures were carried out according to the guidelines of the Animal Ethics Committee of Faculty of Health, Medicine and Life Sciences, Maastricht University, Netherlands.

Blood Pressure Recording (Telemetry)

NOX5 KI and WT Mice were anaesthetized with isoflurane (induction, 3-4%; maintenance, 1.5-2.5%) and echocardiography (ultrasound) was performed (Fig. S8). To implant the telemetry transmitters, 5 days after the ultrasound, mice were anaesthetized with the same protocol and preoperative analgesia was done by subcutaneous injection of 0.05 mg/kg buprenorphine repeated every 12 hours. Each mouse was placed on a heating pad (UNO temperature control unit, UNO Roestvaststaal BV) and body temperature was monitored using a rectal probe and maintained at 37.0°C using a feedback-controlled infrared light. An incision in the skin overlying the carotid artery was made. Via this incision, in the subcutaneous space of

the flank a pocket was created for inserting the telemetry transmitter (TA11PA-C10; Data Sciences, Inc., St. Paul, MN) to monitor blood pressure, heart rate, and motor activity. The left carotid artery was dissected free and 3 ligatures (5-0, silk) were placed: at the bifurcation of the internal and external carotid to close the vessel, at the heart to temporarily close the vessel and one in between to fixate the catheter. Via a small hole cut in the artery, the catheter was introduced and advanced into the aortic arch. Then, the pocket in the flank was filled with 3mL prewarmed saline and the transmitter was placed in the pocket. The wound was then closed using a polysorb 5-0 suture. All surgical procedures were performed under aseptic conditions. Post-operative analgesia was done by subcutaneous injection of 0.05 mg/kg buprenorphine after 6 hr. and 5 mg/kg carprofen after 24 and 48 hr. Mice were allowed to recover for 7-14 days before starting the measurement. Mice were housed individually in a quiet room. Blood pressure was measured over a 72h period, with 10 cycles of 75 sec. per hour. The average per hour was calculated for the 72h period. Radio signals from the transmitter were continuously monitored with a fully automated data-acquisition system (Dataquest A.R.T.; Data Sciences, Inc.). Mice were sacrificed by CO_2/O_2 inhalation and organs were taken out for further analysis. Organ and body weights are presented in Fig. S1.

Myograph

After mice were sacrificed, thoracic aortae, femoral and saphenous arteries were dissected free from perivascular adipose tissue and mounted in a wire myograph (DMT, Aarhus, DK). The organ chamber was filled with Krebs-Ringer bicarbonate-buffered salt solution (KRB) that was continuously aerated with 95% O_2/5% CO_2 and maintained at 37˚C. Passive stretch procedure was performed to mimic the physiologically relevant internal lumen diameter as previously described [65]. Arterial contractile and relaxing responses were recorded at lumen diameters corresponding to a distending pressure of 100 mmHg in thoracic aorta and femoral artery and at 90 % of this diameter in the resistance-sized saphenous artery. This is justified because diastolic arterial blood pressure did not differ significantly between the aged KI and WT mice. In view of the comparable diameter-tension relationships, these diameters did not differ significantly between the two mouse strains (Fig. S8). Part of the isolated thoracic aorta was studied in the absence and part in the continuous presence of 10 μM indomethacin to inhibit production of prostaglandins that can act as endothelium-derived vasoactive factors in

this vessel. The vessels were tested for their contractile response to 40mM K^+, concentration-response curves of phenylephrine (0.01 to 100μM) and endothelin-1 (1 – 256nM) followed by acetylcholine (Ach) (0.01 to 100μM), PAPA/NO (0.01-10μM) or Bay60-2770 (0.01-10μM)-induced relaxations. The wall tension of the vessel segment was continuously recorded with LabChart Pro (ADInstruments, Oxford, UK).

RNA Extraction, cDNA Synthesis and Quantitative Real-Time PCR

Thoracic aortas, femoral arteries and saphenous arteries were isolated from mice and immediately submerged in RNAlater solution (Thermo Fisher Scientific). RNA was extracted using RNeasy® Micro Kit (Qiagen) according to the manufacturer's protocol. cDNA was synthesized from 1 μg total RNA in 20 μl reactions using High Capacity cDNA Reverse Transcription Kit (Thermo Fisher Scientific). After synthesis, the cDNA was stored at –20°C.

RT-qPCR was performed on CFX96™ Real-Time PCR Detection System (Bio-Rad). All reactions were performed in triplicates in a total volume of 20 μl each using TaqMan® Universal PCR Master Mix (Applied Biosystems- Life Technologies) according to manufacturer's instructions. 3 μl cDNA was used as template and pre-designed TaqMan® primers of β-actin and Nox5 were used. The specific assay ID for the primers used are shown in Supplementary Table 1. The standard PCR conditions were as follows: 10 min at 95 °C, followed by 15 s at 95 °C and 1 min at 60 °C, 59 repeats. The amount of mRNA was normalized to the measured expression of β-actin mRNA.

Statistical analysis

All human and animal data are expressed as the mean ± SEM for numeric variables and as the number (percentage) for categorical variables. Comparisons of continuous variables between the two mice groups were performed by unpaired two-tailed Student's t-test and among the three human groups by one-way analysis of variance (ANOVA) followed by Tukey's multiple comparisons test (post-hoc test). Comparisons of categorical variables among the human groups were assessed by a χ^2 (chi square). Comparisons between the two mice groups, in telemetry data were done by two-way repeated measures ANOVA and in myograph by ordinary two-way ANOVA, followed by Sidak's multiple comparisons test. For the subgroup analysis of the NOX5 levels in human subjects, a frequency analysis was carried out, where the bin width is calculated using Sturges' rule [66]. To assess the modality of the data, the output frequencies were

fitted with a single gaussian and sum of two gaussian distributions, and a two-tailed F-test with null hypothesis as Gaussian and alternative hypothesis as sum of two-Gaussians was performed. Additionally, the adjusted r-squared values were compared to select the best fitting distribution for the sample. Given the bimodal nature of the sample, the area under each Gaussian distribution was calculated using the formula "Amplitude*SD/0.3989" and subsequently the proportion of NOX5 mechanotype was reported as the ratio between the two distributions. Data were analyzed using GraphPad Prism Version 8.2 (GraphPad Software Inc., San Diego, CA). A p-value of less than 0.05 was considered to indicate statistical significance after multiple testing correction.

Supplementary Materials

Fig. S1. Body and organs weights in aged WT and KI mice.

Fig. S2. Arterial stiffness in aged WT and KI mice.

Fig. S3. Acetylcholine (Ach)-induced relaxations in arteries of aged WT and KI mice.

Fig. S4. qPCR of NOX5 in thoracic aortas (TAO), femoral arteries (FA) and saphenous arteries (SA) of aged KI mice.

Fig. S5. Contractile responses in arteries of aged WT and KI mice.

Fig. S6. Endothelium-independent relaxations in arteries of aged WT and KI mice.

Fig. S7. Echocardiography in aged WT and KI mice.

Fig. S8. Arteries diameter in aged WT and KI mice.

Table S1. qPCR assays

References

1. M. H. Olsen *et al.*, A call to action and a lifecourse strategy to address the global burden of raised blood pressure on current and future generations: the Lancet Commission on hypertension. *Lancet* **388**, 2665-2712 (2016).
2. L. G. Ogden, J. He, E. Lydick, P. K. Whelton, Long-term absolute benefit of lowering blood pressure in hypertensive patients according to the JNC VI risk stratification. *Hypertension* **35**, 539-543 (2000).
3. R. J. Gryglewski, R. M. Palmer, S. Moncada, Superoxide anion is involved in the breakdown of endothelium-derived vascular relaxing factor. *Nature* **320**, 454-456 (1986).
4. A. T. Kraja *et al.*, New Blood Pressure-Associated Loci Identified in Meta-Analyses of 475 000 Individuals. *Circ Cardiovasc Genet* **10**, (2017).
5. C. Kleinschnitz *et al.*, Post-stroke inhibition of induced NADPH oxidase type 4 prevents oxidative stress and neurodegeneration. *PLoS biology* **8**, (2010).
6. C. E. Holterman *et al.*, Nephropathy and elevated BP in mice with podocyte-specific NADPH oxidase 5 expression. *J Am Soc Nephrol* **25**, 784-797 (2014).
7. J. C. Jha *et al.*, NADPH Oxidase Nox5 Accelerates Renal Injury in Diabetic Nephropathy. *Diabetes* **66**, 2691-2703 (2017).
8. J. C. Jha *et al.*, Endothelial or vascular smooth muscle cell-specific expression of human NOX5 exacerbates renal inflammation, fibrosis and albuminuria in the Akita mouse. *Diabetologia* **62**, 1712-1726 (2019).
9. A. C. Montezano *et al.*, NADPH Oxidase 5 Is a Pro-Contractile Nox Isoform and a Point of Cross-Talk for Calcium and Redox Signaling-Implications in Vascular Function. *J Am Heart Assoc* **7**, (2018).
10. A. L. Barabasi, N. Gulbahce, J. Loscalzo, Network medicine: a network-based approach to human disease. *Nat Rev Genet* **12**, 56-68 (2011).

11. N. Alcaraz *et al.*, De novo pathway-based biomarker identification. *Nucleic Acids Res* **45**, e151 (2017).

12. R. Batra *et al.*, On the performance of de novo pathway enrichment. *NPJ Syst Biol Appl* **3**, 6 (2017).

13. J. Menche *et al.*, Disease networks. Uncovering disease-disease relationships through the incomplete interactome. *Science* **347**, 1257601 (2015).

14. M. Kotlyar, C. Pastrello, Z. Malik, I. Jurisica, IID 2018 update: context-specific physical protein-protein interactions in human, model organisms and domesticated species. *Nucleic Acids Res* **47**, D581-D589 (2019).

15. E. L. Huttlin *et al.*, Architecture of the human interactome defines protein communities and disease networks. *Nature* **545**, 505-509 (2017).

16. S. Choobdar *et al.*, Assessment of network module identification across complex diseases. *Nat Methods* **16**, 843-852 (2019).

17. A. Arenas, A. Fernández, S. Gómez, Analysis of the structure of complex networks at different resolution levels. *New Journal of Physics* **10**, 053039 (2008).

18. P. Jiang, M. Singh, SPICi: a fast clustering algorithm for large biological networks. *Bioinformatics* **26**, 1105-1111 (2010).

19. F. Dignat-George, C. M. Boulanger, The many faces of endothelial microparticles. *Arterioscler Thromb Vasc Biol* **31**, 27-33 (2011).

20. J. Aguirre-Plans *et al.*, Proximal Pathway Enrichment Analysis for Targeting Comorbid Diseases via Network Endopharmacology. *Pharmaceuticals (Basel)* **11**, (2018).

21. A. Mazein *et al.*, Systems medicine disease maps: community-driven comprehensive representation of disease mechanisms. *NPJ Syst Biol Appl* **4**, 21 (2018).

22. N. S. Burns, P. W. Miller, Learning What We Didn't Know - The SPRINT Data Analysis Challenge. *N Engl J Med* **376**, 2205-2207 (2017).

23. A. I. Casas *et al.*, Calcium-dependent blood-brain barrier breakdown by NOX5 limits postreperfusion benefit in stroke. *J Clin Invest* **130**, 1772-1778 (2019).

24. R. F. Furchgott, J. V. Zawadzki, The obligatory role of endothelial cells in the relaxation of arterial smooth muscle by acetylcholine. *Nature* **288**, 373-376 (1980).

25. V. Gebhart, K. Reiss, A. Kollau, B. Mayer, A. C. F. Gorren, Site and mechanism of uncoupling of nitric-oxide synthase: Uncoupling by monomerization and other misconceptions. *Nitric Oxide* **89**, 14-21 (2019).

26. C. B. Mendes-Silverio *et al.*, Activation of haem-oxidized soluble guanylyl cyclase with BAY 60-2770 in human platelets lead to overstimulation of the cyclic GMP signaling pathway. *PLoS One* **7**, e47223 (2012).

27. J. P. Stasch *et al.*, Targeting the heme-oxidized nitric oxide receptor for selective vasodilatation of diseased blood vessels. *J Clin Invest* **116**, 2552-2561 (2006).

28. J. A. Hrabie, J. R. Klose, D. A. Wink, L. K. Keefer, New nitric oxide-releasing zwitterions derived from polyamines. *The Journal of Organic Chemistry* **58**, 1472-1476 (1993).

29. R. Kietadisorn, R. P. Juni, A. L. Moens, Tackling endothelial dysfunction by modulating NOS uncoupling: new insights into its pathogenesis and therapeutic possibilities. *Am J Physiol Endocrinol Metab* **302**, E481-495 (2012).

30. S. Altenhofer *et al.*, The NOX toolbox: validating the role of NADPH oxidases in physiology and disease. *Cell Mol Life Sci* **69**, 2327-2343 (2012).

31. S. Altenhofer, K. A. Radermacher, P. W. Kleikers, K. Wingler, H. H. Schmidt, Evolution of NADPH Oxidase Inhibitors: Selectivity and Mechanisms for Target Engagement. *Antioxid Redox Signal* **23**, 406-427 (2015).

32. F. Augsburger *et al.*, Pharmacological characterization of the seven human NOX isoforms and their inhibitors. *Redox Biol* **26**, 101272 (2019).

33. V. T. Dao *et al.*, Isoform-selective NADPH oxidase inhibitor panel for pharmacological target validation. *Free Radic Biol Med*, (2019).

34. S. Frangos, J. R. Buscombe, Why should we be concerned about a "g"? *European Journal of Nuclear Medicine and Molecular Imaging* **46**, 519-519 (2019).

35. C. Hornsten *et al.*, High blood pressure as a risk factor for incident stroke among very old people: a population-based cohort study. *J Hypertens* **34**, 2059-2065 (2016).

36. T. J. Guzik *et al.*, Calcium-dependent NOX5 nicotinamide adenine dinucleotide phosphate oxidase contributes to vascular oxidative stress in human coronary artery disease. *J Am Coll Cardiol* **52**, 1803-1809 (2008).

37. H. Li *et al.*, Associations of NADPH oxidase-related genes with blood pressure changes and incident hypertension: The GenSalt Study. *J Hum Hypertens* **32**, 287-293 (2018).

38. M. H. Elbatreek, M. P. Pachado, A. Cuadrado, K. Jandeleit-Dahm, H. Schmidt, Reactive Oxygen Comes of Age: Mechanism-Based Therapy of Diabetic End-Organ Damage. *Trends Endocrinol Metab*, (2019).

39. M. Hermann, A. Flammer, T. F. Luscher, Nitric oxide in hypertension. *J Clin Hypertens (Greenwich)* **8**, 17-29 (2006).

40. T. Helbing, C. Olivier, C. Bode, M. Moser, P. Diehl, Role of microparticles in endothelial dysfunction and arterial hypertension. *World J Cardiol* **6**, 1135-1139 (2014).

41. E. Shantsila, Endothelial microparticles: a universal marker of vascular health? *J Hum Hypertens* **23**, 359-361 (2009).

42. D. Burger, M. Turner, M. N. Munkonda, R. M. Touyz, Endothelial Microparticle-Derived Reactive Oxygen Species: Role in Endothelial Signaling and Vascular Function. *Oxid Med Cell Longev* **2016**, 5047954 (2016).

43. A. C. Montezano *et al.*, Nicotinamide adenine dinucleotide phosphate reduced oxidase 5 (Nox5) regulation by angiotensin II and endothelin-1 is mediated via calcium/calmodulin-dependent, rac-1-independent pathways in human endothelial cells. *Circ Res* **106**, 1363-1373 (2010).

44. P. Yu *et al.*, Unique role of NADPH oxidase 5 in oxidative stress in human renal proximal tubule cells. *Redox Biol* **2**, 570-579 (2014).

45. N. E. Hahn *et al.*, NOX5 expression is increased in intramyocardial blood vessels and cardiomyocytes after acute myocardial infarction in humans. *Am J Pathol* **180**, 2222-2229 (2012).

46. C. E. Holterman, J. F. Thibodeau, C. R. Kennedy, NADPH oxidase 5 and renal disease. *Curr Opin Nephrol Hypertens* **24**, 81-87 (2015).

47. G. Bouabout *et al.*, Nox4 genetic inhibition in experimental hypertension and metabolic syndrome. *Arch Cardiovasc Dis* **111**, 41-52 (2018).

48. R. Ray *et al.*, Endothelial Nox4 NADPH oxidase enhances vasodilatation and reduces blood pressure in vivo. *Arterioscler Thromb Vasc Biol* **31**, 1368-1376 (2011).

49. K. Schroder *et al.*, Nox4 is a protective reactive oxygen species generating vascular NADPH oxidase. *Circ Res* **110**, 1217-1225 (2012).

50. C. Veith *et al.*, NADPH oxidase 4 is not involved in hypoxia-induced pulmonary hypertension. *Pulm Circ* **6**, 397-400 (2016).

51. R. P. Brandes, I. Takac, K. Schroder, No superoxide--no stress?: Nox4, the good NADPH oxidase! *Arterioscler Thromb Vasc Biol* **31**, 1255-1257 (2011).

52. H. Miura *et al.*, Role for hydrogen peroxide in flow-induced dilation of human coronary arterioles. *Circ Res* **92**, e31-40 (2003).

53. T. M. Leurgans *et al.*, Endothelin-1 shifts the mediator of bradykinin-induced relaxation from NO to H2 O2 in resistance arteries from patients with cardiovascular disease. *Br J Pharmacol* **173**, 1653-1664 (2016).

54. H. Shimokawa, Hydrogen peroxide as an endothelium-derived hyperpolarizing factor. *Pflugers Arch* **459**, 915-922 (2010).

55. U. Landmesser *et al.*, Oxidation of tetrahydrobiopterin leads to uncoupling of endothelial cell nitric oxide synthase in hypertension. *J Clin Invest* **111**, 1201-1209 (2003).

56. C. Dumitrescu *et al.*, Myocardial ischemia results in tetrahydrobiopterin (BH4) oxidation with impaired endothelial function ameliorated by BH4. *Proc Natl Acad Sci U S A* **104**, 15081-15086 (2007).

57. B. M. Mitchell, A. M. Dorrance, R. C. Webb, GTP cyclohydrolase 1 inhibition attenuates vasodilation and increases blood pressure in rats. *Am J Physiol Heart Circ Physiol* **285**, H2165-2170 (2003).

58. X. Pi *et al.*, NADPH oxidase-generated reactive oxygen species are required for stromal cell-derived factor-1alpha-stimulated angiogenesis. *Arterioscler Thromb Vasc Biol* **34**, 2023-2032 (2014).

59. M. Barton *et al.*, Anatomic heterogeneity of vascular aging: role of nitric oxide and endothelin. *Hypertension* **30**, 817-824 (1997).

60. R. L. Matz, M. A. de Sotomayor, C. Schott, J. C. Stoclet, R. Andriantsitohaina, Vascular bed heterogeneity in age-related endothelial dysfunction with respect to NO and eicosanoids. *Br J Pharmacol* **131**, 303-311 (2000).

61. C. Y. Hsu *et al.*, Increased circulating endothelial apoptotic microparticle to endothelial progenitor cell ratio is associated with subsequent decline in glomerular filtration rate in hypertensive patients. *PLoS One* **8**, e68644 (2013).

62. P. H. Huang *et al.*, Increased circulating CD31+/annexin V+ apoptotic microparticles and decreased circulating endothelial progenitor cell levels in hypertensive patients with microalbuminuria. *J Hypertens* **28**, 1655-1665 (2010).

63. F. Shang *et al.*, MicroRNA-92a Mediates Endothelial Dysfunction in CKD. *J Am Soc Nephrol* **28**, 3251-3261 (2017).

64. Z. Chen *et al.*, Oxidative stress activates endothelial innate immunity via sterol regulatory element binding protein 2 (SREBP2) transactivation of microRNA-92a. *Circulation* **131**, 805-814 (2015).

65. R. Lazor, F. Feihl, B. Waeber, P. Kucera, C. Perret, Endothelin-1 does not mediate the endothelium-dependent hypoxic contractions of small pulmonary arteries in rats. *Chest* **110**, 189-197 (1996).

66. D. W. Scott, Sturges' rule. *Wire computational statistics* **1**, 303-306 (2009).

Acknowledgments: We thank Daniel Marbach and Sven Bergmann for helpful discussions. **Funding**: Financial support (to HHHWS) by the ERC (AdG RadMed '294683' and PoC SAVEBRAIN '737586') and the Horizon 2020 programme (REPO-TRIAL '777111') is gratefully acknowledged. JB is grateful for financial support of his VILLUM Young Investigator grant.

Author contributions: J.D.M. and H.H.H.W Schmidt designed research; M.H.E., S.S., E.A., A.T., P.H.H., C.Y.H., P.S., G.J. and P.K. performed research; M.H.E., S.S. and A.H analyzed the data and prepared figures; M.H.E., S.S., E.G., T.K., A.H., A.W., J.B. and J.D.M contributed to writing and revised the final version of manuscript; M.H.E., J.D.M. and H.H.H.W Schmidt wrote and edited figures and manuscript.

Competing interests: The authors declare no competing interests.

Data and materials availability: All data associated with this study are included in the paper or the Supplementary Materials. We used the interactome from IID database which is available at http://ophid.utoronto.ca/iid. For computational data analysis we used: MONET tool: https://github.com/BergmannLab/MONET and SPICi tool: https://compbio.cs.princeton.edu/spici/. For the NOX module construction by seed gene method, we used our own codes (submitted for publications) which are available from the corresponding author upon reasonable request.

Supplementary Materials:

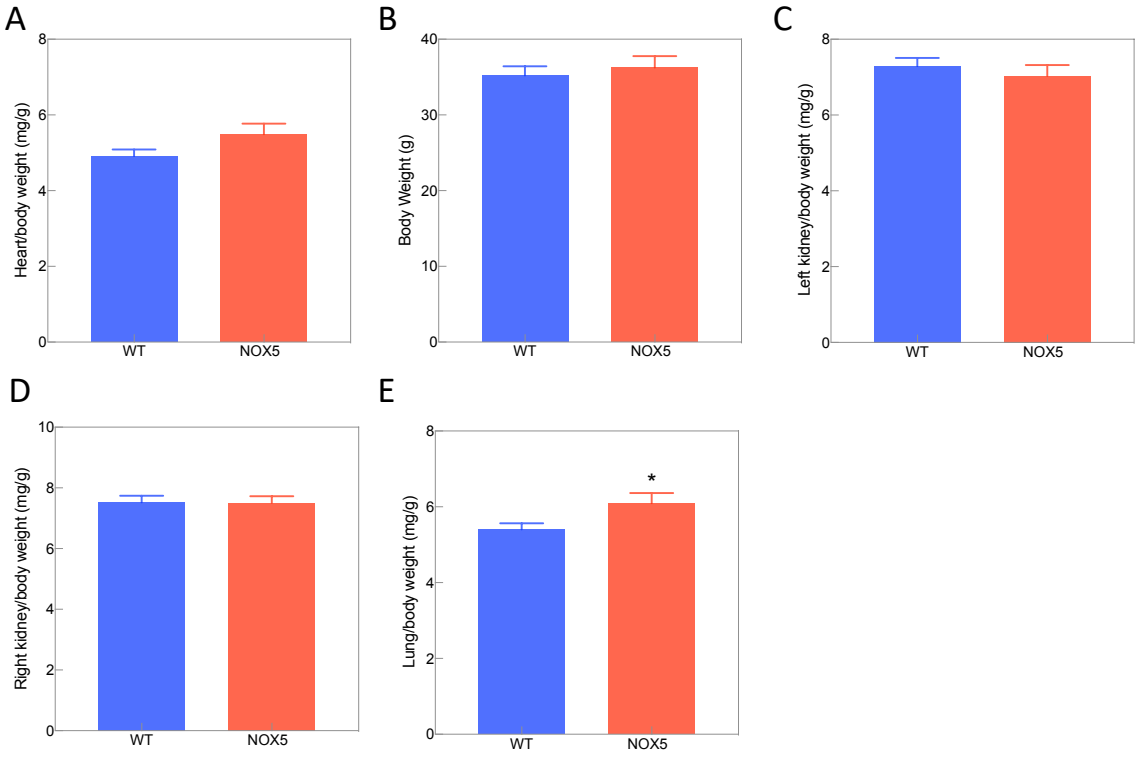

Fig. S1. Body and organs weights in aged WT and KI mice. **A-E.** There was no difference in body, heart and kidneys weights between WT (n=24) and KI mice (n=20), however lung/body weight ratio was higher in KI mice. Comparison between groups were done by two-tailed unpaired T-test. All data are represented as mean ± S.E.M. of n individual animals *P < 0.05.

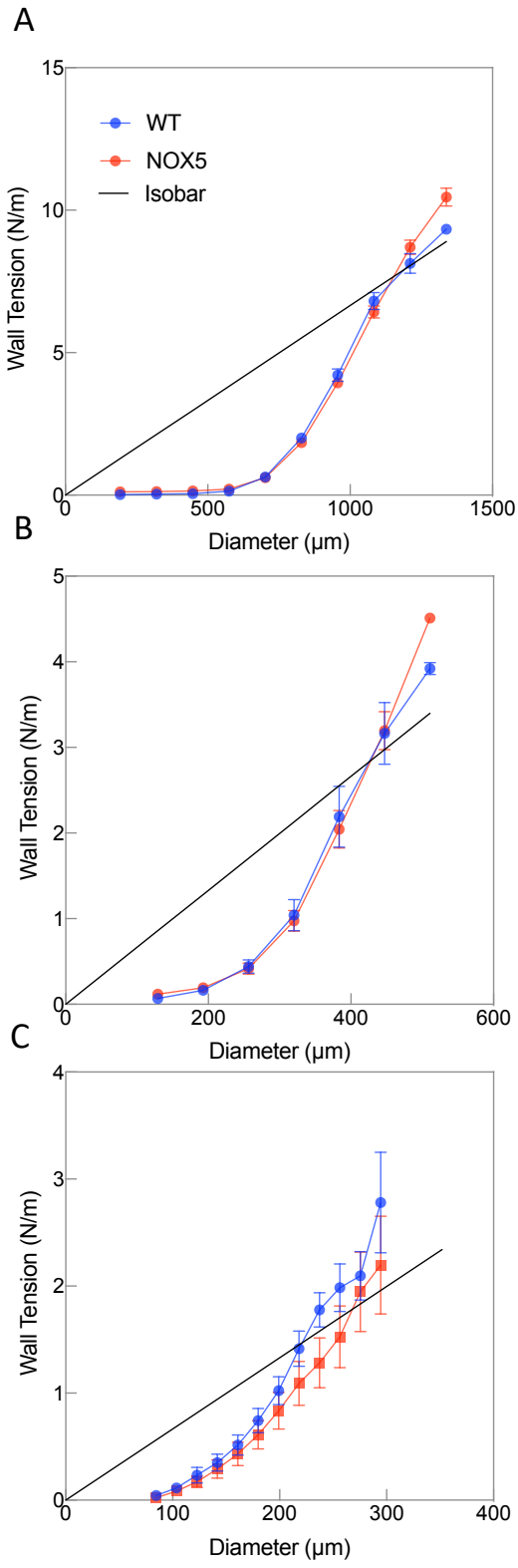

Fig. S2. Arterial stiffness in aged WT and KI mice. **A-C.** The relation between resting wall tension and arterial lumen diameter did not differ between KI (n=9) and WT (n=9) mice in thoracic aortas (A), femoral arteries (B) and saphenous arteries (C). All data are represented as mean ± S.E.M. of n individual animals.

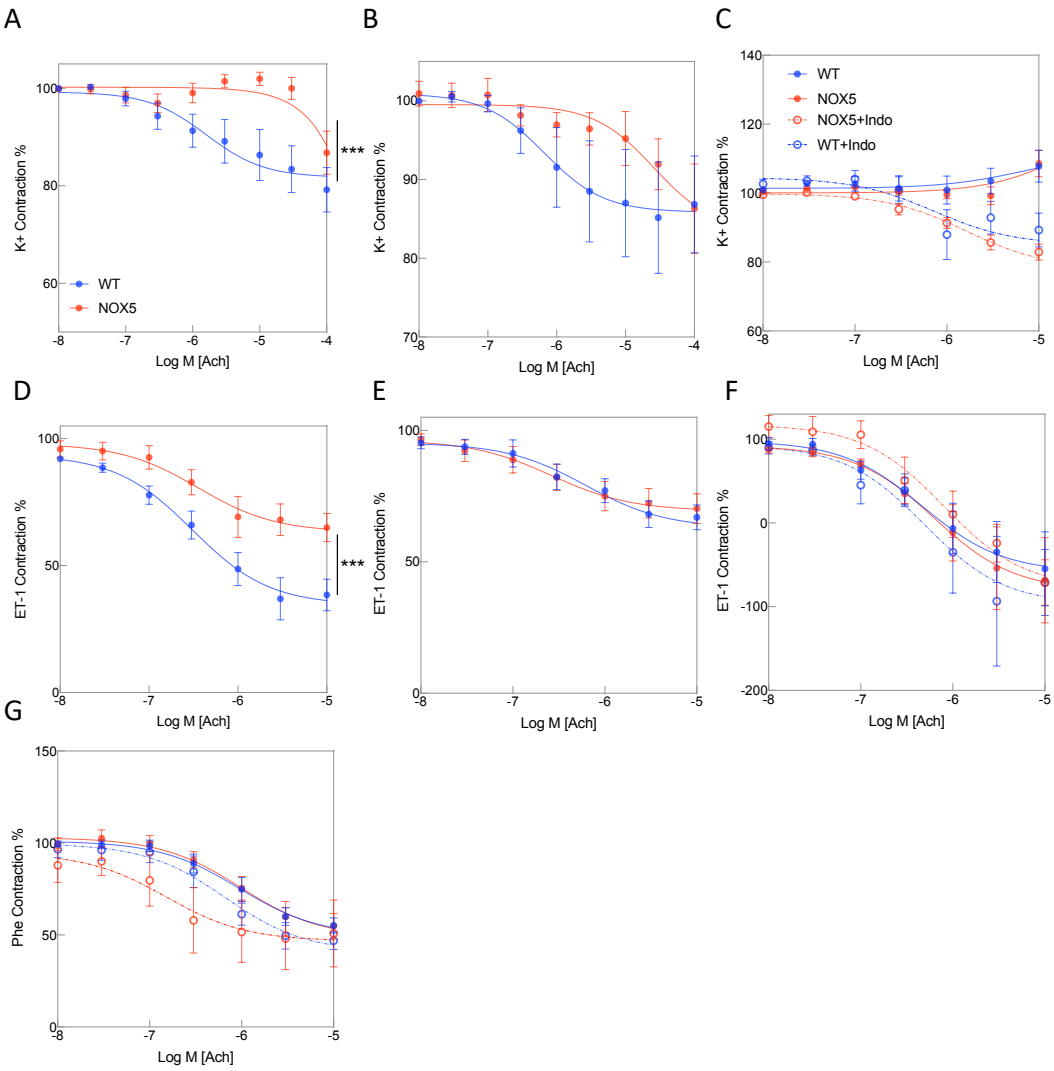

Fig. S3. Acetylcholine (Ach)-induced relaxations in arteries of aged WT and KI mice. **A-C.** Ach-induced relaxations were impaired in femoral arteries (A) of aged KI mice (n=9) compared to WT (n=8-9) but not in saphenous arteries (B) and thoracic aortas (with/without indomethacin) (C) precontracted with K^+. **D-F.** Ach-induced relaxations were impaired in femoral arteries (A) of aged KI mice (n=9) compared to WT (n=8-9) but not in saphenous arteries (B) and thoracic aortas with/without indomethacin (C) precontracted with Endothelin-1. **G.** There was no difference in Ach-induced relaxations in thoracic aortas (with/without indomethacin) precontracted with phenylephrine between WT (n=9) and KI mice (n=9). Myograph data were analyzed by two-way ANOVA followed by Sidak's multiple comparisons test. All data are represented as mean ± S.E.M. of n individual animals ***P < 0.001.

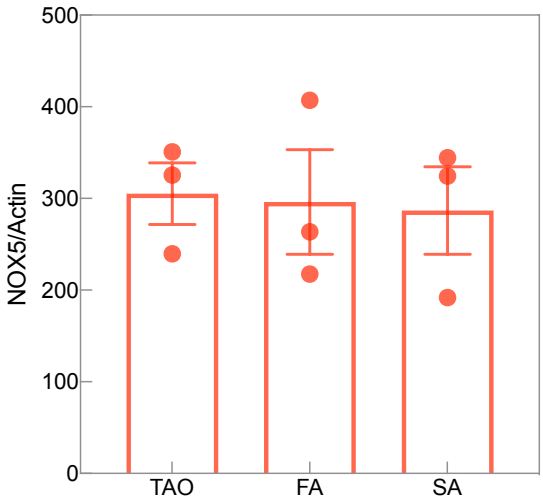

Fig. S4. qPCR of NOX5 in thoracic aortas (TAO), femoral arteries (FA) and saphenous arteries (SA) of aged KI mice. There was no difference in NOX5 gene expression between the three vessel types (n=3, each in duplicates). Comparison were done by one-way ANOVA. All data are represented as mean ± S.E.M. of n individual animals.

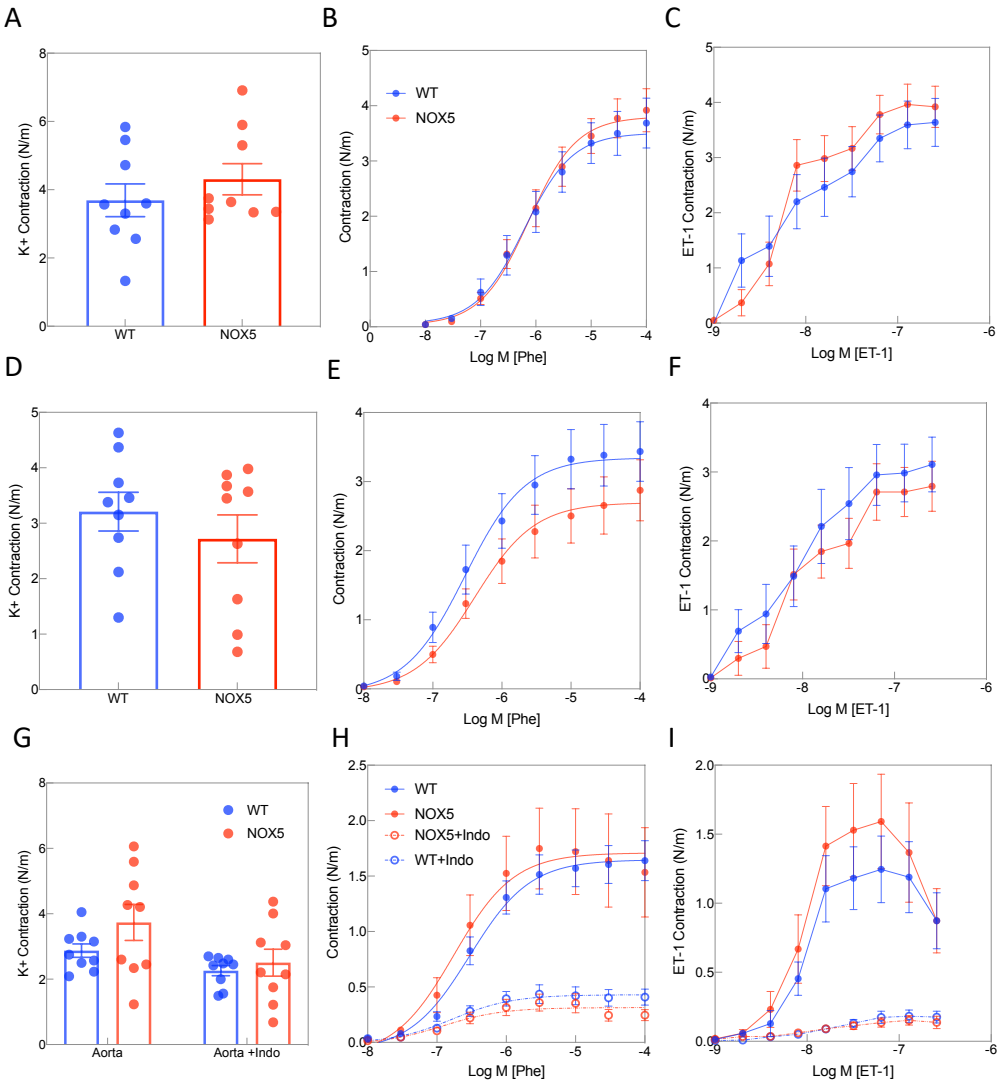

Fig. S5. Contractile responses in arteries of aged WT and KI mice. There was no difference in contractile responses to K^+, phenylephrine and endothelin-1 in femoral arteries **(A-C)**, saphenous arteries **(D-F)** and thoracic aortas (with/without indomethacin) **(G-I)** between WT (n=8-9) and KI mice (n=9). Comparison between 2 groups in contractile responses to K^+ was done by two-tailed T-test. Other myograph data were analyzed by two-way ANOVA followed by Sidak's multiple comparisons test. All data are represented as mean ± S.E.M. of n individual animals.

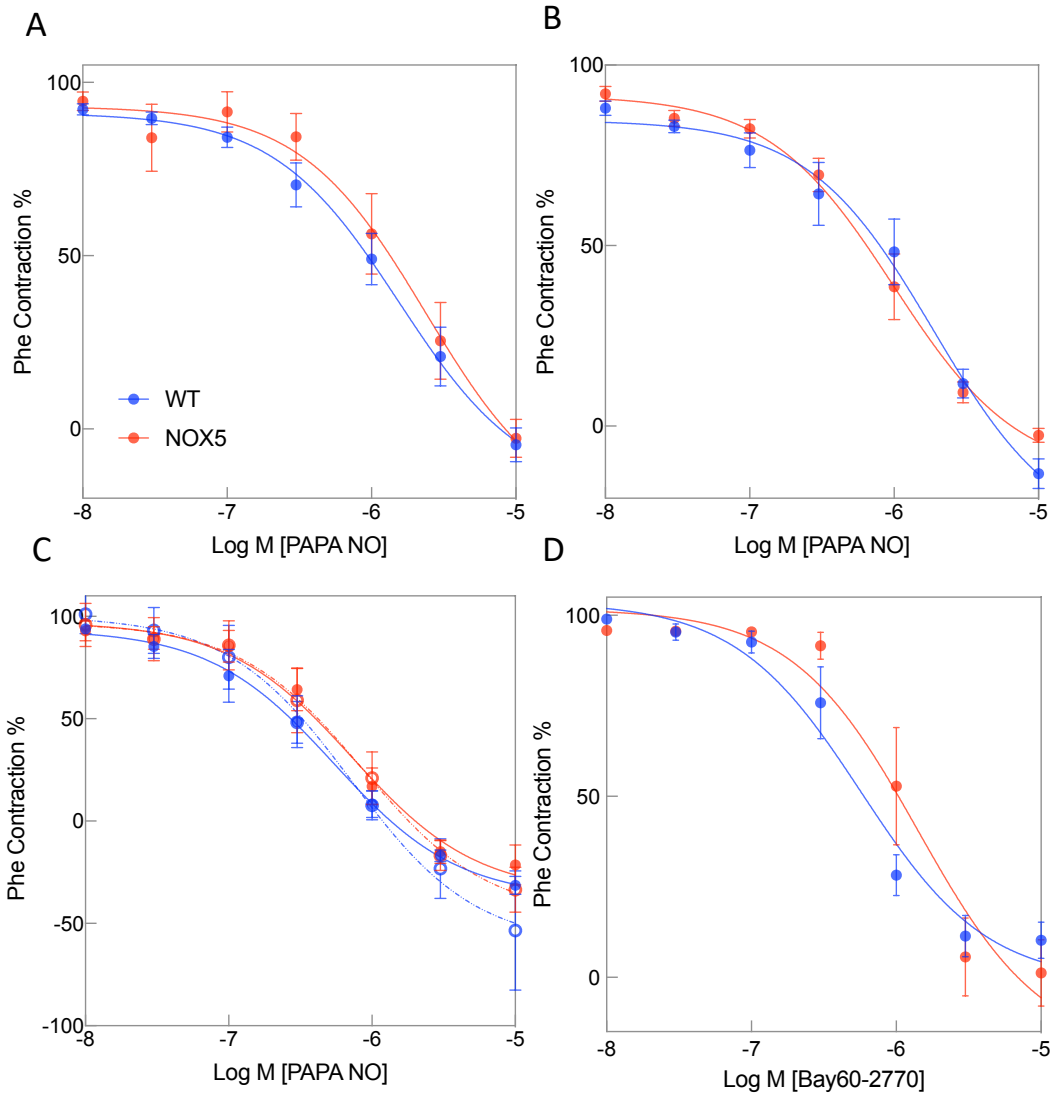

Fig. S6. Endothelium-independent relaxations in arteries of aged WT and KI mice. **A-C.** Relaxations induced by the NO donor, PAPA NO, in femoral arteries (A), saphenous arteries (B) and thoracic aortas (with/without indomethacin) (C) did not differ between WT (n=8-9) and KI mice (n=9). **D.** Relaxations induced by the apo-sGC activator, Bay60-2770, in femoral arteries did not differ between WT (n=4) and KI mice (n=4). Myograph data were analyzed by two-way ANOVA followed by Sidak's multiple comparisons test. All data are represented as mean ± S.E.M. of n individual animals.

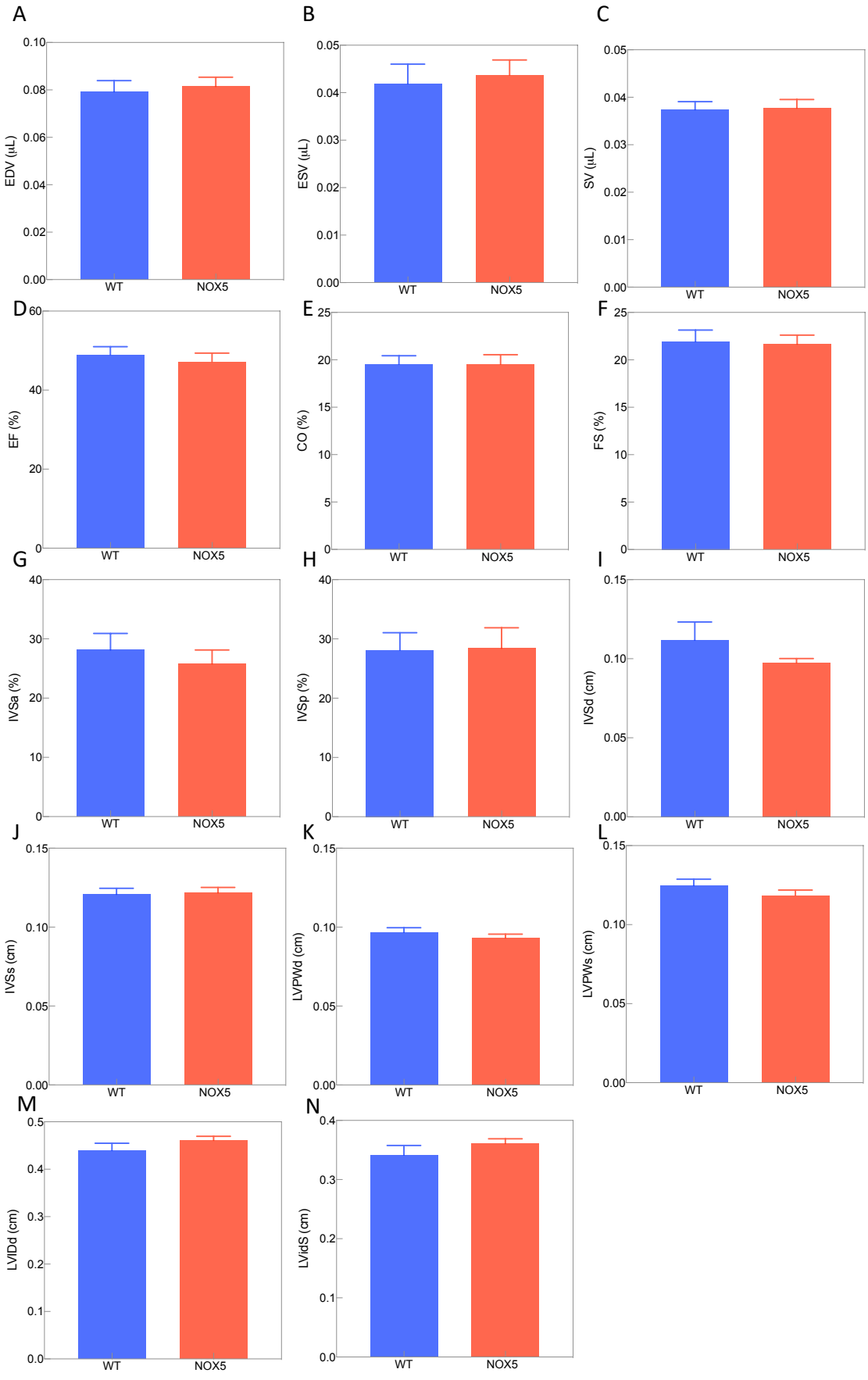
A
EDV (µL)
0.10
0.08
0.06
0.04
0.02
0.00
WT
NOX5
B
ESV (µL)
0.05
0.04
0.03
0.02
0.01
0.00
WT
NOX5
C
SV (µL)
0.05
0.04
0.03
0.02
0.01
0.00
WT
NOX5
D
EF (%)
60
40
20
0
WT
NOX5
E
CO (%)
25
20
15
10
5
0
WT
NOX5
F
FS (%)
25
20
15
10
5
0
WT
NOX5
G
IVSa (%)
40
30
20
10
0
WT
NOX5
H
IVSp (%)
40
30
20
10
0
WT
NOX5
I
IVSd (cm)
0.15
0.10
0.05
0.00
WT
NOX5
J
IVSs (cm)
0.15
0.10
0.05
0.00
WT
NOX5
K
LVPWd (cm)
0.15
0.10
0.05
0.00
WT
NOX5
L
LVPWs (cm)
0.15
0.10
0.05
0.00
WT
NOX5
M
LVIDd (cm)
0.5
0.4
0.3
0.2
0.1
0.0
WT
NOX5
N
LVidS (cm)
0.4
0.3
0.2
0.1
0.0
WT
NOX5

Fig. S7. Echocardiography in aged WT and KI mice. There were no differences in all parameters between WT (n=28) and KI mice (n=29). Comparison between groups were done by two-tailed unpaired T-test. All data are represented as mean ± S.E.M. of n individual animals.

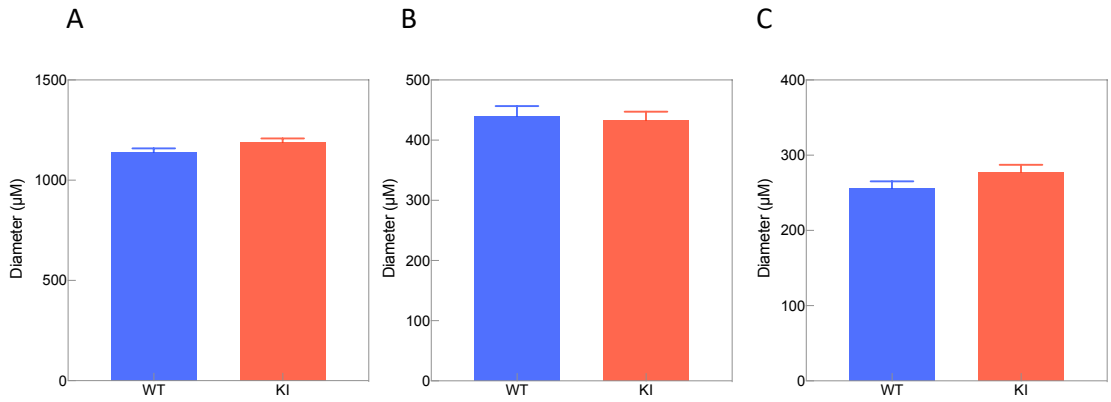

Fig. S8. Arteries diameter in aged WT and KI mice. There were no differences in diameters of thoracic aortas (A), femoral arteries (B) and saphenous arteries (with/without indomethacin) between WT (n=9) and KI mice (n=9). Comparison between groups were done by two-tailed unpaired T-test. All data are represented as mean ± S.E.M. of n individual animals.

Table S1. qPCR assays

Gene	Assay ID
β-actin	Mm02619580_g1
Nox5	Hs00225846_m1

9

GENERAL DISCUSSION

Reactive oxygen-cyclic GMP: Therapeutic targets in common diseases

One key hypothesis of this thesis is that co- or multimorbidities can be explained by a common mechanism that is relevant in different organs and causes symptoms in these organs. Our current organ-based taxonomic approach to medicine, however, artificially separates these and defines independent disease per organ. The component of comorbidity is noticed but without consequence. Not knowing the causal molecular mechanism i.e., the mechanotype of these disease phenotypes results in different symptom-based and rather ineffective therapies in each organ.

Here one such causal disease mechanism was studied as a proof-of-concept, i.e. dysregulated reactive oxygen species (ROS) formation and nitric oxide-cyclic cGMP signaling (ROCG). This module is involved in a cluster of comorbidities including diabetes, atherosclerosis, hypertension and stroke [1-3]. Several key proteins within the ROCG signaling module can be targeted to reinstall the physiological signaling state. These include, NADPH oxidases type 4 and 5 (NOX), NO synthases type 1 and 3 (NOS) and soluble guanylate cyclase (sGC). Despite a uniform module, however, in different diseases and at different stages of a disease such as diabetes different targets are involved in this module requiring thus different drugs to be used. Importantly though, these drug combinations differ from classical combinations of mechanistically unrelated drugs with additive effects; here all drugs target the same causal mechanism and are thus highly synergistic and effective. Patient selection though has to reside not only on the clinical phenotype but also the mechanotype.

In this thesis, two ROCG drug targets were pharmacologically validated in detail, NOX and sGC. With respect to NOX, it was a major obstacle that some of the most commonly used NOX inhibitors lack sufficient isoform-selectivity. An inhibitor panel approach was able to overcome this gap and allowed pharmacological target validation of NOXs in cell-based systems. In other *in vitro* disease models further adaptations of this approach would of course be needed, but feasibility was established. These data and similar results [4] should stimulate focused library synthesis and structure-activity programs for further lead optimization to obtain eventually isoform selective small molecules for single compound target validation and potentially for clinical development.

With respect to NO-activated sGC, chronic exposure to physiological or pathologically elevated NO was found to inactivate sGC and increase the formation of heme-free isoform, apo-sGC, both in health and disease. In physiology, this could be a part of self-limiting direct chemical feedback that was found to be surprisingly independent of canonical cGMP signaling and, in disease, can lead to decreased cGMP formation. To re-install cGMP synthesis, NO-independent sGC stimulators and apo-sGC activators would be therapeutically superior to NO donors. Thus, these findings add to the clinical limitations of NO donors such as their pharmacokinetic tolerance and also to our understanding of apo-sGC as a therapeutic target in disease.

Network pharmacology for ROS/cGMP-related comorbidities

Therapeutically, a disease module such as ROCG, is best targeted, however, at several synergistic sites, an approach termed network pharmacology. In contrast to common combinations of mechanistically unrelated drugs, network pharmacology combines multiple, low-dose synergistic drugs targeting the same module [2, 5, 6]. Here, a network pharmacology approach was applied to target ROCG in stroke with/without diabetes, a high unmet medical need condition [7, 8]. Starting from NOX4 as a primary causal target in stroke and by performing protein–metabolite network analysis, NOS1 could be predicted as the closest target to NOX4. As a validation of these findings, a combination of NOX and NOS inhibitors at subthreshold concentrations/doses in stroke, *in vitro* and *in vivo,* was found neuroprotective. This strategy was then expanded by adding a third target in ROCG, apo-sGC, which is also involved in stroke [8]. Indeed, in stroke, with/without diabetes, a higher neuroprotective effect was observed by using a triple combination of NOX and NOS inhibitors and apo-sGC activator. This network pharmacology approach thus represents an intelligent strategy that reduces the risk of failure in single drug target development by moving toward multiple targeting of de novo causal networks to increase therapeutic efficacy and reduce possible side effects. It would be interesting to extend this approach to other unmet medical need indications.

NOX5: The missing player

Another NOX, NOX5, is currently preclinically highly under-studied because the gene is absent from the mouse and rat genome [9-11]. Using a NOX5 knock-in mouse model, NOX5 was shown to induce hemorrhagic transformation upon induction of stroke in

diabetic mice. Therefore, NOX5 appears as a promising therapeutic target for hemorrhagic transformation that is induced by thrombolytic therapy, the only approved treatment for stroke. Combination of a NOX5 inhibitor with a thrombolytic drug would be an appropriate strategy to overcome thrombolysis side effects and increase the number of patients that can receive this therapy.

In atherosclerosis, another disease where ROCG network is dysfunctional, the role of endothelial NOX5 is unclear, thus its role in a comorbidity model of diabetes-accelerated atherosclerosis was investigated. NOX5 did not aggravate atherosclerosis in both diabetic and non-diabetic mice, however, surprisingly induced aortic aneurysm in diabetes by lowering fibronectin levels.

Dysfunction in NO/cGMP vasodilatory signaling is a characteristic feature in hypertension [12]. Using molecular network analysis, NOX5, but not other ROS sources was identified as the first neighbor to NO/cGMP-related proteins. This connection between NOX5 and NO/cGMP-related proteins was validated clinically, and some hypertensive patients showed high NOX5 levels that were associated with disease severity. Mechanistically, NOX5 was found to cause hypertension in mice upon ageing via uncoupling of NOS resulting in impaired vasodilation. These findings suggest that NOX5-induced NOS uncoupling is a promising theragnostic target of age-related hypertension endotype.

Final Conclusion

This thesis shows that network pharmacology is an excellent approach for curative treatment of mechanistically related comorbidity endotypes. Pharmacological targeting of the ROCG network appears to be beneficial in diabetes, stroke, aortic aneurysm and hypertension and, indeed, phase II drug repurposing trials are currently under preparation suggesting clinical application in the not too far future.

References

1. Langhauser, F. et al. (2018) A diseasome cluster-based drug repurposing of soluble guanylate cyclase activators from smooth muscle relaxation to direct neuroprotection. NPJ Syst Biol Appl 4, 8.
2. Casas, A.I. et al. (2019) From single drug targets to synergistic network pharmacology in ischemic stroke. Proc Natl Acad Sci U S A 116 (14), 7129-7136.
3. Elbatreek, M.H. et al. (2019) Reactive Oxygen Comes of Age: Mechanism-Based Therapy of Diabetic End-Organ Damage. Trends Endocrinol Metab.
4. Augsburger, F. et al. (2019) Pharmacological characterization of the seven human NOX isoforms and their inhibitors. Redox Biol 26, 101272.
5. Hartner, F. et al. (2018) Geometric characterisation of disease modules. Appl Netw Sci 3 (1), 10.
6. Menche, J. et al. (2015) Disease networks. Uncovering disease-disease relationships through the incomplete interactome. Science 347 (6224), 1257601.
7. Chen, R. et al. (2016) Diabetes and Stroke: Epidemiology, Pathophysiology, Pharmaceuticals and Outcomes. Am J Med Sci 351 (4), 380-6.
8. Langhauser, F. et al. (2018) A diseasome cluster-based drug repurposing of soluble guanylate cyclase activators from smooth muscle relaxation to direct neuroprotection. NPJ systems biology and applications 4 (1), 8.
9. Casas, A.I. et al. (2019) Calcium-dependent blood-brain barrier breakdown by NOX5 limits postreperfusion benefit in stroke. J Clin Invest 130, 1772-1778.
10. Touyz, R.M. et al. (2019) Vascular Biology of Superoxide-Generating NADPH Oxidase 5-Implications in Hypertension and Cardiovascular Disease. Antioxid Redox Signal 30 (7), 1027-1040.
11. Zhang, Y. et al. (2019) NADPH oxidases and oxidase crosstalk in cardiovascular diseases: novel therapeutic targets. Nat Rev Cardiol.
12. Gryglewski, R.J. et al. (1986) Superoxide anion is involved in the breakdown of endothelium-derived vascular relaxing factor. Nature 320 (6061), 454-6.

10

SUMMARY

Diabetes, atherosclerosis, hypertension and stroke are common comorbidities and the leading causes of death and disability worldwide. Current therapies are symptom-oriented, do not target the underlying cause and are therefore imprecise. One main reason for this unmet medical need is that these complex diseases are defined by a symptom in an organ and not by a molecular mechanism. Network medicine, however, shows that within the diseasome these comorbidites relate to the same cluster and, thus, likely share common hidden causal pathomechanisms. Targeting these mechanisms would be prefered to syptomatic therapy and, sicne these mechanisms are small signalling modules, network pharmacology is preferable to single-target approaches. One example of such a causal signalling module is the reactive oxygen species (ROS) and cGMP signaling (ROCG) network.

Pharmacologically, several drug classes target this network, including NADPH oxidase (NOX) inhibitors and nitric oxide (NO) donors. In this thesis, a NOX inhibitor panel approach was successfully applied to pharmacologically validate the pathomechanistc involvement of a specific NOX isoform. In addition, NO-cGMP signalling was found to be halted by chronic elevation of NO as part of a chemical feedback loop that converts the NO receptor, soluble guanylate cyclase (sGC), to the heme-free and NO-insensitive apo-sGC. Therefore, other drug classess such as sGC stimulators and apo-sGC activators will be superior to NO donors for chronic use.

In a comorbidity model of stroke plus diabetes, a network pharmacology approach using subthreshold doses of a NOX and an NO synthase (NOS) inhibitor plus apo-sGC activator, resulted in a substantial neuroprotective effect. This approach is now in clinical trials. Also in diabetes, NADPH oxidase 5 (NOX5) was found as the most direct neighbour to NO-cGMP-related proteins. This connection was functionally validated both in a subgroup of hypertensive patients and in NOX5-knock in mice where NOX5 induced NOS uncoupling as a causal mechanism to induce age-related hypertension.

Collectively, network pharmacology targeting causal disease modules represents a new approach to precisely define, diagnose and cure hitherto complex comorbidities such as diabetes, atherosclerosis, hypertension and stroke. Further validations in clinical trials is needed and planned to start in late 2020.

11

VALORISATION

The prevelance of comorbidities is increasing due to aging populations. This will lead to massive medical and socio-economic challenges. Comorbidity is not only associated with worse health outcomes, but also with more complex clinical management, and increased health care costs for public and private insurance payers, individuals, and families. Drug discovery and development does not have only long development times, but for many years its expenses have increased exponentially with a decresing success rate. This is neither sustainable for the pharmaceutical industry but also the health care providers and tax payers who indirectly need to refinance these costs. One key knowledge gap in all of this is our current way of defining and treated diseases, i.e. by symptom without knowing the underlying causal molecular mechains. Obviously this is an imprecise and and error-prone approach in medical valorisation that has to be overcome.

This thesis therefore suggests to redefine comorbidities based on their underlying causal molecular mechanisms as a first key step towards filling this key knowledge gap. Once these diseases are fully endo-phenotyped and mechanistically understood, they will segregate into several distinct mechanotypes that can be treated with different drugs. Both diagnostic and therapeutic approaches herein provide IP and socioeconoímic benefit options. To achieve rapid market entry, a drug repurposing appproach of registered compounds was chosen.

In hypertension, one molecular causal mechanism i.e. NADPH oxidase 5 (NOX5)-induced uncoupling of nitric oxide (NO) synthase (NOS), was identified. This mechanism was found only in some hypertensive patients (around 25%) i.e. as endotype and thus this would suggest that only those patients need to be treated with NOX5 inhibitors and NOS recoupling agents and not all hypertensive patients. These findings open up several lab-to-market opportunities, both in diagnostics and in therapies and deliver at least two products; i) biomarkers for precision diagnosis and ii) a first-in-class mechanism-based therapy. Biomarkers will help stratify the patients based on the underlying pathomechanism and therapeutics will target a causal disease mechanism and therefore are more precise than the current symptomatic treatments. Applying this mechanism-based theragnostic approach (Fig. 1) will decrease the number needed to treat and thus have a great socio-economic relevance.

In stroke only one approved drug is available which is a thrombolytic treatment, rt-PA, and there is no neuroprotective therapy. Here three targets within the ROCG network i.e NOX, NOS and soluble guanylate cyclase (sGC) were identified. This thesis suggests that a combination of NOX and NOS inhibitors and sGC activator as the first broadly applicable, safe and effective neuroprtoective therapy. Using drugs that are already approved or in late clinical development i.e. drug repurposing allows fast testing of this network pharmacology approach in clinical trials. This neuroprotective treatment is a patentable finding that still requires further clinical development, therefore the right strategy for this specific finding is considered to be to further develop the patent into a spin-off company with matching scientific and commercial experience to develop and exploit the findings up to phase IIb/III clinical.

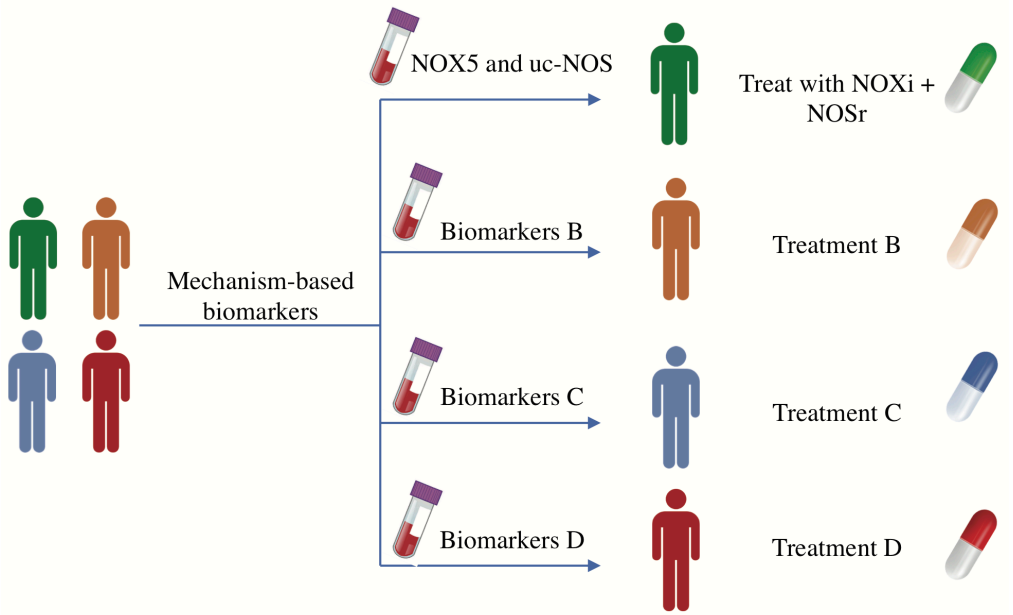

Fig.1| Mechanism-based theragnostic approach in hypertension. NOSr, Nitric oxide synthase recoupling agent; NOX5, NADPH oxidase 5; NOXi, NADPH oxidase inhibitor, uc-NOS, uncoupled NOS.

In conclusion, network pharmacology has several advantages that overcome the current knowledge gaps and unmet medical needs: (i) gathering investigators from different disciplines such as basic biology, clinicians, systems biology, network and data science to work together in addition to collaboration with pharma companies, (ii) drug repurposing within the same disease cluster which decreases time and costs of drug development and omits the need for further preclinical testing and (iii) combination of low-dose drugs for multiple targets within the same network to ensure

high efficacy and less side effects. This approach is of course not limited to the above-mentioned diseases and the ROCG mechanism, but can be applied within any complex, i.e. polygenic disease phenotype and delivers a remarkable and safe innovation for treatments of common comorbidities, which could rapidly save millions of lives of patients, improve the quality of life and decrease research and health care costs.

APPENDICES

LIST OF PUBLICATION

1. Wang R, Wang ST, Wang YD, Wu G, Du Y, **Elbatreek MH**, et al. Stress-responsive heme oxygenase-1 isoenzyme participates in Toll-like receptor 4-induced inflammation during brain ischemia. Neuroreport. 2016.
2. **Elbatreek MH**, Pachado MP, Cuadrado A, Jandeleit-Dahm K, Schmidt H. Reactive Oxygen Comes of Age: Mechanism-Based Therapy of Diabetic End-Organ Damage. Trends Endocrinol Metab. 2019.
3. Dao VT, **Elbatreek MH**, Altenhofer S, Casas AI, Pachado MP, Neullens CT, et al. Isoform-selective NADPH oxidase inhibitor panel for pharmacological target validation. Free Radic Biol Med. 2019.
4. Dao VT, **Elbatreek MH**, Deile M, Nedvetsky PI, Güldner A, Ibarra-Alvarado C, et al. Non-canonical chemical feedback self-limits nitric oxide-cyclic GMP signaling in health and disease. Scientific Reports. 2020.
5. Casas AI, Hassan AA, Larsen SJ, Gomez-Rangel V, **Elbatreek M**, Kleikers PWM, et al. From single drug targets to synergistic network pharmacology in ischemic stroke. Proc Natl Acad Sci U S A. 2019.
6. Casas AI, **Elbatreek MH**, Nogales C, Sadegh S, Kacprowski T, Baumbach J, et al. Network pharmacology reduces diabetes-related poor outcome and hemorrhagic transformation in stroke. (In preparation)
7. Watson A, **Elbatreek MH**, Mathew G, Kleikers P, Schmidt HHHW, Jandeleit-Dahm. Endothelial NOX5 induces aortic aneurysms in diabetic $ApoE^{-/-}$ mice. (In preparation)
8. **Elbatreek MH**, , Sadegh S, Anastasi E, Guney E, Kacprowski T, Hassan AA, et al. NOX5-induced uncoupling of endothelial NO synthase is a causal mechanism and theragnostic target of an age-related hypertension endotype validation. PLOS Biology. 2020.
9. **Elbatreek MH**, Mucke H, Schmidt HHHW. NOX inhibitors: From bench to naxibs to bedside. Reactive oxygen species: network pharmacology and therapeutic applications. Handbook of experimental pharmacology.
10. Dao VT, **Elbatreek MH**, Fuchß T, Grädler U, Schmidt HHHW, et al. Nitric oxide synthase inhibitors into the clinic at last. Reactive oxygen species: network pharmacology and therapeutic applications. Handbook of experimental pharmacology.

APPENDICES

ABOUT THE AUTHOR

Mahmoud was born on October 5th, 1987 in Bilbeis, Egypt. After finishing his high school education in Bilbeis in 2005, he enrolled in the Bachelor program at Faculty of Pharmacy, Zagazig University, Egypt. In 2009, he obtained his Bachelor degree in 'Pharmaceutical Sciences' and then he worked as a pharmacist at Nahdi Medical Company in Saudia Arabia. In 2011, he returned back to Egypt and worked as a demonstrator at Department of Pharmacology and Toxicology in the same faculty where he was graduated. After four years, he got his Master degree under a title of 'Study on the effect of immunosuppressive drugs on kidney injury' and started to work as assistant lecturer in the same department. During his work from 2011 to 2015, he taught several practical pharmacology and toxicology courses to Bachelor students in addition to doing research. Later in 2015, he started a research fellowship at College of Pharmaceutical Sciences, Zhejiang University, China after he had gotten a CSC scholarship from Chinese government. In 2016, he got a PhD scholarship from Ministry of Higher Education and Scientific Research in Egypt and susequentely he started his PhD at Department of Pharmacology and Personalised Medicine, Maastricht University, Netherlands. During his PhD trajectory he attended several courses, workshops and international conferences in addition he was trained in other laboratories in Melbourne, Essen and Bochum. He also served as a reviewer for some journals e.g. PLOS One. Besides, he had a teaching role as a tutor for the second year medical students and he supervised Bachelor and Master intern students. Next to his research and teaching activities, Mahmoud is a soccer player who used to play for his home city, Bilbeis and also joined two teams in the Netherlands during his PhD; DBSV Red Socks and SC Jekerdal. In his private life he married Asmaa in 2012 and she gave birth to their two children: Hamza (2013) and Tala (2019).

APPENDICES

ACKNOWLEDGEMENTS

I would first like to thank Almighty Allah, The Most Generous and The Most Merciful, for giving me the opportunity, strength, knowledge and ability to do my PhD as He always does throughout my life.

In my journey towards this degree, I have found a teacher, a friend and an inspiration, my supervisor, Harald. I cannot find the words that express my gratitude to you. Thanks for all kinds of support and motivation you gave to me and also to my family. Thanks for providing me guidance at all times and giving me the freedom to pursue my research. Thanks for all the happy memories we have shared, and I shall eternally be grateful to you.

I have great pleasure in acknowledging my gratitude to my colleagues in the PPM, Ana, Christian, Alexandra, Mayra, Zeinab, Theodora, Marlou, Ivo, Mohannad and Christopher. Thank you all for encouragement, support, assistance, awesome teamwork and everything I have ever learned from you.

I also wish to thank Vu Thao-Vi, Pamela Kleikers, Peter Lijnen, Jet Bost, Karin Jandeleit-Dahm, Jo De Mey, Paul Schiffers, Stine Mencl, Helma van Essen and Ger Janssen whose assistance was a milestone in the completion of my PhD.

I am thankful to the Egyptian Ministry of Higher Education and Scientific Research for offering me a PhD scholarship and the Department of Pharmacology and Toxicology, Faculty of Pharmacy, Zagazig University for opening the door for me to do my PhD abroad.

My special thanks must go to Ahmed Hassan, Mohamed Darwish, Majed Aldehri, Khalid Shahin, Khalid Eid, Marcel Schoehuijs, Zaid Shaheen and Mohamed Elmongy for their moral support, assistance and motivation.

Finally, there are no proper words to convey my sincere gratitude to my family. My parents, I owe everything to you, and without your love and support, none of this would have been possible. I deeply thank my siblings, Shimaa, Mohammed, Yasmin and Sally and their nuclear families. I am also thankful to my uncles, aunts and parents-in-law. My wife and my life partner, Asmaa, thanks for your patience, tremendous encouragement and countless sacrifices that helped me get to this point. My lovely children, Hamza and Tala, you are the pride and joy of my life, thanks for giving me optimism and hopefulness.

كل الشكر والتقدير والعرفان الى من يجري حبهما في دمي، أبي وأمي، أنتما سبب وجودي ونجاحي، كنتما ولازلتما كالنخلة الشامخة، تعطي بلا حدود، لا أعلم ما الذي يجب أن أقدمه لكما كي أوفيكما حقكما. زوجتي الغالية ورفيقة عمري، شكرا علي تشجيعك ومساندتك الدائمة لي وعلي رعاية أسرتنا الصغيرة. أبنائي الأعزاء، حمزة وتالا أنتما أغلي ما أملك، شكرا جزيلا لأنكما دائما تمنحانني الأمل والتفاؤل والحب.